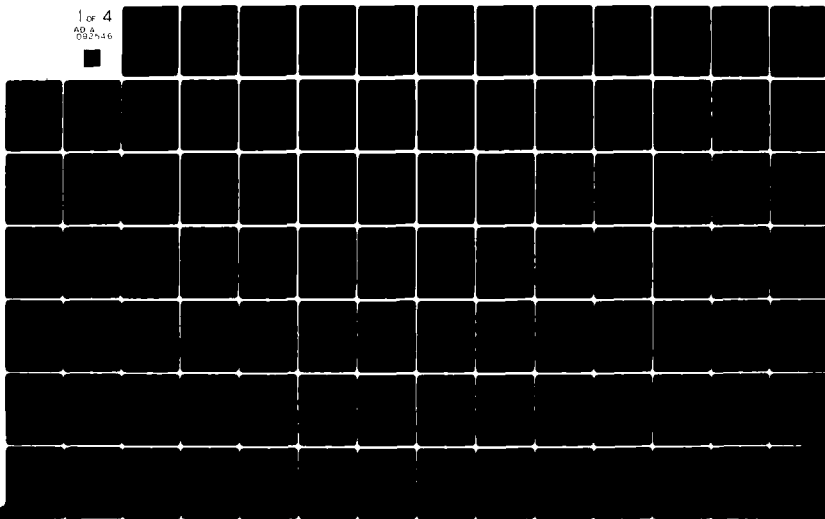


AD-A092 546

AIR FORCE INST OF TECH WRIGHT-PATTERSON AFB OH F/6 7/3  
SPONTANEOUS, METAL-CATALYZED, AND ENZYME-CATALYZED DECARBOXYLAT-ETC(U)  
1980 S L SINCOFF  
UNCLASSIFIED AFIT-CI-80-27D

NL

1 of 4  
AD A  
092 546



UNCLASS

SECURITY CLASSIFICATION OF THIS PAGE (When Data Entered)

## REPORT DOCUMENTATION PAGE

READ INSTRUCTIONS  
BEFORE COMPLETING FORM

1. REPORT NUMBER

80-270

2. AVT ACCESSION NO.

3. RECIPIENT'S CATALOG NUMBER

AD-A092546

4. TITLE (and Subtitle)

Spontaneous, Metal-Catalyzed, and Enzyme-  
Catalyzed Decarboxylation of Oxalosuccinic  
Acid

5. TYPE OF REPORT &amp; PERIOD COVERED

THESIS/DISSERTATION

6. PERFORMING ORG. REPORT NUMBER

8. CONTRACT OR GRANT NUMBER(s)

7. AUTHOR(s)

Capt Steve L. Sincoff

9. PERFORMING ORGANIZATION NAME AND ADDRESS

AFIT STUDENT AT: The Ohio State University

10. PROGRAM ELEMENT, PROJECT, TASK  
AREA & WORK UNIT NUMBERS

11. CONTROLLING OFFICE NAME AND ADDRESS

AFIT/NR  
WPAFB OH 45433

12. REPORT DATE

1980

13. NUMBER OF PAGES

309

14. MONITORING AGENCY NAME &amp; ADDRESS (if different from Controlling Office)

15. SECURITY CLASS. (of this report)

UNCLASS

15a. DECLASSIFICATION/DOWNGRADING  
SCHEDULE

16. DISTRIBUTION STATEMENT (of this Report)

APPROVED FOR PUBLIC RELEASE; DISTRIBUTION UNLIMITED

DTIC  
SELECTE  
DEC 08 1980

17. DISTRIBUTION STATEMENT (of the abstract entered in Block 20, if different from Report)

E

18. SUPPLEMENTARY NOTES

APPROVED FOR PUBLIC RELEASE: IAW AFR 190-17  
FREDRIC C. LYNCH, Major, USAF  
Director of Public AffairsAir Force Institute of Technology (ATC)  
Wright-Patterson AFB, OH 45433

19. KEY WORDS (Continue on reverse side if necessary and identify by block number)

20. ABSTRACT (Continue on reverse side if necessary and identify by block number)

ATTACHED

DD FORM 1 JAN 73 1473

EDITION OF 1 NOV 65 IS OBSOLETE

UNCLASS

SECURITY CL.

CLASSIFICATION OF THIS PAGE (When Data Entered)

AD A092546

CIRC FILE  
300

SPONTANEOUS, METAL-CATALYZED, AND ENZYME-CATALYZED

DECARBOXYLATION OF OXALOSUCCINIC ACID

by

Captain Steven L. Sincoff, PhD in Analytical Chemistry

United States Air Force

The Ohio State University, 1980

309 Pages

Professor Daniel Leussing, Advisor

Decarboxylation rates of oxalosuccinic acid, a tricarboxylic acid, has been studied in detail. It was shown that the keto forms of the acid spontaneously decarboxylate. The catalytic effect of three metals were examined. The overall effectiveness of the metals were  $Zn^{(2+)} > Mn^{(2+)} > Mg^{(2+)}$ . This catalysis resulted from the formation of a 1:1 complex between the acid and the metal ions. The enzyme isocitrate dehydrogenase (ICDH) was able to catalyze the reaction without the aid of a metal ion. Kinetically, protonated and deprotonated ICDH-oxas<sup>(3-)</sup> complexes were shown to exist. The effect of two divalent metals were studied. The rate constants for the  $Zn^{(2+)}-ICDH-oxas^{(3-)}$  and  $Mg^{(2+)}-ICDH-oxas^{(3-)}$  ternary complexes were nearly identical. It was also found that the  $Mg^{(2+)}$  ternary complex could ionize ( $pK_a = 5.72$ ) as well as the  $Mg^{(2+)}-ICDH$  binary complex ( $pK_a = 7.64$ ). It was concluded that (1) the actual binding site on the enzyme was different for each metal; and (2) the role of the metal ion is to create a more favorable geometry at the active site on the enzyme. This new geometry establishes a structure within the enzyme for other functional groups at the active site to better promote decarboxylation.

SPONTANEOUS, METAL-CATALYZED, AND ENZYME-CATALYZED

DECARBOXYLATION OF OXALOSUCCINIC ACID .

Doctor of Philosophy

DISSERTATION

Presented in Partial Fulfillment of the Requirements for the  
Degree Doctor of Philosophy in the Graduate School of  
The Ohio State University

ADAFIT-2I-10-27D

By

Captain Steven L. Sincoff, BS, MS in ChE

United States Air Force

\*\*\*\*\*

The Ohio State University

1980

Accession For	
NTIS GRA&I	<input checked="checked" type="checkbox"/>
DDC TAB	<input type="checkbox"/>
Unannounced	<input type="checkbox"/>
Justification	
By _____	
Distribution/	
Availability Codes	
Dist.	Avail and/or special
A	

Reading Committee:

Professor L. B. Anderson

Professor D. L. Leussing

Professor R. L. McCreery

Approved By

*Daniel L. Leussing*  
Advisor  
Department of Chemistry



#### ACKNOWLEDGMENTS

The author wishes to thank Dr. Daniel L. Leussing for his expert guidance and direction in the preparation and presentation of this project. The detailed discussions and advice of my fellow colleagues are also appreciated.

The author also wishes to express sincere thanks to the United States Air Force, who released him from all military duties in order to pursue this research work on a full-time basis.

The encouragement and moral support from the author's wife, Connie, for her help in the preparation of this manuscript as well as her tolerance of the author during his period of intense research is most appreciated. The author also wishes to thank his two children, Kristy and Carrie, who had to live with numerous fatherless evenings and weekends during this period.

# VITA

April 17, 1948 . . . . . Born - Bronx, New York

June 4, 1969. . . . . B.S. in Chemical Engineering,  
New Jersey Institute of Technology,  
Newark, New Jersey

September 27, 1970 . . . . . Entered active duty as a Second  
Lieutenant, United States Air Force

June 5, 1972 . . . . . M.S. in Chemical Engineering,  
New Jersey Institute of Technology,  
Newark, New Jersey

June 1977 - June 1980. . . . . Graduate Student, Department of  
Chemistry, The Ohio State Univ.,  
Columbus, Ohio, under sponsorship  
of the Air Force Institute of  
Technology, Wright-Patterson Air  
Force Base, Ohio

## TABLE OF CONTENTS

	Page
ACKNOWLEDGMENTS . . . . .	ii
VITA . . . . .	iii
LIST OF TABLES . . . . .	vi
LIST OF FIGURES . . . . .	viii
 Chapter	
I. LITERATURE REVIEW . . . . .	1
II. EXPERIMENTAL PROCEDURES . . . . .	30
A. Reagents	30
B. Equilibrium Investigations	38
C. Kinetic Investigations	42
III. PHYSICAL DATA ON OXALOSUCCINATE . . . . .	50
A. Ultraviolet	51
B. Infrared	55
C. Nuclear Magnetic Resonance	60
D. Equilibrium Data	68
IV. DECARBOXYLATION AND TAUTOMERIZATION OF OXALOSUCCINIC ACID	97
Summary	135
V. ZINC CATALYZED DECARBOXYLATION OF OXALOSUCCINATE. . . .	137
Summary	152
VI. MAGNESIUM AND MANGANESE CATALYZED DECARBOXYLATION OF	
OXALOSUCCINATE . . . . .	154
Summary	166

## CONTENTS (CONT'D)

	Page
VII. ENZYME ASSISTED DECARBOXYLATION OF OXALOSUCCINATE	169
A. ICDH Assisted Decarboxylation of Oxalosuccinate	171
B. Zinc(II) and Magnesium(II) Assisted Decarboxylation of the ICDH-Oxalosuccinate System	198
C. Summary	235
REFERENCES . . . . .	238
APPENDICES	
A. Absorbance Data for the Various Oxalosuccinate-Metal- $\alpha$ -ketoglutarate Systems . . . . .	242
B. pH Titration Data . . . . .	255
C. Decarboxylation Rate Data for the Various Enzyme- Oxalosuccinate-Metal Systems . . . . .	261
D. Computer Listing of the Program CORNEK . . . . .	278
E. Computer Listing of the Various FITFC Subroutines Used For the Program CORNEK . . . . .	289
F. Investigation of the Spontaneous Tautomerization of Oxalosuccinate via the Method of Iodination . . . . .	293

# LIST OF TABLES

Table	Page
1. Published Rate Constants for Various Oxalosuccinate Systems . . . . .	7
2. Decarboxylation Rate Constants for Oxaloacetate Species and Metal-Oxaloacetate Complexes . . . . .	12
3. Decarboxylation Rate Constants for 3-Oxoglutarate Species and Metal-3-Oxoglutarate Complexes . . . . .	15
4. Linear Range of pH Indicators . . . . .	45
5. Comparison of Infrared Energies for Oxalosuccinate, Citrate, and Isocitrate Inorganic Salts (cm <sup>-1</sup> ). . . . .	61
6. Extinction Coefficients and pK <sub>a</sub> Values for Alpha-ketoglutaric Acid . . . . .	72
7. Oxalosuccinate Absorbance Data at 260 nm . . . . .	75
8. Extinction Coefficients for Oxalosuccinate at Various Wavelengths . . . . .	77
9. Spectrophotometric Titration of the Enolate Species at 272 nm . . . . .	84
10. Summary of Data: Acid Protonation Constants and Metal Formation Constants . . . . .	86
11. Magnesium - Oxalosuccinate Absorbance Data at 260 nm . . . . .	91
12. Zinc - Oxalosuccinate Absorbance Data at 255 nm . . . . .	92
13. Zinc - Oxalosuccinate Absorbance Data at 284 nm . . . . .	93
14. Comparison of Spectrophotometric, pH Stat, pH Indicator, and Manometric Determinations of the Decarboxylation Rate Constants. . . . .	109
15. Spontaneous Decarboxylation of Oxalosuccinic Acid . . . . .	115

# TABLES (CONT'D)

Table	Page
16. Keto/Enol Ratios of Oxalosuccinic Acid . . . . .	130
17. Observed Rate Constants at Higher Levels of Zinc <sup>2+</sup> . . . . .	151
18. Summary of Formation Constants and Decarboxylation Rate Constants for Metal-Oxalosuccinate Systems . . . . .	167
19. Alpha-ketoglutarate Inhibition of the ICDH-Oxalosuccinate System . . . . .	184
20. EDTA Inhibition on the Metal-Free System . . . . .	186
21. Metal Content of ICDH . . . . .	193

# LIST OF FIGURES

Figure		Page
1.	Ultraviolet Spectrum of $\alpha$ -Ketoglutarate . . . . .	53
2.	Ultraviolet Spectrum of Oxalosuccinate - Low pH . . . . .	54
3.	Ultraviolet Spectrum of Oxalosuccinate - High pH . . . . .	56
4.	Infrared Spectrum of $\alpha$ -Ketoglutarate. . . . .	58
5.	Infrared Spectrum of Oxalosuccinate . . . . .	59
6.	Nuclear Magnetic Resonance Spectrum of $\alpha$ -Ketoglutarate. .	63
7.	Nuclear Magnetic Resonance Spectrum of Oxalosuccinate . .	65
8.	pH Titration of $\alpha$ -Ketoglutarate . . . . .	69
9.	Spectrophotometric Titration of $\alpha$ -Ketoglutarate . . . . .	70
10.	Spectrophotometric Titration of Oxalosuccinate . . . . .	78
11.	Wavelength Dependence of the Extinction Coefficients for the Oxalosuccinate Species. . . . .	79
12.	Ultraviolet Spectra of Oxalosuccinate Versus pH at High pH. . . . .	82
13.	Spectrophotometric Titration of the Oxalosuccinate Enolate Species at 272 nm . . . . .	83
14.	pH Titrations of Metal/ $\alpha$ -ketoglutarate Solutions for Magnesium, Manganese, and Zinc . . . . .	88
15.	Ultraviolet Spectrum of the Magnesium-Oxalosuccinate Solution . . . . .	95
16.	Ultraviolet Spectrum of the Zinc-Oxalosuccinate Solution	96
17.	Spectrophotometric Decarboxylation of Oxalosuccinate. . .	98
18.	Reaction Spectra Versus Time: Slow Scan Rates . . . . .	99

Figure	FIGURES (CONT'D)	Page
19.	Reaction Spectra Versus Time: Longer Times . . . . .	101
20.	Rapid Scanning Spectra Versus Time: Longer Times . . . . .	102
21.	Rapid Scanning Spectra Versus Time: Short Times . . . . .	104
22.	Observed Decarboxylation Rate Constants Versus pH . . . . .	111
23.	Dependence of the Fast Relaxation on the Concentration of Acetate . . . . .	119
24.	Rate Constant for the Fast Relaxation Versus pH . . . . .	121
25.	Experimental Trace from the Cary 14 for the Determination of the Enol Content of Oxalosuccinate . . . . .	126
26.	Percent Oxalosuccinate Enolized Versus pH . . . . .	128
27.	Time Dependence of the Ultraviolet Spectra for the Zinc <sup>2+</sup> -Oxalosuccinate System . . . . .	139
28.	Sample Reaction Trace for the Zinc-Oxalosuccinate System	142
29.	Tautomerization Rates for the Zinc-Oxalosuccinate System	144
30.	Observed Decarboxylation Rate Constants Versus Zinc Concentration . . . . .	146
31.	Observed Decarboxylation Rate Constants Versus pH for the Zinc-Oxalosuccinate System. . . . .	149
32.	Time Dependence of the Ultraviolet Spectra for the Magnesium <sup>2+</sup> -Oxalosuccinate System . . . . .	155
33.	Observed Decarboxylation Rate Constants Versus Magnesium Concentration . . . . .	158
34.	Observed Decarboxylation Rate Constants Versus pH for the Magnesium-Oxalosuccinate System . . . . .	161



# FIGURES (CONT'D)

Figure	Page
35. Observed Decarboxylation Rate Constants Versus Manganese Concentration . . . . .	164
36. Observed Decarboxylation Rate Constants Versus pH for the Manganese-Oxalosuccinate System . . . . .	165
37. Spectrophotometric Titration of Isocitrate Dehydrogenase	172
38. Observed Rate Constants for the ICDH - Oxalosuccinate System as a Function of pH . . . . .	177
39. Observed Rate Constants for the ICDH-Oxalosuccinate System as a Function of the Concentration of Oxalosuccinate	179
40. EDTA Inhibition on the ICDH-Oxalosuccinate System: Rate Constant versus [EDTA] . . . . .	188
41. EDTA Inhibition on the ICDH-Oxalosuccinate System: Rate Constant versus pH . . . . .	190
42. Observed Rate Constants for the ICDH-Zinc-Oxalosuccinate System as a Function of pH . . . . .	202
43. Observed Rate Constants for the ICDH-Zinc-Oxaloussccinate System as a Function of the Zinc Concentration . . . . .	204
44. Observed Rate Constants for the ICDH-Magnesium-Oxalo-succinate System as a Function of pH. . . . .	209
45. Observed Rate Constants for the ICDH-Magnesium-Oxalo-succinate System as a Function of the Magnesium Concentration . . . . .	211
46. Observed Rate Constants for the ICDH-Magnesium-Oxalo-succinate System as a Function of the Oxalosuccinate Concentration . . . . .	213
47. Comparison of the Enzyme Models for the ICDH-Magnesium-Oxalosuccinate System Versus pH . . . . .	216
48. Comprison of Enzyme Models for the ICDH-Magnesium-Oxalosuccinate System Versus the Magnesium Concentration	218

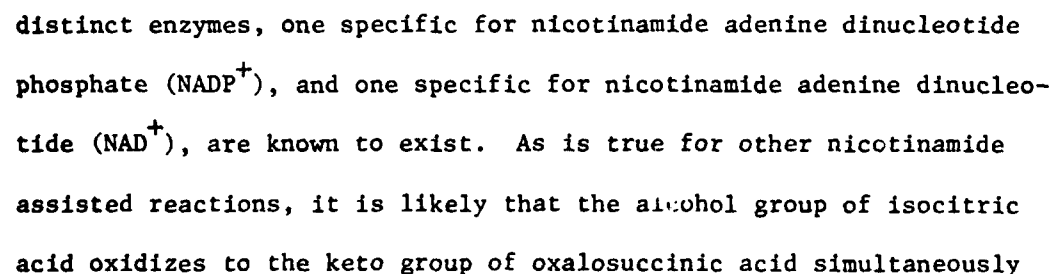
FIGURES (CONT'D)

Figure	Page
49. Tautomerization Rate and Iodination Rate versus pH	295

## I. LITERATURE REVIEW

Historically, reaction mechanisms have been a prime area of research in the study of chemistry. The reason for this is fairly obvious: by determining the correct sequence of reactions and elucidation of intermediate structures, chemists can make predictions of other reactions as well as verifying theoretical models. The area of biochemical reactions offers some very useful and interesting applications. New drugs for the treatment of biological disorders and disease control are two subjects that can be well defined with proper knowledge of reaction mechanisms. Unfortunately, biochemical reactions are very complicated. First, most require an enzyme for reaction catalysis. This creates a serious problem since enzymes, which are large (molecular weights of at least 10,000 daltons) molecules and are very specific for a particular substrate, cannot, at this time, be synthesized in the laboratory. Second, many enzymes require a coenzyme, a smaller molecule which binds to the enzyme and substrate, for the catalytic effect. Finally, many enzyme reactions need a metal ion for increased activity.

In spite of the complexity of these reactions, a great deal of mechanistic information can be obtained by examining the non-enzymatic metal/substrate reaction. By first studying this portion of the

$$\begin{array}{c} \text{O} \\ \parallel \\ \text{HO}-\text{C}-\text{CH}_2-\text{CH}-\text{C}-\text{C} \xrightarrow{\quad} \text{O} \quad \text{O} \quad \text{O} \\ \parallel \quad \parallel \quad \parallel \quad \parallel \\ \text{HO} \quad \text{OH} \quad \text{HO} \quad \text{OH} \\ \text{O} \quad \text{OH} \\ \text{I} \qquad \qquad \qquad \text{II} \end{array} + \text{CO}_2 \quad (1)$$


with the reduction of  $\text{NAD(P)}^+$  to  $\text{NAD(P)H}$  by direct hydrogen transfer.

There is much support for the reaction sequences shown above. It has already been established that isocitric acid decarboxylates with the aid of an enzyme-metal ion-nicotinamide coenzyme complex. This decarboxylation results in the formation of  $\alpha$ -ketoglutarate, although the exact reaction mechanism is subject to investigation. Direct conversion seems unlikely since  $\beta$ -hydroxy acids, like isocitric acid, decarboxylate much slower than  $\beta$ -keto acids, such as oxalosuccinic acid, because the  $\beta$ -hydroxy functionality cannot serve as a useful electron sink. This implies that direct decarboxylation of isocitric acid to  $\alpha$ -ketoglutaric acid without the oxalosuccinic acid intermediate is unlikely. A reasonable assumption, then, would be conversion of the  $\beta$ -hydroxy moiety to form the  $\beta$ -keto acid, which has a low energy path for decarboxylation. It is apparent that the conversion of the  $\beta$ -hydroxy to the  $\beta$ -keto takes place anyway, since the location of the keto group of the product,  $\alpha$ -ketoglutaric acid, is the same as the hydroxy group of the starting material, isocitric acid.

There is also experimental evidence that oxalosuccinate is indeed a reaction intermediate in the conversion of isocitrate to  $\alpha$ -ketoglutarate. Ochoa (1) showed that oxalosuccinate is formed as an intermediate in the decarboxylation of isocitrate. He later showed (2) spectrophotometrically that reactions 1 and 2 are reversible.

He started out with 0.109 micromoles of d-isocitrate and 0.074 micromoles of  $\text{NADP}^+$  in a 1.0 cm cell. He monitored the reaction at 340 nm, a wavelength where only NADPH absorbs. After adding some enzyme, he observed an absorbance increase, which leveled off after about 15 min. He next observed an absorbance decrease when 0.495 micromoles of oxalosuccinate was added. This was due to the formation of  $\text{NADP}^+$  from NADPH, indicating that reaction 2 was going from right to left. After adding 1.8 micromoles  $\text{MnCl}_2$ , the absorbance rapidly increased to the value calculated for 100% conversion to NADPH. Further addition of alpha-ketoglutarate caused a decrease in absorbance, showing that NADPH is being oxidized. The only way this can happen is due to carboxylation of alpha-ketoglutarate followed by the reduction of oxalosuccinate to isocitrate.

Moyle and Dixon (3,4,5) and Siebert et al. (6,7) showed that synthetic oxalosuccinate undergoes catalytic decarboxylation with the  $\text{Mn}^{2+}$ -enzyme complex independent of the  $\text{NADP}^+$  coenzyme. In the presence of NADPH, exogenous oxalosuccinate can be reduced by the enzyme to isocitrate. Further experiments on the overall isocitrate reaction showed that oxalosuccinate cannot be trapped during normal catalysis by carbonyl reagents, such as potassium cyanide.

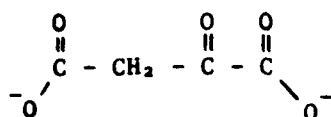
Studies on the decarboxylation of isocitrate by chromatographic techniques (8) failed to demonstrate any buildup of oxalosuccinate.

Also, when exogenous oxalosuccinate is added to carbon-14 labeled isocitrate, the specific activity of the oxalosuccinate pool was unaltered. From those experiments, it was concluded that oxalosuccinate must remain tightly bound to the enzyme and cannot dissociate during the reaction sequence, since it is chemically reasonable that oxalosuccinate is indeed formed as a finite intermediate.

The first reported study on the decarboxylation of oxalosuccinate was presented by Ochoa, who was also the first to stabilize the acid as the barium salt (9). His method of study was by carbon dioxide evolution in a Warburg vessel. He also examined the decarboxylation of oxaloacetate, IV, using the same apparatus. Ochoa reported the following decarboxylation rate constants at a pH of 5.1 and 25°C:

$$k_{\text{oxaloacetate}} = 5.37 \times 10^{-5} \text{ s}^{-1}$$

$$k_{\text{oxalosuccinate}} = 4.49 \times 10^{-4} \text{ s}^{-1}$$



IV

Lynen and Scherer (10) also studied the decarboxylation of oxalosuccinate and oxaloacetate at 20°C and 30°C at a pH of 6.0. The results they obtained were:

$$\begin{aligned}
 k_{\text{oxalosuccinate}}^{20^\circ\text{C}} &= 2.11 \times 10^{-4} \text{ s}^{-1} \\
 k_{\text{oxalosuccinate}}^{30^\circ\text{C}} &= 6.85 \times 10^{-4} \text{ s}^{-1} \\
 k_{\text{oxaloacetate}}^{30^\circ\text{C}} &= 4.00 \times 10^{-5} \text{ s}^{-1}
 \end{aligned}$$

If the rate constant obeys the Arrhenius relationship, then the data at 20°C and 30°C can be used to calculate a value at 25°C. This calculated rate constant was  $3.82 \times 10^{-4} \text{ s}^{-1}$ , which is in excellent agreement with Ochoa. In the same paper, Lynen and Scherer evaluated the decarboxylation rates of oxalosuccinate with various metal ions. These rate constants are summarized in Table 1. The relative rates, in order of decreasing effectiveness, are  $\text{Al}^{3+} > \text{Zn}^{2+} > \text{Fe}^{3+} > \text{Mn}^{2+} > \text{Mg}^{2+} > \text{Ca}^{2+}$ . This agrees closely with the independent work of Ochoa (9), who reported  $\text{Al}^{3+} > \text{Fe}^{3+} > \text{Cu}^{2+} > \text{Fe}^{2+} > \text{Zn}^{2+} > \text{Mg}^{2+} > \text{Mn}^{2+} > \text{Ca}^{2+}$ .

The first ultraviolet (UV) spectrophotometric study on the decarboxylation of oxalosuccinate was reported by Kornberg, Ochoa, and Mehler (11). They investigated the spontaneous reaction of the free acid as well as the effects of  $\text{Al}^{3+}$  and  $\text{Mn}^{2+}$  on the rate, both enzymatically and non-enzymatically. They observed, in all cases involving a metal, a rapid absorbance increase followed by a slower absorbance decrease when monitored at 252 nanometers (nm). This absorbance increase was attributed to the formation of the stable enol forms of the metal-oxalosuccinate complexes, while the slower absorbance decrease was the actual decarboxylation reaction. The metal-oxalosuccinate decarboxylation rate constants are also summarized in Table 1.



TABLE 1  
PUBLISHED RATE CONSTANTS FOR VARIOUS  
OXALOSUCCINATE SYSTEMS

Metal Ion	[(Metal)]	[(OXAS)]	pH	Temp	K(obs)	Ref
---	---	7.73E-3	6.00	20	2.11E-4	10
---	---	7.73E-3	6.00	30	6.85E-4	10
---	---	7.73E-3	6.00	25	3.82E-4	10 <sup>a</sup>
---	---	6.40E-4	5.10	25	4.49E-4	9
---	---	6.43E-3	5.60	14	5.96E-4	2
AL(III)	4.00E-3	8.16E-3	6.00	30	3.01E-3	10
AL(III)	1.25E-4	2.50E-4	7.30	25	8.90E-4	1
FE(III)	4.00E-3	8.16E-3	6.00	30	8.96E-4	10
ZN (II)	4.00E-3	8.16E-3	6.00	30	1.42E-3	10
CR (II)	4.00E-3	8.16E-3	6.00	30	6.64E-4	10
MN (II)	4.00E-3	8.16E-3	6.00	30	6.75E-4	10
MN (II)	1.67E-3	2.50E-4	7.30	25	2.50E-4	1
MN (II)	1.29E-3	6.43E-3	5.60	14	1.09E-3	2
MG (II)	4.00E-3	8.16E-3	6.00	30	5.40E-4	10
CA (II)	4.00E-3	8.16E-3	6.00	30	4.13E-4	10

<sup>a</sup> Interpolated value from the first two data points by assuming an Arrhenius plot.

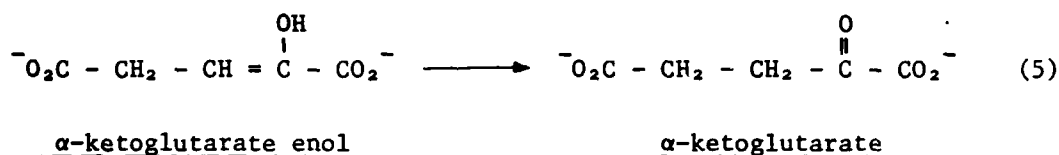
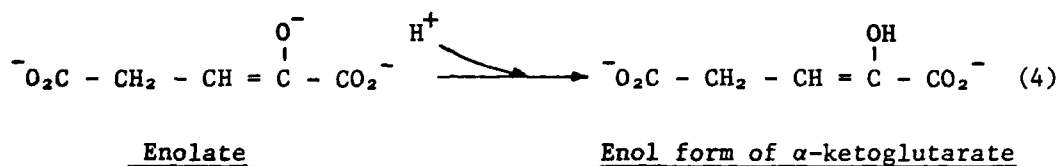
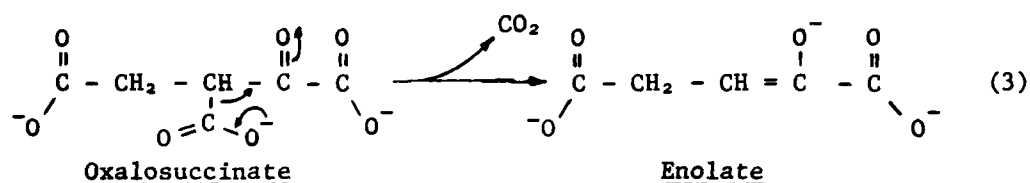
Notes:

1. Concentration is in units of molarity.
2. The temperature is in degrees Celcius
3. The units of the rate constants are 1/seconds.

$$\begin{array}{ccccccc} \text{O} & & \text{OH} & & \text{T} & & \text{O} \\ \parallel & & | & & | & & \parallel \\ -\text{O}-\text{C}- & \text{CH}- & \text{C}- & \text{CH}_2- & \text{C}- & \text{O}- \\ & & | & & & & \\ & & \text{C} & & & & \\ & & \parallel & & & & \\ & & \text{O} & & & & \text{O} \end{array}$$

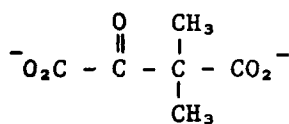
isocitrate dehydrogenase reaction. From this they concluded that the enol form of oxalosuccinate was not the active decarboxylating species, since the proton in the  $\beta$  position would be lost during the enolization. This agrees with the observations of other  $\beta$ -keto acids, such as  $\alpha,\alpha$ -dimethylacetoacetic acid (13) and dimethyloxaloacetate (14), which cannot enolize, but readily decarboxylate. In another experiment, Lienhard and Rose (15) studied the oxidative decarboxylation of isocitrate in tritiated water. They reported that the

carboxylate group that is lost was replaced by a  $T^+$  from the medium. The same observations were reported by Danziel and Londesborough (16), who studied the reductive carboxylation of  $\alpha$ -ketoglutarate. This is shown below in reactions (3) through (5).



The electron-withdrawing carbonyl shifts the electrons, causing cleavage of the  $\alpha$  carbon- $\beta$  carbon bond and releases carbon dioxide (reaction 3). The enolate formed rapidly consumes a proton from the solvent to form the enol of  $\alpha$ -ketoglutarate. In strongly basic solutions, the enol will remain deprotonated since the  $\text{pK}_a$  of the enol proton is ca 13. The final step in the reaction sequence is the rapid tautomerization of the enol to the more stable keto isomer (reaction 5).

Pederson (13) provided evidence for this mechanism by showing that  $\alpha,\alpha$ -dimethyloxaloacetate, VI, which cannot enolize, readily



VI

decarboxylates, and therefore the keto form of the acid is the reactive form. The formation of the enol intermediate was concluded from halogen trapping experiments. Pederson (18) found that the rates of iodination and bromination coincided with the manometric rate of decarboxylation of VI. Steinberger and Westheimer (14) found spectroscopic evidence of enol formation in the decarboxylation of the same dimethyl derivative of oxaloacetate. The presence of the enol was confirmed by bromine titrations. The lifetime of this enol was found to be pH, buffer, and metal ion dependent.

For oxaloacetate, the rate determining step is decarboxylation. This was verified by Leussing and Raghaven (19), who studied the copper (II) catalyzed decarboxylation of oxaloacetate using four separate experiments. The first experiment was manometric carbon dioxide evolution; the second was a pH stat experiment, which measures the proton consumption from the solvent; the third method was spectrophotometrically at 320 nm; and finally, by monitoring the change in pH of the solution (unbuffered) with methyl orange at 514 nm. The

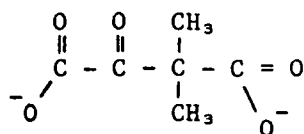
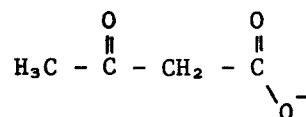
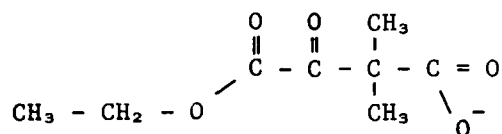
rate constants evaluated in each experiment were comparable in value. Therefore, the rate of carbon dioxide release is equivalent to the rate of proton uptake. The only way that both rate constants could be the same is if the first reaction were to be rate limiting. Thus, decarboxylation and carbon dioxide release is the slow, rate determining step.

From the data in Table 2, it can be seen that, in the absence of metal ions, the reactivity order for oxaloacetate is monoanion > dianion > neutral acid. The rate increase that results from deprotonation of the neutral acid to form the monoanion was expected, since the proton on the leaving carboxylate group must be removed prior to decarboxylation. However, removal of the second proton reduces the reactivity by a factor of 3.7. One possible reason is that the  $\alpha$ -carboxylic acid group can stabilize the enolic transition state through hydrogen bonding. A second possibility is that the  $\alpha$ -carboxylic acid group can better inductively stabilize the enolic intermediate as compared to the  $\alpha$ -carboxylate group.

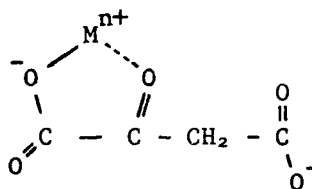
It is observed that  $\beta$ -ketodiacids, such as oxaloacetate, oxalosuccinate, and  $\alpha,\alpha$ -dimethyloxaloacetate (VII) are catalyzed by metal ions, while  $\beta$ -ketomonoacids, such as acetoacetate (VIII), are not. It has also been shown that the monoethyl ester of  $\alpha,\alpha$ -dimethyloxaloacetate, IX, which decarboxylates, is not metal ion dependent.

TABLE 2  
DECARBOXYLATION RATE CONSTANTS FOR OXALOACETATE SPECIES  
AND METAL-OXALOACETATE COMPLEXES

Species/Complex	$10^3 k \text{ (min}^{-1}\text{)}$	Reference
H <sub>2</sub> Oxac	0.345	20
H Oxac	15.4	20
Oxac	4.2	20
CaOxac	144	21
MnOxac	390	21
CoOxac	1440	21
NiOxac	1380	21
CuOxac	3960	21
ZnOxac	1860	21

VIIVIIIIX

All the diacids that are metal catalyzed have a carboxyl group  $\alpha$  to the keto carbon, such that a stable, five member ring (X) can occur.

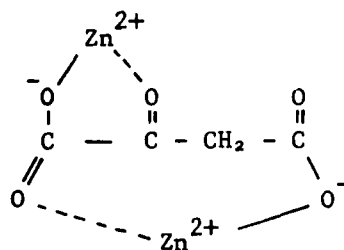
X

The metal, which is a stronger Lewis acid than the proton, significantly enhances the electron withdrawing effect of the carbonyl. This creates a stronger electron sink, which further weakens the carbon-carbon bond undergoing cleavage. This five member chelate ring has been shown to exist based on NMR data (22). On the other hand,

acetoacetic acid, which does not have an  $\alpha$  carboxyl group (IX) prevents metal chelation, thus eliminating any dependence on metal ions for catalysis.

Normally, there is a close relationship between catalytic activity of the metal ion and the formation constants of the metal complexes. Thus, the catalytic activity should follow the Irving-Williams natural stability order, which is  $\text{Cr}^{2+} < \text{Mn}^{2+} < \text{Fe}^{2+} < \text{Co}^{2+} < \text{Ni}^{2+} < \text{Cu}^{2+} > \text{Zn}^{2+}$ . For oxaloacetate, this order is validated in Table 2. Copper (II) has the largest formation constant and is about 1000 times more reactive than the oxaloacetate dianion. Table 3 shows similar data for 3-oxoglutaric acid. In this case, the same order for catalytic activity is noted; the copper complex is about 2000 times more reactive than the dianion.

Gelles and Salama (23) noted metal ion inhibition at higher concentrations of zinc, and they attributed this to the formation of a five and seven member chelate ring (XI). Kosicki and Lipovak (24) attributed the inhibition of magnesium solutions at higher pH values to the formation of a 1:1 deprotonated enolate, shown in equation 6.



XI

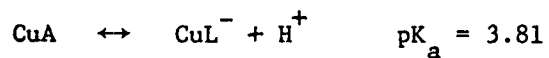


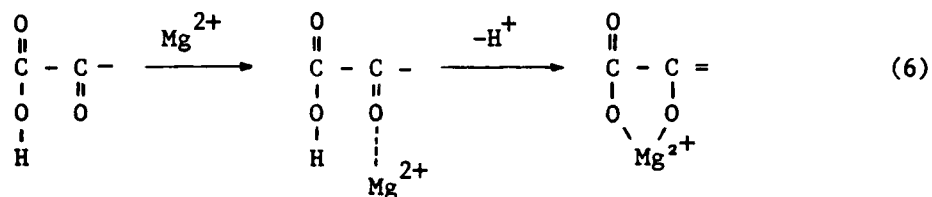
TABLE 3  
 DECARBOXYLATION RATE CONSTANTS FOR 3-OXOGLUTARATE SPECIES  
 AND METAL-3-OXOGLUTARATE COMPLEXES

Species/Complex	$10^3 k \text{ (min}^{-1}\text{)}$
$H_2A$	1.25
$HA^-$	2.90
$A^{2-}$	0.1
CoA	2.1
NiA	3.15
CuA	201
$CuL^-$	5.6
ZnA	1.5

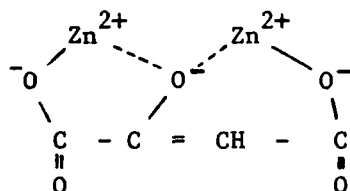
Notes:

1. All data was from reference 25.
2.  $A^{2-}$  is the dianion of 3-oxoglutarate.
3. The  $CuL^-$  complex is the deprotonated copper complex. The equilibrium reaction is:





Leussing (26) attributed the inhibition to a dinuclear, deprotonated complex,  $\text{Zn}_2\text{H}_{-1}\text{oxac}$  (XII). Based on their kinetic data, the formation constant of complex XII was found to be  $0.0692 \text{ M}^{-1}$ .



XII

During the spectrophotometric investigations of the decarboxylation of oxaloacetate and oxalosuccinate, a rapid absorbance increase, followed by a slower absorbance decrease, was observed. Gelles and Hay (27) interpreted the increase to the formation of the pyruvate enol intermediate. This agreed with Steinberger and Westheimer's view (14). Gelles and Hay recognized that metal-oxac enol complexes were formed; unfortunately, they assumed that this occurred immediately after mixing. In contrast to this, Kosicki and Lipovak (24) stated that the initial absorbance increase was due to the real time formation of the highly absorbing enolic form of the metal-oxac chelate, which does not decarboxylate. Raghaven and Leussing (19), in the

copper oxaloacetate system, calculated concentration-time profiles for the major species in the reaction. They found that both the copper-pyruvate enol and the copper-oxaloacetate enol were formed immediately, but the concentration of the copper-oxaloacetate enol was significantly higher than the concentration of the copper-pyruvate enol at all times. In the same paper, previous data for the zinc-oxaloacetate system was recalculated, and the findings were identical to the copper system.

As noted previously in this section, the biological decarboxylation of oxalosuccinate is catalyzed by the enzyme isocitrate dehydrogenase (ICDH). In many of the early research investigations, it was thought that the enzyme isocitrate dehydrogenase catalyzed the oxidation of isocitrate to oxalosuccinate, while a separate enzyme, oxalosuccinate carboxylase, catalyzed the decarboxylation step (10,29). However, Moyle and Dixon (4) isolated the enzymes in a highly pure state and proved that both reactions were catalyzed by a single enzyme. The enzyme was extracted from pig heart and was  $\text{NADP}^+$  specific.

Analysis of the enzyme by Moyle and Dixon (5) showed that it was largely protein in nature, but it contained a small portion of lipid material. It was shown that the lipid portion was actually tissue lipid which had been adsorbed onto the enzyme during the purification process. Enzymatic activity was related to the protein content and not to the lipid content.

Some of the physical properties of the enzyme were also investigated. The enzyme retained 100% activity when held for 30 minutes at 0°C in the pH range of 3.9 to 8.0. The absorption spectrum from 230 nm to 520 nm showed a single band centered at 280 nm. Based on their work, they determined that 0.90 absorbance units corresponded to a protein concentration of 1 mg/ml when measured in a 1 cm cell at 280 nm. The molecular weight of the enzyme was estimated to be 64,000. This was somewhat higher than the currently accepted value of 58,000 (30).

Kinetically, ICDH required  $\text{NADP}^+$  and  $\text{Mn}^{2+}$  for activity. The mechanism proposed for the oxidation/decarboxylation of isocitrate was that, after the oxidation step, the intermediate product, oxalosuccinate, was not released by the enzyme. Following decarboxylation, the product,  $\alpha$ -ketoglurate, was released by the enzyme, since it only forms a weak complex. The active sites in the protein for the two reactions must be close since both reactions were reversible.

In addition to this enzyme, an  $\text{NAD}^+$ -linked enzyme has been isolated. This enzyme was slightly larger (molecular weight of 105,000 daltons) and existed as a dimer. Using an enzyme isolated from commercial baker's yeast, Atkinson and coworkers (31) have shown that this protein had two catalytic sites, with isocitrate,  $\text{NAD}^+$ , and  $\text{Mg}^{2+}$  bound at each site. They also provided good experimental evidence for the existence of two adenosine 5'-monophosphate (AMP)

effector sites and two additional isocitrate effector sites. It has also been shown (31) that citrate was an effector of the reaction, presumably interchanging with isocitrate at an effector site.

The exact biological roles of the two distinct enzymes were unclear for some time, but it is now clear (32) that the  $\text{NAD}^+$ -linked enzyme, located in the mitochondria, is responsible for most of the isocitrate oxidation via the Krebs Cycle. The  $\text{NADP}^+$ -linked enzyme, located in the mitochondria and cytoplasm, appears to function as a source of NADPH that is needed to drive other reactions. The  $\text{NAD}^+$  enzyme is subject to strong allosteric control by ADP. High concentrations of ATP and NADH inhibit the reaction. The  $\text{NADP}^+$  enzyme is not subject to the control of ADP.

Since the commercially available isocitrate dehydrogenase (from the Sigma Chemical Company) was extracted from pig hearts and  $\text{NADP}^+$  specific (E.C. no. 1.1.1.42), the remainder of this chapter will deal exclusively with the kinetics and properties of that particular protein.

The equilibrium constant for the reaction:



was investigated by Londesborough and Dalziel (33). They first verified that  $\text{CO}_2$  and not  $\text{HCO}_3^-$  was the actual substrate in the reaction. By defining the pressure and concentration equilibrium constants,  $K_p$  and  $K_c$ , as

$$K_p = \frac{(NADPH)(\alpha-KG^{2-})}{(NADP^+)(isocitrate^{3-})} \frac{p}{760}$$

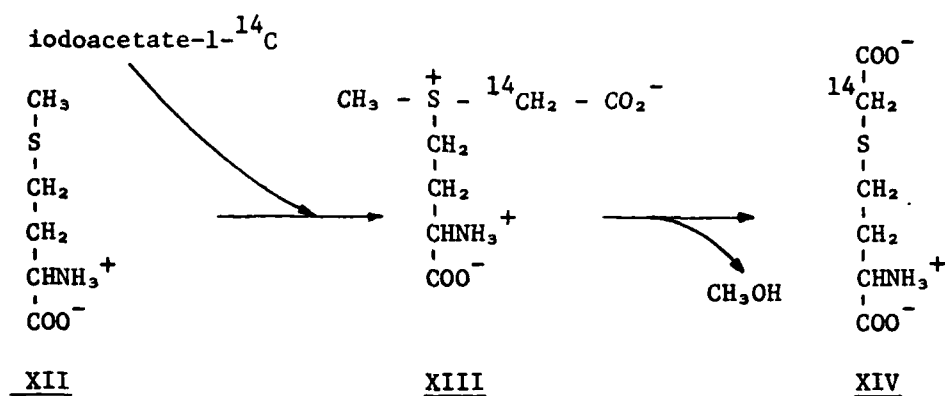
$$K_c = \frac{(NADPH)(\alpha-KG^{2-})(CO_2)}{(NADP^+)(isocitrate^{3-})}$$

where  $p$  is the partial pressure of carbon dioxide in millimeters of mercury, they found that, at a pH of 7.1 at 25°C and an ionic strength of 0.104, values of 25.8 atmospheres for  $K_p$  and 0.86 M for  $K_c$ . The reaction therefore lies far to the right, favoring the oxidation and decarboxylation of isocitrate.

Colman (34) published a paper concerning the reaction between the enzyme and iodoacetate and the resulting enzyme inactivation. Inclusion of iodoacetate did not change the structure of the enzyme, since no change in molecular weight, ultraviolet absorption spectra, or optical rotatory dispersion was observed. Treatment of isocitrate dehydrogenase with iodoacetate below a pH of 6 resulted in a significantly greater loss in dehydrogenase activity compared to decarboxylation activity. Thus, the active sites of the two reactions must be at least partially separable. Inactivation of the enzyme was prevented by the addition of isocitrate to the reaction mixture. This suggested that iodoacetate caused a modification in the functional group at the active site.

Other data presented by Colman led to the conclusion that the amino acid residue at the alkylation site was methionine. Evidence

for this was shown by comparing the amino acid analysis of the protein before and after treating the enzyme with iodoacetate. This comparison showed a decrease of one methionine (XII) residue and the appearance of a carboxymethylhomocystein (XIV) residue in the treated enzyme. This can result from the conversion of the uncharged thioether group of methionine to the dipolar carboxymethylmethionine (XIII), which decomposes to yield XIV.



In another paper (30), Colman and Ehrlich incubated the protein with ethoxyformic anhydride. In this investigation, loss of dehydrogenase activity from pH 5 to pH 6.7 follows the deprotonation of an ionizable group with a  $\text{pK}_a$  of 5.67, a value comparable to histidine. The loss of decarboxylation activity follows the deprotonation of a functional group with a  $\text{pK}_a$  of 7.05. Identification of this group, however, could not be accomplished due to evidence of other functional group interactions at higher pH values.

Colman and Villafranca (35) did NMR and binding studies to investigate the complexes of the enzyme and the manganous ion with various substrates. They reported that the enzyme binds one mole of  $\text{Mn}^{2+}$  per mole of enzyme and had a dissociation constant of 45 micromolar. Dissociation constants for the ternary complex of enzyme- $\text{Mn}^{2+}$ -isocitrate was calculated to be  $2 \pm 1$  micromolar, while the enzyme- $\text{Mn}^{2+}$ - $\alpha$ -ketoglutarate complex had a dissociation constant of  $290 \pm 80$  micromolar. They also reported that the metal-free enzyme binds  $\alpha$ -ketoglutarate with a dissociation constant of 10.3 micromolar.

Villafranca and Levy (36) used electron paramagnetic resonance (epr) spectra to obtain dissociation constants for binary metal-enzyme complexes: cobalt $^{2+}$ ,  $K_d = 300$  micromolar; magnesium $^{2+}$ ,  $K_d = 2$  micromolar; manganese $^{2+}$  (in 10 micromolar NADPH),  $K_d = 280$  micromolar. Note that the dissociation constant for the  $\text{Mn}^{2+}$ -enzyme complex in a saturated solution of NADPH was six times larger than the value for the complex in the absence of NADPH. No reasons for this were offered.

Some dehydrogenase enzymes, such as alcohol dehydrogenase from liver, contain zinc as an integral part of the enzyme. In order to investigate this possibility in isocitrate dehydrogenase, Colman (37) examined the enzyme for metal content by atomic absorption. She found that a 6.64 micromolar enzyme solution contained less than 0.10 micromolar manganese $^{2+}$ , while a 5.54 micromolar solution of isocitrate dehydrogenase also contained less than 0.10 micromolar zinc. Thus, these low concentrations of metals rules out the



consideration of isocitrate dehydrogenase as a zinc or manganese metalloenzyme. These results are verified by epr studies (36) which showed no  $\text{Mn}^{2+}$  signal for the apoenzyme.

One important point in enzyme kinetics, and one that was often very elusive, was the actual nature of the substrate. In a series of experiments using  $\text{Mn}^{2+}$  and isocitrate, Colman (37) evaluated Michaelis constants for  $\text{Mn}^{2+}$ , which were found to be dependent on the total concentration of isocitrate. Similarly, the Michaelis constants for isocitrate was found to be a function of the total metal concentration. However, the Michaelis constants calculated for the  $\text{Mn}^{2+}$ -isocitrate complex was constant for three orders of magnitude with respect to manganese.

In another experiment, the total concentration of the metal-isocitrate complex was held constant. Thus, as the concentration of isocitrate increased, the corresponding concentration of metal decreased in order to maintain a constant concentration of the complex. The exact concentrations of metal and isocitrate were determined by solving the set of equilibrium equations that govern the system. It was found that the rate of the reaction decreased by only 25% while the total metal and isocitrate concentrations varied by two orders of magnitude. These two experiments provided good evidence that the actual substrate was the metal-isocitrate complex. Colman (38) also provided evidence that the enzyme binds only one mole of metal ion and

one mole of isocitrate per mole of isocitrate dehydrogenase under all conditions.

Further information of the binding of  $\text{Mn}^{2+}$  and substrates to isocitrate dehydrogenase comes from epr studies (36). The spectrum of  $\text{Mn}(\text{H}_2\text{O})_6^{2+}$  consists of six hyperfine lines due to the interaction of the electron spin moment with that of the nucleus. The spectrum was altered upon addition of the enzyme. Although a sextet still appeared, the lines sloped downward and were no longer symmetrical. Thus, the electronic environment of the metal ion is still isotropic. When threo-D<sub>s</sub>-isocitrate was added, an extremely anisotropic powder spectrum was formed. This strongly suggested that isocitrate binded directly to or extremely near the manganous ion. However, the spectrum of the ternary  $\text{Mn}^{2+}$ -enzyme- $\alpha$ -ketoglutarate complex resembled the spectrum of the binary  $\text{Mn}^{2+}$ -enzyme complex. This showed that  $\alpha$ -ketoglutarate binds much weaker to the metal-enzyme complex than isocitrate, since the metal appeared to be more influenced by bound solvent molecules rather than by  $\alpha$ -ketoglutarate.

After adding NADPH to the ternary enzyme- $\text{Mn}^{2+}$ -isocitrate complex, the resulting spectrum contained features peculiar to both enzyme- $\text{Mn}^{2+}$ -isocitrate and enzyme- $\text{Mn}^{2+}$ -NADPH spectra. First, the sextet signal intensity increased, indicating that more free manganous ion existed in solution, an observation associated with NADPH binding. Second, an additional low field signal was split into a doublet, which may have indicated the existence of a quarternary enzyme- $\text{Mn}^{2+}$ -isocitrate-NADPH

complex. When  $\text{NADP}^+$  was added to the solution containing isocitrate dehydrogenase, isocitrate,  $\text{Mn}^{2+}$ , and NADPH, the resulting spectrum resembled the enzyme- $\text{Mn}^{2+}$ - $\alpha$ -ketoglutarate-NADPH spectrum. This was precisely the anticipated spectrum if it was assumed that  $\text{NADP}^+$  has a greater affinity for the enzyme complex than NADPH. If that assumption were true, then all the reactants were present to drive the reaction to completion. This was obviously the case since the final spectrum resembled that of the reaction products.

Ultrafiltration experiments by Ehrlich and Colman (39) using carbonyl  $^{14}\text{C}$ - $\text{NADP}^+$  showed the existence of two sites on the enzyme. The dissociation constant for the labeled  $\text{NADP}^+$  at each site was 49 micromolar, which was more than ten times greater than the corresponding Michaelis constant. If it was assumed that the reaction proceeds via a random mechanism, then  $\text{NADP}^+$  should bind to isocitrate dehydrogenase independently of the substrate, and therefore the dissociation constant for  $\text{NADP}^+$  should equal its Michaelis constant. It was therefore concluded that the isocitrate dehydrogenase reaction does not occur through a random mechanism.

Ehrlich and Colman took advantage of the fact that NADPH fluoresces (with a peak at 465 nm) when excited at its absorption maximum of 340 nm to determine that there was only one site for NADPH per peptide chain. The dissociation constant for NADPH was found to be 1.45 micromolar, which was comparable to the Michaelis constant. It was also found that  $\text{NADP}^+$  and the  $\text{Mn}^{2+}$ -isocitrate substrates

weakens the binding of NADPH. Further fluorescence studies by Ehrlich and Colman suggested that free NADPH, and not the metal complex, binds to the enzyme. Additional evidence provided in their investigation indicated that the enzyme maintained a different configuration towards the bound reduced and oxidized coenzymes. This agreed with the idea presented earlier by Rose (40), who postulated that NADPH kept isocitrate dehydrogenase in a conformation suitable for the binding of  $\alpha$ -ketoglutarate. In this conformation, the  $Mn^{2+}$ -isocitrate substrate would be unable to bind to the enzyme.

Although most studies of isocitrate dehydrogenase use either magnesium or manganese as the metal cofactor, other metals will catalyze the reaction. Colman (37) showed that cadmium was an effective metal. Kratochvil, Boyer, and Hicks (41) added zinc and cobalt to the list of metal activators, whereas copper, nickel, and cadmium inhibit the reaction. The relative rates of metal activation was a function of all the species concentrations as well as the pH, and therefore sequential ordering of the metals based on their catalytic effect was very difficult. However, it appeared that, under similar conditions, manganese<sup>2+</sup> provided the most catalytic activity among the metal activators (37,41).

Ingebretsen and Sanner (42) studied the effect of EDTA on the reaction. They found that the rate of NADPH formation increased with increasing amounts of EDTA, then decreased. The peak was reached

when the concentration of EDTA was comparable to the metal ion concentration. The inhibition at higher EDTA concentrations was due, according to the investigators, to the reduced  $\text{Mg}^{2+}$ -isocitrate concentration, since EDTA binds magnesium better than isocitrate. This seems unlikely for the following reason. Using the appropriate concentrations given in the paper corresponding to the amount of EDTA needed for peak activation, 3.6% of the magnesium was complexed with isocitrate, while 28.8% was complexed with EDTA. When the amount of EDTA was doubled, 2.7% of the magnesium was bound to isocitrate, and 46.6% was bound to EDTA. It seems unlikely that the fourfold decrease in the rate was due to the lower concentration of the  $\text{Mg}^{2+}$ -isocitrate substrate. Since free magnesium can bind to the enzyme, it would be reasonable to attribute the inhibition to a dead-end enzyme- $\text{Mg}^{2+}$ -EDTA complex and/or a dead-end enzyme-EDTA complex.

Kratochvil, et al. (41) used EDTA to determine the concentrations of various metals in solution. Their results showed that the rate initially increased upon addition of EDTA, then decreased as more EDTA was added. The initial increase in the rate as EDTA was first added appeared to be caused by adsorption of manganese on the walls of the spectrophotometric cell to give a thin film that was still able to activate the enzyme. The adsorbed material was assumed to contain manganese because this effect was not seen at lower  $\text{Mn}^{2+}$  concentrations. That is, at lower metal ion concentrations, the rate

decreased when the amount of EDTA increased. After the equivalence point, further addition of EDTA continued to lower the reaction rate. As before, this could be due to the formation of inhibitory complexes between isocitrate dehydrogenase, EDTA, and the metal.

O'Leary and Limburg (43) studied the role of metal ions on the enzyme reaction by studying the isotope effect. In their study using nickel<sup>2+</sup> and magnesium<sup>2+</sup> as metal catalysts, they concluded that, based on <sup>13</sup>C and <sup>2</sup>H effects, the difference in rates for the two metals must have resulted from the effects of the metals on substrate and product binding and dissociation, rather than the effect on catalysis. This finding was similar to the enzymatic decarboxylation of oxaloacetate with pyruvate kinase (44). In the case of the latter, the actual rate of decarboxylation for the metal/oxaloacetate/enzyme complex was independent of the metal cation. For example, the decarboxylation rate constants for the magnesium ternary complex and the manganese ternary complex differ by less than 10%, while the rate constant for the zinc ternary complex was less than five times slower. These rate differences were relatively small considering that, nonenzymatically, zinc-oxaloacetate decarboxylates eighteen times faster than the corresponding magnesium complex.

Research Objectives. A great deal of work has been published on the decarboxylation of  $\beta$ -keto acids and, in particular, the dicarboxylic

acid oxaloacetic acid. This work includes metal catalysis and inhibition, reaction mechanisms, intermediate structures, and the effect of various tautomerization equilibria. In order to determine the applicability of the above work, it was necessary to investigate a different  $\beta$ -keto acid. Thus, the center of study of this research was oxalosuccinic acid, a triacid that has the unique distinction of possessing carboxylate groups that are  $\alpha$ ,  $\beta$ , and  $\gamma$  to the keto functional group.

Therefore, the specific goals of this research work are:

1. Establish solution properties of oxalosuccinate, such as all three pK values and the stability constants of the acid with various metals;
2. Obtain pH-rate profiles of the free acid and determine the individual rate constants of the various protonated forms;
3. Investigate the influence of magnesium<sup>2+</sup>, manganese<sup>2+</sup>, and zinc<sup>2+</sup>, on the decarboxylation rate;
4. Investigate the kinetics of the decarboxylation of the free acid with the enzyme isocitrate dehydrogenase; and
5. Investigate the effect of two metals on the enzymatic decarboxylation.

## II. EXPERIMENTAL PROCEDURES

### Reagents

Water. The water used in all solutions was first distilled, then demineralized, and redistilled. This water was obtained from The Ohio State University Laboratory Stores. It was then boiled for approximately 30 minutes to remove dissolved carbon dioxide prior to useage.

Oxalosuccinic Acid. The barium salt of oxalosuccinic acid was purchased from the Sigma Chemical Company, and was stored desiccated in the freezer. The manufacturer's assay of the solid was approximately 70% barium oxalosuccinate and 30% barium  $\alpha$ -ketoglutarate. Analysis of the mixture, accomplished by monitoring the decarboxylation of the acid spectrophotometrically, showed that the actual content was 69.6% barium oxalosuccinate. This solid was not purified any further for the kinetic investigations, since  $\alpha$ -ketoglutarate, which was stable for all experiments, only provided a constant background.

Ochao's method (9) of preparation of the acid was modified for all investigations. After dissolving a known amount of the acid mixture, usually 20 mg, in 1 ml of 1.0 N HCl, a stoichiometric amount of 2.0 N H<sub>2</sub>SO<sub>4</sub> was added to precipitate the barium as BaSO<sub>4</sub>. The precipitate was filtered in a glass-frit filter presaturated with BaSO<sub>4</sub>. Sodium hydroxide was used to adjust the pH. The entire procedure was carried out in an ice bath, and all solutions used in the preparation were at 0°C. Due to the instability of



oxalosuccinate, the prepared solutions were good for three hours when kept at 0°C.

α-Ketoglutaric Acid. Reagent grade α-ketoglutarate was purchased from the Sigma Chemical Company and used without further preparation. It was stored desiccated in the freezer when not in use. The solid was assayed at 97.0% pure by a potentiometric titration against a standard solution of sodium hydroxide.

Zinc(II) Chloride. The 20 mesh granulars ('Baker Analyzed' 99.9% reagent grade), purchased from the J. T. Baker Chemical Company, was washed for two hours with dilute hydrochloric acid, rinsed several times with distilled water, then dried overnight at 110°C. The solid was then weighed in a volumetric flask and dissolved for several hours in a slight excess of concentrated hydrochloric acid. After filtering, the precise concentration of the solution was determined via an EDTA titration as described by Scharzenbach and Flaska (45).

Manganese(II) Chloride. Mallinckrodt reagent grade  $\text{MnCl}_2 \cdot 4\text{H}_2\text{O}$  was weighed and dissolved in water. The concentration was determined by an EDTA titration (45).

Magnesium(II) Chloride. Mallinckrodt reagent grade  $\text{MgCl}_2 \cdot 6\text{H}_2\text{O}$ , minimum purity of 99.2%, was prepared and analyzed as described above for manganese(II) chloride.

Sodium Chloride. This salt, obtained from the Fisher Scientific Company, was weighed and dissolved in water. It was then filtered to

remove foreign particles. The molarity was calculated based on the weight and volume used.

Ethylenediaminetetraacetic Acid, EDTA. The salt ( $\text{Na}_2\text{EDTA}\cdot 2\text{H}_2\text{O}$ ), purchased from the Fischer Scientific Company, was dried in the oven at  $80^\circ\text{C}$  for four hours. After cooling in a desiccator, it was dissolved in water. Zinc(II) solutions were used to standardize the EDTA.

Ammonia-Ammonium Chloride Buffer. A 100 milliliter solution of this pH - 10 buffer was required for all EDTA titrations performed in this research. It was prepared by dissolving 6.80 grams of  $\text{NH}_4\text{Cl}$  (Allied Chemical Company) with 57 milliliters of concentrated ammonia (Mallinckrodt), then diluted to volume.

Acetate Buffer. Crystalline sodium acetate,  $\text{NaOAc}\cdot 3\text{H}_2\text{O}$  (Mallinckrodt Analytical Reagent) was dissolved into a precalculated volume of glacial acetic acid (Baker Analyzed 99.8%) and diluted to volume. This resulted in a series of pH buffer solutions in the range of 3.7 to 5.7.

Hydrochloric Acid, HCl. "Baker Analyzed" reagent grade hydrochloric acid, purchased as a 37% solution, was diluted to the working concentration and standardized against NaOH to a phenolphthalein endpoint.

Sulfuric Acid,  $\text{H}_2\text{SO}_4$ . Obtained through the Ohio State University Laboratory Stores at the desired concentration, it was standardized against NaOH to a phenolphthalein endpoint.

Sodium Hydroxide, NaOH. This was obtained through the Ohio State University Laboratory Stores at the desired concentration. The molarity was determined by titrating against a standard HCl solution using a phenolphthalein endpoint.

Deuterium Chloride, DCl. A 20% solution of 100 atom % deuterium chloride in D<sub>2</sub>O was purchased from the Sigma Chemical Company. It was stored in a vial capped with a septum in a desiccator. The atmosphere in the vial was dry nitrogen. The solution was used for the NMR work without any additional preparation.

Iodine (I<sub>3</sub><sup>-</sup>). A stock solution was prepared by first adding a weighed amount of potassium iodide, KI ("Baker Analyzed" 100.1%), and diluting to approximately 90% of the final volume. Resublimed iodine crystals (Mallinckrodt Analytical Reagent) were weighed and added to the KI solution. The solution was diluted to the final volume and mixed until completely dissolved. This resulted in a solution that was approximately  $2 \times 10^{-3} \text{ M I}_3^-$  in 1.0 M KI. After filtering to remove any foreign particles, the solution was stored in the dark under a nitrogen atmosphere to retard the oxidation of I<sub>3</sub><sup>-</sup>. Solutions used in this research, which were stored in this manner, only lost about 30% activity after a three month period. The concentration was determined spectrophotometrically, since the extinction coefficient of I<sub>3</sub><sup>-</sup> has been accurately determined to be 24,500 at a wavelength of 352 nm (46).

2,4-Dinitrophenylhydrazine. Obtained from the Eastman Kodak Chemicals Division, it was used as purchased. The solution was prepared by stirring the calculated amount into 100 ml of a 2 N HCl at 40°C. The solution was stored at room temperature and was stable for about two weeks.

Monochloroacetic Acid. The acid, certified by Fisher Scientific Company as 99% pure, was used as a buffer ( $pK_a = 2.86$ ) without further purification. The solutions were prepared by mixing a known amount of acid into water, then adjusting the pH with HCl or NaOH. The pH range used was 1.9 to 3.7.

$\beta$ -Nicotinamide Adenine Dinucleotide, Reduced Form, NADH. The disodium salt,  $C_{21}H_{27}O_{14}N_7P_2Na_2$ , was obtained from the Sigma Chemical Company, who prepared the salt enzymatically from yeast using alcohol dehydrogenase. It was assayed by Sigma as 98% pure based on a lactate dehydrogenase determination. A spectrophotometric assay at 340 nm (extinction coefficient of  $6.20 \times 10^3$ ) (47) verified the analysis from Sigma. The salt was stable when stored in a desiccator at room temperature.

Glutamate Dehydrogenase, E.C. No. 1.4.1.3. This enzyme, prepared from extracts of bovine livers, was purchased from the Sigma Chemical Company. The enzyme was a crystalline suspension in 2.0 M  $NH_4SO_4$  with a 0.50 M sodium phosphate buffer, pH = 7.5. It was stored in the refrigerator. The concentration of the enzyme was 10 mg/ml. Each

milligram of enzyme had 48 units of activity. By definition, one unit will reduce one micromole of  $\alpha$ -ketoglutarate to L-glutamate per minute at a pH of 7.3 and 25°C in the presence of  $\text{NH}_4^+$ .

Isocitric Dehydrogenase, E.C. No. 1.1.1.42. This enzyme, purchased from the Sigma Chemical Company, was extracted from porcine hearts. The enzyme was in a 50% glycerol solution. The concentration was 10 mg/ml, and there were approximately 1.4 units per milligram of enzyme. For this protein, one unit will convert 1.0 micromoles of isocitrate to  $\alpha$ -ketoglutarate per minute at pH 7.8 at 25°C.

2(N-Morpholino)ethanesulphonic Acid, MES. This zwitterionic biological buffer from the Sigma Chemical Company,  $\text{pK}_a = 6.1$  at 25°C, was used without further purification. Solutions were prepared analogous to monochloroacetic acid. The useful pH range was 5.5 to 6.7.

4-(2-hydroxyethyl)-1-piperazineethanesulfonic Acid, HEPES. This zwitterionic biological buffer, also purchased from the Sigma Chemical Company,  $\text{pK}_a = 7.5$  at 25°C, was used without further purification. Solutions were prepared analogous to monochloroacetic acid. The useful pH range was 6.8 to 8.2.

Isocitric Acid Substrate. Isocitrate acid substrate, purchased from the Sigma Chemical Company, was used exclusively for the assay of the enzyme isocitrate dehydrogenase. The solution, which was used

as purchased, contained 10 micromoles of DL-isocitrate and 160 micromoles of triethanolamine buffer per milliliter. The solution had a pH of 7.8 at 25°C, and was stored in the refrigerator.

β-Nicotinamide Adenine Dinucleotide Phosphate, NADP<sup>+</sup>. The sodium salt, 98-100% pure, was purchased from the Sigma Chemical Co., and was used for the ultraviolet determination of the enzyme isocitrate dehydrogenase. The salt was in preweighed vials, with 1.0 mg of NaNADP per vial. For the assay, 1.0 mg of NADP<sup>+</sup> was dissolved in 1.0 ml water (concentration of  $1.248 \times 10^{-3}$  M) and was used without further purification. The solid was stored in the freezer. The solutions were prepared just prior to use.

Standard Buffers. Three buffers, prepared according to the National Bureau of Standards (NBS) procedures, were used routinely to standardize the pH meter. They were:

1. Potassium hydrogen phthalate, 0.050 molal, pH = 4.004 at 25°C;
2. Potassium dihydrogen phosphate/disodium hydrogen phosphate, 0.0250 molal, pH = 6.863 at 25°C; and
3. Sodium tetraborate decahydrate (Borax), 0.010 molal, pH = 9.183 at 25°C.

#### Assay of Isocitrate Dehydrogenase

The concentration of the enzyme isocitrate dehydrogenase (ICDH) was determined spectrophotometrically. Since an absorbance of 0.91 absorbance units at 280 nm represents a concentration of 1.0 mg/ml of

protein (36), then the concentration of a sample of  $V_{en}$  milliliters of the protein sample mixed into  $V_s$  milliliters of water is

$$C_{en} = \frac{(Abs)(V_s + V_{en})}{0.91V_{en}} \quad \text{mg/ml}$$

where Abs is the absorbance at 280 nm of  $(V_s + V_{en})$  milliliters of solution.

The activity of the enzyme was determined in the following manner. One milligram of the NaNADP salt, contained in the preweighed vial, was dissolved in 1.0 milliliters of water. This solution was transferred to a 1.0 cm square quartz cell. Next, a 1.0 milliliter aliquot of 0.030 M  $MnCl_2$  and 1.0 milliliters of the isocitrate substrate was also added to the cell. Addition of a buffer solution was unnecessary since the isocitrate substrate solution contained 0.160 M triethanolamine buffer at a pH of 7.8. All solutions were initially at 25°C. The cell was then placed in the jacketed vessel of the Gilford Model 250 Spectrophotometer and maintained at 25°C. The instrument was set at a wavelength of 340 nm and adjusted to read 0.6 absorbance units as full scale. Once this was done, 10 microliters of the enzyme solution was syringed into the cell. After waiting three minutes for the system to equilibrate, the absorbance was measured for two minutes.

For the purpose of this report, one unit of enzyme activity converts one micromole of isocitrate to  $\alpha$ -ketoglutarate per minute at 25°C at a pH of 7.8. Thus, in terms of the measured absorbance change, the number of units of enzyme activity per milligram of enzyme is

$$\text{Units/mg enzyme} = \frac{A}{C_{\text{en}} (2.07)}$$

where

A = absorbance change per minute

C<sub>en</sub> = concentration of the enzyme in the cell

2.07 = absorbance change of one micromole of NADPH in a 3 ml solution, based on an extinction coefficient of  $6.22 \times 10^3 \text{ M}^{-1} \text{ cm}^{-1}$ .

To convert the number of units at 25°C to the number of units at 37°C, multiply the above equation by 2.7 (48).

#### Equilibrium Experiments

Potentiometric Titrations. A Radiometer Model 26 pH Meter equipped with a Corning Glass 476024/Corning Calomel K4312 electrode pair was used for all pH work. The pH meter was standardized daily using two NBS buffers covering the region under investigation. All measurements were made at  $25 \pm 0.2^\circ\text{C}$ . A Teflon-coated magnetic stirrer was used to insure solution homogeneity. The titrant, either HCl or NaOH, was added using a Radiometer ABU12 Autoburette. After each increment was added, the pH was manually recorded.



Spectrophotometric Data. A Cary 14 Spectrophotometer equipped with a thermostatted cell compartment was used for all equilibrium spectrophotometric experiments in this study. The scan rate was usually set at 1.0 nm/second, however, some of the faster reactions being monitored were run at a scan rate of 2.5 nm/second.

Some of the reactions were so fast that the spectra versus time data could not be obtained accurately on the Cary 14. For these experiments, a rapid scanning spectrophotometer built by Dr. McCreery, consisting of a GCA/McPherson UV-Visible source, a J-Y monochrometer, and a Hayden stepping motor to control the grating drive was used. The experiment was controlled by a Hewlett-Packard HP21MX minicomputer. Using this system, scan rates of 100 nm/second were routinely used. A thermostatted cell compartment was not used since the reactions studied in this manner were completed in ten minutes or less. The data was recorded on a Hewlett-Packard HP7225A Data Plotter.

For the spectrophotometric data, the solutions required were brought to the desired pH by using HCl or NaOH as required, then pipetting into a 1.0 cm quartz cell (Precision Cells Inc.). For the UV work, the Cary 14, a double beam instrument, was calibrated at a reference point under the conditions of two blank matched cells, one each in the reference and sample compartment, at a wavelength of 300 nm. The rapid scanning spectrophotometer, a single beam instrument, was zeroed by placing a blank cell in the sample compartment. The experimental method for the spectra/time

investigations were identical to the method used in all kinetic work and will therefore be described in detail in that section.

In order to determine the amount of enol present, the technique (49,50) of iodine uptake was employed. In this method, a solution of  $I_3^-$  was diluted into approximately 2.7 ml of water in a 1.0 cm quartz cell (the concentration of  $I_3^-$  in the cell was approximately equal to the concentration of oxalosuccinate), then placed in the Cary 14 for an initial absorbance reading at 352 nm. With the recorder on, a 0.3 ml sample was injected directly into the cell through a light-tight injection port. The amount of enol present was calculated from the following equation

$$\text{Fraction Enol} = \frac{0.9(\text{Abs}_0) - \text{Abs}_1}{24,500C_{\text{oxas}}}$$

where:

$\text{Abs}_0$  = initial absorbance of  $I_3^-$  prior to sample injection

$\text{Abs}_1$  = absorbance immediately following the sample injection

0.9 = correction factor due to dilution of  $I_3^-$

24,500 = extinction coefficient of  $I_3^-$

$C_{\text{oxas}}$  = concentration of oxalosuccinate in the sample

Data Analysis. Due to the complexities of these systems, a NOVA 3 minicomputer was used to analyze the data. Peripheral equipment for the 32k memory computer included a fixed head disk, twin floppy disk drives, an eight channel analogue-to-digital converter, teletype,

Hazeltine video terminal, Centronics Model 305 line printer, fast paper tape punch, and a fast paper tape reader.

All pH titration data were analyzed by using the FORTRAN program PHFIT. This program can determine  $pK_a$  or  $pK_b$  values for acids and bases as well as evaluating formation constants of metal-ligand complexes based on pH data alone. PHFIT uses the least-squares curve-fitting routine to calculate the best value of the formation constants by minimizing the function  $X^2$ , defined as:

$$X^2 = \sum_i ([H^+]_{obs,i} - [H^+]_{calc,i})^2$$

where

$$\begin{aligned} [H^+]_{obs} &= 10^{(-pH_{obs})} \\ [H^+]_{calc} &= (\gamma_{H^+})(H^+)_{calc} \\ \gamma_{H^+} &= \text{activity coefficient of } H^+ \end{aligned}$$

$[H^+]_{calc}$  is the calculated equilibrium concentration of  $H^+$  and is evaluated by solving mass balances on all the species. A subroutine in PHFIT, GENDIS, calculates the concentration of all species and complexes present at a given pH based on total concentrations of starting materials and the formation (association) constants of all complexes. With this subroutine, some or all of the formation constants can be optimized iteratively to provide the minimum  $X^2$ . Since the ionic strength of all experiments were maintained at 0.1M,  $\gamma_{H^+}$  was set at 0.83 (51).

The absorbance data was analyzed by CORNEK, which differs from PHFIT only by the optimization function  $X^2$ , defined here as:

$$X^2 = \sum_i (A_{\text{obs},i} - A_{\text{calc},i})^2$$

Here,  $A_{\text{obs}}$  and  $A_{\text{calc}}$  are the observed and calculated absorbances respectively. The calculated absorbances are a function of each species or complex and their extinction coefficients by Beer's Law:

$$A_{\text{AB}} = \epsilon_{\text{AB}} (AB) \quad (1)$$

$$A_{\text{AB}} = \epsilon_{\text{AB}} \beta_{\text{AB}} (A)(B) \quad (2)$$

In the above equations,  $\epsilon_{\text{AB}}$  is the extinction coefficient of the complex AB, while  $\beta_{\text{AB}}$  is the formation constant of the complex.

#### Kinetic Experiments

pH Stat. The proposed decarboxylation sequence of oxalosuccinate actually consists of three consecutive reactions. In the first reaction, the actual loss of carbon dioxide results in an enolate intermediate. The enolate rapidly consumes a proton from the solvent to form the enol, which rapidly tautomerizes to yield  $\alpha$ -ketoglutarate, the final product. If this is the correct mechanism, a proton is consumed equal to the decarboxylation rate, since the enol is formed very rapidly. If  $\text{H}^+$  can be added and monitored externally as the reaction progresses, then the reaction can be followed. This is a pH stat experiment.

The instrumentation included, in addition to a pH meter and autoburette previously described, a Radiometer type TTT1 titrator. The pH of the experiment is set by the titrator. As the pH increases due to the loss of the proton from the solvent, a solenoid-actuated valve allows a small amount of HCl to enter the reactor vessel. Once the pH has been reestablished at the preset value, the valve is closed, and the HCl cannot flow. Therefore, the HCl is only added when the pH changes. Data is recorded directly into the NOVA 3 computer in the following manner. The burette was mechanically connected to a variable resistor. This resistor was in the feedback loop of an operational amplifier, thus creating a voltage follower circuit. As HCl was added to the solution, the motion of the burette altered the resistance in the feedback loop. This signal was sent through the analog-to-digital converter into the computer, where it was stored for further processing.

There were several advantages to the pH stat experiment. First, only one reaction was observed. Complicated side reactions, such as tautomerization, did not interfere. Second, it provided another technique with which one may cross-check kinetic data. Lastly, due to the nature of the experiment, the pH was held constant without the use of buffers. Thus, any possible buffer catalysis was eliminated.

Spectrophotometric Investigations. The decarboxylation/tautomerization kinetics were studied via absorbance changes on the Cary 14 or the Gilford 250 spectrophotometer. This was the preferred method due to convenience and ease of use. The Gilford 250 was the

primary instrument. It was equipped with a Gilford model 2451-A Automatic Cuvette Positioner. Data was recorded on a Heath Company Model SR-205 Single Pen Chart Recorder, which was capable of recording multiple sets of data. Thus, as many as three experiments could be monitored simultaneously, provided all were detected at the same wavelength. In most experiments, a rapid increase in absorbance was seen, followed by a slower decrease in absorbance. This slower decrease was monitored for about five half-lives to insure maximum confidence in the data analysis. In most cases, a final value for the absorbance,  $A_{\infty}$ , could not be observed due to the very slow absorbance increase that followed. These absorbance changes will be discussed in greater detail in later chapters.

A modification of the pH stat experiment can be done on the Gilford 250. As was mentioned before, the decarboxylation process consumes a proton from the solvent, resulting in a pH increase (less acidic) as the reaction progresses. If an experiment is set up at a given pH that falls within the transitional pH range of a colored indicator, then the change in pH from the reaction causes the indicator to change color, and that can be monitored spectrophotometrically. For this research, four suitable indicators were found and these indicators are summarized in Table 4.

Although this is another way to record the reaction rate based on proton consumption, it was not as accurate as the pH stat. This is because this method depends on a change in the pH; since the reaction

TABLE 4  
LINEAR RANGE OF pH INDICATORS

Indicator	Wavelength (nm)	Linear Range of pH
Bromophenyl Blue	591	3.3 - 3.8
Bromocresol Green	618	4.0 - 5.6
Bromocresol Purple	590	4.8 - 6.4
Phenyl Red	560	6.6 - 8.2

was pH dependent, the observed kinetic rate constant will be an average. However, it can be used as a good approximation.

Sample Preparation. The procedure for these experiments was as follows. Using a 1.0 centimeter quartz cell, one and one half milliliters of the supporting solution, composed of the buffer, trace EDTA to retard metal catalysis, and sodium chloride electrolyte to control the final ionic strength at 0.1, was syringed into the reaction vessel. This solution was maintained at approximately 55°C in a water bath. Next, one and one half milliliters of the oxalosuccinate solution, adjusted to the appropriate pH value, was added. The oxalosuccinate solution had been stored at 0°C in an ice bath for stability. Using this method, the temperature was quickly brought up to 25°C  $\pm$  0.5, and the starting time for the reaction was well defined. For the metal catalyzed studies, a slight modification was used. One milliliter of buffer at 55°C was added to the cell. Following this, one milliliter of metal solution, containing the supporting electrolyte for ionic strength control, was added. Finally, one milliliter of the oxalosuccinate solution adjusted to the experimental pH and maintained at 0°C, was added. As before, this last step initiated the reaction.

For the pH stat experiments, an equivalent concentration of sodium chloride was substituted for the buffer, since the buffer was not needed. This substitution was also done for the spectrophotometric kinetics using the pH indicators.



Data Analysis. All kinetic data was analyzed by the program RLXFT. These calculations were done in the NOVA 3 computer. The change in absorbance for a first order reaction is an exponential decay and fits the equation

$$A(t) = A_{\infty} + A_1 \exp(-k_1 t) \quad (3)$$

where

$A(t)$  = observed absorbance at time  $t$

$t$  = time (seconds)

$k_1$  = rate constant (seconds<sup>-1</sup>)

$A_{\infty}$  = final value of absorbance at  $t = \text{infinity}$

$A_1$  = total absorbance change observed.

If more than one relaxation was observed, equation (3) can be expanded to

$$A(t) = A_{\infty} + A_1 \exp(-k_1 t) + A_2 \exp(-k_2 t) + \dots \quad (4)$$

Although  $A(t)$  was defined here as the absorbance, it can refer to any variable used to monitor the reaction. For example, in the pH stat, the voltage from the amplifier was plotted versus time and fit to equation (3).

In RLXFT, the variable minimized in the least squares analysis was  $\chi^2$ , defined as

$$\chi^2 = \sum_1 (A(t)_{\text{obs}} - A(t)_{\text{calc}})^2 \quad (5)$$

where  $A(t)_{\text{calc}}$  was defined by equation (3) or equation (4). In order to minimize  $\chi^2$ , any or all of the variables,  $A_\infty$ ,  $A_1$ ,  $k_1$ ,  $A_2$ ,  $k_2$ , etc., can be optimized.

Theoretically it should be possible to evaluate the data in a two relaxation process, however, in reality, severe errors can occur. In practice, data involving two relaxations, for example, rapid tautomerization followed by slow decarboxylation, can be analyzed with confidence if the two rate constants vary by at least a factor of 5.

The rate constant is often expressed in the literature as the relaxation time,  $\tau_i$ , defined as:

$$\tau_i \equiv 1/k_i$$

The reaction half life is defined as:

$$t_{1/2} = \tau \ln 2$$

The decarboxylation rate is pH and total species dependent. One reason is that the distribution of a tricarboxylic acid is pH dependent, and each of the protonated forms has a distinct rate constant. To evaluate this profile, the program CORNEK (52) was used. This program can evaluate rate constants for individual species and complexes. It can also be used to evaluate formation constants, since the formation of a complex species is a function of the pH and the formation constant.

The program CORNEK used a least-squares analysis of the data. It can vary formation constants or rate constants as specified by the user. A subroutine in CORNEK was GENDIS, which calculates the equilibrium distribution of species and complexes based on initial concentrations and formation constants. The heart of CORNEK is the subroutine FITFC. In FITFC, the actual equation that corresponds to a particular reaction mechanism was placed. This subroutine is specified by the user and changes for each system. The equations that were required for this subroutine will be developed in the chapter pertaining to that system. A list of all the subroutines used for this research can be found in Appendix E.

### III. PHYSICAL DATA ON OXALOSUCCINATE

Very little work has been done on oxalosuccinate since it was first synthesized by Ochoa in 1948. Therefore, spectral data on this compound are lacking. It is necessary, then, to gather spectral data to characterize the acid as well as to aid in the interpretation of research data. This section will be divided into three sections of spectroscopic data: ultraviolet, infrared, and nuclear magnetic resonance. Each section will present the spectra obtained, the instrument that was used, and an interpretation of the data.

Before beginning this chapter, it is imperative to point out one basic problem encountered with the spectra. It was mentioned in Chapter II, Experimental Procedures, under Section A, Reagents, that the oxalosuccinic acid purchased commercially, was the barium salt, which was only 70% pure. The bulk of the remaining 30% was the barium salt of  $\alpha$ -ketoglutaric acid. Separation via chromatography was impractical owing to the instability of oxalosuccinate. Recrystallization of the free acid, as reported by Lynnen and Scherer (10), cannot be possible since the free acid was very unstable. These experiments must therefore be done with the oxalosuccinate/ $\alpha$ -ketoglutarate mixture. This restriction did not affect the kinetic data, since  $\alpha$ -ketoglutarate was unreactive under the experimental conditions in this study and therefore, only contributed to the

background. Unfortunately, this mixture did cause problems in obtaining the spectral data. Therefore, each section also includes a discussion on the spectra of  $\alpha$ -ketoglutarate; data which must be considered along with the actual results of oxalosuccinate.

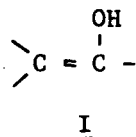
The ultraviolet data will be presented in two sections. In Part A, the spectra for the two compounds will be analyzed on a strictly qualitative level. This can be done because the general shape of the spectra are unchanged for pH values less than nine, only the actual absorbance values change. Therefore, for this portion of the chapter, it is not necessary to know the  $pK_a$  values for the acid or the species distribution. This data, including the extinction coefficients of each species, will be discussed in detail in Part D, which will present in depth the quantitative nature of the ultraviolet spectra.

#### A. Ultraviolet

The ultraviolet (UV) spectra of  $\alpha$ -ketoglutarate and oxalosuccinate are pH dependent due to the different absorptivities of the protonated forms of the acids. However, the relative shapes of the spectra are relatively unchanged for pH values less than nine. Thus, only one spectrum for each compound at low pH will be presented and discussed. A Cary 14 was used to obtain these spectra. It should also be pointed out that all spectra were obtained at 0°C.

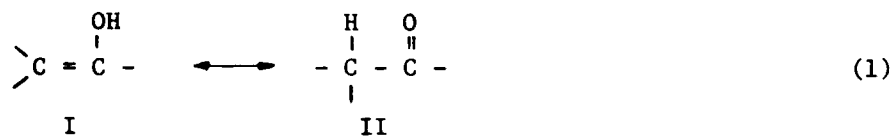
A typical UV spectrum for  $\alpha$ -ketoglutarate, at a pH of 4.98 is shown in Figure 1. Aside from the end absorption at low wavelengths, the only feature on this spectrum is the small peak at 315 nm (extinction coefficient of  $31 \text{ M}^{-1} \text{ cm}^{-1}$ ). This arises from the forbidden  $n \rightarrow \pi^*$  transition of the carbonyl. There is no shoulder in the spectrum near 270 nm, indicating the complete lack of any enol, which has a typical extinction coefficient of  $11,000 \text{ M}^{-1} \text{ cm}^{-1}$ .

A typical UV spectrum of oxalosuccinate at a pH of 3.68 is shown in Figure 2. In addition to the carbonyl peak at 315 nm and the end absorption at low wavelengths, a slight shoulder can be seen at 270 nm. This was due to the strongly absorbing enol chromophore, I. The presence of a slight amount of enol was confirmed by



halogenation experiments. These will be discussed in detail in the Equilibrium Data section of this chapter.

At pH values less than nine, the enol (I) is in equilibrium with the keto tautomer, II, as shown in the reaction below. However,



at more basic pH values, the enol proton can be removed, forming an enolate compound, III. Thus, the equilibrium shown in reaction (2) also exists.

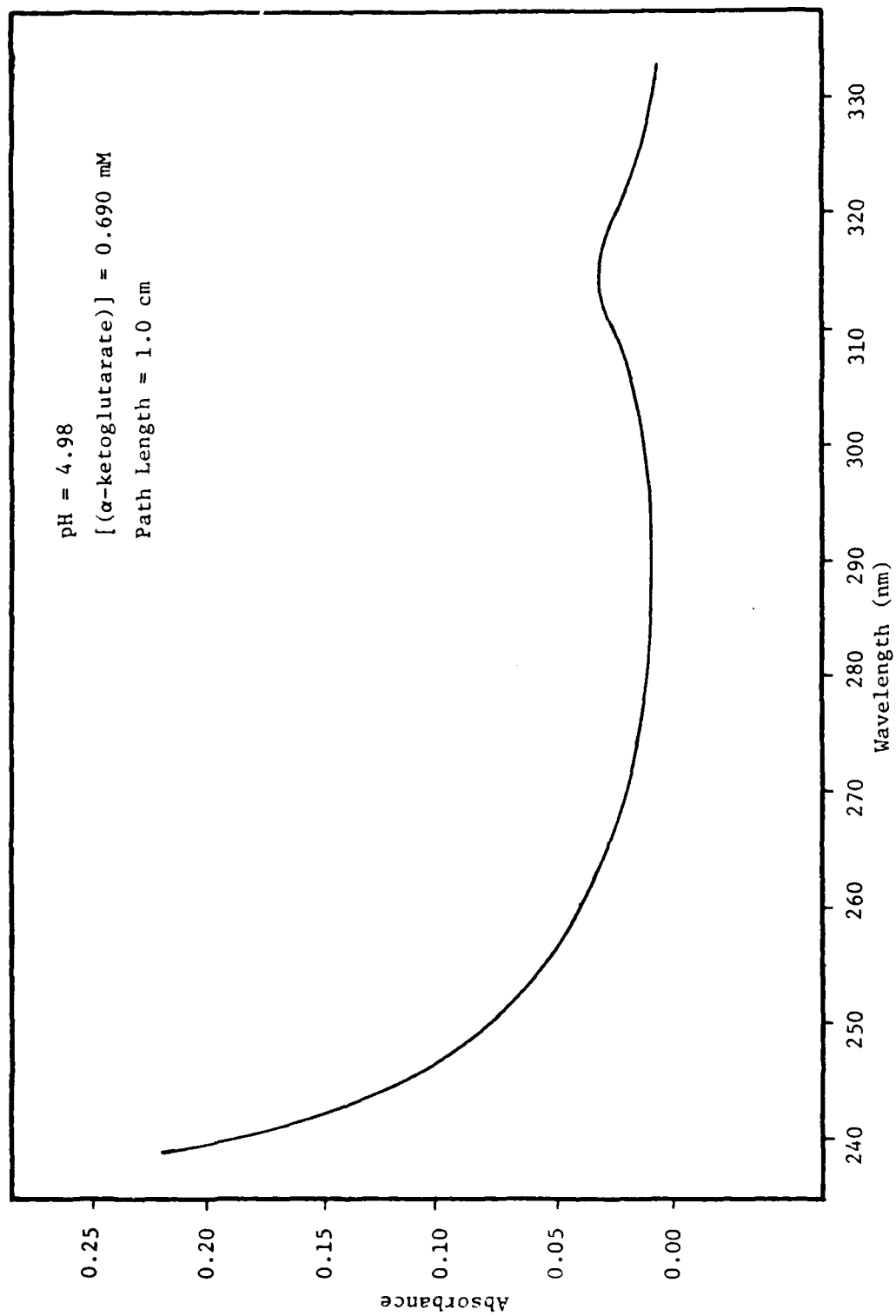


Figure 1. Ultraviolet spectrum of  $\alpha$ -Ketoglutarate.

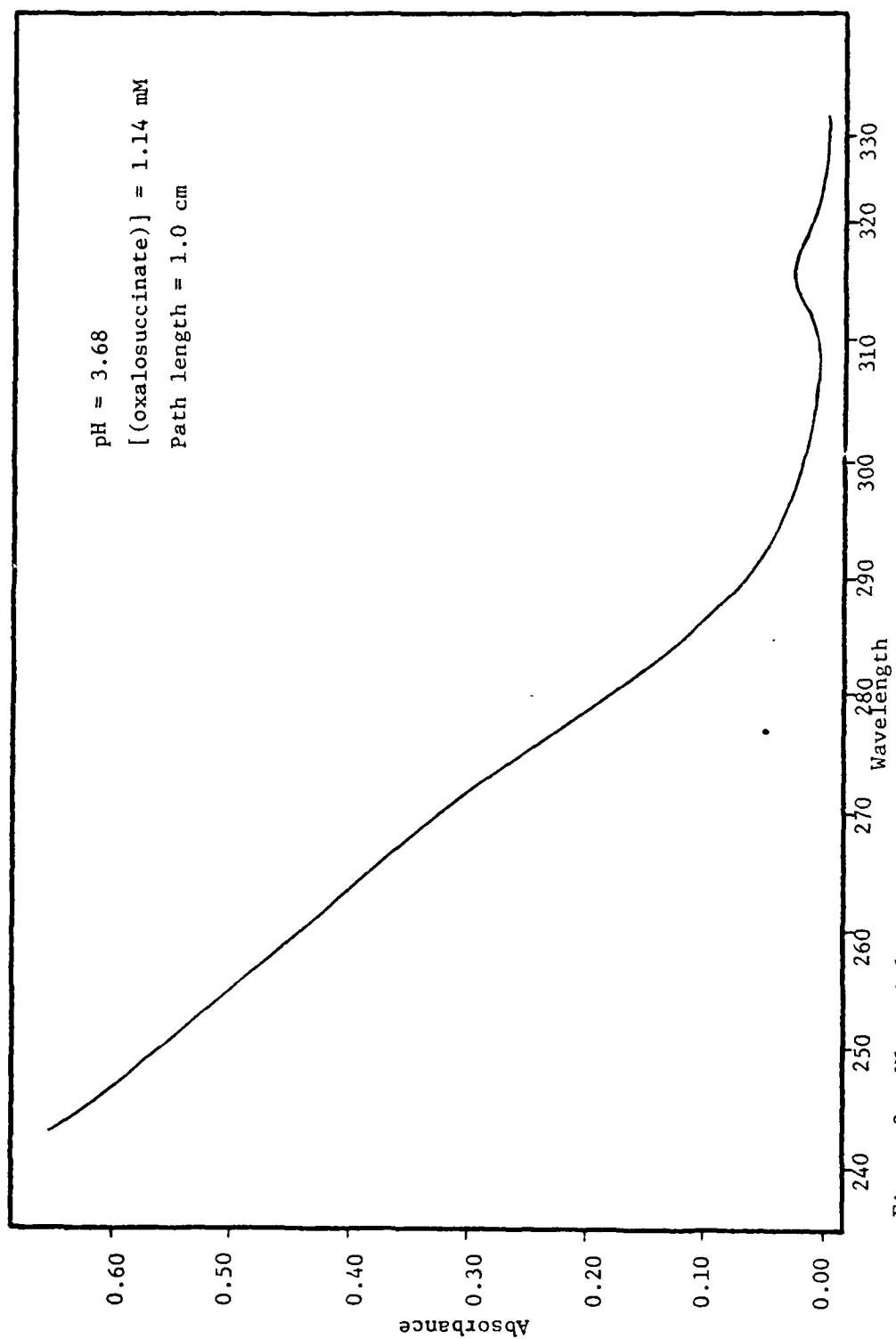
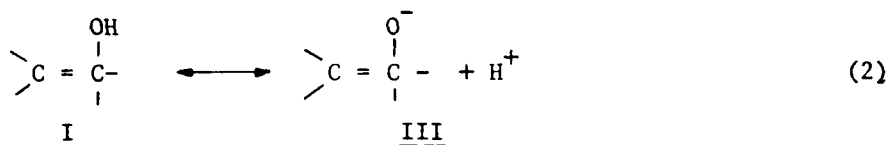


Figure 2. Ultraviolet Spectrum of Oxalosuccinate, Low pH.





As the pH increases from acidic to basic, some enol is deprotonated as shown in equation (2). However, in order to maintain the equilibrium shown in reaction (1), some keto must tautomerize to yield more enol. This implies that the UV spectrum of oxalosuccinate at elevated pH values should show a peak representing the high amount of enol-to-enolate in solution. Examination of Figure 3, the UV spectrum of oxalosuccinate at a pH of 13.11, verifies the above analysis. The strong enolate peak appears at 272 nm, with an extinction coefficient of  $15,250 \text{ M}^{-1} \text{ cm}^{-1}$ .

In summary, this section presented the UV spectrum of oxalosuccinate at both high and low pH values, plus the acid spectrum of  $\alpha$ -ketoglutarate. This analysis was strictly on a qualitative level. Numerical analysis of the UV data, including the pH dependence of the extinction coefficients of all species and complexes as well as formation constants, appear later in this chapter under Equilibrium Data.

#### B. Infrared

All infrared (IR) spectra presented in this section were obtained on a Perkin-Elmer Model 283b Infrared Spectrometer. Since both  $\alpha$ -ketoglutarate and oxalosuccinate are solids at room temperature, the

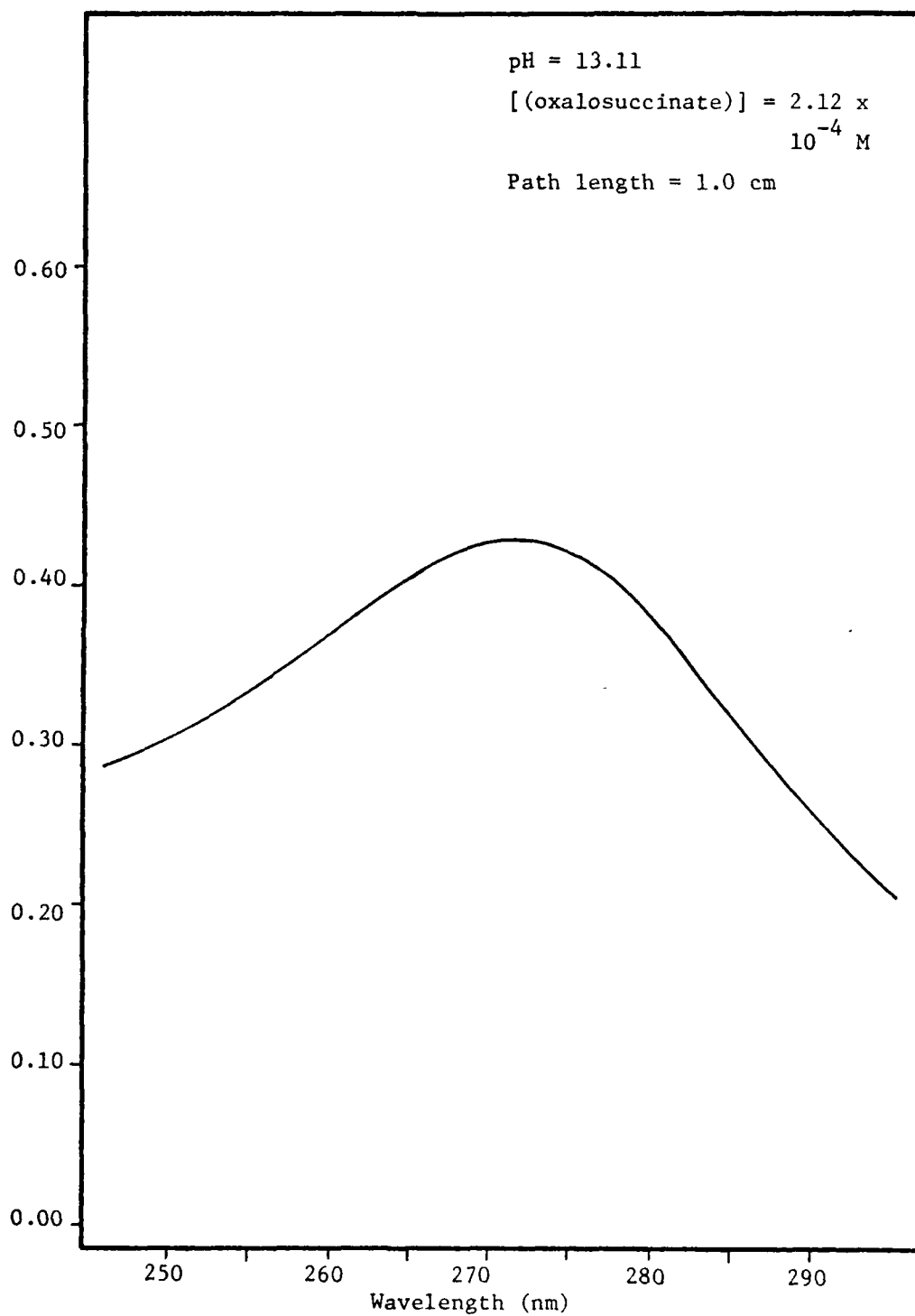


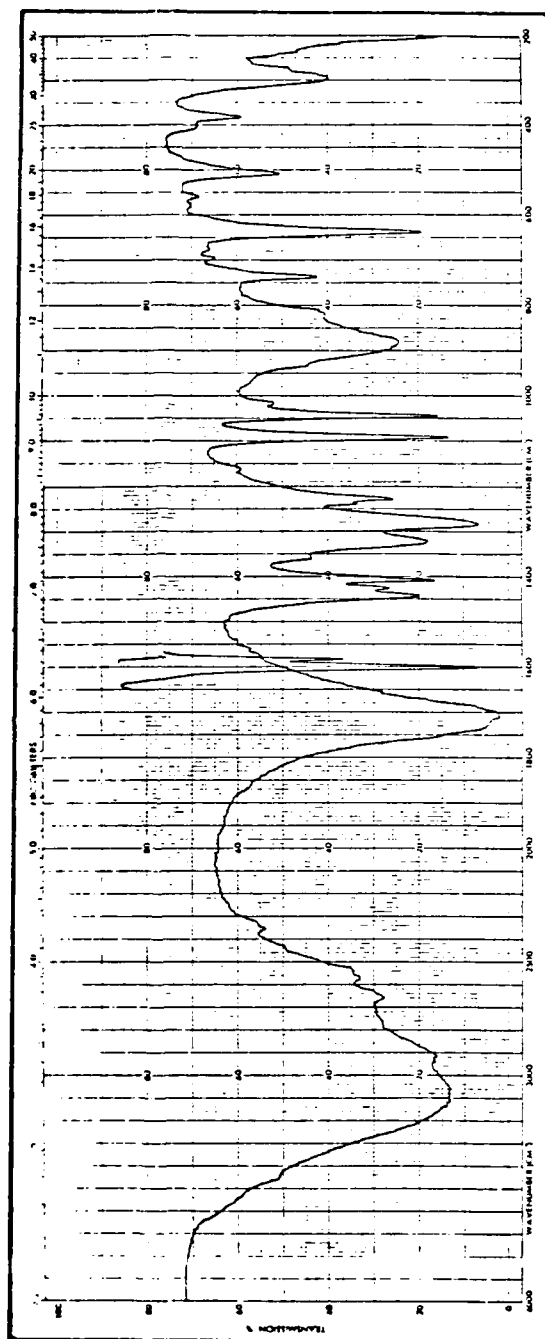
Figure 3. Ultraviolet Spectrum of Oxalosuccinate, High pH.

spectra were obtained as KBr pellets. The pellets were prepared by using approximately one part sample to fifteen parts dry KBr and pressed at 6000 pounds pressure for 20 minutes. The resulting clear pellets were placed in the cell of the instrument for the recording of the spectra. The entire IR spectrum was obtained in 20 minutes at room temperature.

The IR spectrum of  $\alpha$ -ketoglutarate, shown in Figure 4, was identical to the one previously published (53). There is a broad band centered at  $1710\text{ cm}^{-1}$ , which represents all the carbonyl and carbonyl stretching modes. The bands at  $1400\text{ cm}^{-1}$  and  $1275\text{ cm}^{-1}$  are indicative of a carboxylic acid. The small peak at  $2918\text{ cm}^{-1}$  represents  $\text{CH}_2$  asymmetrical stretching, while the peak at  $738\text{ cm}^{-1}$  indicates  $-\text{CH}_2-\text{CH}_2-$ . The absence of strong bands at  $3030\text{ cm}^{-1}$ ,  $1670\text{ cm}^{-1}$ ,  $1345\text{ cm}^{-1}$ , and  $840\text{ cm}^{-1}$  clearly indicates the lack of any alkene, providing further evidence that solid  $\alpha$ -ketoglutarate is 100% keto.

The IR spectrum of the oxalosuccinate/ $\alpha$ -ketoglutarate (barium salts) mixture is shown in Figure 5. The most striking feature of this spectrum is the set of carbonyl bands at  $1707\text{ cm}^{-1}$ ,  $1620\text{ cm}^{-1}$ , and  $1562\text{ cm}^{-1}$ . The doublet centered at  $1704\text{ cm}^{-1}$  was due to the free keto group of both acids, while the other two bands represent the carboxyl group of oxalosuccinate. The latter two bands for the  $-\text{C}=\text{O}$  stretching are shifted to slightly lower energies due to the presence of the salts of  $\alpha$ -ketoglutarate (IV) and oxalosuccinate (V), compared to the

KBr pellet

Figure 4. Infrared spectrum of  $\alpha$ -ketoglutarate.

KBr pellet

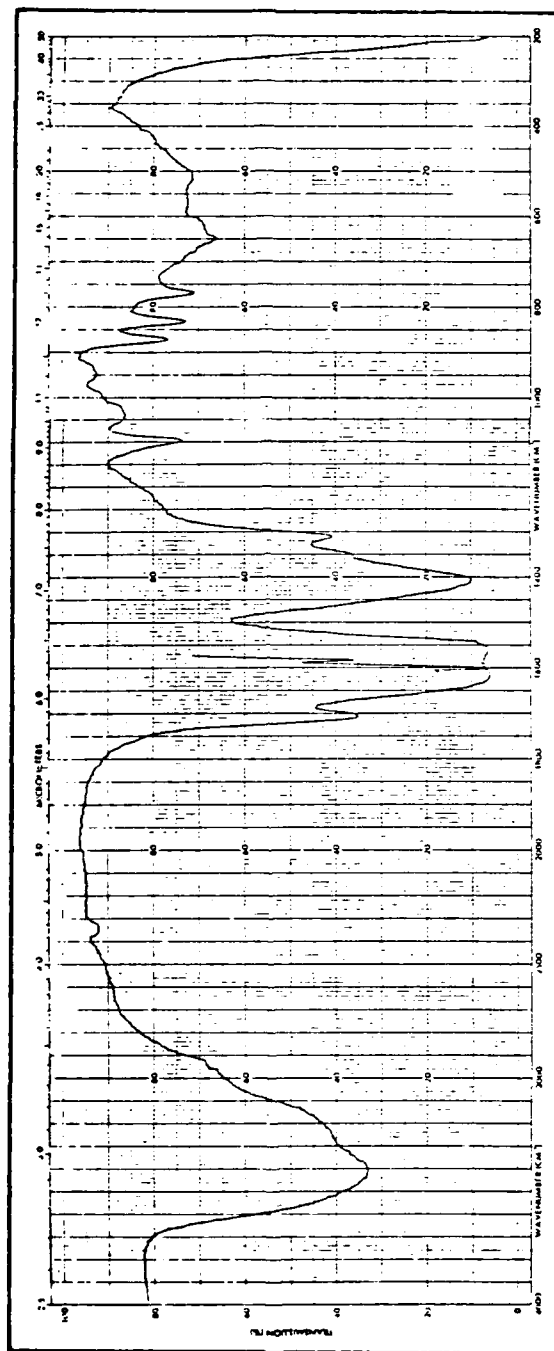


Figure 5. Infrared spectrum of oxalosuccinate.

$$\text{Ba} - \text{O} - \overset{\overset{\text{O}}{\parallel}}{\text{C}} - \text{CH}_2 - \underset{\underset{\text{O}=\text{C}}{\parallel}}{\text{CH}} - \overset{\overset{\text{O}}{\parallel}}{\text{C}} - \overset{\overset{\text{O}}{\parallel}}{\text{C}} - \text{O} - \text{Ba}^{2+}$$

anticipated energy of free acid stretches. Of the doublet at  $1704\text{ cm}^{-1}$ , the band at  $1701\text{ cm}^{-1}$  represents the keto group of oxalosuccinate that is present in the seven member ring, while the band at  $1707\text{ cm}^{-1}$  was due to the keto group from  $\alpha$ -ketoglutarate.

The IR spectrum for the barium salt of oxalosuccinate was compared to the IR spectra of the barium salt of citrate and the sodium salt of isocitrate. This can be seen in Table 5. Aside from the peak at  $1701\text{ cm}^{-1}$  due to the keto group of oxalosuccinate, other peaks compare quite well for all three spectra. The conclusion that can be drawn from this section was that the IR spectrum could represent oxalosuccinate. However, a final determination will not be made until all of the spectra in this chapter are analyzed.

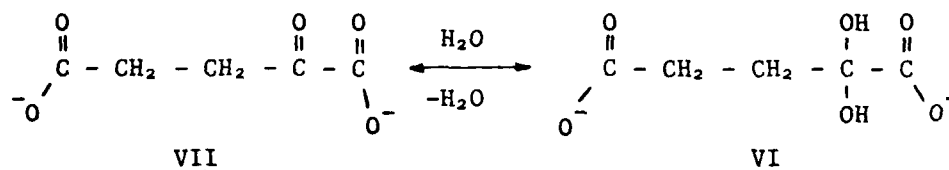
The nuclear magnetic resonance (NMR) spectra reported in this section were obtained on a Bruker HX90 Fourier Transform NMR

TABLE 5  
COMPARISON OF INFRARED ENERGIES FOR OXALOSUCCINATE,  
CITRATE, AND ISOCITRATE, INORGANIC SALTS ( $\text{cm}^{-1}$ )

Barium Oxalosuccinate	Sodium Isocitrate	Barium Citrate
3400 (m)	3400 (m)	3400 (m)
1710 (m)		
1620 (s)	1600 (s)	1575 (s)
1560 (s)		
1410 (s)	1470/1450 (s)	1420 (s)
1310 (m)	1360 (m)	1380 (m)
	1350 (m)	
	1250 (w)	
	1200 (w)	1190 (w)
	1140 (m)	1160 (m)
1100 (s)	1080 (w)	1070 (w)
1040 (w)	1040 (m)	
950 (w)	950 (w)	910 (w)
870 (m)	920 (w)	890 (w)
840 (m)	860 (m)	840 (m)

spectrometer. The sample was held in a constant temperature bath at 0°C. The oxalosuccinate sample was dissolved in a DCl/D<sub>2</sub>O mixture such that the calculated pD was 1.16. α-Ketoglutarate was dissolved in D<sub>2</sub>O, and the pD was adjusted with a calculated amount of DCl. The reference compound was tetramethylsilane, while the chemical shifts were reported as δ parts per million.

The NMR spectrum for α-ketoglutarate is given in Figure 6. Since a detailed analysis of this spectrum has already been published (54), this paragraph will only summarize the results. The doublets at 3.2 parts per million, ppm, with a coupling constant, J, of 2.2 Hz, 3.06 ppm (J=7.7 Hz), 2.80 ppm (J=6.6 Hz), and 2.68 ppm (J=1.9 Hz) were assigned to the methylene protons that form an A<sub>2</sub>B<sub>2</sub> system on the hydrate of α-ketoglutarate (VI). The slightly distorted doublet at 3.34 ppm (J=6.5 Hz) and the broad band at 3.73 ppm represents the



shift for the non-hydrated form, VII. At the pH of this sample, approximately 53% of α-ketoglutarate is hydrated, while only 10% is hydrated at a pH greater than four. The slight distortion in the signals assigned to the non-hydrated species was due to the formation of a lactol, VIII, formed by the nucleophilic attack on the carbonyl by the γ carboxyl group.



Note: 0.0 ppm = TMS

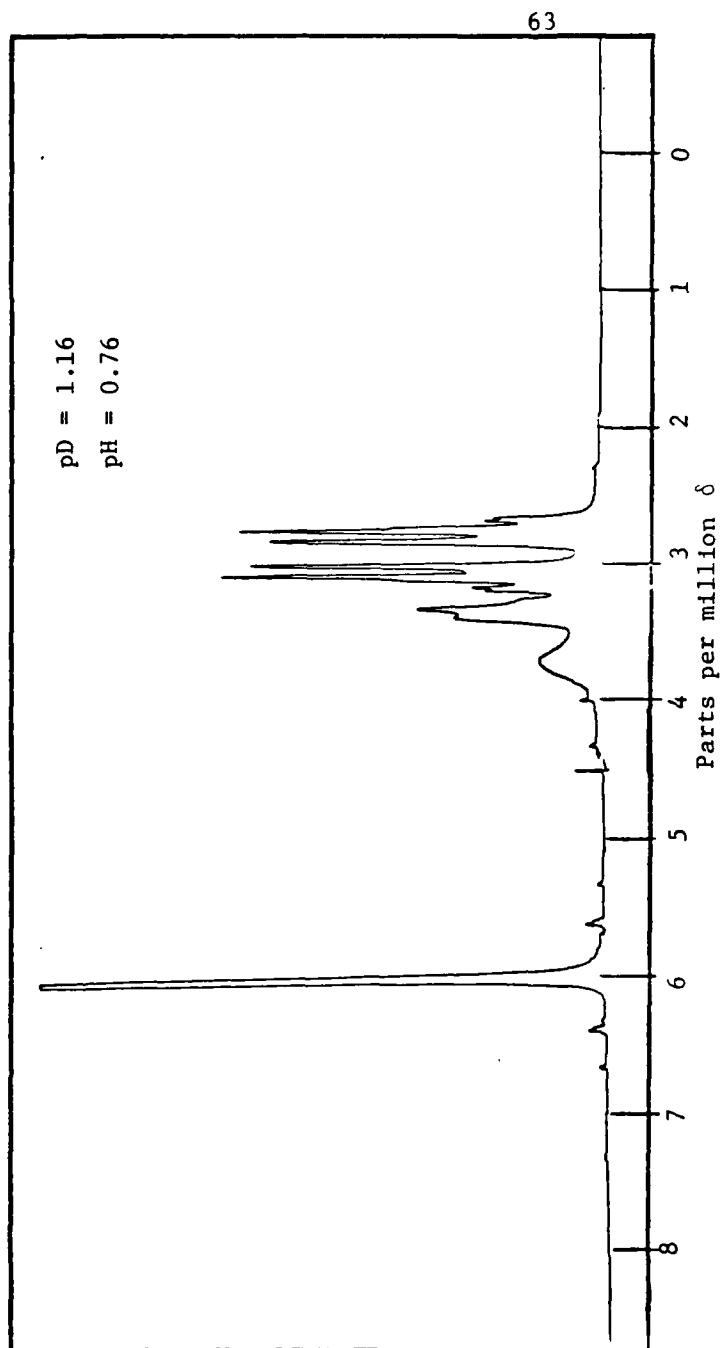
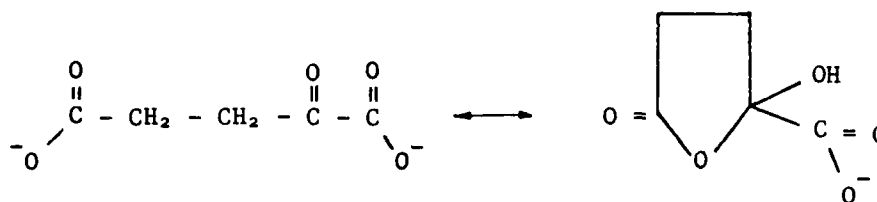
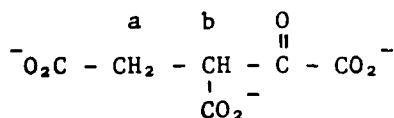


Figure 6. Nuclear magnetic resonance spectrum of  $\alpha$ -ketoglutarate.

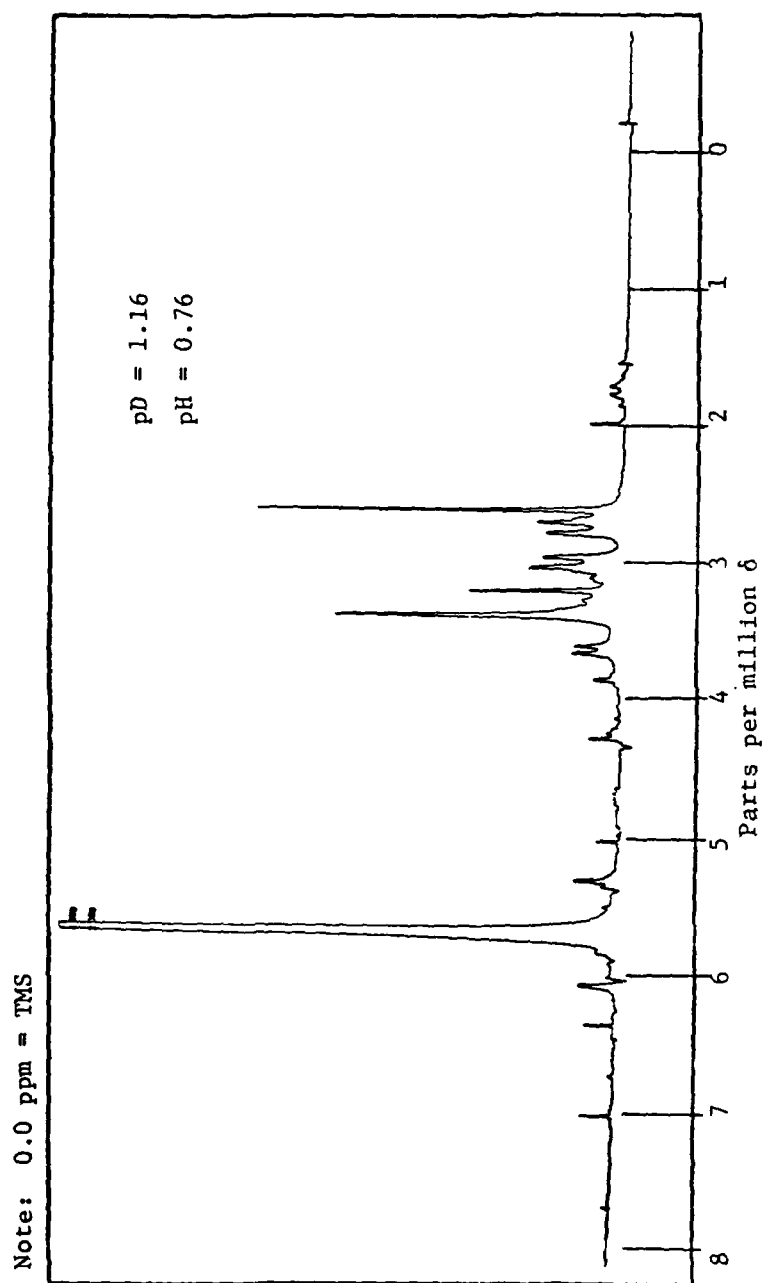


VIII

The NMR spectrum of oxalosuccinate is shown in Figure 7. Since the oxalosuccinate mixture contains approximately 30%  $\alpha$ -ketoglutarate, then the features just described in the preceding paragraph should, and do, appear. The peaks at 3.06 ppm, 2.98 ppm, 2.80 ppm, 2.73 ppm ( $J=6.75$  Hz for each doublet), and the small peak at 3.14 ppm represent the methylene protons of the  $\alpha$ -ketoglutarate hydrate, while the peaks at 3.30 ppm and 3.88 ppm are the signals for the non-hydrated isomer. The doublet at 3.68 ppm and 3.63 ppm represents the methylene protons of oxalosuccinate keto, which is split into the doublet by the methine proton. These are the protons labeled "a" in IX. This shift was comparable to the reported shift for the methylene protons in  $\beta$ -ketoglutarate, which is 3.55 ppm, and the methylene protons in the diethyl ester of oxaloacetate (3.84 ppm).

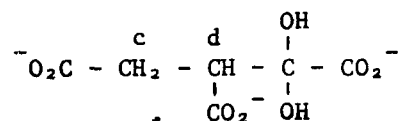


IX



The peak at 3.23 ppm represents the methine proton of the keto form of oxalosuccinate. This is proton "b" in IX. This shift was in the range of other protons in similar compounds, such as 1,2,4-butanetricarboxylic acid (large singlet at 2.7 ppm), 2,3-dimethyl-2-phenyl succinic acid (3.41 ppm), and 1,2,3-propanetricarboxylic acid (3.22 ppm). The relative integrated area of this signal was 0.262, while the area of the methylene doublet was 0.519, or approximately twice as much.

The large peak at 2.64 ppm was attributed to the methine proton of the hydrated form of oxalosuccinate. This is proton "d" of X.



X

This peak corresponds closely to the methine peak of the hydrate of oxalo-2-propionic acid, which was 2.66 ppm. The relative area of this peak, 0.437, was roughly half of the area under the peak at 3.41 ppm (0.838), which represents the methylene protons on the hydrate of oxalosuccinate. These are protons "c" in X. The ratio of the relative areas for the methylene protons of the hydrate to the non-hydrate was 1.61, and the ratio of the areas for hydrate to non-hydrate of the methine protons were 1.67. This means that at a pD of 1.16, which

corresponds to a pH of 0.76, oxalosuccinate was approximately 62% hydrated. This was in fairly good agreement with other keto acids at that pH. For example,  $\alpha$ -ketoglutarate was 53% hydrate, while pyruvate was 65% hydrate. Other values include  $\alpha$ -ketobutyric acid, 63% hydrate, and oxaloacetate, which was 80% hydrated at a pH of 1.68 at 38°C.

The large peak at 5.71 ppm was the peak due to HOD, and the six smaller peaks from 4.2 ppm to 7.1 ppm were the spinning side bands from that peak. All those peaks can therefore be ignored. The source for the small singlet at 2.01 ppm and the small quartet at 1.8 ppm cannot be determined. These peaks are therefore assigned as impurities in the sample.

#### Summary and Conclusions

Based on the spectra presented in this section, it can be concluded that the compound under investigation in this research was oxalosuccinate, with a structure shown in IX above. From the UV spectrum, a slight amount of the enol isomer was detected. The IR spectrum was typical for inorganic salts of tricarboxylic acids. The NMR spectrum, in addition to the peaks anticipated for the keto acid, showed peaks that were attributed to a hydrated species. Based on the spectrum, it was concluded that a pH of 0.76, oxalosuccinate was 62% hydrated.

#### D. Equilibrium Data

The UV spectral data obtained for this investigation will be analyzed numerically in this section. Other equilibrium experiments, such as titrations, will also be analyzed. The end result of this analysis will be numerical values for the UV extinction coefficients and formation constants for the various species and complexes included in this research. This information will be used to aid in the interpretation of the experimental kinetic data obtained.

In order to evaluate the acid formation constants (equilibrium constants), normal titration techniques were used. The pH titration of  $\alpha$ -ketoglutarate against a standard solution of 0.10 N NaOH is shown in Figure 8. The solution was maintained at a constant ionic strength of 0.1 by the addition of NaCl. Therefore, for the analysis of the data by PHFIT, an activity coefficient of 0.825 (51) was used. The results of the computer fit, summarized in Table 10, yield a value of 2.02 for  $pK_{1a}$  and 4.64 for  $pK_{2a}$ . This is in good agreement with other published values for this acid.

An alternate method for the determination of the acid formation constants was to perform a spectrophotometric titration. This was done by determining the pH dependence of the absorption spectra which, for  $\alpha$ -ketoglutarate, can be seen in Figure 9. The figure shows plots for the wavelengths of 255 nm and 284 nm. The data was adjusted to reflect the absorbance corresponding to a total concentration of 0.70 mM. These adjustments were made according to Beer's Law as it applies to mixtures, which is:

$[\alpha\text{-ketoglutarate}] = 0.0159 \text{ M}$

$[\text{NaOH}] = 0.100 \text{ M}$

Initial volume = 20.0 ml

$T = 25^\circ\text{C}$

$I = 0.1 \text{ M}$

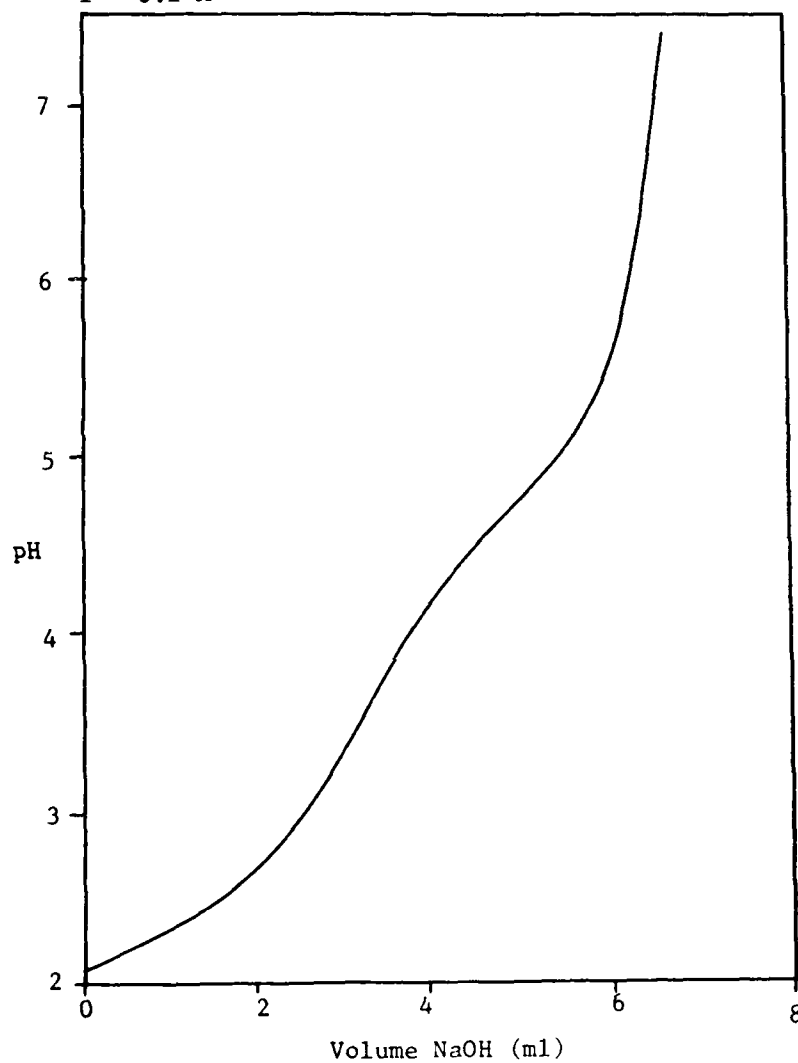


Figure 8. pH titration of  $\alpha$ -ketoglutarate.

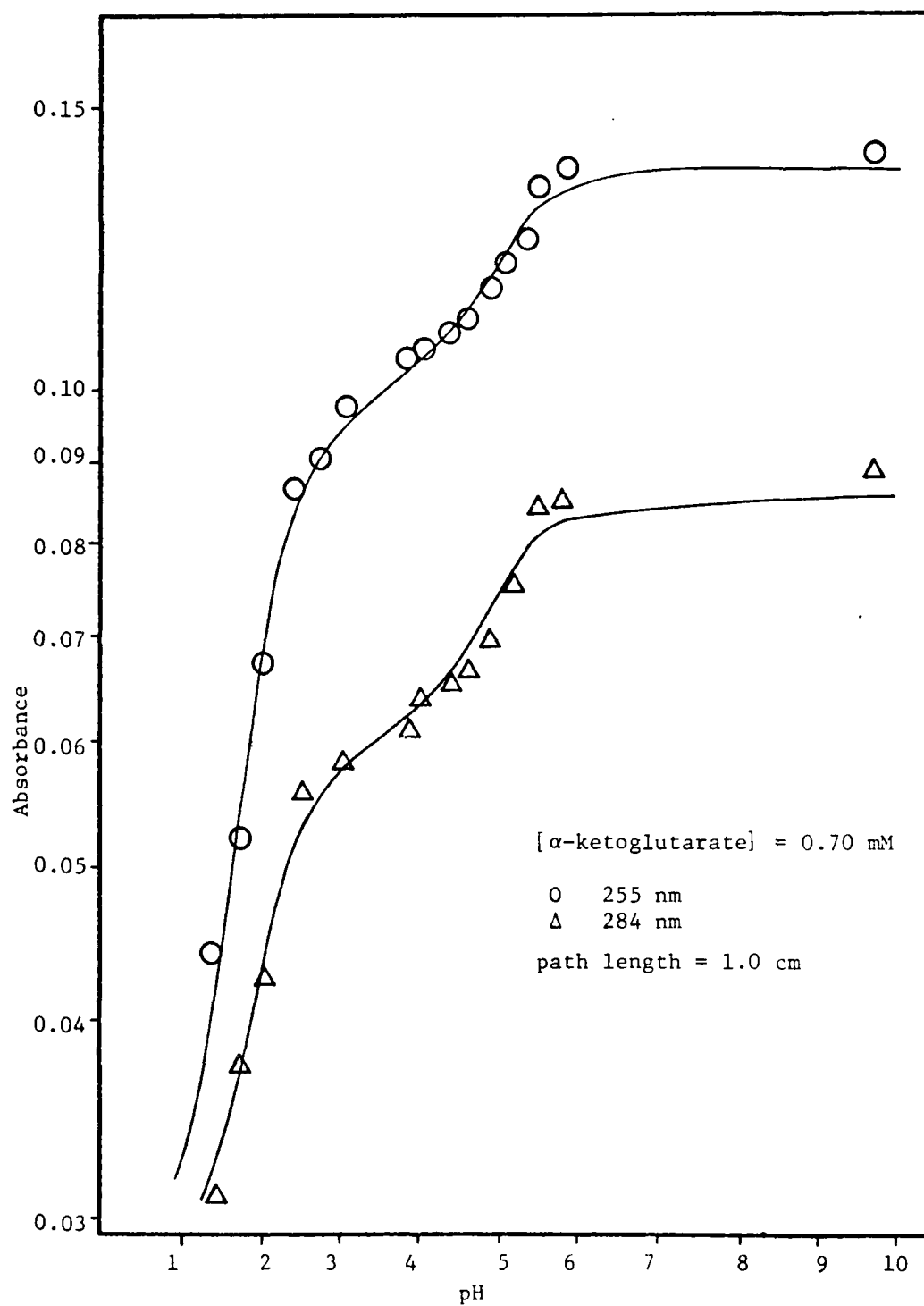


Figure 9. Spectrophotometric titration of  $\alpha$ -ketoglutarate.



$$A_{\text{calc}} = \epsilon_{\alpha\text{-KG}} [\alpha\text{-KG}^{2-}] + \epsilon_{\text{H}\alpha\text{-KG}} [\text{H}\alpha\text{-KG}^-] + \epsilon_{\text{H}_2\alpha\text{-KG}} [\text{H}_2\alpha\text{-KG}] \quad (1)$$

Noting that the formation constants are defined as:

$$\beta_{\text{H}\alpha\text{-KG}} = \frac{[\text{H}\alpha\text{-KG}^-]}{[\alpha\text{-KG}^{2-}][\text{H}^+]}$$

and

$$\beta_{\text{H}_2\alpha\text{-KG}} = \frac{[\text{H}_2\alpha\text{-KG}]}{[\alpha\text{-KG}^{2-}][\text{H}^+]^2}$$

equation (1) becomes

$$A_{\text{calc}} = [\alpha\text{-KG}^{2-}] \left\{ \epsilon_{\alpha\text{-KG}} + \epsilon_{\text{H}\alpha\text{-KG}} [\text{H}^+] + \epsilon_{\text{H}_2\alpha\text{-KG}} \beta_{\text{H}_2\alpha\text{-KG}} [\text{H}^+]^2 \right\} \quad (2)$$

By using the data points shown in Figure 9, the apparent extinction coefficients for all species and complexes can be evaluated by using published values of the formation constants as an initial estimate. Further refinement of the formation constants and the extinction coefficients results in a best solution for each wavelength. The extinction coefficients and formation constants are summarized in Table 6.

The solid lines in Figure 9 were calculated from the best values using equation (2). The program CORNEK was used for the optimization.

Several attempts were made to titrate the solution of oxalosuccinate against a standard solution of NaOH, but none of these pH titrations were very useful. This was due to the fact that oxalosuccinate was reacting as the titration was in progress. Thus, by the

TABLE 6  
EXTINCTION COEFFICIENTS AND  $pK_a$  VALUES FOR  
ALPHA-KETOGLUTARIC ACID

$pK_{1a} = 2.02$	}	at 25°C via a titration with NaOH
$pK_{2a} = 4.64$		
$pK_{1a} = 1.92$	}	at 0°C via a spectrophotometric titration
$pK_{2a} = 4.86$		

<u>Species</u>	<u>Extinction Coefficient at:</u>			
	<u>255 nm</u>	<u>260 nm</u>	<u>272 nm</u>	<u>284 nm</u>
H <sub>2</sub> a-Ketoglutarate	34.1	24.8	17.6	15.8
H a-Ketoglutarate <sup>-</sup>	143.6	123.9	107.0	86.8
a-Ketoglutarate <sup>2-</sup>	195.4	172.5	146.8	121.8

Metal/alpha-ketoglutarate formation constants (potentiometric titration):

<u>Metal</u>	<u>Log Beta</u>
Magnesium	0.353
Manganese	0.692
Zinc	1.630

(Spectrophotometric titration):

MgKetoglutarate	---	200.00	---	---
ZnKetoglutarate	905.	---	---	256.0

end of the titration, more than half of the oxalosuccinate was converted to  $\alpha$ -ketoglutarate. In an effort to speed up the experiment, a computer was used to perform the titration. Although it took only 6 minutes to complete, the results were poor. The reason was that this method was not sensitive enough to titrate five protons, oxalosuccinate and  $\alpha$ -ketoglutarate, from compounds that were in millimolar concentrations. Thus, a spectrophotometric titration was attempted. The UV spectra of the oxalosuccinate/ $\alpha$ -ketoglutarate mixture were obtained at various pH values. The resulting data was then analyzed at four wavelengths (255 nm, 260 nm, 272 nm, and 284 nm) by the program CORNEK.

However, even at 0°C, oxalosuccinate was not stable. In the time frame used for the titration, some of the oxalosuccinate had already decarboxylated. To account for this, the following was done. Based on previously published rate constants, the half life for decarboxylation is approximately 26 minutes at 25°C. If we invoke a rule of thumb in kinetics, that claims a 50% decrease in reaction rate for every 10°C change in temperature, then the half life of this reaction at 0°C is about 65 minutes. Since the entire titration was completed in about 30 minutes, then 25% of the oxalosuccinate had reacted. Thus, roughly 1% of the oxalosuccinate was converted to  $\alpha$ -ketoglutarate between each of the 21 data points. Therefore, the concentration of the total oxalosuccinate was decreased by 1%, while the concentration of

$\alpha$ -ketoglutarate was increased by 1%, for each successive data point. Since the purpose of this titration was to estimate the  $pK_a$  values, and since the data at 0°C is only an approximate value for the same data at 25°C, then precise values of the oxalosuccinate  $pK_a$ 's were not needed; only the estimates were required.

The data for one of these titrations is given in Table 7, which shows the titration at 260 nm. The data for the remaining titrations can be found in Appendix A. The calculated values resulted from applying the extinction coefficients and  $pK$  values from Table 7 into equation (3), which is shown below. A visual representation of the data taken at 255 nm and 284 nm is shown in Figure 10. The lines represent the values calculated via the equation

$$A_{\text{calc}} = A_{\alpha\text{-KG}} + [\text{ox}^{3-}] \left\{ \epsilon_{\text{ox}} + \epsilon_{\text{Hox}} \beta_{\text{Hox}} [\text{H}^+] + \epsilon_{\text{H}_2\text{ox}} \beta_{\text{H}_2\text{ox}} [\text{H}^+]^2 + \epsilon_{\text{H}_3\text{ox}} \beta_{\text{H}_3\text{ox}} [\text{H}^+]^3 \right\} \quad (3)$$

where  $A_{\alpha\text{-KG}}$  is the total absorbance due to  $\alpha$ -ketoglutarate, defined by equation (2). The extinction coefficients for oxalosuccinate are summarized in Table 8, while the formation constants are summarized in Table 10.

The data for the extinction coefficients for oxalosuccinate are shown graphically in Figure 11, which presents a plot of the extinction

TABLE 7  
OXALOSUCCINATE ABSORBANCE DATA AT 260 nm

<u>Species/Complex</u>		<u>Extinction Coefficient</u>	<u>Std. Dev</u>
Oxas		224.7	3.31
H Oxas		407.6	7.25
H <sub>2</sub> Oxas		337.0	9.01
H <sub>3</sub> Oxas		236.4	7.86
a-KG		173.0	
H a-KG		124.0	
H <sub>2</sub> a-KG		24.8	

---

<u>Complex</u>	<u>Log Beta</u>
H <sub>3</sub> Oxas	9.277
H <sub>2</sub> Oxas	7.402
H Oxas	4.631
H <sub>2</sub> a-KG	6.780
H a-KG	4.861

---

Exp			pH	<u>Absorbance</u>		<u><math>\sigma</math> %</u> Dev.
				Obs	Calc	
1	1.27E-3	9.00E-4	8.55	0.431	0.441	-2.35
2	1.25E-3	9.05E-4	6.42	0.430	0.440	-2.31
3	1.23E-3	9.11E-4	6.17	0.433	0.438	-1.21
4	1.21E-3	9.17E-4	6.01	0.440	0.437	0.81
5	1.21E-3	9.19E-4	5.69	0.448	0.443	1.14
6	1.18E-3	9.25E-4	5.22	0.473	0.456	3.66
7	1.16E-3	9.33E-4	4.76	0.504	0.487	3.35
8	1.15E-3	9.41E-4	4.17	0.543	0.538	0.94
9	1.14E-3	9.51E-4	3.68	0.552	0.557	-0.86
10	1.12E-3	9.61E-4	3.31	0.540	0.548	0.26

Table 7 (continued)

Exp	(Oxas)	(a-KG)	pH	Obs	Calc	Dev.
11	1.11E-3	9.70E-4	3.03	0.521	0.532	-2.13
12	1.10E-3	9.80E-4	2.88	0.504	0.519	-2.96
13	1.08E-3	9.91E-4	2.66	0.490	0.493	-0.56
14	1.07E-3	1.00E-3	2.54	0.472	0.477	-1.07
15	1.05E-3	1.01E-3	2.40	0.457	0.454	0.60
16	1.04E-3	1.02E-3	2.26	0.436	0.433	0.59
17	1.03E-3	1.03E-3	2.14	0.422	0.414	1.79
18	1.01E-3	1.04E-3	2.04	0.408	0.395	3.22
19	9.99E-4	1.05E-3	1.87	0.362	0.369	-1.79
20	9.87E-4	1.07E-3	1.57	0.332	0.328	1.09
21	9.73E-4	1.08E-3	1.29	0.294	0.298	-1.49

## Notes:

1. Concentration units are molar.
2. A 1.0 cm quartz cell was used.
3. The experiment was carried out at 0°C.
4. The units of the extinction coefficients were  $M^{-1} cm^{-1}$ .

TABLE 8  
EXTINCTION COEFFICIENTS FOR OXALOSUCCINATE  
AT VARIOUS WAVELENGTHS

Species	Extinction Coefficient at			
	255 nm	260 nm	272 nm	284 nm
H <sub>3</sub> Oxalosuccinate	354	236	125	74
H <sub>2</sub> Oxalosuccinate	467	337	150	56
H Oxalosuccinate	447	408	267	126
Oxalosuccinate	277	225	102	41
ZnOxalosuccinate	2205	--	--	210
MgOxalosuccinate	--	329	--	--
H <sup>-1</sup> Oxalosuccinate (enolate)	--	--	15,250	--

Notes:

1. The unit for the extinction coefficients are  $M^{-1} cm^{-1}$ .
2. The data in this table was obtained by analyzing the appropriate spectrophotometric titration by the program CORNEK.

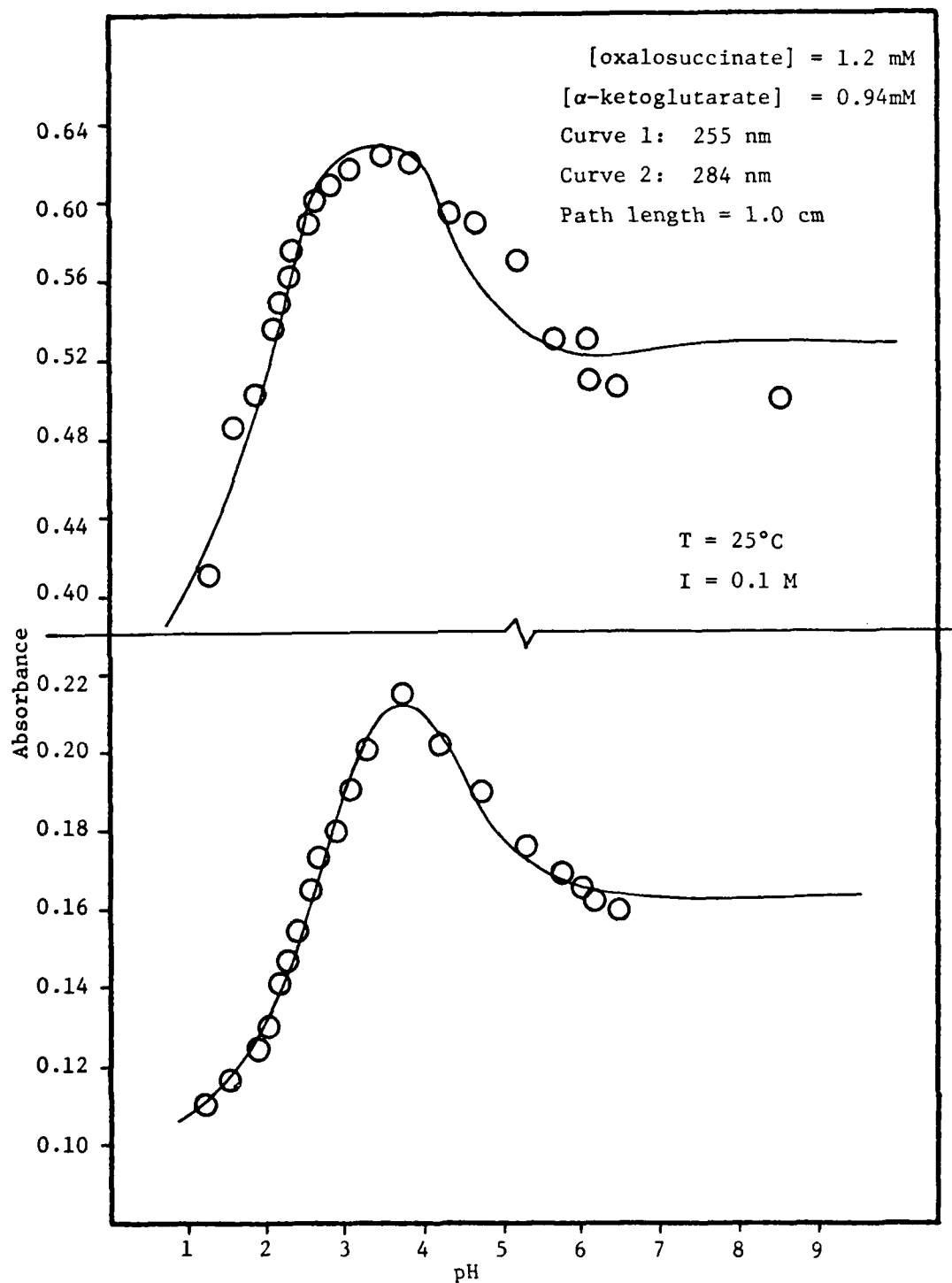


Figure 10. Spectrophotometric titration of oxalosuccinate



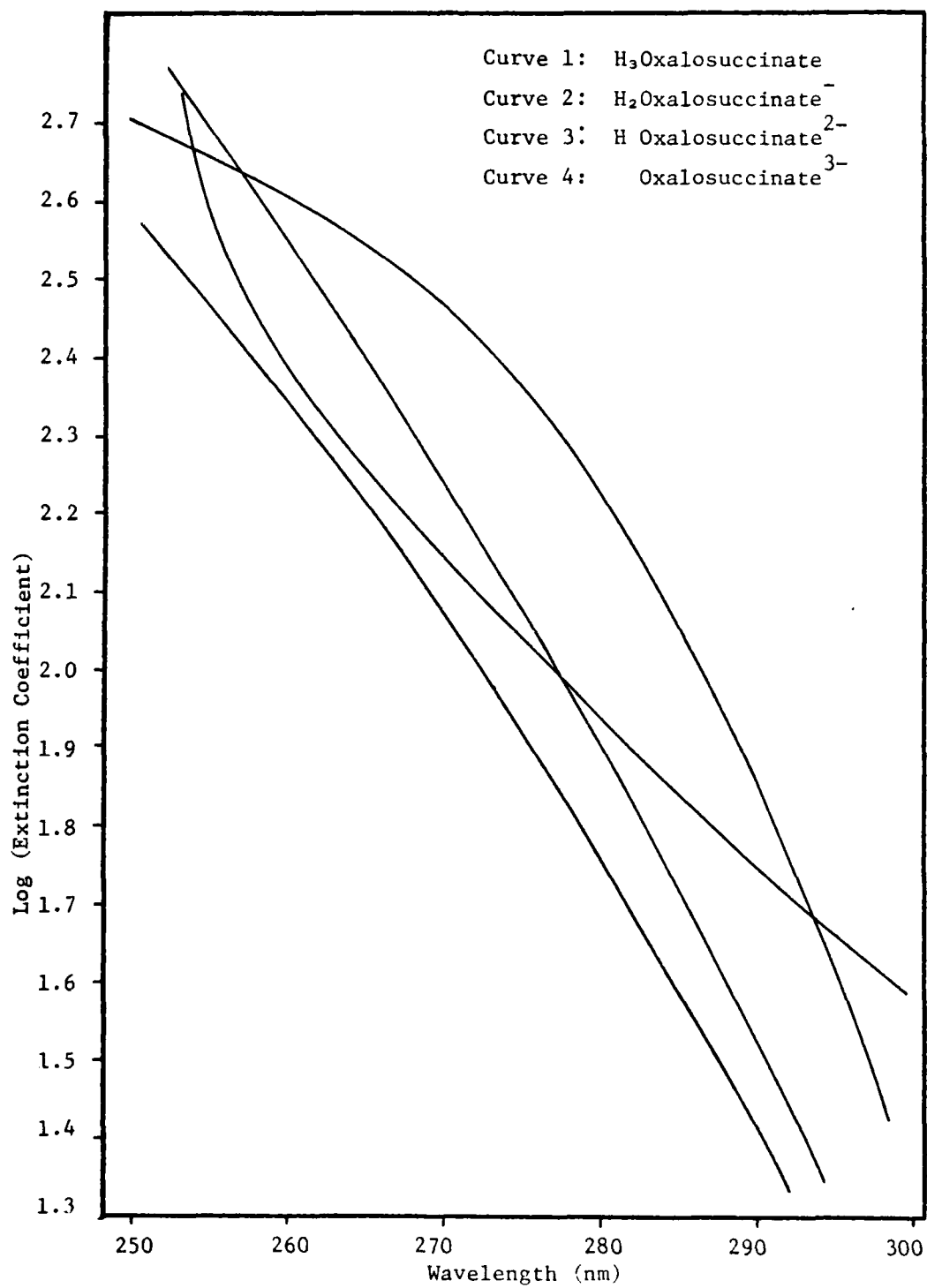
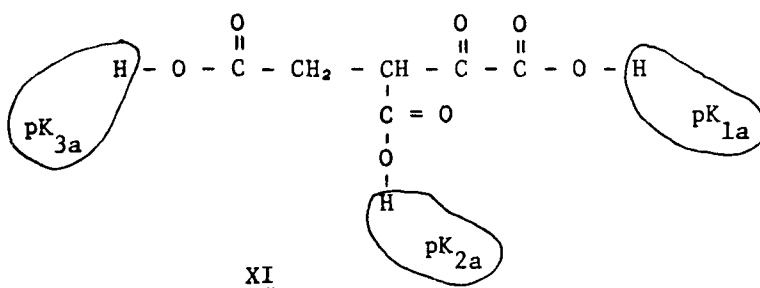


Figure 11. Wavelength dependence of the extinction coefficients for the oxalosuccinate species.

coefficients versus wavelength (250 nm to 290 nm) for each species and complex. By using the data in the figure along with the distribution of oxalosuccinate calculated from the formation constants, the theoretical absorbance of a solution of oxalosuccinate at any pH can be evaluated.

The observed pK values for oxalosuccinate, determined by CORNEK, were 1.88, 2.77, and 4.63 for  $pK_{1a}$ ,  $pK_{2a}$ , and  $pK_{3a}$  at 0°C. The protons corresponding to these values are shown in XI. These values were similar to other acidic protons that are  $\alpha$ ,  $\beta$ , and  $\gamma$  to a keto group. For comparison, pK values for other comparable acids are:  $\alpha$ -keto-glutarate, 2.02; pyruvic acid, 2.26; and oxaloacetic acid, 2.22. A



good example of a  $\beta$ -keto acid to use for comparison was acetone dicarboxylic acid ( $\beta$ -ketoglutaric acid), which has a  $pK_{1a}$  of 2.74. The  $pK_{3a}$  for oxalosuccinate, corresponding to the carboxylate group  $\gamma$  to the keto, compares favorably to the same moiety on  $\alpha$ -ketoglutarate, which has a pK value for that proton of 4.64. Thus, the results from

the spectrophotometric titration compares well to published data for other similar acids.

From halogenation experiments, it was shown that a small amount of enol was present in a solution of oxalosuccinate. Since the strongly basic enol can deprotonate, it became necessary to characterize the enolate species. A series of UV spectra at various pH values are shown in Figure 12. These spectra show a peak at 272 nm that increases in intensity as the pH increases. This arose from the  $H_{-1}ox^{4-}$  enolate species.

The absorbance data in Figure 12 was analyzed according to equation (5). Realizing that the formation constant for the enolate,

$$A_{obs} = \epsilon_{ox} [ox^{3-}] + \epsilon_{H_{-1}ox} [H_{-1}ox^{4-}] \quad (5)$$

$\beta_{H_{-1}ox}$ , is defined as  $[H_{-1}ox^{4-}][H^+]/[ox^{3-}]$ , equation (5) reduces to:

$$A_{obs} = (\epsilon_{ox} + \epsilon_{H_{-1}ox} \beta_{H_{-1}ox} / [H^+]) ([ox^{3-}]) \quad (6)$$

The absorbance data was evaluated for the formation constant of the enolate species as well as the apparent extinction coefficients for the species  $ox^{3-}$  and  $H_{-1}ox^{4-}$ . This data is shown in Figure 13. The solid line in the figure is the theoretical fit calculated from equation (6). The program CORNEK was used to optimize the data, which is summarized in Table 9.

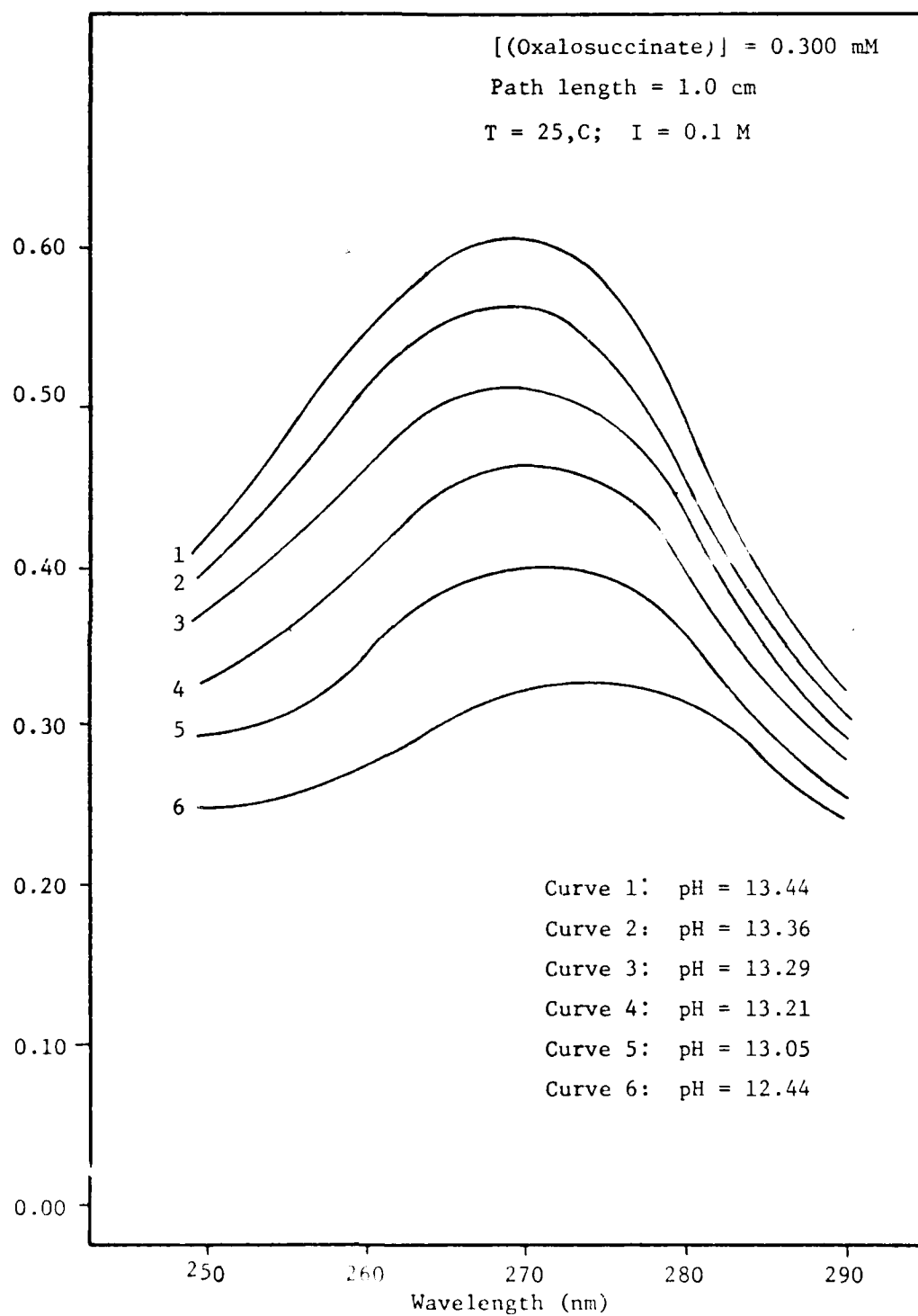


Figure 12. Ultraviolet spectra of oxalosuccinate vs. pH at high pH.

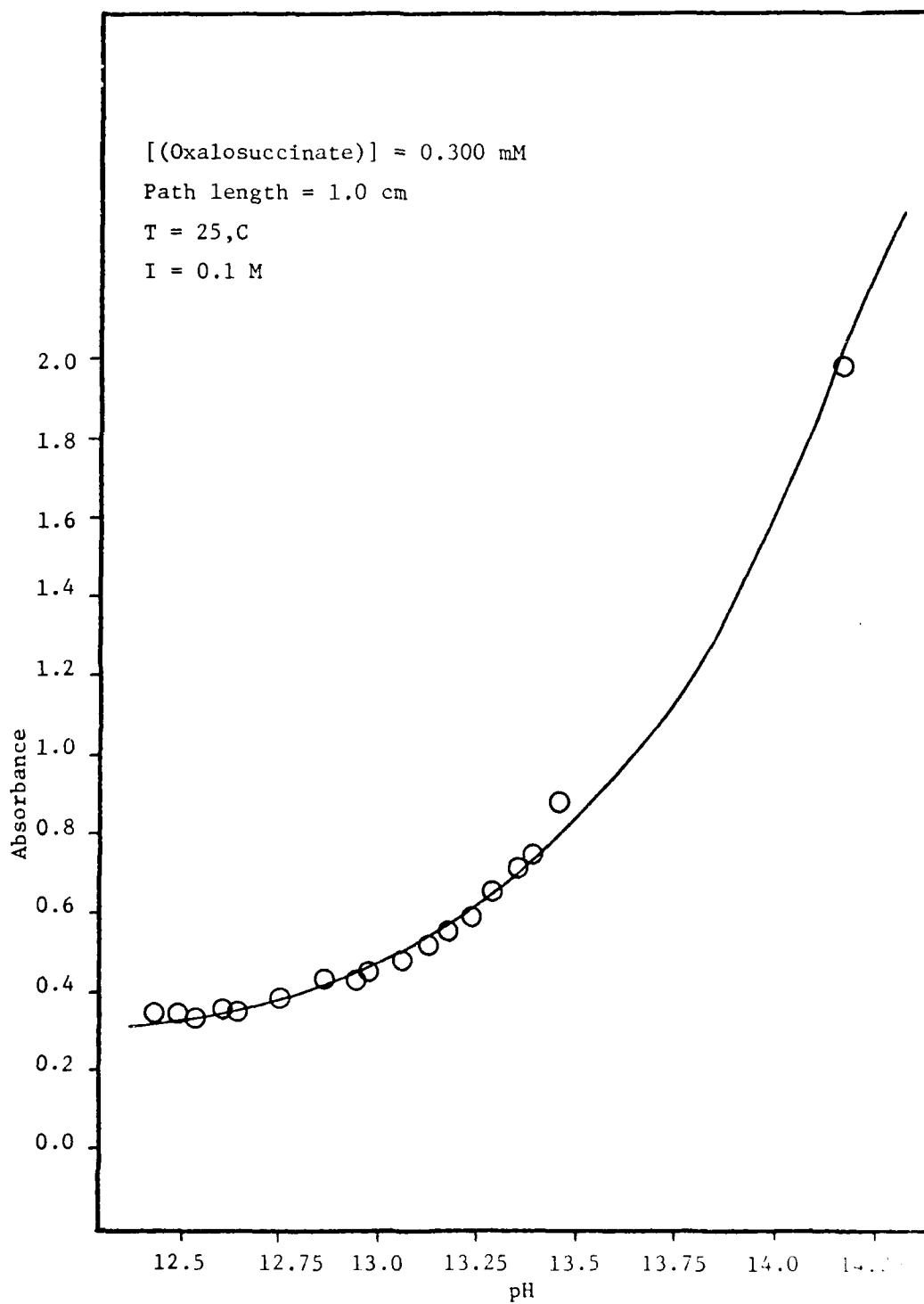


Figure 13. Spectrophotometric titration of the oxalosuccinate-enolate species at 272 nm.

AD-A092 546

AIR FORCE INST OF TECH WRIGHT-PATTERSON AFB OH  
SPONTANEOUS, METAL-CATALYZED, AND ENZYME-CATALYZED DECARBOXYLAT-ETC(U)  
1980 S L SINCOFF  
UNCLASSIFIED AFIT-CI-80-27D

F/6 7/3

NL

2 of 4  
AD A  
092 546

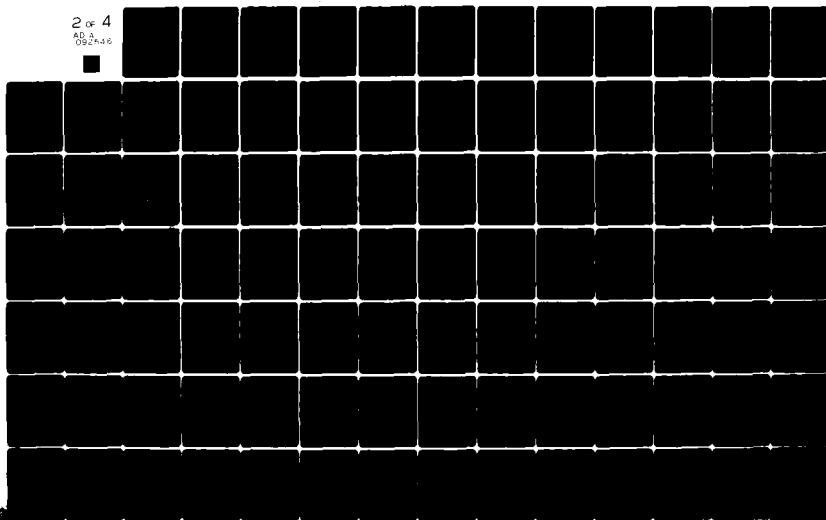


TABLE 9  
SPECTROPHOTOMETRIC TITRATION OF THE ENOLATE SPECIES AT 272 nm

Species		Extinction Coefficient	Std Dev
Oxas Enol <sup>3-</sup>		836	38.7
Oxas Enolate <sup>4-</sup>		15,250	3,108
$\alpha$ -Ketoglutarate <sup>2-</sup>		147	

---

Species	pK <sub>a</sub>
Oxas Enolate <sup>4-</sup>	14.31

---

Exp.	[(Oxas)]	[( $\alpha$ -KG)]	pH	Absorbance		% Dev.
				Obs	Calc	
1	9.34E-4	4.52E-4	12.44	1.090	1.025	5.93
2	2.92E-4	1.26E-4	12.50	0.348	0.326	6.20
3	9.32E-4	4.51E-4	12.54	1.100	1.068	2.87
4	2.86E-4	1.25E-4	12.62	0.356	0.339	4.64
5	9.29E-4	4.50E-4	12.64	1.120	1.121	-0.13
6	2.81E-4	1.23E-4	12.75	0.362	0.361	0.28
7	2.75E-4	1.20E-4	12.87	0.373	0.386	-3.40
8	9.13E-4	4.43E-4	12.94	1.260	1.364	-8.26
9	2.70E-4	1.18E-4	12.97	0.392	0.412	-5.18
10	2.64E-4	1.15E-4	13.05	0.404	0.435	-7.64
11	2.59E-4	1.13E-4	13.11	0.421	0.454	-7.75
12	2.54E-4	1.11E-4	13.16	0.441	0.470	-6.48
13	2.49E-4	1.09E-4	13.21	0.466	0.487	-4.52
14	2.44E-4	1.06E-4	13.25	0.491	0.500	-1.84

Table 9 (continued)

Exp	[(Oxas)]	[( $\alpha$ -KG)]	pH	Obs	Calc	% Dev
15	2.39E-4	1.04E-4	13.29	0.522	0.514	1.53
16	2.34E-4	1.02E-4	13.33	0.542	0.529	2.42
17	2.29E-4	1.00E-4	13.36	0.570	0.538	5.68
18	2.25E-4	9.81E-5	13.39	0.564	0.549	2.65
19	2.20E-4	9.62E-5	13.41	0.584	0.551	5.64
20	2.16E-4	9.42E-5	13.44	0.616	0.563	8.63
21	2.12E-4	9.24E-5	13.46	0.623	0.567	8.93
22	2.60E-4	1.13E-4	14.13	1.670	1.721	-3.02

## Notes:

1. Concentration units are molar.
2. A 1.0 cm quartz cell was used.
3. The experiment was carried out at 0°C.
4. The units of the extinction coefficients are  $M^{-1}cm^{-1}$ .



TABLE 10  
SUMMARY OF DATA: ACID PROTONATION CONSTANTS AND METAL FORMATION CONSTANTS

Species	T (°C)	Log Beta	pK <sub>1a</sub>	pK <sub>2a</sub>	pK <sub>3a</sub>	pK <sub>4a</sub>	Method
Oxalosuccinic Acid	0	--	1.88	2.77	4.63	14.31	A
Oxalosuccinic Acid	0	--	1.89	2.60	4.40	--	B
Oxalosuccinic Acid	25	--	1.86	2.66	4.47	--	C
Zn-Oxalosuccinate	0	3.02	--	--	--	--	A
Zn-Oxalosuccinate	25	3.02	--	--	--	--	C
Mg-Oxalosuccinate	0	1.92	--	--	--	--	A
Mg-Oxalosuccinate	25	1.99	--	--	--	--	C
Mn-Oxalosuccinate	25	2.57	--	--	--	--	C
α-Ketoglutaric Acid	25	--	2.02	4.64	--	--	D
Mg-α-Ketoglutarate	25	0.353	--	--	--	--	D
Mg-α-Ketoglutarate	25	0.692	--	--	--	--	D
Zn-α-Ketoglutarate	25	1.630	--	--	--	--	D

A = Spectrophotometric titration

B = pH profile of the keto/enol ratio

C = Kinetic data (to be found in Chapters IV, V, and VI).

D = Potentiometric titration.

Above a pH of 11, direct pH readings on the pH meter are inaccurate due to sodium ion error. Therefore, the pH values reported in Figures 12 and 13 were determined by calculating the concentration of hydroxide ion present in the solution. This method was valid due to the high concentration of hydroxide present during the titration. For example, a pH of 12.44, which was the lowest value, corresponds to a 0.04 M solution of NaOH. This was a relatively strong solution in comparison to a 0.001 M solution of oxalosuccinate.

In order to evaluate the formation constants of the metal/ $\alpha$ -ketoglutarate complex, a pH titration of a solution composed of 0.010 M  $\alpha$ -ketoglutarate and 0.030 M metal was performed against a standard NaOH solution. The metal/ligand concentration ratio of three was used to insure that the primary complex present was the metal-monoligand complex, ML, rather than higher order complexes, such as ML<sub>2</sub>. In this way the equilibrium investigation was consistent with the kinetic study, since the kinetic studies involved metal/ligand ratios of at least eight.

A plot of each titration is shown in Figure 14. To evaluate the data, mass balance equations, shown below, were required.

$$[M]_{\text{total}} = [M] + [MKG] \quad (7)$$

$$[KG]_{\text{total}} = [KG] + [HKG] + [H_2KG] + [MKG] \quad (8)$$

$$[H]_{\text{total}} = [H] - [OH] + [HKG] + 2[H_2KG] \quad (9)$$

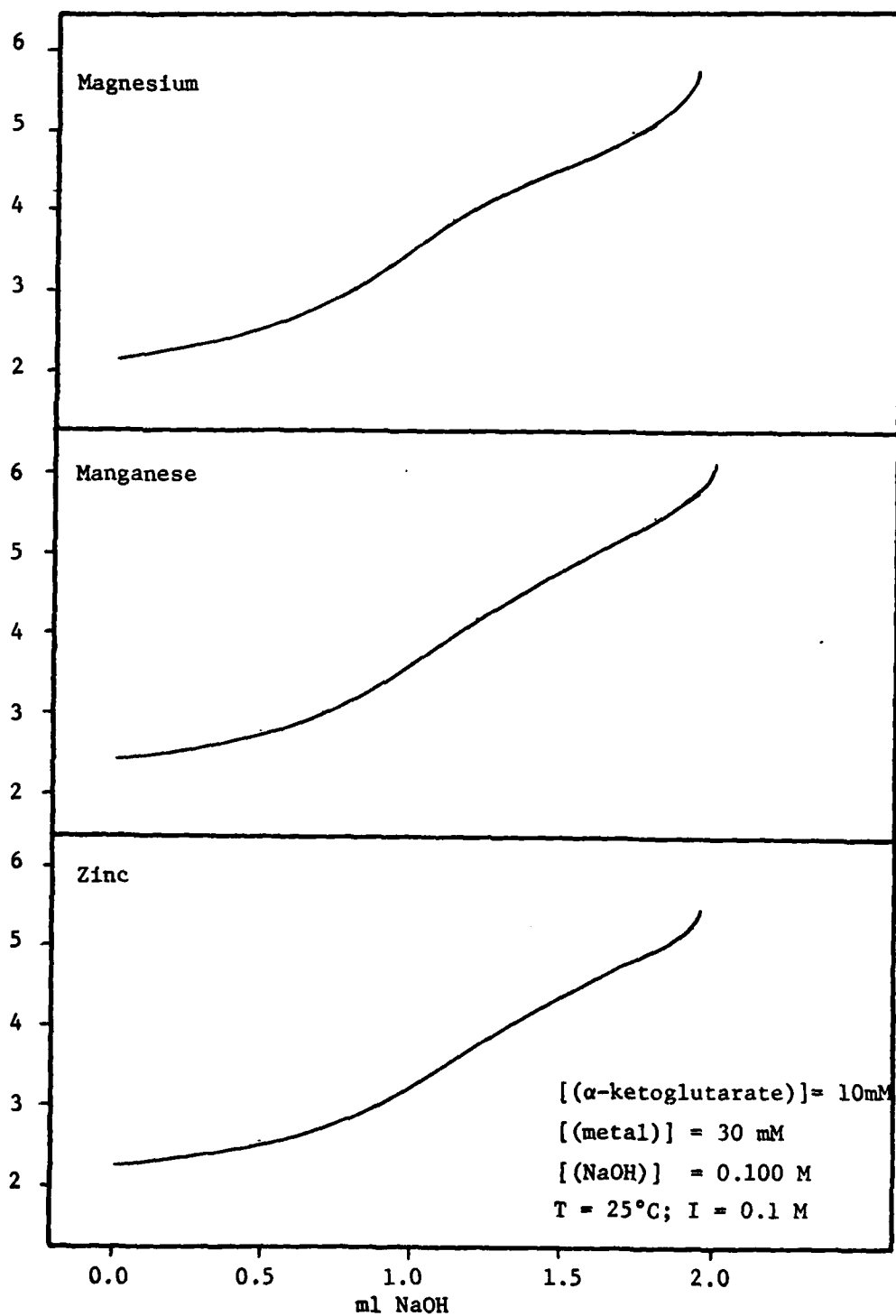


Figure 14. pH titration of metal/ $\alpha$ -ketoglutarate solutions for magnesium, manganese, and zinc.

The metal-ligand formation constants are defined as:

$$\beta_1 = \frac{[\text{HKG}]}{[\text{H}^+][\text{KG}]}$$

$$\beta_2 = \frac{[\text{H}_2\text{KG}]}{[\text{H}^+]^2[\text{KG}]}$$

$$\beta_{\text{MKG}} = \frac{[\text{MKG}]}{[\text{M}][\text{KG}]}$$

Substitution of these relationships into equations (7) through (9) yields:

$$[\text{M}]_{\text{total}} = [\text{M}](1 + \beta_{\text{MKG}}[\text{KG}]) \quad (10)$$

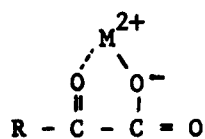
$$[\text{KG}]_{\text{total}} = [\text{KG}](1 + \beta_1[\text{H}^+] + \beta_2[\text{H}]^2 + \beta_{\text{MKG}}[\text{M}]) \quad (11)$$

$$[\text{H}]_{\text{total}} = [\text{KG}](1 + \beta_1[\text{H}^+] + 2\beta_2[\text{H}]^2) - K_w/[\text{H}^+] \quad (12)$$

For a given point on the titration curve,  $[\text{H}]_{\text{total}}$  can be calculated from the volume of base added, and  $[\text{H}^+]$  can be calculated from the experimental pH. Since  $K_w = 1 \times 10^{-14}$ , the formation constants given, and the total concentration of species also given, then the only unknowns are  $[\text{M}]$ , the concentration of free metal,  $[\text{KG}]$ , or the concentration of free  $\alpha$ -ketoglutarate, and the metal/ $\alpha$ -ketoglutarate formation constant. These unknowns were found by solving equations (10) to (12) above. This analysis was done on the computer by the

program PHFIT. The results are shown in Table 10. The binding of the metals to the ligand follows the Irving-Williams natural stability order, which was  $\text{Zn}^{2+} > \text{Mn}^{2+} > \text{Mg}^{2+}$ .

In a similar manner, an analogous set of equations can be used for an absorbance titration, which can be extended for an oxalo-succinate titration by simply accounting for all absorbing species and complexes. The absorbance data for the magnesium-oxalosuccinate absorbance titration at 260 nm is shown in Table 11. The log of the formation constant, determined by CORNEK, was found to be 1.92. The zinc-oxalosuccinate absorbance data at 255 nm and 284 nm are shown in Tables 12 and 13 respectively. The log of the formation constant for the zinc complex was found to be 3.02 at both wavelengths. The corresponding values for the metal/oxaloacetate formation constants were 1.96 and 3.20 respectively. The values were expected to be reasonable close since the metals complex the ligands in a similar manner, as shown in XII.



XII

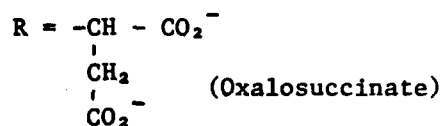
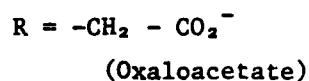


TABLE 11  
MAGNESIUM-OXALOSUCCINATE ABSORBANCE DAT AT 260 nm

Species/Complex	Ext. Coef.	Std. Dev.
MgOxas	329.2	9.61
Mg Akg	200.0	
Oxas	225.0	
H Oxas	408.0	
H2Oxas	337.0	
H3Oxas	236.0	
Akg	173.0	
H Akg	124.0	
H2Akg	24.8	

---

Complex	Log Beta
MgOxas	1.918
MgAkg	1.630
H Oxas	4.631
H2Oxas	7.402
H3Oxas	9.277

---

Exp	[(Mg)]	[(Oxas)]	[(Akg)]	pH	Absorbance	
					Obs.	Calc
1	5.00E-3	7.71E-4	3.37E-4	4.88	0.283	0.281
2	4.99E-3	7.58E-4	3.42E-4	5.32	0.273	0.263
3	4.98E-3	7.32E-4	3.51E-4	5.50	0.257	0.254
4	4.97E-3	7.21E-4	3.56E-4	5.83	0.251	0.248
5	4.96E-3	7.08E-4	3.62E-4	6.63	0.253	0.243
6	1.20E-2	6.92E-4	3.65E-4	6.57	0.261	0.255
7	1.20E-2	6.79E-4	3.71E-4	6.22	0.248	0.252
8	1.19E-2	6.65E-4	3.76E-4	5.44	0.245	0.251
9	1.19E-2	6.52E-4	3.81E-4	4.84	0.262	0.257
10	1.18E-2	6.36E-4	3.85E-4	4.78	0.243	0.257

## Notes:

1. Concentration units are molar.
2. A 1 cm quartz cell was used.
3. The experiment was carried out at 0°C.

TABLE 12  
ZINC-OXALOSUCCINATE ABSORBANCE DATA AT 255 nm

Species/Complex	Ext. Coef.	Std. Dev.				
ZnOxas	2205.0	68.49				
Zn Akg	956.0					
Oxas	277.0					
H Oxas	447.0					
H2Oxas	467.0					
H3Oxas	353.0					
Akg	195.0					
H Akg	143.0					
H2 Akg	34.1					
-----						
Complex	Log Beta					
ZnOxas	3.017					
Zn Akg	1.630					
H Oxas	4.631					
H2Oxas	7.402					
H3Oxas	9.277					
-----						
Exp.	[(Zn)]	[(Oxas)]	[(Akg)]	pH	Absorbance	
					Obs	Calc
1	4.96E-4	7.35E-4	3.49E-4	5.89	1.200	1.457
2	4.96E-3	7.19E-4	3.55E-4	6.35	1.360	1.439
3	1.21E-2	6.83E-4	3.69E-4	5.83	1.480	1.554
4	1.20E-2	6.65E-4	3.76E-4	5.16	1.480	1.480
5	1.20E-2	6.48E-4	3.83E-4	4.86	1.410	1.410
6	1.19E-2	6.29E-4	3.90E-4	4.09	1.240	1.149
7	1.19E-2	6.12E-4	3.98E-4	3.63	1.020	0.865
8	1.89E-2	5.93E-4	4.05E-4	3.46	0.946	0.857
9	1.88E-2	5.74E-4	4.13E-4	4.29	1.280	1.224
10	1.87E-2	5.58E-4	4.22E-4	4.64	1.330	1.276
11	1.87E-2	5.41E-4	4.32E-4	5.15	1.360	1.317
12	1.86E-2	5.24E-4	4.42E-4	5.88	1.350	1.325

## Notes:

1. Concentration units are molar.
2. A 1 cm quartz cell was used.
3. The experiment was carried out at 0°C.

TABLE 13  
ZINC-OXALOSUCCINATE ABSORBANCE DATA AT 284 nm

Species/Complex		Ext. Coef.	Std. Dev.
ZnOxas		209.7	14.00
Zn Akg		256.0	
Oxas		41.4	
H Oxas		126.0	
H2Oxas		56.5	
H3Oxas		73.6	
Akg		122.0	
H Akg		86.8	
H2 Akg		30.5	

---

Complex		Log Beta
ZnOxas		3.017
Zn Akg		1.630
H Oxas		4.631
H2Oxas		7.402
H3Oxas		9.277

---

Exp	[(ZN)]	[(OXAS)]	[(AKG)]	pH	Absorbance	
					Obs	Calc
1	5.00E-3	7.71E-4	3.37E-4	4.92	0.151	0.175
2	4.98E-3	7.53E-4	3.43E-4	5.21	0.177	0.177
3	4.96E-4	7.35E-4	3.49E-4	5.89	0.232	0.180
4	4.96E-3	7.19E-4	3.55E-4	6.35	0.255	0.179
5	1.21E-2	6.83E-4	3.69E-4	5.83	0.257	0.193
6	1.20E-2	6.65E-4	3.76E-4	5.16	0.209	0.184
7	1.20E-2	6.48E-4	3.83E-4	4.86	0.189	0.177
8	1.19E-2	6.29E-4	3.90E-4	4.09	0.148	0.153
9	1.19E-2	6.12E-4	3.98E-4	3.63	0.117	0.134
10	1.89E-2	5.93E-4	4.05E-4	3.46	0.117	0.132
11	1.88E-2	5.74E-4	4.13E-4	4.29	0.152	0.159
12	1.87E-2	5.58E-4	4.22E-4	4.64	0.153	0.167
13	1.87E-2	5.41E-4	4.32E-4	5.15	0.158	0.177
14	1.86E-2	5.24E-4	4.42E-4	5.88	0.175	0.183

## Notes

1. Concentration units are molar.
2. A 1 cm quartz cell was used.
3. The experiment was carried out at 0°C.



A typical spectrum for magnesium/oxalosuccinate is shown in Figure 15. As with the free acid, no peaks or shoulders are seen. This indicates that the keto form of the chelate predominates. This was verified by iodination experiments, which showed that about 1% of the magnesium/oxalosuccinate complex is enol. The spectrum for the manganese/oxalosuccinate complex was similar in that no peaks or shoulders were observed. However, the spectrum for zinc/oxalosuccinate, shown in Figure 16, has a strong peak appearing at 255 nm. It was concluded that zinc forms a very stable complex with the enol. The apparent extinction coefficient of this peak, evaluated by CORNEK, was  $2205 \text{ M}^{-1} \text{ cm}^{-1}$ . Assuming that the true extinction coefficient of the enolic complex was  $9500 \text{ M}^{-1} \text{ cm}^{-1}$ , a value typical for metal/oxaloacetate enol complexes, then 23% of the zinc/oxalosuccinate complex was enolized. A spectrum for zinc/ $\alpha$ -ketoglutarate indicated the complete absence of enol. Therefore, any enol found in the solution arose from the oxalosuccinate complex with zinc.

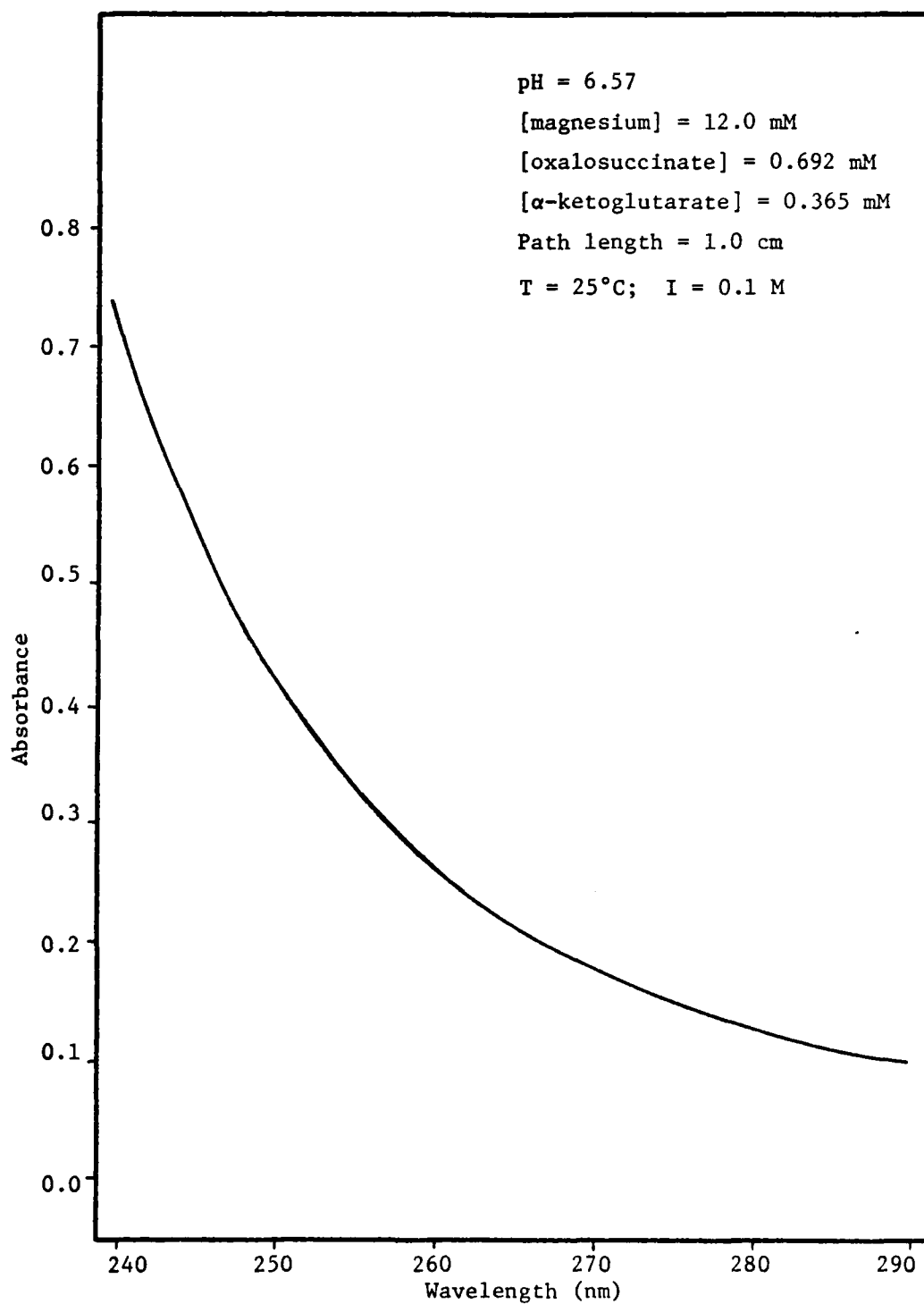


Figure 15. Ultraviolet spectrum of the magnesium/oxalosuccinate solution.

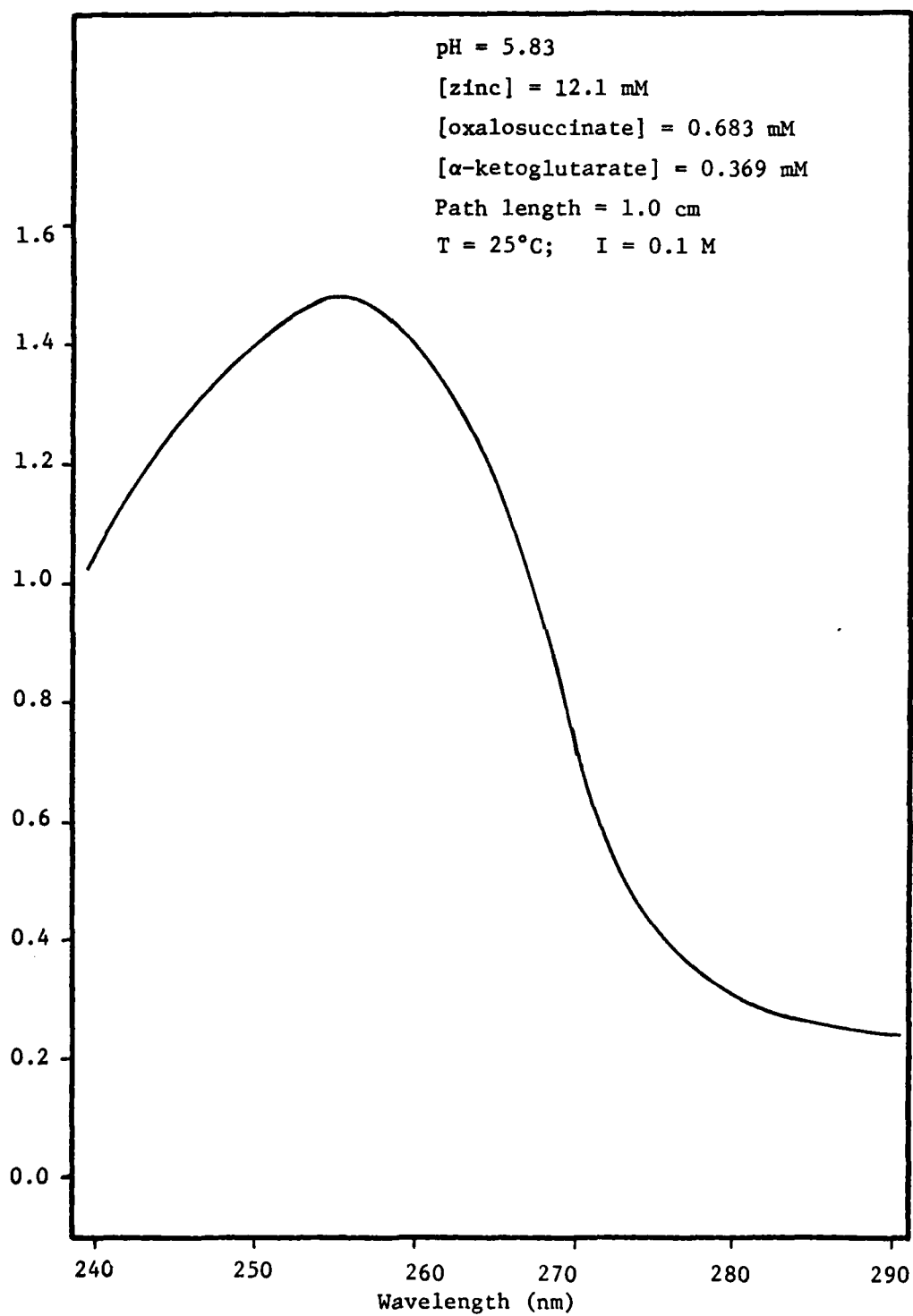


Figure 16. Ultraviolet spectrum of the zinc/oxalosuccinate solution.

#### IV. DECARBOXYLATION AND TAUTOMERIZATION OF OXALOSUCCINIC ACID

This chapter will discuss the kinetics of the free acid decarboxylation reaction. Unfortunately, a discussion of system kinetics cannot be done independently of equilibrium considerations, that is, the interpretation of the kinetic investigations is very dependent on the constants provided by equilibrium studies. Also, the equilibrium investigations require a knowledge of the kinetic processes and must be performed within the constraints of the kinetics of the system in order to be valid. It is important that the experimenter recognize the interplay between equilibrium and kinetic processes and to recognize that the results from one may effect the interpretation of the other.

When observing the buffered decarboxylation of oxalosuccinate spectrophotometrically at 255 nm, three distinct regions appear, as shown in Figure 17. It is the objective of this section to determine what reaction is reflected in each region, and, if applicable, resolve the kinetics of that region.

In order to do this, the first step is to follow the reaction by monitoring the UV spectrum of the solution at various times. The first experiment is shown in Figure 18, and was taken on the Cary 14 spectrophotometer. The scan rate for each spectrum was 1 nm/second, or 70 seconds for each scan. It can be seen that there is an absorbance

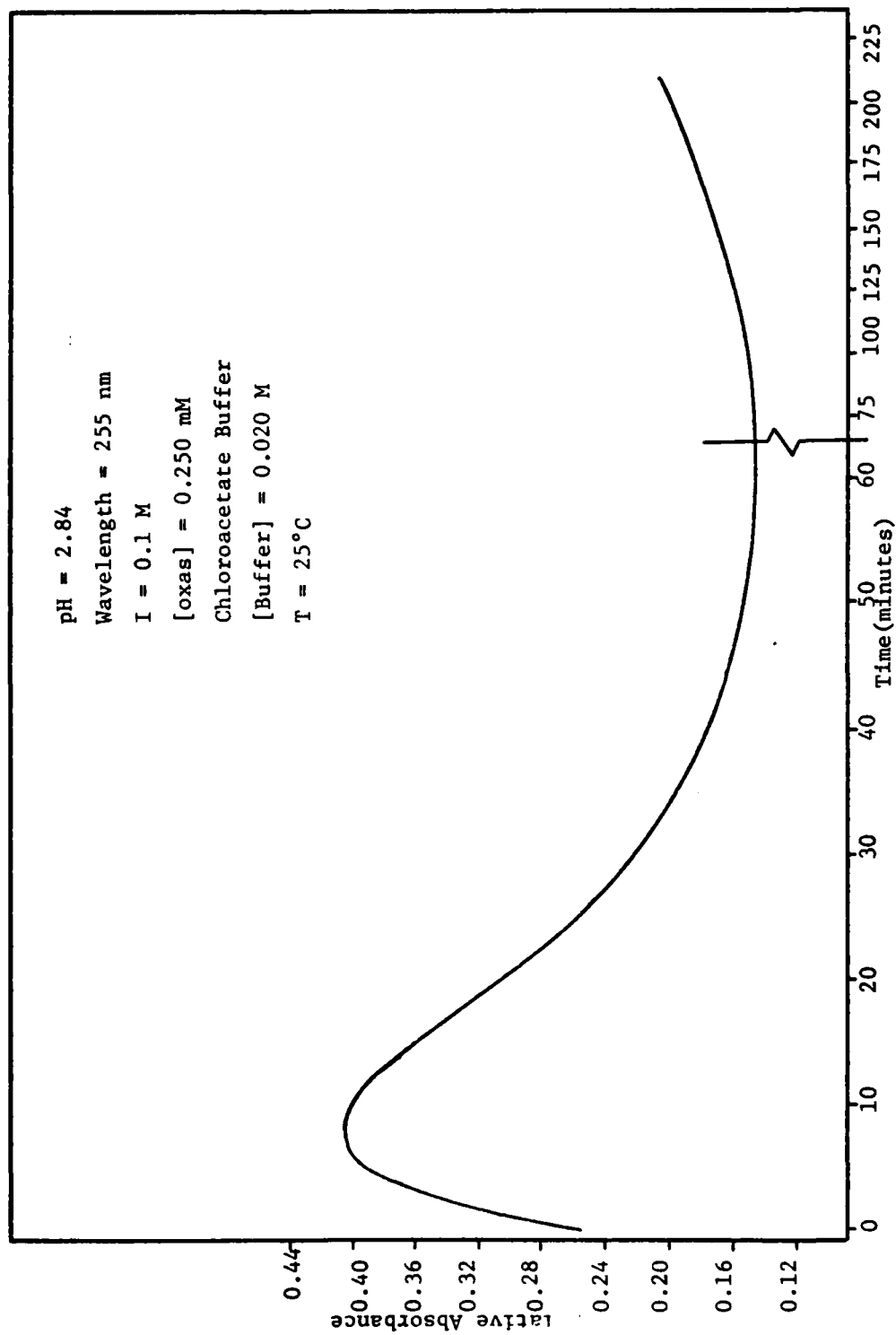


Figure 17. Spectrophotometric decarboxylation of oxalosuccinate.

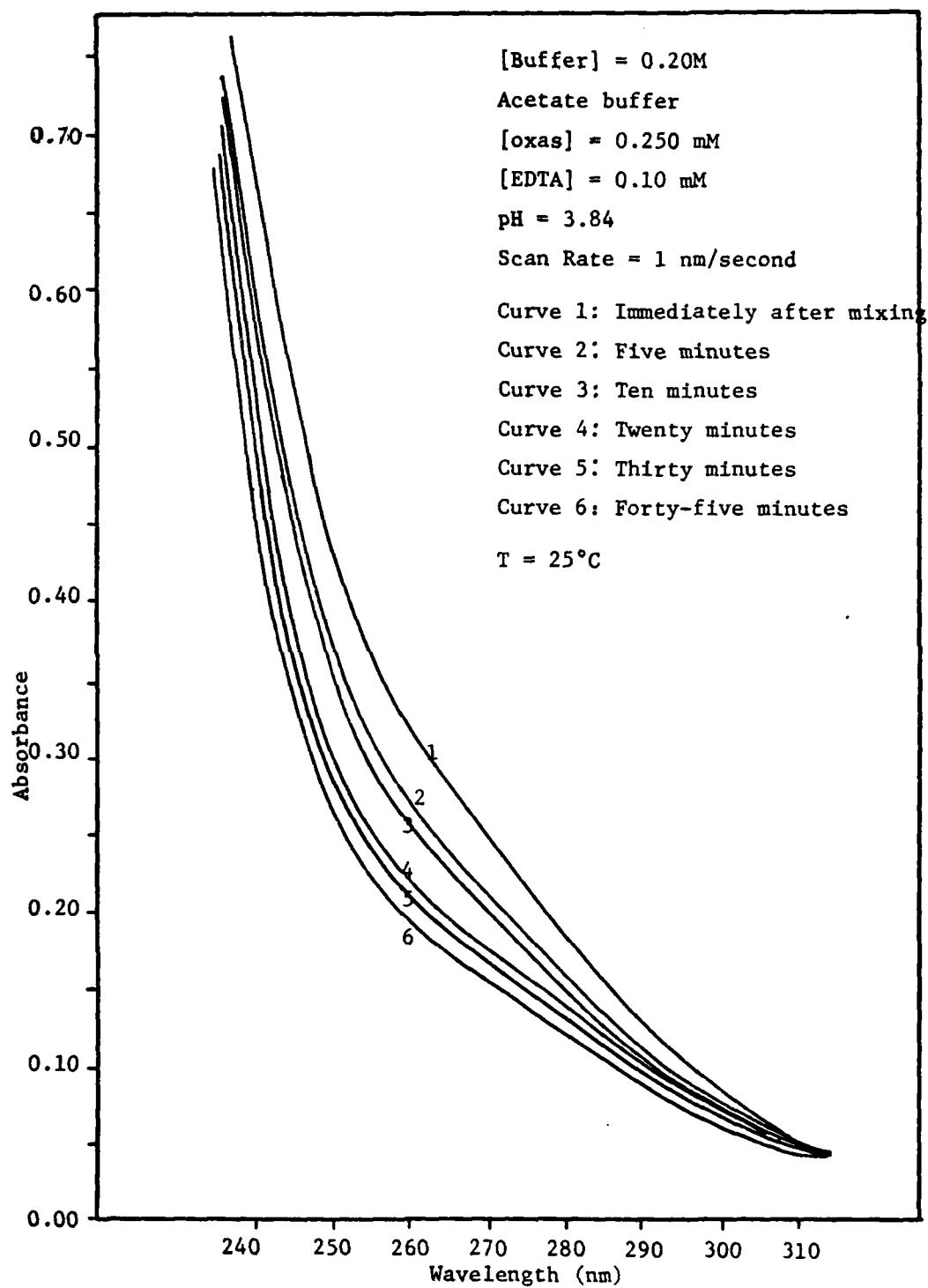


Figure 18. Reaction spectra versus time: slow scan rates.

decrease through the entire range of wavelengths. The spectrum taken after 45 minutes was nearly identical to the spectrum taken after 60 minutes, therefore, it is safe to assume that the reaction being observed is completed. Since the conversion of oxalosuccinate to  $\alpha$ -ketoglutarate results in an absorbance decrease (the extinction coefficients of  $\alpha$ -ketoglutarate are lower), then the absorbance decrease followed in Figure 18 was tentatively assigned the decarboxylation step.

However, Figure 19 shows the same reaction mixture at longer times. In this time scale, a slow absorbance increase, represented as region III in Figure 17, is observed. This is in contrast to the oxaloacetate system, which does not show any spectral changes after the decarboxylation step. Further discussion of this reaction will be deferred to a later portion of this chapter. At this point, the nature of the reaction is unknown.

Unfortunately, spectral changes in the fast reaction (region I of Figure 17) were not observed at these slow scan rates. Consequently, a reaction solution was observed in a rapid scanning instrument. At a scan rate of 100 nm/second, the entire spectrum was obtained in 0.60 seconds. The first of these plots is shown in Figure 20, which is a series of rapid scans taken 500 seconds apart. Scan number 1, taken about 15 seconds after mixing shows a slight shoulder at 270 nm, owing to the presence of oxalosuccinate enol. The remaining four spectra, however, converge on an isobestic point

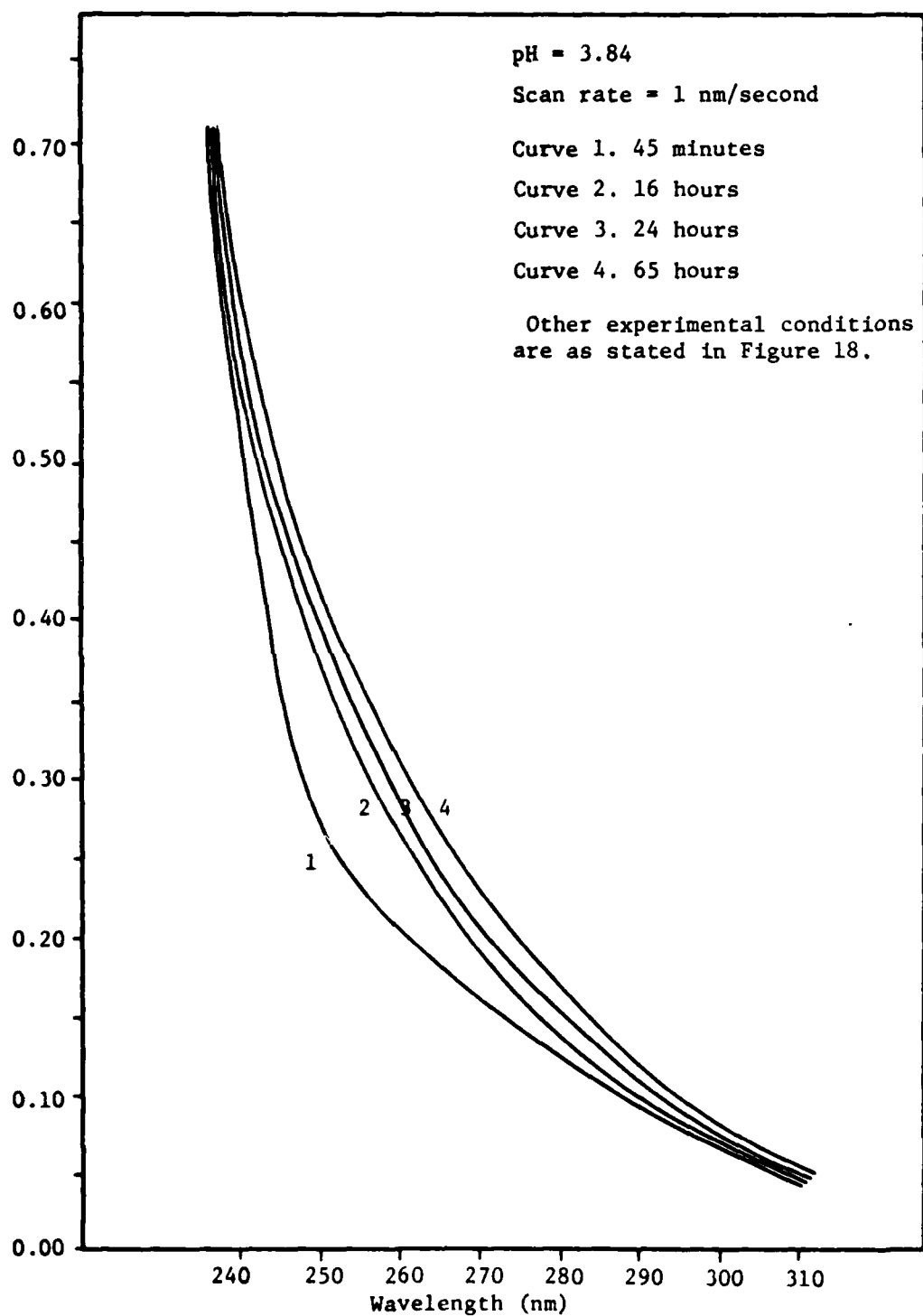


Figure 19. Reaction spectra versus time: longer times.



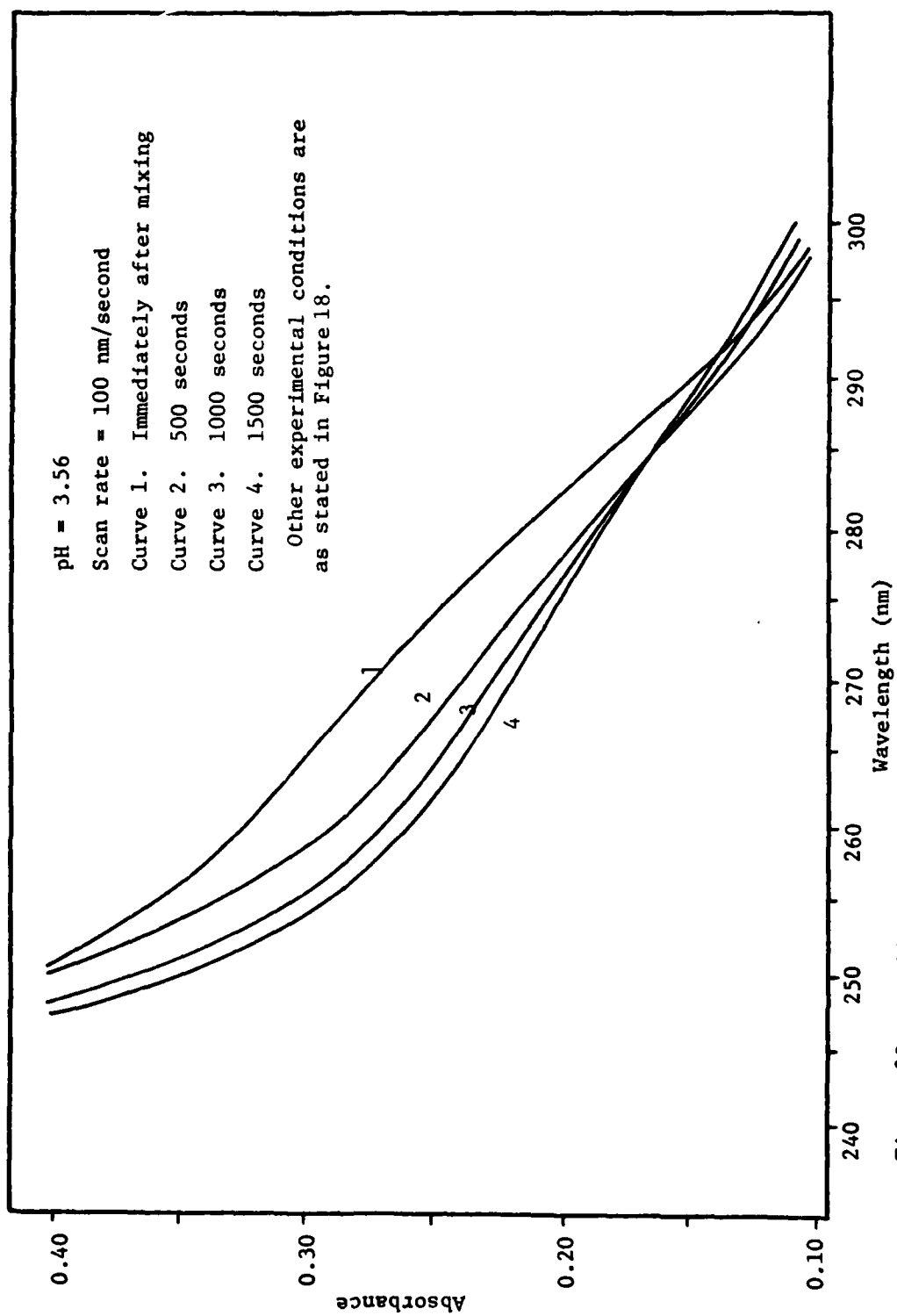
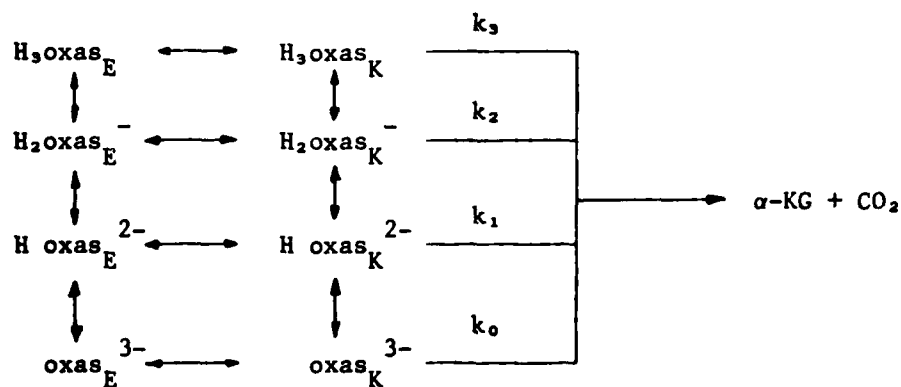


Figure 20. Rapid scanning spectra versus time; longer times.

at 285 nm. The appearance of this point indicates that a simple reaction is occurring. This has already been labeled as the decarboxylation step. Figure 21 shows why scan 1 does not pass through the isosbestic point. In this figure, the scans are taken at 10 second intervals. It is evident from this plot that a second isosbestic point, now at 257 nm, appears. Scan 1 on this figure, which is the same as scan 1 on Figure 20, passes through this point. As before, this indicates a simple but different reaction occurring. This faster reaction is the enolization of oxalosuccinate. Additional discussion of this reaction will also be deferred, since the reaction that is being considered, decarboxylation, will be covered first.

The reaction scheme proposed is shown below. The subscripts K and E refer to the keto and enol forms of the acid respectively.



Since the proton exchange between the solvent and oxyanions are very rapid, all verticle reactions can be considered to be in virtual equilibrium. Initially, let it also be assumed that tautomerization

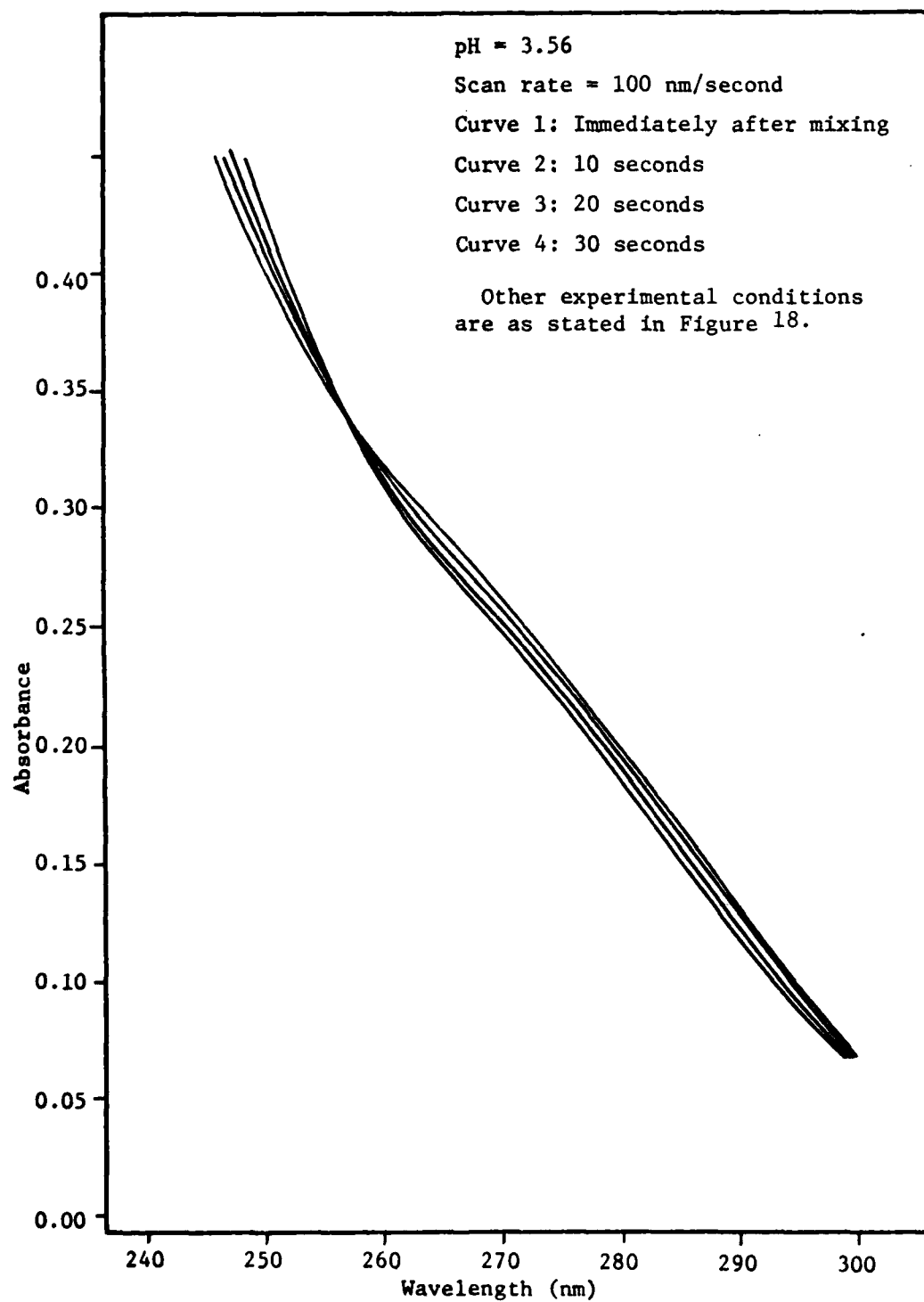


Figure 21. Rapid scanning spectra versus time: short times.

is rapid compared to decarboxylation. Therefore, the rate of formation of  $\alpha$ -ketoglutarate is

$$\frac{d[\alpha\text{-KG}]}{dt} = k_{\text{obs}} [\text{oxas}]_{\text{total}} = k_3 [\text{H}_3\text{oxas}_K] + k_2 [\text{H}_2\text{oxas}_K^-] + k_1 [\text{Hoxas}_K^{2-}] + k_0 [\text{oxas}_K^{3-}] \quad (1)$$

In this equation,  $k_{\text{obs}}$  is the observed rate constant, while  $[\text{oxas}]_{\text{total}}$  is the total concentration of all species of oxalosuccinate, or

$$[\text{oxas}]_{\text{total}} = [\text{H}_3\text{oxas}] + [\text{H}_2\text{oxas}] + [\text{Hoxas}^{2-}] + [\text{oxas}^{3-}] \quad (2)$$

By dividing equation (1) by  $[\text{oxas}]_{\text{total}}$  and defining the fraction of each species as  $\text{Fr}(n) = [\text{H}_n\text{oxas}]/[\text{oxas}]_{\text{total}}$ , one obtains

$$k_{\text{obs}} = k_3\text{Fr}(3) + k_2\text{Fr}(2) + k_1\text{Fr}(1) + k_0\text{Fr}(0) \quad (3)$$

Equation (3) states that the observed rate constant is a concentration-weighted average of the individual rate constants for the species present. The fraction of each species can be calculated in the following manner. Two mass balance equations are:

$$[\text{oxas}]_{\text{total}} = [\text{H}_3\text{oxas}_K] + [\text{H}_3\text{oxas}_E] + [\text{H}_2\text{oxas}_K^-] + [\text{H}_2\text{oxas}_E^-] + [\text{Hoxas}_K^{2-}] + [\text{Hoxas}_E^{2-}] + [\text{oxas}_K^{3-}] + [\text{oxas}_E^{3-}] \quad (4)$$

$$\begin{aligned}
[\text{H}]_{\text{total}} = & 3[\text{H}_3\text{oxas}_K] + 3[\text{H}_3\text{oxas}_E] + 2[\text{H}_2\text{oxas}_K^-] + 2[\text{H}_2\text{oxas}_E^-] + \\
& [\text{Hoxas}_K^{2-}] + [\text{Hoxas}_E^{2-}] - [\text{OH}^-] + [\text{H}^+]
\end{aligned} \quad (5)$$

where  $[\text{H}]_{\text{total}}$  is the total titratable hydrogen ion concentration.

By defining the keto to enol ratio,  $K_{T_n}$ , as

$$K_{T_n} = [\text{H}_n\text{oxas}_K] / [\text{H}_n\text{oxas}_E]$$

and noting the stepwise association constants,  $\beta_n$ , as

$$\beta_n = \frac{[\text{H}_n\text{oxas}]}{[\text{oxas}^{3-}][\text{H}^+]^n}$$

equations (4) and (5) reduce to

$$\begin{aligned}
[\text{oxas}]_{\text{total}} = & [\text{oxas}^{3-}] \left\{ \left(1 + \frac{1}{K_{T_n}}\right) \beta_3 [\text{H}^+]^3 + \left(1 + \frac{1}{K_{T_n}}\right) \beta_2 [\text{H}^+]^2 \right. \\
& \left. + \left(1 + \frac{1}{K_{T_1}}\right) \beta_1 [\text{H}^+] + \left(1 + \frac{1}{K_{T_0}}\right) \right\}
\end{aligned} \quad (6)$$

$$\begin{aligned}
[\text{H}]_{\text{total}} = & [\text{oxas}^{3-}] \left\{ 3\left(1 + \frac{1}{K_{T_3}}\right) \beta_3 [\text{H}^+]^3 + 2\left(1 + \frac{1}{K_{T_2}}\right) \beta_2 [\text{H}^+]^2 \right. \\
& \left. + \left(1 + \frac{1}{K_{T_1}}\right) \beta_1 [\text{H}^+] \right\} - [\text{OH}^-] + [\text{H}^+]
\end{aligned} \quad (7)$$

By solving equation (6) for  $[\text{oxas}^{3-}]$  and substituting that result into equation (7), the result is

$$[H]_{\text{total}} =$$

$$[oxas]_{\text{total}} \left\{ \frac{3(1 + \frac{1}{K_{T_3}})\beta_3 [H^+]^3 + 2(1 + \frac{1}{K_{T_2}})\beta_2 [H^+]^2 + (1 + \frac{1}{K_{T_1}})\beta_1 [H^+]}{(1 + \frac{1}{K_{T_0}}) + (1 + \frac{1}{K_{T_1}})\beta_1 [H^+] + (1 + \frac{1}{K_{T_2}})\beta_2 [H^+]^2 + (1 + \frac{1}{K_{T_3}})\beta_3 [H^+]^3} \right\} \\ + [H^+] - [OH^-] \quad (8)$$

From equation (8), it is evident that the fraction of each species can be defined as

$$Fr(0) = \frac{1 + \frac{1}{K_{T_0}}}{D} \quad (9)$$

$$Fr(n) = \frac{(1 + \frac{1}{K_{T_n}})\beta_n [H^+]^n}{D} \quad (10)$$

where D, the denominator in the first term of equation (8), is

$$D = (1 + \frac{1}{K_{T_0}}) + (1 + \frac{1}{K_{T_1}})\beta_1 [H^+] + (1 + \frac{1}{K_{T_2}})\beta_2 [H^+]^2 + (1 + \frac{1}{K_{T_3}})\beta_3 [H^+]^3$$

As shown in Chapter I, the mechanism for the decarboxylation of  $\beta$ -keto acids is to first form an  $\alpha$ -ketoglutarate enolate intermediate, which very rapidly consumes a proton from the solvent to form an enol,

followed by ketonization of the enol intermediate. To show the validity of this mechanism, three different techniques were employed to evaluate rate data. The first method was to observe the reaction spectrophotometrically. A second method was pH stat, that is, monitoring the amount of HCl added to the reaction in order to maintain a constant pH. A third method was to follow the spectral change of a specific pH indicator in an unbuffered solution. The first method follows the spectral change of the reactant to the product, while the last two monitor the uptake of the proton directly following the decarboxylation step.

A comparison of the methods is shown in Table 14. The table compares the slower rate constants evaluated through these methods. Also shown are the rate constants determined manometrically by various other workers. Based on the data, the rate of CO<sub>2</sub> evolution and the rate of proton uptake from the solvent agree with the rate of absorbance decrease at 255 and 240 nm. Thus, the convenience of monitoring the reaction spectrophotometrically can be used, since the slower absorbance decrease was the decarboxylation of oxalosuccinate.

The data in Table 14 verifies that the decarboxylation mechanism of oxalosuccinate is typical of  $\beta$ -keto acids. This mechanism, given in Chapter I, is the loss of CO<sub>2</sub> from oxalosuccinate (I), forming an enolate (II). This enolate rapidly protonates, forming the enol of the reaction product,  $\alpha$ -ketoglutarate. This enol rapidly ketonizes, completing the reaction sequence (III).

TABLE 14  
COMPARISON OF SPECTROPHOTOMETRIC, pH STAT, pH INDICATOR, AND  
MANOMETRIC DETERMINATIONS OF THE DECARBOXYLATION RATE CONSTANT

Rate Constant	pH	Method
4.49E-04	5.10	A
3.54E-04	5.45	B
3.27E-04	5.44	C
2.55E-04	5.91	C
2.70E-04	6.04	B
7.18E-04	4.78	D
6.83E-04	4.57	E
6.71E-04	4.57	B
1.41E-03	3.50	D
1.47E-03	3.17	C
1.39E-03	3.58	B
1.43E-03	3.64	E

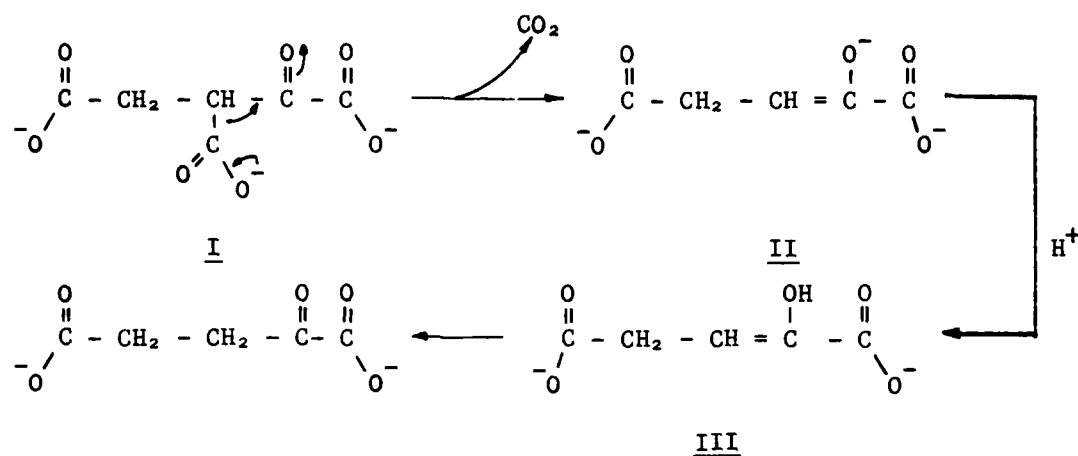
Methods:

- A = Manometric data of OCHAO (2)
- B = Spectrophotometric, 240 nm
- C = pH stat
- D = pH indicators
- E = Spectrophotometric, 255 nm

Note:

The rate constant has units of 1/seconds.





The data for the observed rate constant as a function of pH is shown in Figure 22. Rate data taken spectrophotometrically at 255 and 280 nm, pH stat, and pH indicator are all indicated. The rate constants were obtained by curve-fitting the response (absorbance, volume HCl) versus time data into the program RLXFT, which evaluated the rate constant via the equation

$$A_{\text{obs}} = A_1 \exp(-k_1 t) + A_2 \exp(-k_2 t) + A_{\infty} \quad (12)$$

where  $A_{\text{obs}}$  is the observed response at time  $t$ , and  $A_{\infty}$  is the final response at  $t = \infty$ . Also shown on this figure is the data point evaluated by Ochoa (2) manometrically.

Figure 22

Observed decarboxylation rate constant versus pH

- Spectrophotometric data at 240 nm
- Spectrophotometric data at 255 nm
- pH stat data
- △ pH indicator data
- × Manometric data by Ochoa

$I = 0.1 \text{ M}$

$[\text{oxas}] = 0.400 \text{ mM}$

$[\text{buffer}] = 0.020 \text{ M}$

<u>pH range</u>	<u>Buffer used</u>
2.0 - 3.8	Chloroacetate
3.7 - 5.6	Acetate
5.6 - 6.5	MES
6.5 - 9.0	HEPES

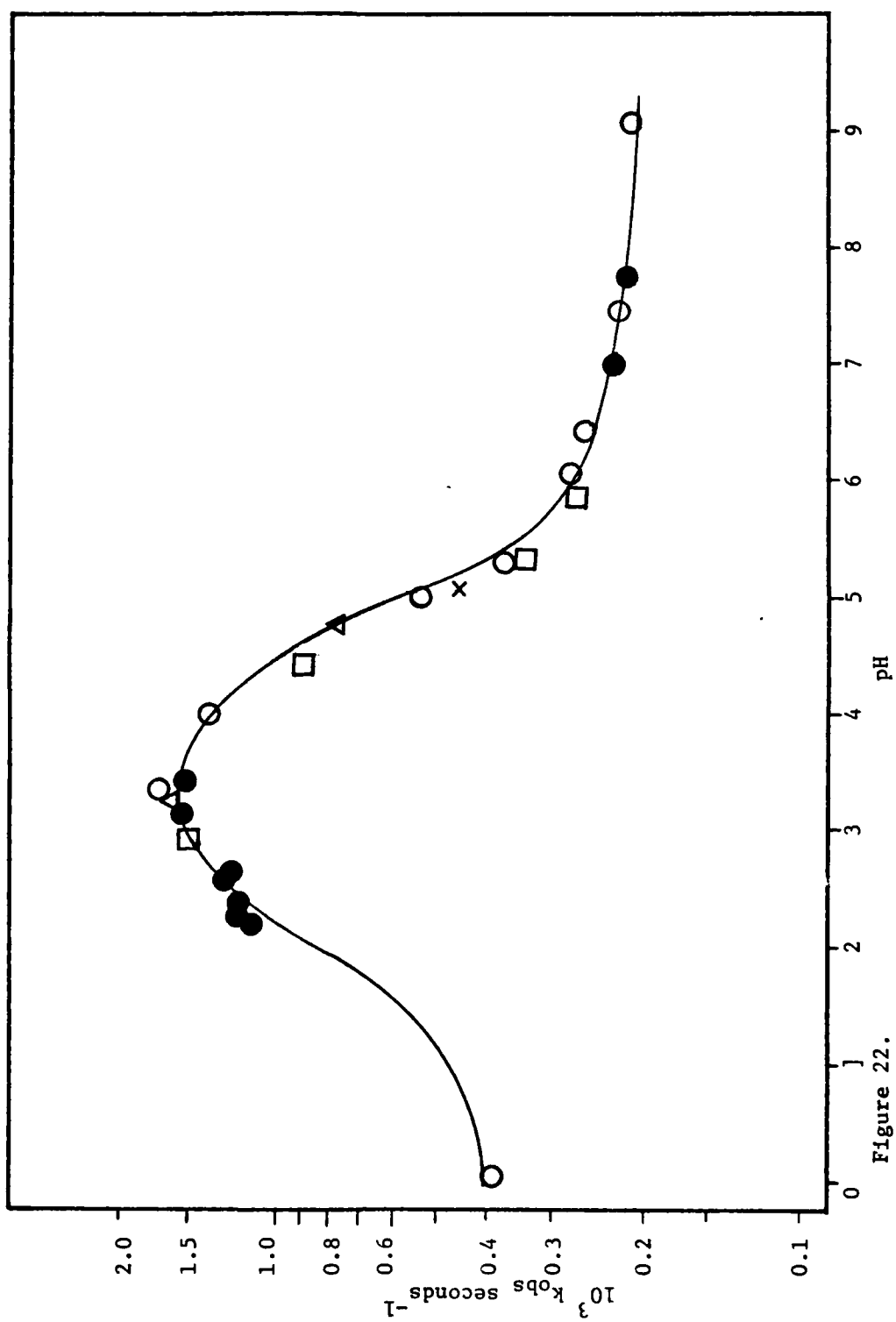


Figure 22.

The solid line is the theoretical curve calculated from equation (3). The fraction of each species was calculated via equations (9) to (11). For this data, it was assumed that oxalosuccinate was predominantly in the keto form. Thus,  $K_{T_n}$  was large, and  $1/K_{T_n}$  was negligible compared to 1. The simplified equations for the fractions therefore become

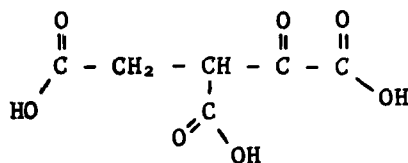
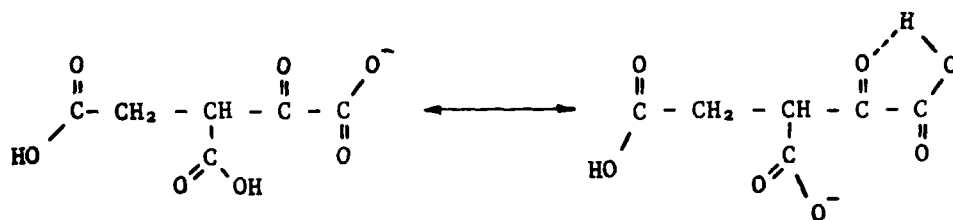
$$\text{Fr}(0) = \frac{1}{1 + \beta_1[\text{H}^+] + \beta_2[\text{H}^+]^2 + \beta_3[\text{H}^+]^3} \quad (13)$$

$$\text{Fr}(n) = \frac{\beta_n [\text{H}^+]^n}{1 + \beta_1[\text{H}^+] + \beta_2[\text{H}^+]^2 + \beta_3[\text{H}^+]^3} \quad (14)$$

The individual rate constants  $k_0$ ,  $k_1$ ,  $k_2$ , and  $k_3$  as well as the formation constants were all evaluated using the program CORNEK (see Appendix D). In order to gain maximum utility from the program, fairly accurated estimates were required. These were obtained in the following way. The initial formation constants were those obtained at 0°C by the spectrophotometric titration. The initial values of 4.6, 7.4, and 9.3 for  $\log \beta_1$ ,  $\log \beta_2$ ,  $\log \beta_3$  respectively were close to the kinetically determined values of 4.5, 7.1, and 9.0. The initial rate constants were also fairly easy to obtain. The rate constant observed spectrophotometrically at a pH of 0.037 was the initial guess for  $k_3$ , since most of the oxalosuccinate at that pH is in the form of

$\text{H}_3\text{oxas}$ . Similarly, the spectrophotometrically determined rate constant at  $\text{pH} = 9.14$  became the initial guess for  $k_0$ . At a  $\text{pH}$  equal to  $\text{pK}_{3a}$ , the distribution of oxalosuccinate is approximately half oxalosuccinate<sup>3-</sup> and half Hoxalosuccinate<sup>2-</sup>. Since, under these conditions,  $k_{\text{obs}} = \frac{1}{2}k_0 + \frac{1}{2}k_1$ , then  $k_1 = 2k_{\text{obs}} - k_0$ . Also, at a  $\text{pH}$  equal to  $\text{pK}_{1a}$ , oxalosuccinate is approximately half  $\text{H}_3\text{oxalosuccinate}$  and half  $\text{H}_2\text{oxalosuccinate}^-$ . In this case,  $k_2 = 2k_{\text{obs}} - k_3$ .

The results of the fit are shown in Table 15. As one would expect, the diprotonated form, Va, decarboxylates faster than the

IVVaVb

triprotonated form, IV. This is due to the fact that the unionized molecule IV must first lose a proton to the solvent before it can

TABLE 15

## SPONTANEOUS DECARBOXYLATION OF OXALOSUCCINIC ACID

Reaction		Rate Constant	Std Dev
H3Oxas $\rightarrow$ CO <sub>2</sub> + $\alpha$ KG		3.704E-04	2.655E-05
H2Oxas $\rightarrow$ CO <sub>2</sub> + $\alpha$ KG		1.036E-03	9.085E-05
H Oxas $\rightarrow$ CO <sub>2</sub> + $\alpha$ KG		1.697E-03	4.535E-05
Oxas $\rightarrow$ CO <sub>2</sub> + $\alpha$ KG		2.222E-04	5.709E-06

Complex	Log Beta
H3Oxas	4.467
H2Oxas	7.127
H Oxas	8.991

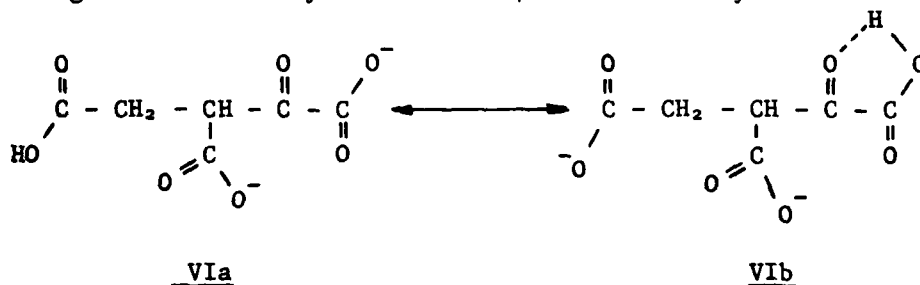
  

Exp	[(Oxas)]	pH	K(Obs)	K(Calc)	% Dev
1	4.00E-04	0.04	3.90E-04	3.91E-04	- 0.27
2	4.00E-04	2.36	1.18E-03	1.10E-03	6.84
3	4.00E-04	2.51	1.22E-03	1.20E-03	1.95
4	4.00E-04	2.56	1.22E-03	1.23E-03	- 0.57
5	4.00E-04	2.84	1.30E-03	1.38E-03	- 5.80
6	4.00E-04	2.89	1.25E-03	1.40E-03	-11.73
7	4.00E-04	3.17	1.47E-03	1.48E-03	- 0.65
8	4.00E-04	3.46	1.50E-03	1.50E-03	0.35
9	4.00E-04	3.50	1.61E-03	1.49E-03	7.41
10	4.00E-04	3.58	1.74E-03	1.48E-03	15.04
11	4.00E-04	3.64	1.43E-03	1.47E-03	- 2.45
12	4.00E-04	4.06	1.36E-03	1.28E-03	6.26
13	4.00E-04	4.49	9.06E-04	9.41E-04	- 3.84
14	4.00E-04	4.78	7.19E-04	7.06E-04	1.86
15	4.00E-04	5.05	5.49E-04	5.29E-04	3.81
16	4.00E-04	5.15	4.49E-04	4.76E-04	- 6.00
17	4.00E-04	5.44	3.54E-04	3.64E-04	- 2.87
18	4.00E-04	5.45	3.27E-04	3.61E-04	-10.47
19	4.00E-04	5.91	2.55E-04	2.74E-04	- 7.28
20	4.00E-04	6.04	2.70E-04	2.61E-04	3.48
21	4.00E-04	6.41	2.61E-04	2.39E-04	8.49
22	4.00E-04	7.06	2.30E-04	2.26E-04	1.75
23	4.00E-04	7.44	2.27E-04	2.24E-04	1.42
24	4.00E-04	7.48	2.31E-04	2.24E-04	3.19
25	4.00E-04	9.14	2.20E-04	2.22E-04	- 1.02

## Notes:

1. Molar concentrations are used.
2. Units on the rate constants are 1/sec.

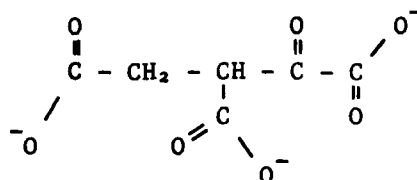
decarboxylate. The monoanion, Va, can exist in equilibrium as Vb, which can readily decarboxylate. Hydrogen bonding of the carboxyl proton  $\alpha$  to the carbonyl forms a stable ring, further enhancing the electron withdrawing ability of the carbonyl group. Removal of another proton, yielding structure Via, causes a 60% increase in the decarboxylation rate. This structure is in equilibrium with Vib via an intramolecular hydrogen shift. In this case, the increased reaction rate could be caused by two effects. First, the formation of a stable ring through hydrogen bonding creates a stronger electron sink in the carbonyl, and, second, an inductive effect caused by the charge on the carboxylate that is  $\gamma$  to the carbonyl.



This inductive effect does not appear on the diprotonated species Vb.

However, the unprotonated form, VII, decarboxylates slower than any of the species. In fact, it decarboxylates about 40% slower than the fully protonated molecule. This is in contrast to the

oxaloacetate system, in which the deprotonated form decarboxylates about 67% faster than the fully protonated species, owing to the extensive hydration of H<sub>2</sub>oxac.



### VII

It was mentioned at the outset of this chapter that the initial absorbance increase observed in the decarboxylation reaction was the tautomerization of oxalosuccinate. This will now be verified by some experimental evidence. Before presenting this evidence, however, it is necessary to first discuss the source of the absorbance increase.

The procedure for the preparation of an oxalosuccinate solution was reported in Chapter II. After dissolving the barium salt in HCl and precipitating out the barium, the pH of the solution at 0°C was adjusted to a value close to that of the experiment being conducted. Therefore, the equilibration of oxalosuccinate between the enol, keto, and hydrate forms at 0°C at the experimental pH should be complete before the experiment begins. This cold solution was rapidly brought to 25°C with the hot buffer as the experiment began. Because the equilibrium constants are thermodynamic functions, the distribution



of the species will shift as the temperature changes. The net result was a temperature jump experiment, in which the different forms of oxalosuccinate must reequilibrate simultaneously to the decarboxylation of the keto at the new temperature, 25°C. This temperature perturbation is the cause of the faster absorbance increase.

Since it is now established that the first relaxation resulted from a shift in the equilibrium species, the question is: is this relaxation due to hydration/dehydration or the keto/enol tautomerization? The first piece of evidence is seen in Figure 23, which shows the dependence of the relaxation rate on the buffer concentration. For this investigation, the buffer concentration was adjusted from 0.016 M to 0.080 M, while maintaining the ionic strength at 0.1 M by the addition of NaCl. From this data then, it is apparent that the relaxation rate is a strong function of the buffer concentration. Unfortunately, this investigation cannot determine the actual nature of the relaxation since tautomerization and hydration are buffer dependent. But one can conclude that the absorbance change is not due to the formation of the  $\alpha$ -ketoglutarate enolate intermediate, since the formation of the enolate is independent of the buffer concentration.

Additional evidence dealing with the nature of the relaxation reaction can be seen in Figure 21, which shows a series of UV scans taken every ten seconds at a rate of 100 nm/second. This figure shows the definite presence of an isosbestic point, indicating that only one

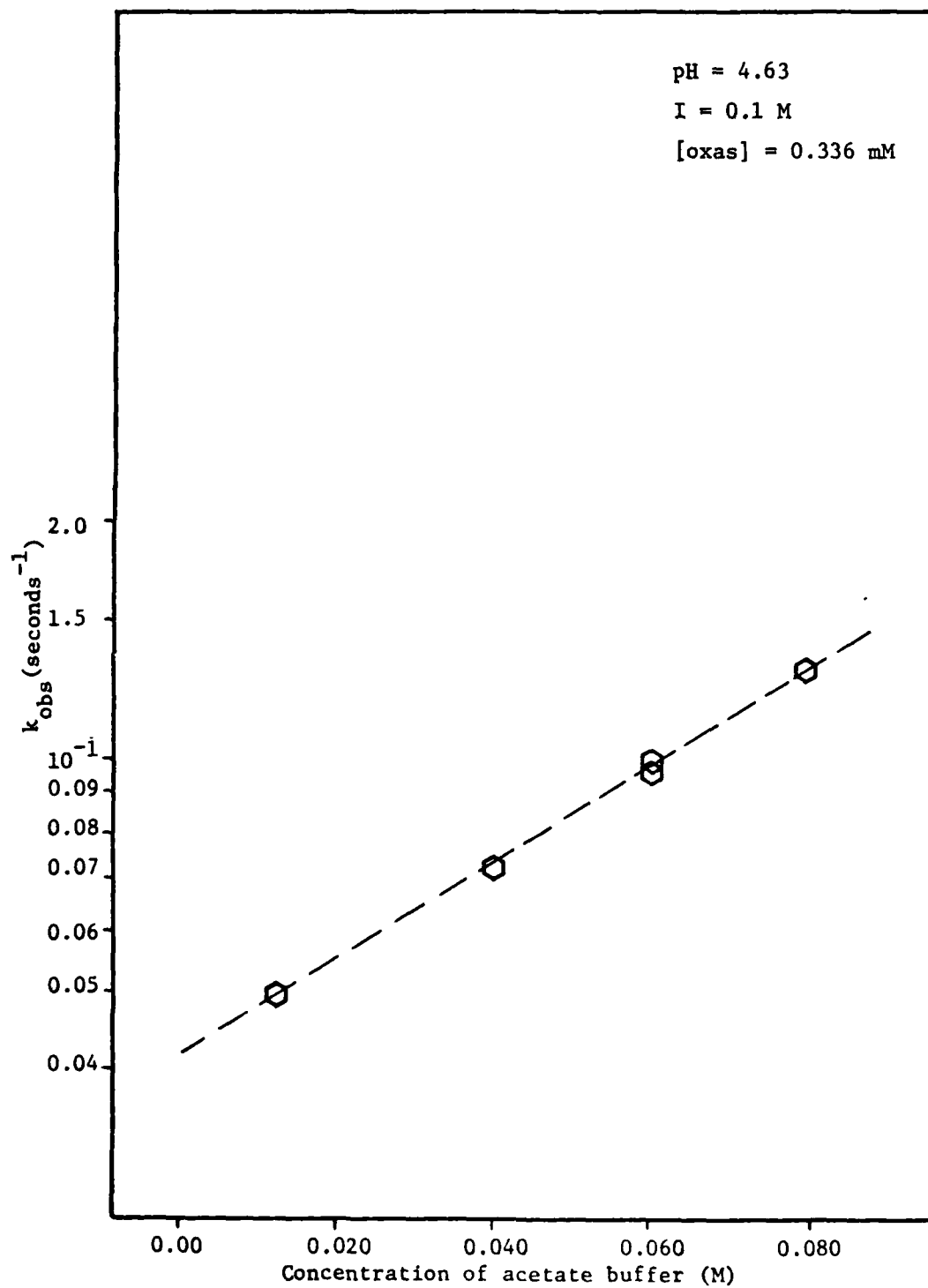


Figure 23. Dependence of the fast relaxation on the concentration of acetate.

reaction is occurring. Close inspection of the shape of successive scans shows that the size of the shoulder is increasing. Of the three forms, only the enol has a spectral band typical to that seen in this set of scans. Since only one reaction is occurring, it must therefore be the tautomerization equilibrium and not hydration/dehydration.

Now that the nature of the relaxation is resolved, the next step is to examine the tautomerization rates in relation to the observed decarboxylation. The tautomerization rates are plotted in Figure 24 as a function of pH. These rates were determined by analyzing the biphasic absorbance changes (as shown in Figure 17) by the program RLXFT, which gave the decarboxylation rate constant ( $k_1$  in Equation (12)) as well as the tautomerization relaxation rate ( $k_2$  in Equation (12)) for a particular experiment. Therefore, the experimental conditions for the data in Figure 24 are identical to those of the decarboxylation rate profile, Figure 22.

Inspection and comparison of the two figures reveals the following. At pH values greater than 4, the tautomerization relaxation rate is at least a full order of magnitude faster than decarboxylation. At low pH values, this rate is at least 50% faster than decarboxylation. Therefore, this rate always exceeds the rate of  $\text{CO}_2$  loss. From kinetics, this relaxation rate is equal to the sum of the forward rate constant plus the backward rate constant, or, for this reaction,

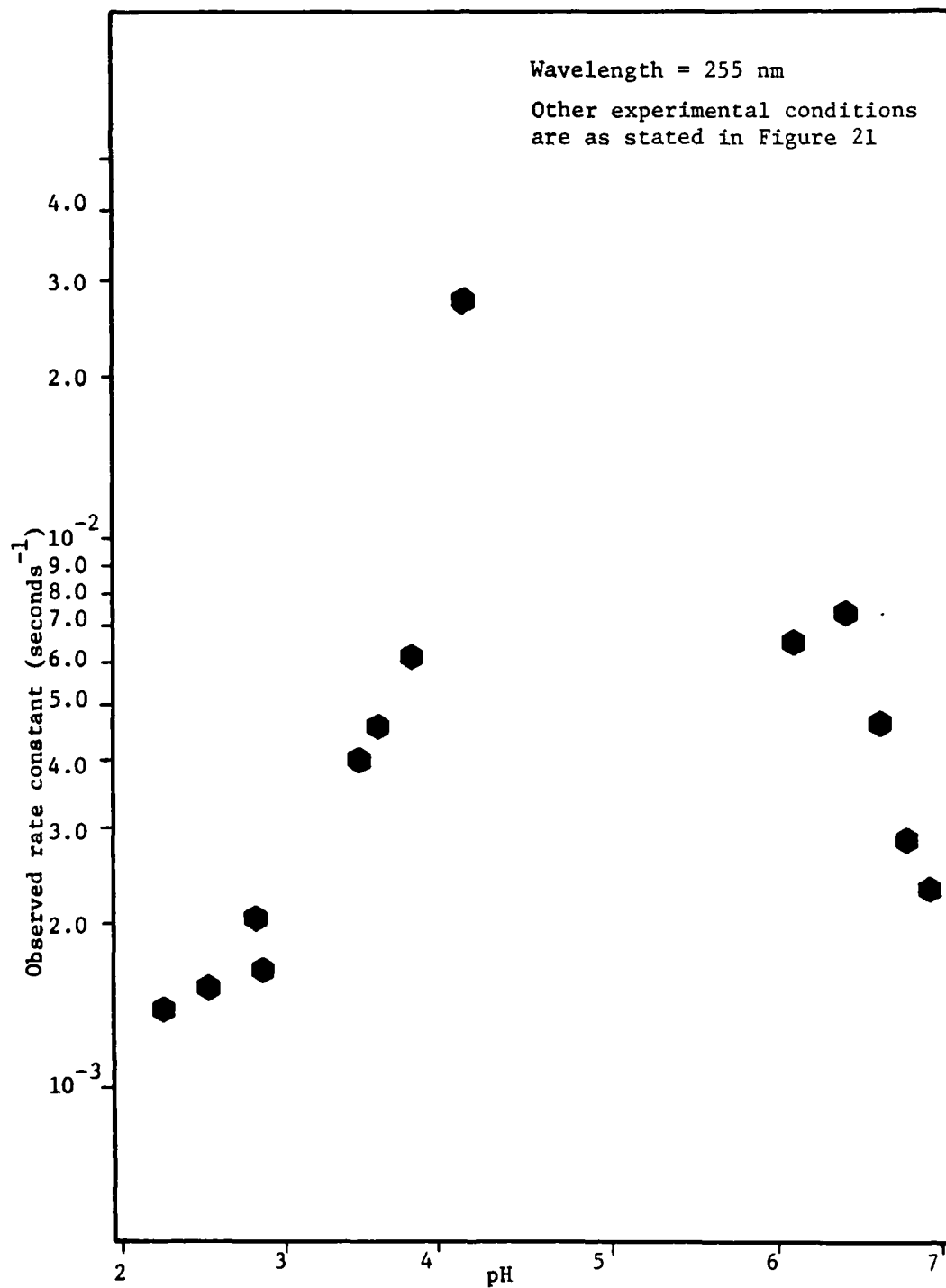


Figure 24. Rate constant for the fast relaxation versus pH.



the rates plotted in Figure 24 are:

$$k_{\text{obs}} = k_f + k_b \quad (16)$$

From the data for the tautomerization relaxation rate profile shown in Figure 24, the individual rate constants,  $k_f$  and  $k_b$ , can be evaluated. Noting that the equilibrium constant for reaction (15),  $K_T$ , is  $k_f/k_b$ , then equation (16) becomes

$$k_{\text{obs}} = k_f (1 + 1/K_T)$$

Therefore, the individual rate constants for the tautomerization relaxation can be evaluated from the two equations below.

$$k_f = k_{\text{obs}} / (1 + 1/K_T)$$

$$k_b = k_f / K_T$$

The equilibrium constant  $K_T$ , will be discussed shortly. However, the results of that investigation will be used here. Some representative values for  $k_f$  and  $k_b$ , as well as the decarboxylation rate constant  $k_{-\text{CO}_2}$ , are shown below as a function of pH. The rate constants have units of seconds<sup>-1</sup>.

pH	$10^3 k_{\text{obs}}$	$K_T$	$10^3 k_f$	$10^5 k_b$	$10^3 k_{-\text{CO}_2}$
2.36	1.53	364	1.53	0.42	1.10
2.89	2.13	303	2.13	0.70	1.40
3.56	4.08	289	4.08	1.41	1.48
3.93	6.27	300	6.27	2.09	1.32
4.06	28.7	312	28.7	9.20	1.28
4.63	51.2	375	51.2	13.7	0.75
5.91	7.13	444	7.13	1.61	0.27
6.53	4.91	458	4.91	1.07	0.23
6.92	2.34	465	2.43	0.50	0.22

From these values, some observations can be made. The rate of enolization is slow relative to decarboxylation. However, the rate of formation of the decarboxylating keto species is considerably larger than the rate of decarboxylation. In fact, at pH values greater than 4, ketonization is a full order of magnitude faster than decarboxylation. Notice also that the amount of keto is at least 289 times greater than the amount of enol at equilibrium. Because oxalosuccinate is primarily keto and the enol to keto transformation is rapid compared to decarboxylation, it is concluded that the keto-enol relaxation equilibrium will not interfere with the analysis of the decarboxylation data.

It is apparent from this discussion that the kinetics are dependent upon the keto/enol ratio. To determine the amount of enol

present, the following investigation was performed. A 1.0 cm quartz cell was partially filled with 2.30 ml H<sub>2</sub>O and 0.40 ml solution composed of 0.258 mM I<sub>3</sub><sup>-</sup>. The cell was then placed in a Cary 14 spectrophotometer. The Cary 14 was set at a wavelength of 352 nm to monitor the consumption of I<sub>3</sub><sup>-</sup>. The recorder, operating at 8 inches per minute, was switched to RUN. The absorbance reading of this solution gave the initial concentration of I<sub>3</sub><sup>-</sup>. While the recorder was running, 0.30 ml of an unbuffered solution of oxalosuccinate was syringed directly into the cell through a light-tight opening in the cell compartment. Upon this injection, an absorbance decrease was immediately observed. This decrease resulted from two sources: dilution of the iodine in the cell as well as the loss of iodine due to its reaction with the enol. Because the initial iodine solution was diluted by 10%, then the amount of iodine consumed by the reaction was  $(0.9A_0 - A_1)/24,500$ , where  $A_0$  is the initial absorbance in the cell,  $A_1$  is the absorbance after the addition of oxalosuccinate, and 24,500 is the extinction coefficient of I<sub>3</sub><sup>-</sup> in M<sup>-1</sup>cm<sup>-1</sup> at 352 nm. Therefore, the fraction of oxalosuccinate that is enol is

$$\text{fraction enol} = \frac{0.9A_0 - A_1}{(24,500)C_{\text{oxas}}} \quad (17)$$

As an example, consider the experiment represented in Figure 25. In this experiment, at a pH of 3.49, the initial absorbance  $A_0$  of

the iodine solution just prior to the addition of oxalosuccinate was 0.905. Upon the addition of 0.30 ml of an oxalosuccinate solution at a concentration of 1.03 mM (A in the figure), the absorbance quickly dropped and subsequently dropped further at a semi-linear rate (in this time frame). This decay curve can be extrapolated back to the point of injection, which corresponds to an absorbance of 0.723. If no enol was present, this value should correspond to the initial absorbance corrected for dilution, or  $(0.9)(0.905) = 0.815$ . This experiment shows that the amount of iodine consumed by the enol was  $(0.815 - 0.723)/24,500$ , or  $3.73 \times 10^{-6} \text{ M}$ . Since this is equal to the concentration of enol, then the fraction enol is  $3.73 \times 10^{-6} / 1.03 \times 10^{-3}$ , or  $3.63 \times 10^{-3}$ .

This data point as well as data at nine other pH values are plotted in Figure 26. The data was analyzed by the program CORNEK in a manner analogous to the decarboxylation pH profile. Since proton exchange is very rapid, then the observed keto/enol ratios must be an average of all the species present. Thus, the observed ratio,  $K_T$ , is

$$K_{T_{\text{obs}}} = K_{T_0} \text{Fr}(0) + K_{T_1} \text{Fr}(1) + K_{T_2} \text{Fr}(2) + K_{T_3} \text{Fr}(3) \quad (18)$$

where  $\text{Fr}(n)$  is the fraction of the oxalosuccinate species containing  $n$  protons.

Initially, the data was analyzed by using the kinetically determined formation constants. Once the approximate ratios are found, then the



Figure 25

Experimental trace from the Cary 14 for the determination of the enol content of oxalosuccinate.

$$T = 25^{\circ}\text{C}$$

$$\text{pH} = 3.49$$

$$[\text{oxas}] = 1.03 \text{ mM}$$

$$V_{\text{oxas}} = 0.30 \text{ ml}$$

$$[\text{I}_3^-] = 3.82 \times 10^{-5} \text{ M (prior to the addition of oxas)}$$

$$V_{\text{I}_3^-} = 0.40 \text{ ml}$$

$$V_{\text{total}} = 3.0 \text{ ml}$$

$$\text{Path length} = 1.0 \text{ cm}$$

At Point A, the oxas is added (see text)

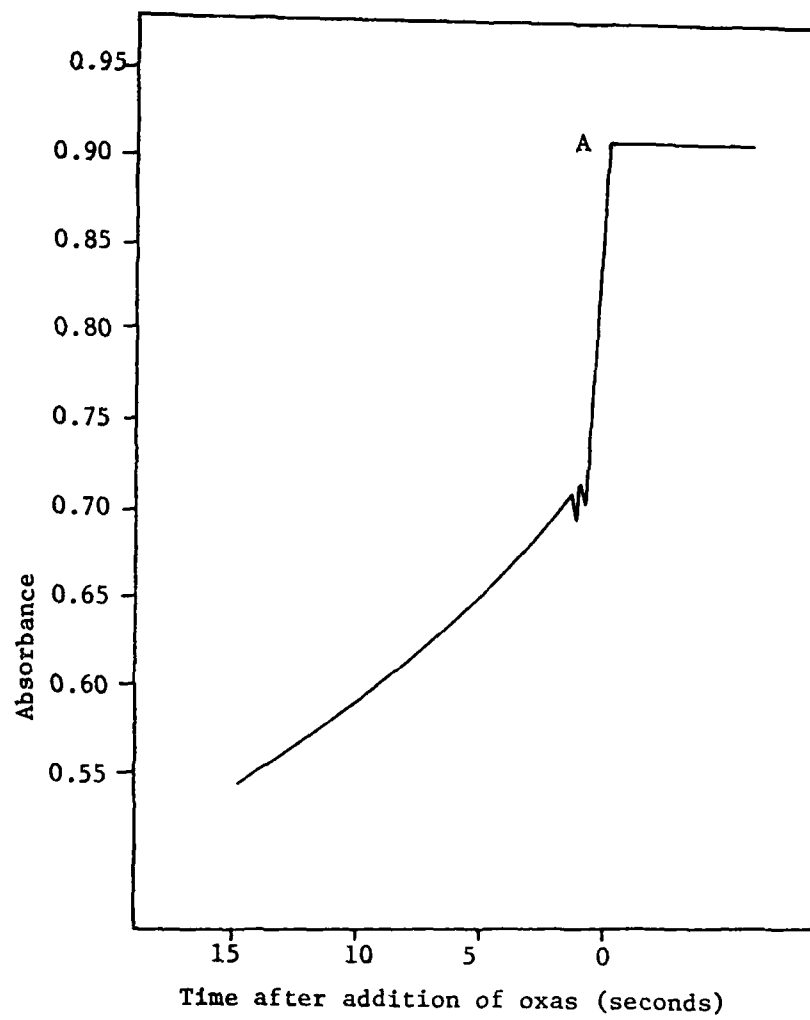


Figure 25.

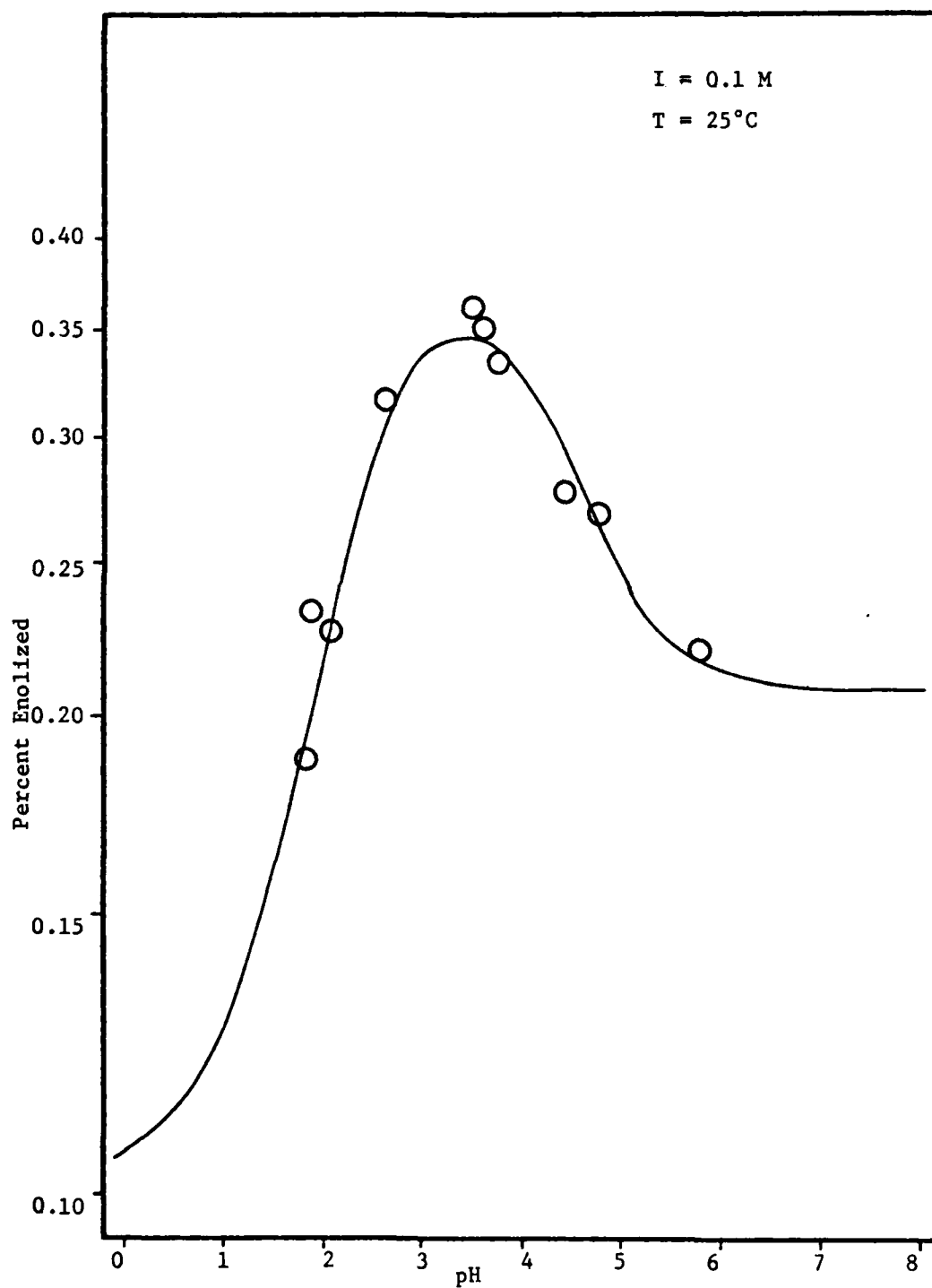
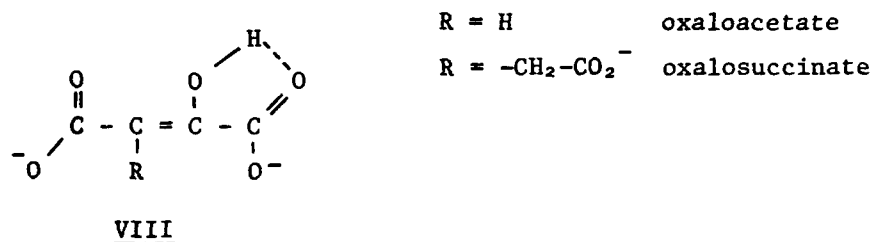


Figure 26. Percent oxalosuccinate enolized versus pH.

formation constants can be optimized to obtain the best fit for the data. The results of this computer fit are shown in Table 16. The calculated values are represented as the solid line in Figure 26. These low values are in contrast to oxaloacetate, which is about 5-12% enolized.

The low amount of enol in equilibrium with the keto (relative to oxaloacetate) can be explained by examining the structure of the enols of the two compounds. This is shown in VIII. The enol would be the preferred structure if it were more stable than the keto form. The



stabilization of the enol can result from three sources: hydrogen bonding of the enol proton to the carboxylate group, conjugation of the double bond, while the third is inductive stabilization. The effect of substituting  $-\text{CH}_2 - \text{CO}_2^-$  group, an electron donating group, on oxalosuccinate for the proton on oxaloacetate is to destabilize the enol due to the high electron charge density on the double bond.

Since the keto/enol ratio,  $K_T$ , ranges from 269 to 943, the term  $1 + 1/K_T$  can be approximated as 1.0. Thus, the simplified equations

TABLE 16  
KETO/ENOL RATIOS OF OXALOSUCCINIC ACID

Species	Fraction Enol	Std Dev
H3Oxas	1.060E-03	4.688E-04
H2Oxas	2.830E-03	4.272E-04
H Oxas	3.720E-03	1.722E-04
Oxas	2.090E-03	1.376E-04

---

Complex	Log Beta
H3Oxas	4.402
H2Oxas	6.999
H Oxas	8.889

---

Exp	[(Oxas)]	pH	FR(Obs)	FR(Calc)	% Dev
1	1.07E-03	1.78	1.90E-03	1.95E-03	-2.71
2	1.06E-03	1.89	2.34E-03	2.11E-03	10.10
3	1.05E-03	2.13	2.27E-03	2.46E-03	-8.23
4	1.04E-03	2.61	3.17E-03	3.08E-03	2.73
5	1.03E-03	3.49	3.63E-03	3.46E-03	4.60
6	1.02E-03	3.61	3.52E-03	3.44E-03	2.31
7	1.01E-03	3.76	3.35E-03	3.38E-03	-1.03
8	3.22E-04	4.42	2.76E-03	2.89E-03	-4.61
9	9.60E-04	4.74	2.68E-03	2.60E-03	2.87
10	8.11E-04	5.81	2.21E-03	2.15E-03	2.66

Notes:

1. The ionic strength was set at 0.1 M.
2. The experiment was carried out at 25°C.

for the fractional distribution, (13) and (14), apply. Another consequence of the large value of the keto/enol ratio, according to equation (19), is that the observed rate constant for each species is accurate and does not need to be adjusted.

$$k_n(\text{actual}) = k_n(\text{obs}) / (1 + K_{T_n}) \quad (19)$$

Inspection of Figure 25 reveals that iodination is very rapid compared to the rate of tautomerization. It is demonstrated in the figure that the consumption of iodine by the enol initially present in solution was completed in about two seconds. From the tautomerization analysis, the slowest half-life observed for the forward rate (ketonization) is 23 seconds at a pH of about 4. This verifies that iodination, under the experimental conditions in Figure 25, is very fast compared to tautomerization.

Based on the fact that less than  $\frac{1}{2}\%$  of the oxalosuccinate is in the enol form and that the rate of ketoinization is much faster than decarboxylation, it can be concluded that the tautomerization reaction does not interfere with the decarboxylation step. Therefore, the complex analysis of tautomerization data (26,55) is not necessary for the decarboxylation study. It can also be concluded that the enol form of oxalosuccinate is solely responsible for the initial rapid absorbance increase of the reaction, and not the enol of  $\alpha$ -ketoglutarate.

This is due to the fact that the tautomerization relaxation rate is at least four times faster than the rate of decarboxylation. Thus, keto/enol equilibration is essentially complete before decarboxylation becomes significant.

Upon completion of the decarboxylation of oxalosuccinate, a very slow absorbance increase is observed. The time dependence of the spectra was previously shown in Figure 19. From these spectra, it can be seen that the decarboxylation was completed in about 45 minutes, while the next reaction was still in progress after 65 hours. Calculations based on the observed extinction coefficients indicate that the spectrum at 45 minutes is  $\alpha$ -ketoglutarate at a concentration of 1.45 mM. Therefore, this very slow absorbance increase is due to a reaction involving  $\alpha$ -ketoglutarate. The rate, measured at a pH of 3.56, was  $2.7 \times 10^{-5}$  seconds<sup>-1</sup>. This is two orders of magnitude slower than the decarboxylation. The half life of this reaction is 7.13 hours.

Several experiments were conducted in an attempt to deduce the nature of the reaction. One experiment was to monitor the concentration of  $\alpha$ -ketoglutarate at various times, by using the enzyme glutamate dehydrogenase in an assay procedure, as outlined in the literature (56). The objective was to sample the reaction mixture at one hour intervals, starting one hour after the reaction was initiated. Although the enzyme reaction with  $\alpha$ -ketoglutarate should be completed in 5 minutes,

the actual reaction took about 2 hours. This indicates that something in the mixture inhibited the reaction with glutamate dehydrogenase, and this procedure could not be used.

A second approach was to assay for  $\alpha$ -ketoglutarate colorimetrically by the reaction with 2,4-dinitrophenylhydrazine (57). The reaction mixture was sampled hourly during the daytime for a period of three days. The concentration of  $\alpha$ -ketoglutarate determined by this method was unchanged for the entire period. Since hydrazines react with all ketones, the only conclusion reached is that the keto functionality is maintained during the course of the reaction.

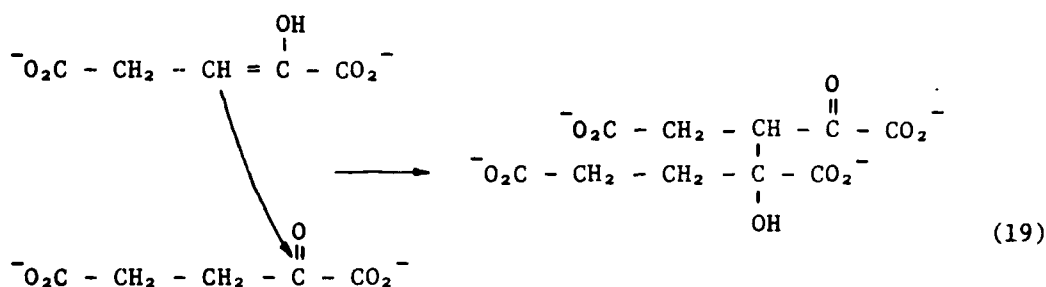
The next experiment was to determine the amount of iodine initially consumed by the reaction mixture at various times. The results were similar to the 2,4-dinitrophenylhydrazine experiments, that is, the amount of iodine consumed was fairly constant over a two day period. However, there seemed to be a general trend towards larger iodine consumption, but the trend was very small. The conclusion was that there are double bonds present, but the amount remains fairly constant.

From these experiments, very little can be concluded. There are published reports on the non-enzymatic oxidation of  $\alpha$ -ketoglutarate (58,59). The rates published are comparable in the order of magnitude to those observed here. But the main product of the reaction, succinic



acid, has a lower extinction coefficient than  $\alpha$ -ketoglutarate. This reaction should therefore occur with an absorbance decrease rather than an absorbance increase. Therefore, non-enzymatic oxidation of  $\alpha$ -ketoglutarate is probably not occurring.

Another possibility is the formation of a dimer or trimer of  $\alpha$ -ketoglutarate. A lead<sup>2+</sup>-catalyzed trimer of  $\alpha$ -ketoglutarate has been reported (60). The formation of a dimer would result from the condensation of the keto and enol forms, as shown in reaction (19). This mechanism is similar to the dimerization of pyruvate (61). Due



to the larger chromophores, the dimer should have a greater absorbance than the monomer. The extinction coefficients of the pyruvate dimer are slightly higher than the monomer (61). But since the concentration of the dimer is half of the monomer, the conversion to the dimer results in a net absorbance decrease for pyruvate. It therefore appears that polymerization of  $\alpha$ -ketoglutarate is not occurring.

The possibility of  $\alpha$ -ketoglutarate dimerization was investigated by placing a 1.0 mM solution of  $\alpha$ -ketoglutarate, buffered to a pH of

4.61 with 0.02 M acetate, and monitoring the reaction at 255 nm. After one hour, no spectral change was observed. Therefore, the blank solution of  $\alpha$ -ketoglutarate does not dimerize.

It is obvious that more experiments are needed in order to determine the nature of this reaction. One approach is to attempt a separation of the reaction components using high performance liquid chromatography. This would allow the experimenter to isolate the species in the system as well as to monitor the concentrations of each species. However, this reaction is very slow and does not interfere with the decarboxylation reaction. Further work on the slow reaction will therefore not be continued in this study.

#### Summary

The UV spectral change observed during the decarboxylation of oxalosuccinate in buffered solutions showed three distinct relaxation processes. The first relaxation was tautomerization. The second reaction was the decarboxylation of oxalosuccinate, because this process was comparable in rate to manometric and pH stat data. The third relaxation was very slow, and the nature of this reaction is unknown. Further evidence for these processes was provided by rapid scanning UV spectra as a function of time.

A mathematical model for the reaction sequence was proposed and verified by experimental data. This model is typical for the

decarboxylation mechanism of other  $\beta$ -keto acids. Although oxalosuccinate enolizes in solution, the amount of enol is small. Furthermore, the conversion rate of enol to keto is very rapid when compared to decarboxylation. Therefore, tautomerization does not interfere with decarboxylation, and can therefore be treated as a pre-equilibrium reaction.

## V. ZINC CATALYZED DECARBOXYLATION OF OXALOSUCCINATE

The zinc promoted tautomerization and decarboxylation of oxalosuccinate will be discussed in this chapter. The material in this chapter, in general, will also apply to the discussion of the manganese and magnesium assisted reactions. This is due to the fact that the metal/oxalosuccinate decarboxylation mechanisms are similar for all three metals; the only difference is the actual data. Therefore, this chapter will discuss in greater detail the data analysis, mechanisms, and the overall chemistry of the system. In the following chapter, pertaining to the manganese and magnesium systems, the discussions will be briefer, however, more detailed analysis will be included when necessary.

Equilibrium data pertaining to this system was discussed in some detail in Chapter III. A repeat of that discussion is not necessary. However, reference will be made to that information and its application to the kinetics of the system.

Kinetically, upon the addition of metal to a solution of oxalosuccinate, the following processes should take place:

(a) extremely fast complexation and deprotonation; (b) a slower shift in keto/enol ratios to the equilibrium values; and (c) the relatively slower decarboxylation step. Reaction (a) is very fast and

can be assumed to occur instantaneously with respect to the other processes. Reactions (b) and (c) are much slower and can be observed without the use of stopped-flow techniques.

A series of UV spectra versus time for the zinc-oxalosuccinate system is shown in Figure 27. Each spectrum was obtained in 0.75 seconds and recorded at two second intervals. In this system, tautomerization of the zinc-oxalosuccinate enol complex must be extremely rapid since the first spectrum shows the presence of the enol, while succeeding spectra show a simple reaction occurring. In other words, enolization was completed during the first few seconds after mixing. This reaction will be discussed in more detail later in the chapter.

The first spectrum in Figure 27 shows a relatively large shoulder at 290 nm, whereas each succeeding spectrum shows lower overall absorbances and smaller shoulders. The final spectrum has a small shoulder, consistent with the spectrophotometric data for zinc- $\alpha$ -ketoglutarate. This data showed that the zinc- $\alpha$ -ketoglutarate complex was about 8% enolized. Therefore, the series of spectra in the figure map out the spectral change in the zinc catalyzed decarboxylation of oxalosuccinate. Based on this figure, it was decided to monitor the reaction at 284 nm.

With careful experimental technique, the spectral change of the reaction can be recorded within one second after mixing. This was

Figure 27

Time dependence of the ultraviolet spectra for the zinc<sup>2+</sup>-oxalosuccinate system.

[acetate buffer] = 0.020 M

T = 25°C

pH = 3.49

Scan rate = 100 nm/second

[zinc<sup>2+</sup>] = 10.0 mM

[oxas<sup>3-</sup>] = 0.336 mM

Curve 1: 1 second after mixing

Curve 2: 3 seconds

Curve 3: 5 seconds

Curve 4: 7 seconds

Curve 5: 9 seconds

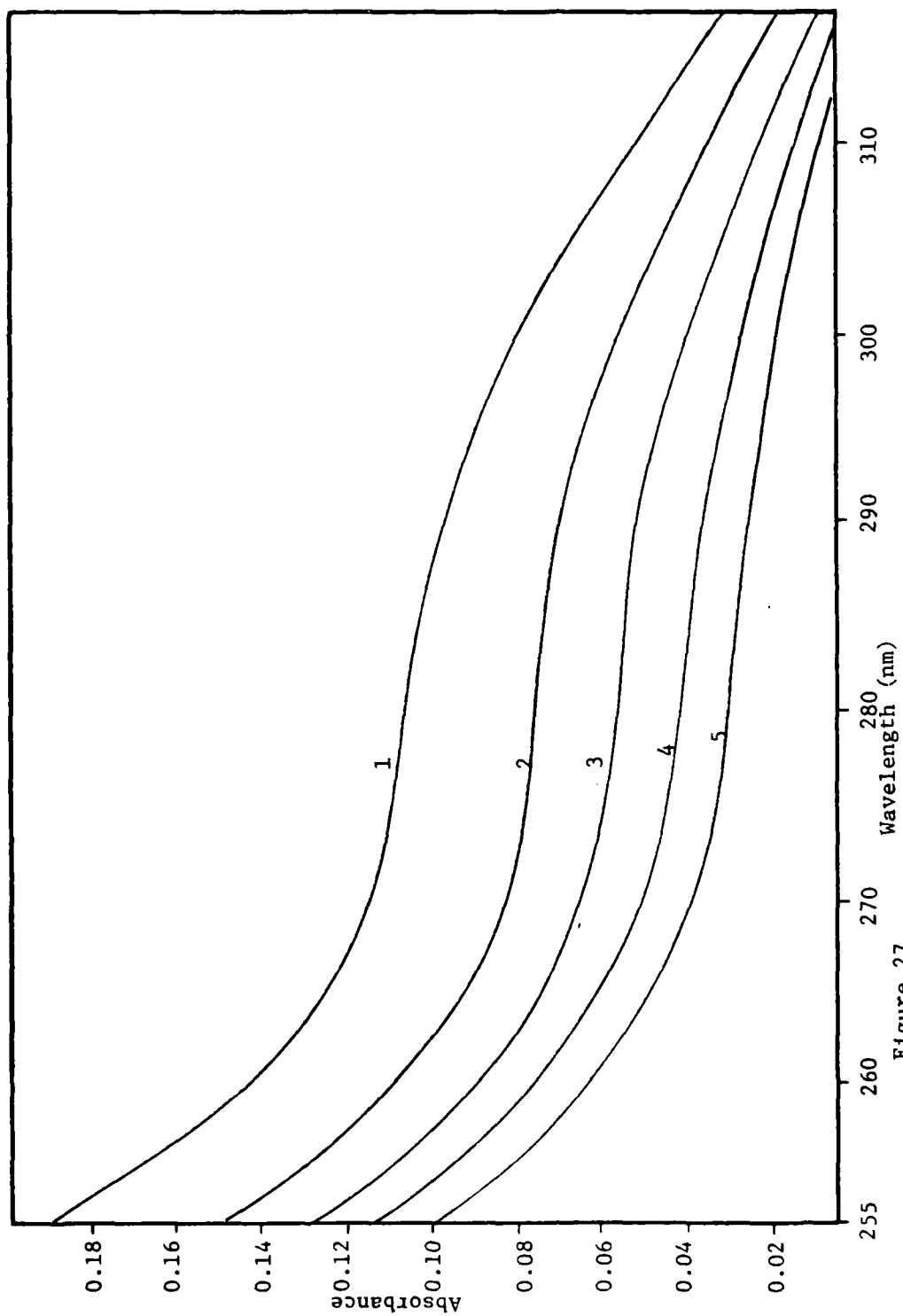


Figure 27.

done in the following way. A 1.0 ml aliquot of the oxalosuccinate solution was mixed with 1.0 ml of the appropriate buffer in a 1.0 cm cell. This cell was placed in the Gilford 250 Spectrophotometer, and the recorder was switched to RUN. Then, 1.0 ml of the zinc solution was syringed into the cell. The cell compartment was immediately closed, and the data was then recorded.

Using this method, two relaxations, corresponding to tautomerization and decarboxylation, can be monitored. A sample trace is shown in Figure 28, which shows the reaction for a 0.267 mM oxalosuccinate/13.3 mM zinc<sup>2+</sup> solution at a pH of 3.96. Under these conditions, about 75% of the oxalosuccinate was complexed to the zinc ion. The absorbance data can be analyzed in the program RLXFT, where the observed absorbance,  $A_{\text{obs}}$ , is related to the rate constants for the two relaxations,  $k_1$  and  $k_2$ , by the expression  $A_{\text{obs}} = A_{\infty} + A_1 e^{-k_1 t} + A_2 e^{-k_2 t}$ . Thus, both rate constants can be extracted. Note that the reaction was essentially completed within one minute after mixing.

It was shown in the last chapter that tautomerization of oxalosuccinate did not interfere with the decarboxylation. It was therefore not included in the detailed analysis of the decarboxylation kinetics. However, it is necessary to discuss the tautomerization side equilibria for the zinc system.

Based on the equilibrium investigations given in Chapter II, it was found that the zinc-oxalosuccinate complex is 23% enolized. The



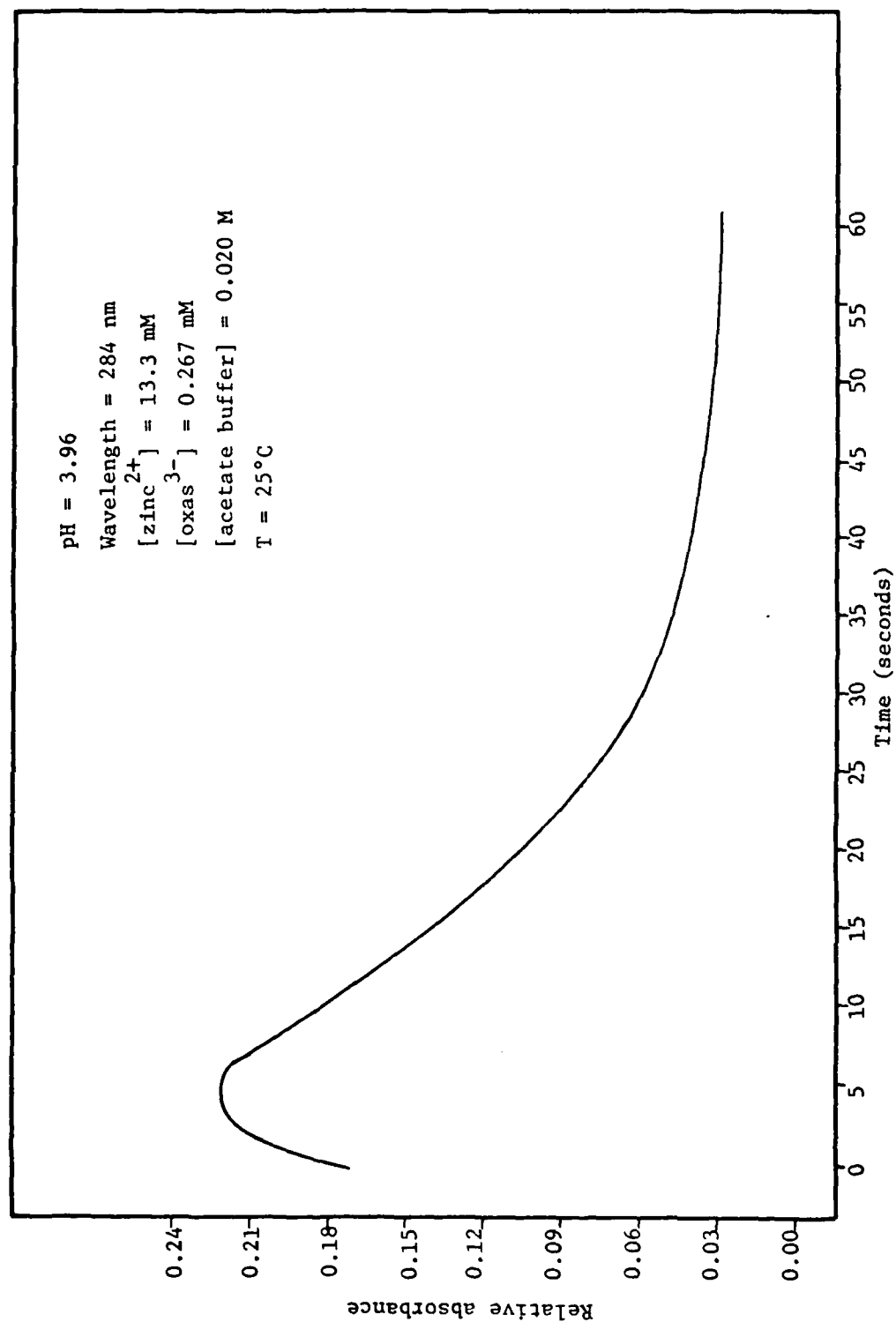
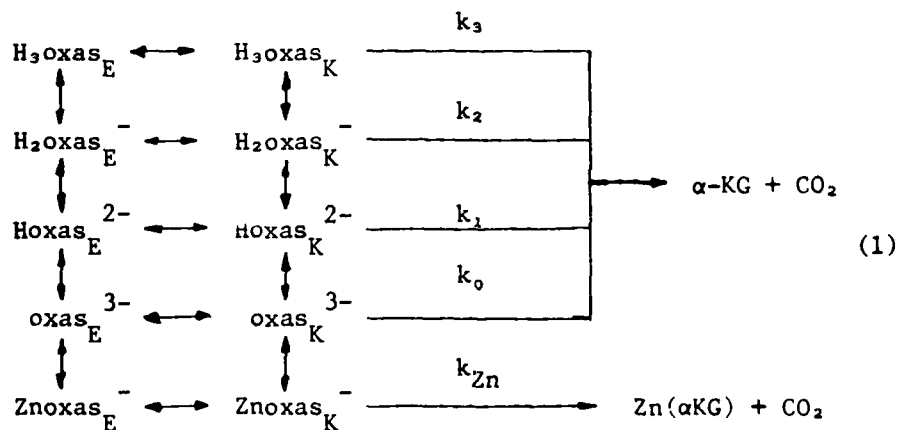


Figure 28. Sample reaction trace for the zinc-oxalosuccinate system.

observed tautomerization rates as a function of the zinc concentration are shown in Figure 29. The rates were determined by the program RLXFT by analyzing the biphasic absorbance changes at 284 nm. From this figure, it can be seen that the slowest observed rate constant was  $0.2 \text{ s}^{-1}$ . This observed rate is  $k_f + k_b$ , where  $k_f$  is the rate of enolization and  $k_b$  is the rate of ketonization. Since  $k_b = k_f/K_{eq}$ , then  $0.2 = k_f(1 + 1/K_{eq})$ , or  $k_f = 0.037 \text{ s}^{-1}$ . This implies that  $k_b$  is  $0.163 \text{ s}^{-1}$ . This rate is considerably larger than the fastest observed decarboxylation rate constant, which is  $0.1 \text{ s}^{-1}$ . Therefore, it can again be concluded that tautomerization does not interfere with the decarboxylation kinetics, and this side reaction will be considered to be in virtual equilibrium.

The complete reaction scheme is shown below in reaction (1). All equilibria are fast relative to decarboxylation.



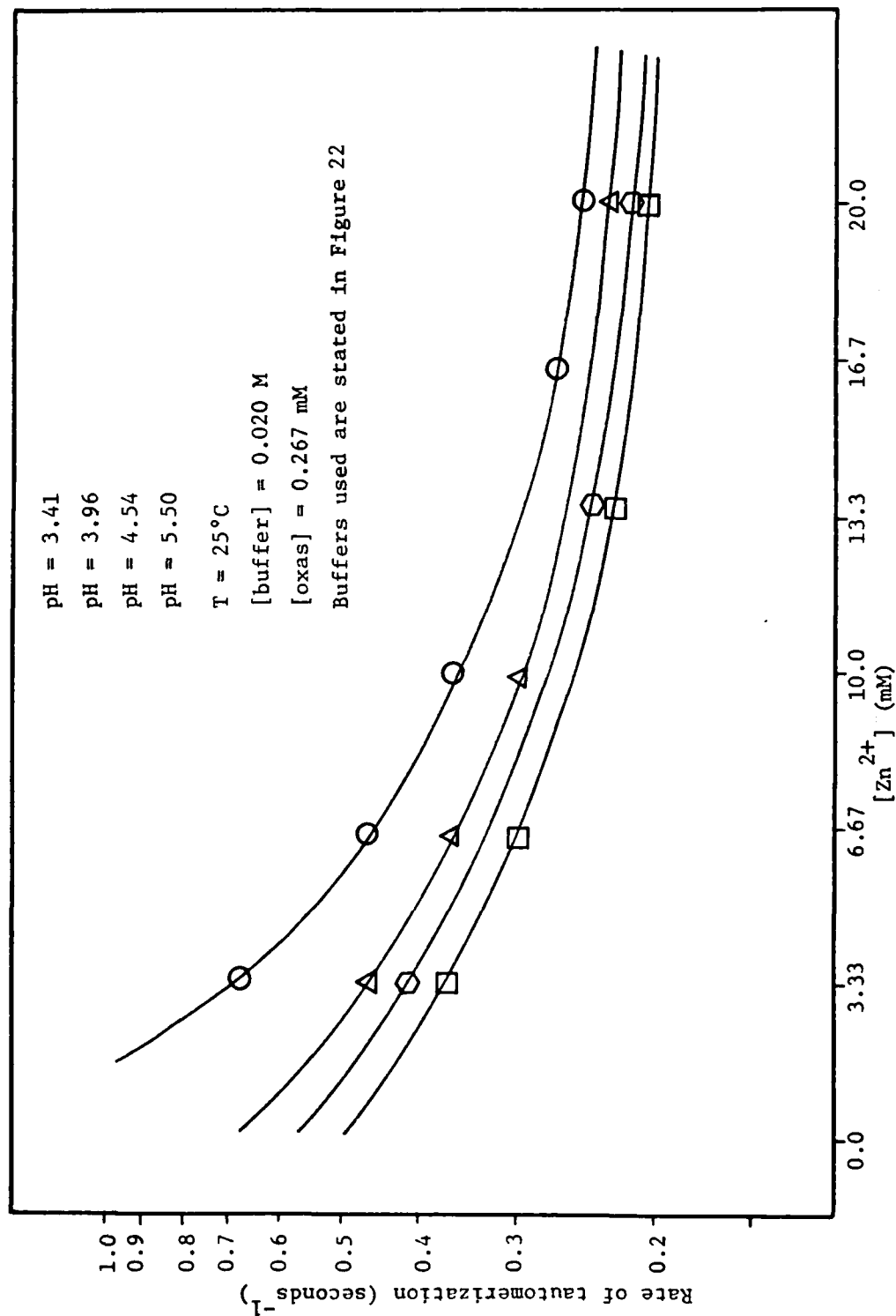


Figure 29. Tautomerization rates for the zinc-oxalosuccinate system.

The rate law governing this scheme is:

$$-\frac{d(\text{oxas})_{\text{total}}}{dt} = k_{\text{obs}} [\text{oxas}]_{\text{total}} = k_0 [\text{oxas}_K^{3-}] + k_1 [\text{Hoxas}_K^{2-}] + k_2 [\text{H}_2\text{oxas}_K^-] + k_3 [\text{H}_3\text{oxas}_K] + k_{\text{Zn}} [\text{Znoxas}_K^-] \quad (2)$$

By dividing equation (2) by  $[\text{oxas}]_{\text{total}}$  and recalling that the fraction of each species, Fr, is equal to the concentration of each complex divided by the total concentration of oxalosuccinate, then the above equation reduces to

$$k_{\text{obs}} = k_0 \text{Fr}_{\text{oxas}} + k_1 \text{Fr}_{\text{Hoxas}} + k_2 \text{Fr}_{\text{H}_2\text{oxas}} + k_3 \text{Fr}_{\text{H}_3\text{oxas}} + k_{\text{Zn}} \text{Fr}_{\text{Znoxas}} \quad (3)$$

Some of the data for the observed decarboxylation rate constant versus the zinc ion concentration is shown in Figure 30. A complete table of the data can be found in Appendix C. The lines in the figure are the theoretical values calculated from Equation (3). Based on the kinetic data, the rate constant for the zinc<sup>2+</sup>-oxalosuccinate keto complex is 0.136 seconds<sup>-1</sup>. The log of the formation constant is 3.02. In the data analysis, zinc complexation with the chloroacetate ion (log formation constant = 0.80) and the acetate ion (log formation constant = 1.248) in the buffer solutions were considered. It should

Figure 30

Observed decarboxylation rate constants versus zinc concentration.

I = 0.1 M

T = 25°C

[buffer] = 0.020 M

[oxas<sup>3-</sup>] = 0.267 mM

◇ pH = 3.17

▽ pH = 3.41

□ pH = 3.61

⬡ pH = 3.96

△ pH = 4.54

○ pH = 7.18

Buffers used are stated in Figure 22

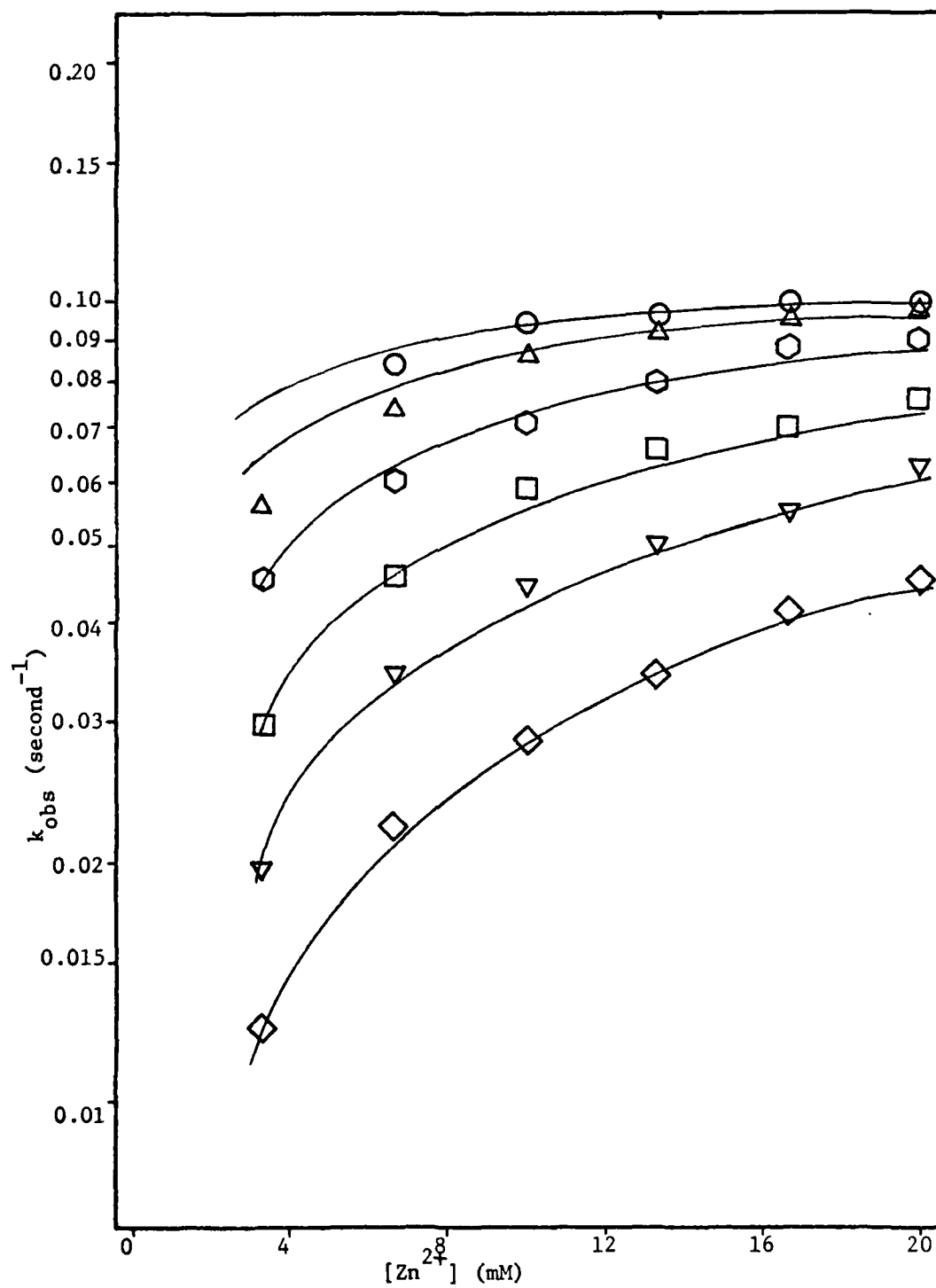
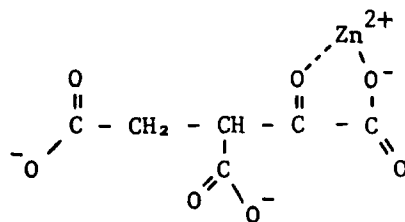


Figure 30.

be pointed out that the formation constant determined spectrophotometrically at two wavelengths at 0°C was identical to that obtained kinetically.

The rate constant for this complex is approximately 70 times faster than the monoprotinated oxalosuccinate complex, which is the most reactive of the non-metal catalyzed forms of the acid. The overall effectiveness of the zinc ion as a catalyst for decarboxylation can be seen in Figure 31, which is a plot of the observed rate constant versus the pH. As in the previous figure, the solid line is the theoretical curve calculated from Equation (3).

The data presented thus far clearly indicates that zinc forms a stable five member chelate ring with the oxalosuccinate trianion, as shown in I. The zinc ion, which is a much better Lewis acid than the proton, enhances the carbonyl as an electron sink, making the carboxylate group  $\beta$  to the keto a better leaving group. It also aids the reaction by stabilizing the  $\alpha$ -ketoglutarate enolate intermediate.



I

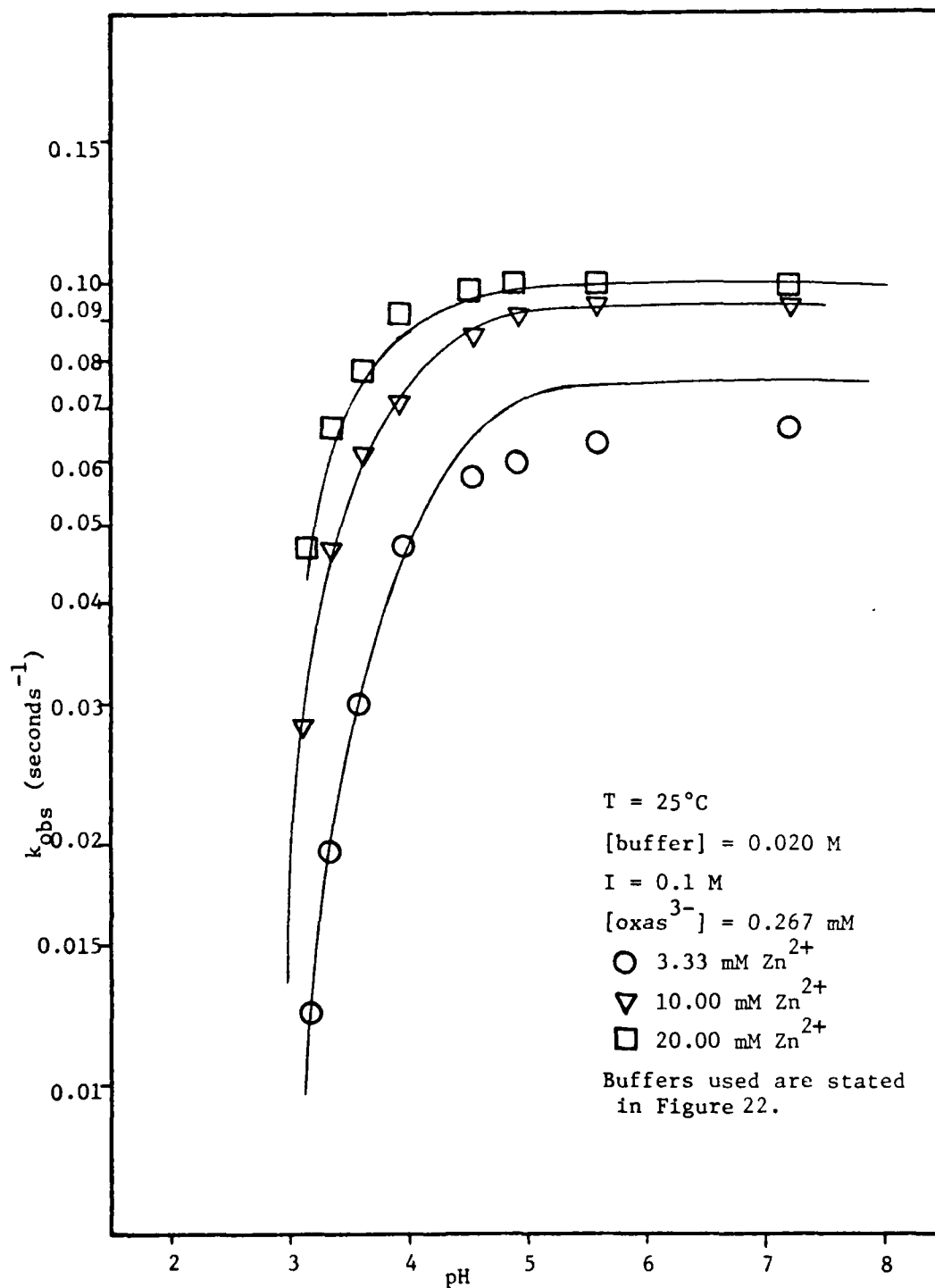


Figure 31. Observed decarboxylation rate constants versus pH for the zinc-oxalosuccinate system.



It was stated in Chapter I that metal ion inhibition was observed in the oxaloacetate system at higher metal concentrations and elevated pH values. The next step in this investigation, then, was to increase the zinc ion concentration in an attempt to detect this inhibition. In all work pertaining to this research, the ionic strength was maintained at 0.1 M. Ignoring the contribution of oxalosuccinate and  $\alpha$ -ketoglutarate, the highest concentration of the zinc ion that could have been used without exceeding the ionic strength limitation (buffer concentration = 20.0 mM) was 26.7 mM. In the data presented thus far, the maximum concentration of zinc was 20.0 mM. Inhibition was not seen at that concentration at pH values of 7.8 or below. It is apparent that the ionic strength limitation of 0.1 M must be exceeded in order to study greater concentrations of the zinc ion. However, the data obtained for zinc solutions greater than 26.7 mM must be analyzed with caution, since the ionic strength will be larger than 0.1 M.

A series of experiments were conducted using 30 mM and 40 mM zinc<sup>2+</sup> solutions. One experiment, using a 90.9 mM zinc<sup>2+</sup> solution, was also done. This data is shown in Table 17. The calculated values in the table came from equation (3) using the data from Figure 30; that is,  $k_{\text{Znoxas}} = 0.136 \text{ s}^{-1}$ ,  $K_{\text{enol}} = 0.23$ , and  $\log \beta_{\text{Znoxas}} = 3.02$ . It can be seen that four of the values agree quite well with the

TABLE 17  
OBSERVED RATE CONSTANTS AT HIGHER LEVELS OF ZINC<sup>2+</sup>

[Zinc <sup>2+</sup> ]	pH	k <sub>obs</sub>	k <sub>calc</sub>	% Dev
3.00E-02	3.91	9.16E-02	8.75E-02	4.49
4.00E-02	3.88	8.97E-02	8.98E-02	-0.10
3.00E-02	4.44	9.19E-02	9.37E-02	-1.97
4.00E-02	4.39	7.70E-02	9.49E-02	-23.29
4.00E-02	4.96	8.43E-02	9.66E-02	-14.62
3.00E-02	6.32	8.65E-02	9.63E-02	-11.33
4.00E-02	6.35	7.83E-02	9.72E-02	-24.14
9.09E-02	3.76	8.86E-02	9.34E-02	-5.48

Notes:

1. The concentration of oxalosuccinate for all experiments was 2.67E-04 M.
2. The concentrations in the table are molar.
3. The units for the rate constants are seconds<sup>-1</sup>.

model (reaction scheme (1)), while two others deviate by less than 15%. The other data points are somewhat lower, indicating the possible presence of a  $\text{Zn}_2\text{H}_{-1}\text{oxas}$  dead-end complex, as suggested by Leussing and coworkers (26,55). However, when all the data was analyzed for the existence of the dead-end complex, a very poor fit resulted. It is therefore concluded that an unreactive complex is not responsible for the lower than expected observed rate constants.

One explanation for these lower values is the effect of the ionic strength. The ionic strength of a 40.0 mM zinc<sup>2+</sup> solution with 20.0 mM buffer is 0.14 M, which is considerably higher than the 0.1 M standard. As the ionic strength of the solution increases, metal/ligand formation constants decrease. Thus, the lower observed rates could easily be accounted for by the lower amount of complex actually present due to the lower formation constant, rather than by the presence of a dead-end inhibition complex.

### Summary

The tautomerization and decarboxylation of the zinc<sup>2+</sup>-oxalo-succinate system was studied. Although the complex is 23% enolized, tautomerization is very rapid compared to decarboxylation and can therefore be considered to be in virtual equilibrium. The decarboxylation rate profile at various zinc<sup>2+</sup> concentrations from a pH of 3.17 to a pH of 7.18 follows the decarboxylation of a 1:1 complex

with a log formation constant of 3.02. The rate constant for this complex is approximately 450 times larger than the oxalosuccinate trianion. Under the conditions of this investigation, there was no observed inhibition at higher zinc concentrations or elevated pH values. Although the observed rate constant was lower at higher concentrations of the zinc cation, this effect was due to lower concentrations of the zinc-oxalosuccinate complex than predicted. This resulted from the lower formation constant due to the higher ionic strength used in those experiments. The lower rate constants did not result from the formation of a  $\text{Zn}_2\text{H}_{-1}\text{oxas}$  dead-end complex.

## VI. MAGNESIUM AND MANGANESE CATALYZED DECARBOXYLATION OF OXALOSUCCINATE

This chapter will discuss the magnesium and manganese catalyzed decarboxylation of oxalosuccinate. The two metals will be treated together since the mechanisms are the same; only the rates and formation constants will vary. In the previous chapter on zinc, it was shown that tautomerization did not interfere with the reaction kinetics. It was also shown that inhibition at elevated zinc concentrations and high pH values was not observed. If these effects did not occur in the zinc system, they certainly would not appear in systems composed of metal ions that are weaker Lewis acids, such as magnesium and manganese. Also, recall from Chapter II that the UV analysis as well as iodination experiments showed that the magnesium and manganese complexes with oxalosuccinate were both about 1% enol, whereas the zinc complex was 23% enol. Therefore, this chapter will not be concerned with inhibition complexes and will also treat the tautomerization reaction as being in virtual equilibrium.

A series of UV scans, obtained at 135 second intervals at a rate of 100 nm/second, is shown in Figure 32. This figure shows that the final four scans have an isosbestic point at 277 nm, while the first scan does not pass through this point. This is very similar to the

Figure 32

Time dependence of the ultraviolet spectra for the magnesium<sup>2+</sup>-oxalosuccinate system.

T = 25°C

[acetate buffer] = 0.020 M

pH = 3.52

Scan rate = 100 nm/second

[magnesium<sup>2+</sup>] = 10.0 mM

[oxalosuccinate<sup>3-</sup>] = 0.336 mM

Curve 1: immediately after mixing

Curve 2: 135 seconds

Curve 3: 270 seconds

Curve 4: 405 seconds

Curve 5: 540 seconds

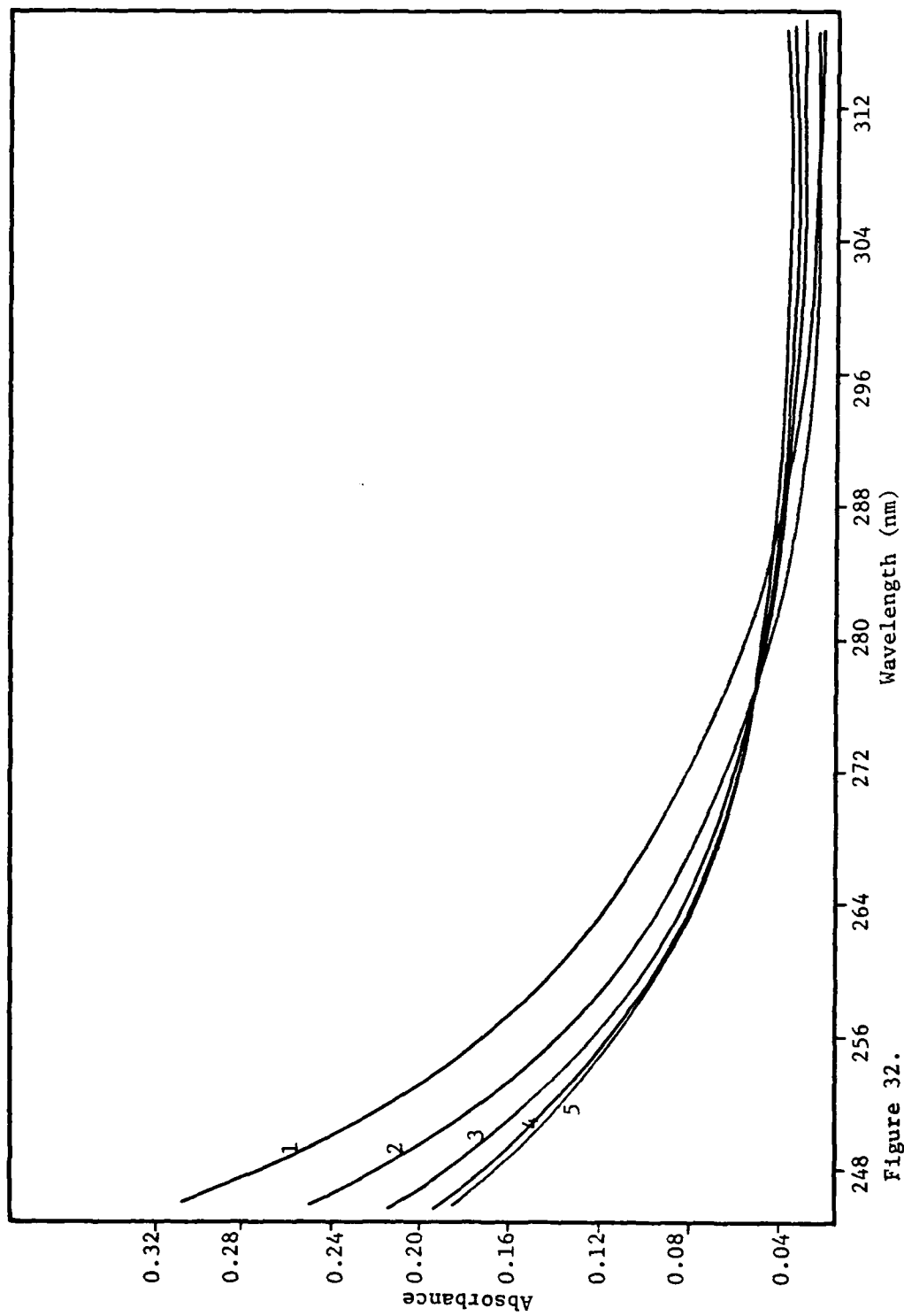


Figure 32.

scans for the free acid reaction presented in Chapter III. One would therefore expect a similar trace while monitoring the reaction at a wavelength of 260 nm. That is, one would see a slight absorbance increase, due to enolization, followed by an absorbance decrease, which is decarboxylation. This is precisely what is observed.

By fitting the data for each experiment in the program RLXFT, the observed decarboxylation rate constant can be determined. A plot of the data is shown in Figure 33. This is a plot of the observed rate constant versus magnesium. Each set of points represents constant pH. If we assume that the same decarboxylation model of zinc applies to magnesium, then the observed rate constant should be

$$k_{\text{obs}} = \text{Fr}_{\text{Moxas}} k_{\text{Moxas}} + \sum_1^4 \text{Fr}_n k_{\text{H}_n \text{oxas}} \quad (1)$$

This model was used to fit the data points in Figure 33 in the program CORNEK. The solid lines in the figure are the theoretical results from the program. The log formation constant of the magnesium-oxalosuccinate complex evaluated from the kinetics is 1.99. This is in excellent agreement with the value of 1.92 determined via a spectrophotometric titration. The rate constant is  $0.0125 \text{ seconds}^{-1}$ , which is about seven times faster than  $\text{Hoxas}^{2-}$ , and about eleven times slower than the zinc-oxalosuccinate keto complex. It is readily apparent that, under the range of experimental parameters, there is no inhibition at higher magnesium concentrations or elevated pH values.



Figure 33

Observed decarboxylation rate constants versus magnesium concentration.

$T = 25^{\circ}\text{C}$

$I = 0.1 \text{ M}$

$[\text{oxas}^{2-}] = 0.267 \text{ mM}$

○ pH = 2.84

△ pH = 3.30

⬡ pH = 3.54

□ pH = 4.03

▽ pH = 4.59

◇ pH = 7.71

$[\text{buffer}] = 0.020 \text{ M}$

Buffers used are stated in Figure 22.

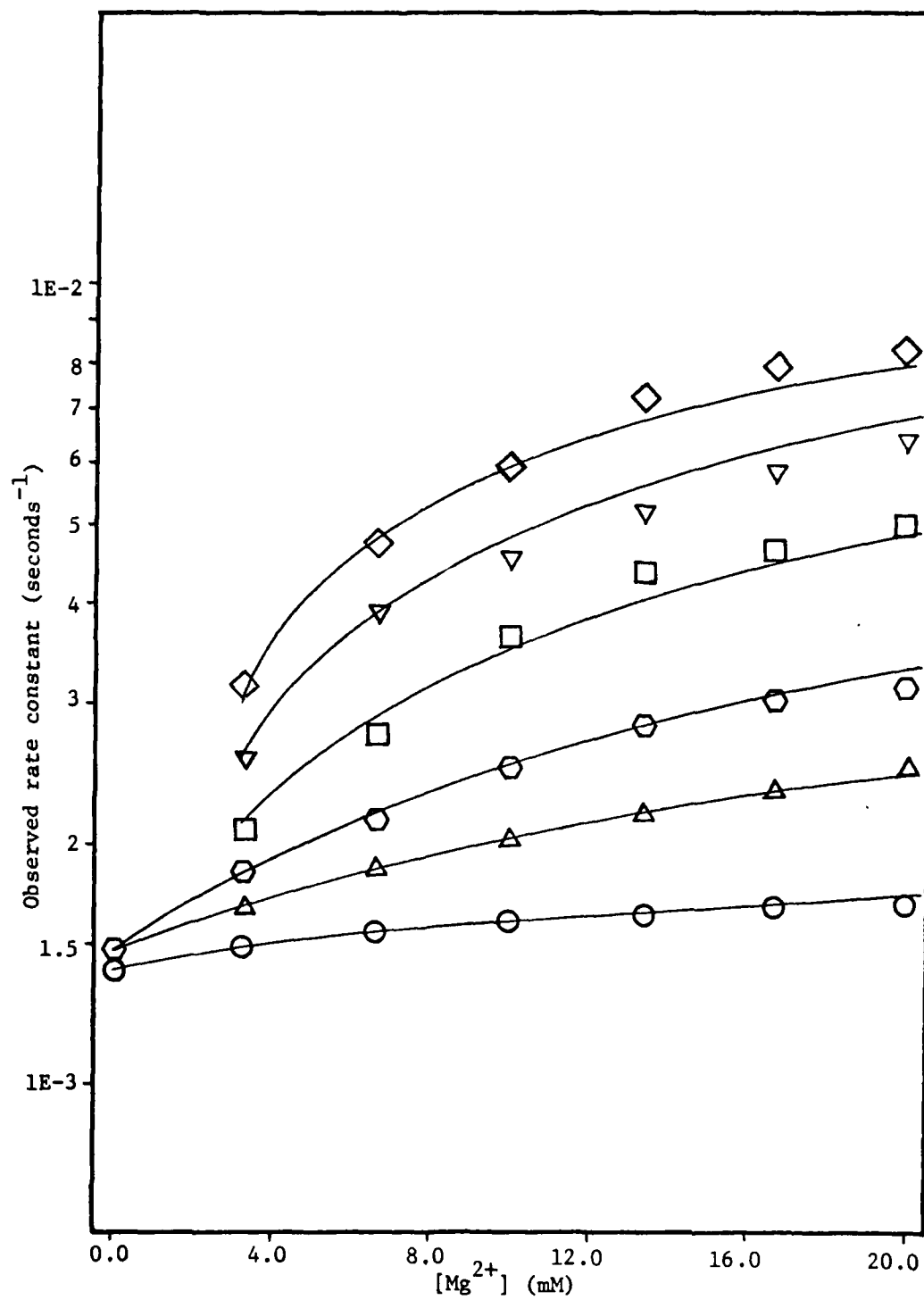


Figure 33.

The overall effectiveness of magnesium as a metal catalyst can be seen in Figure 34. In this figure, the observed rate constant is plotted as a function of pH. Included in this figure for reference is the rate profile for the free acid. This figure shows that, at biological pH values, a 3.28 mM solution of magnesium<sup>2+</sup> in 0.267 mM oxalosuccinate decarboxylates about ten times faster than oxalosuccinate itself, while a 20.0 mM solution of magnesium in oxalosuccinate decarboxylates about 35 times faster. This is considerably slower than the zinc complex. In the zinc system, the decarboxylation rate is about 400 times faster in a 20.0 mM solution of zinc at biological pH when compared to the oxalosuccinate trianion.

Also shown in this figure are two data points evaluated by monitoring the change in solution pH by following the color change of an appropriate pH indicator. These solutions were unbuffered. These points are shown in the figure as the darkened triangles. The experimental conditions for these points were the same as for the open triangles. Each point was plotted at the average pH of the solution. Although these points are not as precise as the other data points on that line, it is very apparent that the rate of proton uptake from the solvent is identical to the rate of absorbance decrease monitored in the UV region, which is the decarboxylation step.

Thus, the magnesium system behaves similarly to the zinc system, except that about 1% of the magnesium-oxalosuccinate complex is

Figure 34

Observed decarboxylation rate constants versus pH for the magnesium-oxalosuccinate system.

$$[\text{oxas}^{3-}] = 0.267 \text{ mM}$$

○ 3.28 mM  $\text{Mg}^{2+}$

△ 10.00 mM  $\text{Mg}^{2+}$

□ 20.00 mM  $\text{Mg}^{2+}$

▲ 10.00 mM  $\text{Mg}^{2+}$ ; from pH indicator experiments

(see text)

Experimental conditions are as stated in Figure 33.

The lower curve represents the free acid decarboxylation.

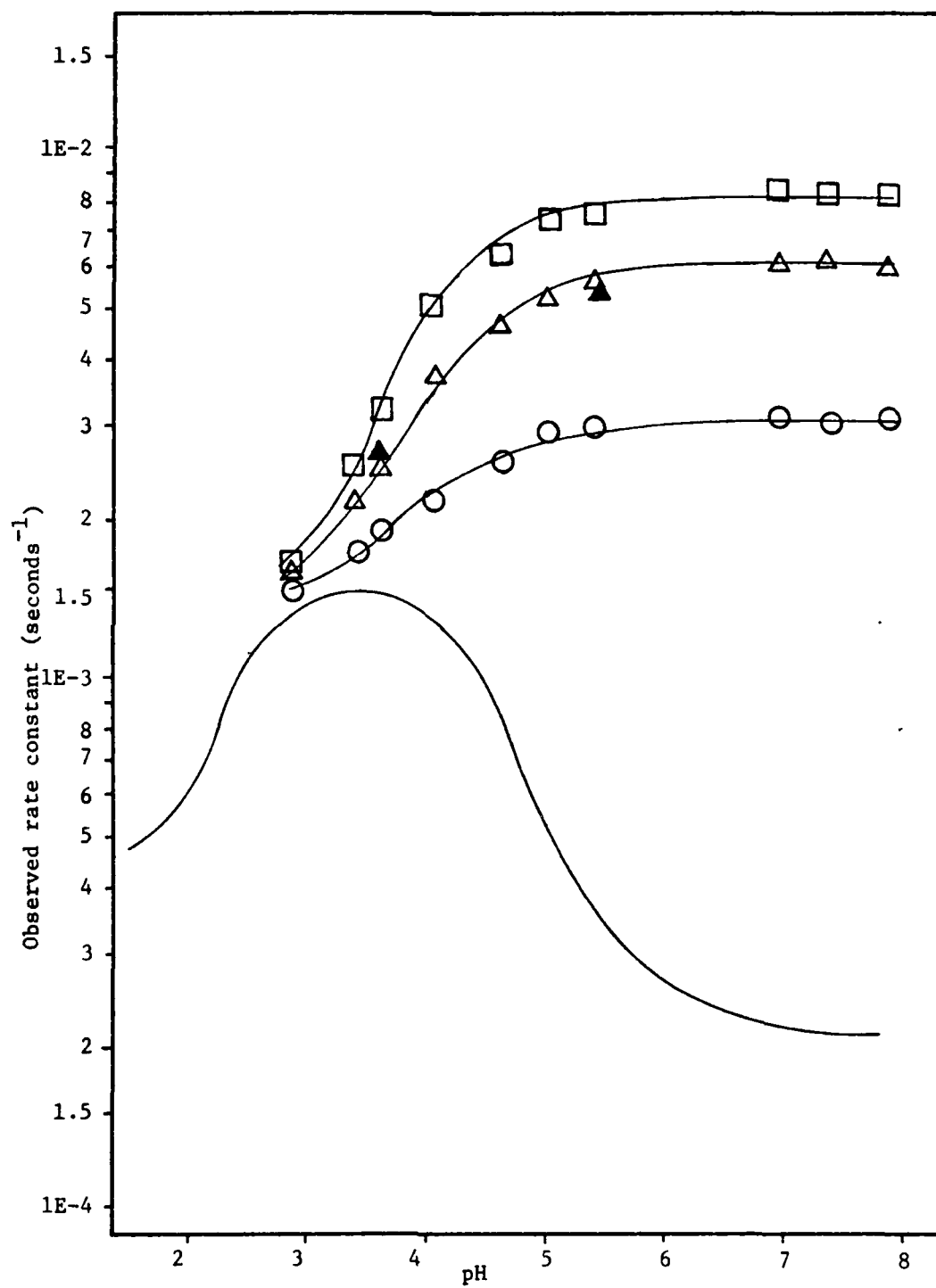


Figure 34.

enolized. The manganese system is nearly identical to the magnesium system. The only difference is the actual numbers, although the manganese-oxalosuccinate complex is also about 1% enolized. The UV spectral change with time for a solution of manganese and oxalosuccinate is not shown since it is identical qualitatively to the magnesium spectra in Figure 32.

The observed rate constants for the manganese catalyzed reaction are shown in Figure 35. This is a plot of rate versus manganese concentration at four different pH values. A table of all the data can be found in Appendix C. The data was analyzed by the program CORNEK using equation (1). From this analysis, the formation constant for the manganese-oxalosuccinate complex is  $10^{2.565}$ , while the rate constant for the complex is  $0.0200 \pm 0.00048 \text{ seconds}^{-1}$ . The calculated fit of the data is represented as the solid line in Figure 35.

The overall effectiveness of manganese as a catalyst can be seen in Figure 36, which plots the observed rate versus pH. As before, the solid lines were calculated from equation (1). Also shown on this figure, for reference, is the pH profile of the non-metal catalyzed reaction. The solid triangles in this figure are the rate constants of an unbuffered manganese-oxalosuccinate solution obtained by monitoring the pH change in the solution by using the appropriate pH indicator. As before, these points lie very close to the theoretical curve,

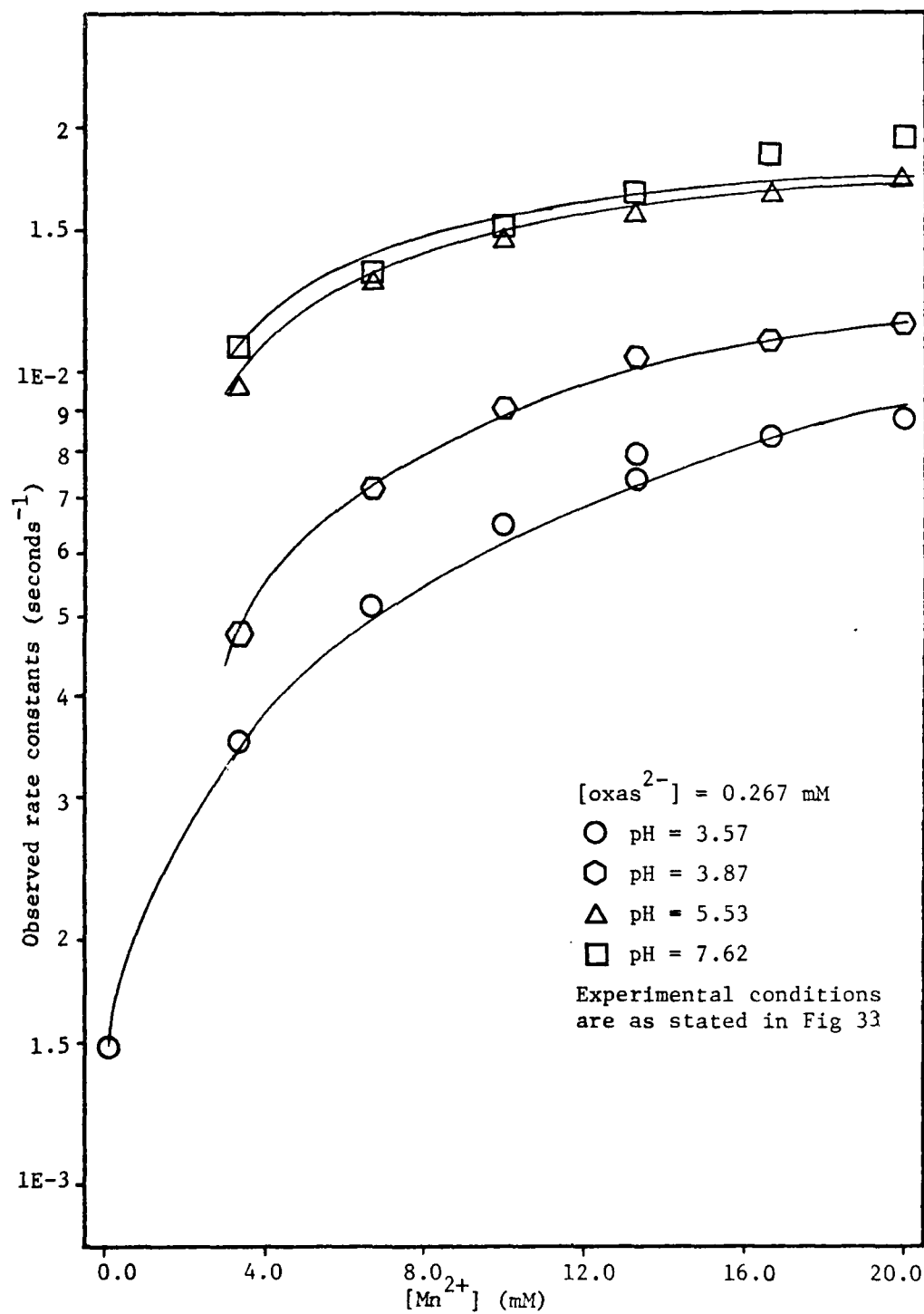


Figure 35. Observed decarboxylation rate constants versus manganese concentration.

The lower curve represents the free acid decarboxylation.

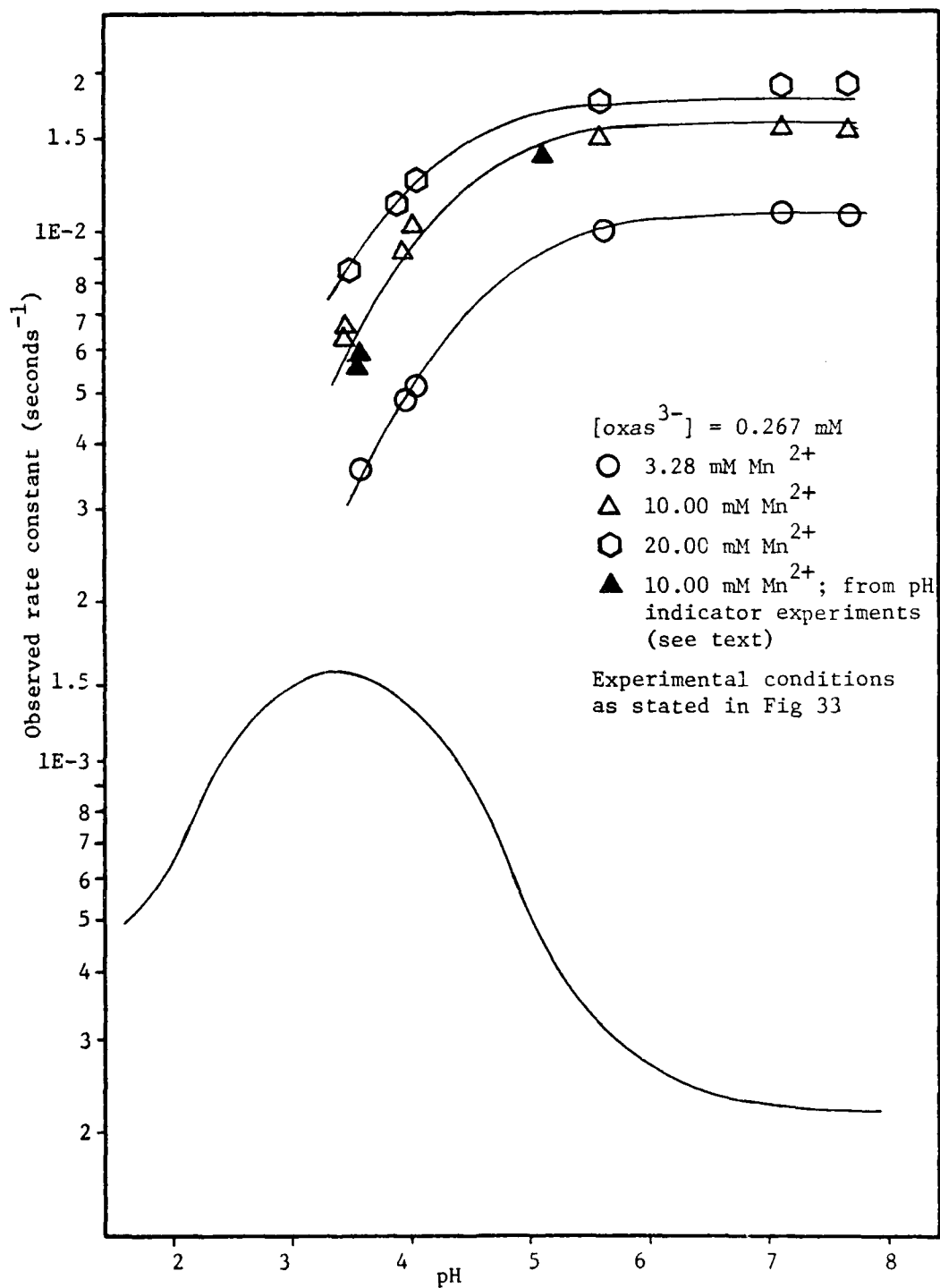


Figure 36. Observed decarboxylation rate constants versus pH for the manganese-oxalosuccinate system.



indicating that the rate of proton uptake from the solvent is nearly identical to the UV spectral change of an equivalent buffered solution.

Figure 36 shows that a 20.0 mM solution of  $\text{Mn}^{2+}$  in 0.267 mM oxalosuccinate decarboxylates 70 times faster than the free acid at physiological pH. Thus, of the three metals, zinc is the best catalyst, while manganese is somewhat less effective than zinc, and magnesium is the least effective. This is the same order observed by Ochoa (1) in his initial experiments with oxalosuccinate. It is also the same catalytic order observed for other  $\beta$ -keto acids, such as oxaloacetate (see Table 2) and 3-oxoglutarate (see Table 3).

#### Summary

The catalytic effect of  $\text{Mg}^{2+}$ ,  $\text{Mn}^{2+}$ , and  $\text{Zn}^{2+}$  on the decarboxylation of oxalosuccinate was studied. In each case, the kinetics observed matched the predicted rates based on the formation of a 1:1 metal<sup>2+</sup>/oxas<sup>3-</sup> complex. The formation constants determined kinetically were nearly identical to those found via spectrophotometric titrations. Tautomerization was very fast relative to decarboxylation, and was therefore considered to be in equilibrium at all times. Inhibition at high metal ion concentrations or elevated pH values was not observed with any of these metals.

The data from these last two chapters are summarized in Table 18. The stability constant for the metal/oxas complex as well as the decarboxylation rate constant for each complex follows the Irving-Williams natural stability order, which is  $\text{Mg}^{2+} < \text{Mn}^{2+} < \text{Zn}^{2+}$ . The

TABLE 18  
 SUMMARY OF FORMATION CONSTANTS AND DECARBOXYLATION RATE  
 CONSTANTS FOR METAL-OXALOSUCCINATE SYSTEMS

	Magnesium <sup>2+</sup>	Manganese <sup>2+</sup>	Zinc <sup>2+</sup>
Log $\beta_{\text{Moxas}}$	1.993	2.565	3.016
$k_{-\text{CO}_2}$ (seconds <sup>-1</sup> )	0.0125	0.0200	0.136
$K_{\text{enol}}$	$\sim 0.01$	$\sim 0.01$	0.23
Relative decarboxy- lation rate of a 3.28 mM solution of $\text{M}^{2+}$ at pH = 7.0 ( $\text{oxas}^{3-} = 1.0$ )	13.6	48.2	333.2

zinc complex was 23% enolized, while the magnesium and manganese complexes were about 1% enol. The relative observed decarboxylation rate constant, which is a good way to analyze the effect of greater stability coupled with a faster rate constant, is shown on the last line in the table. The decarboxylation rate of a 3.28 mM  $\text{Zn}^{2+}$ /0.267 mM oxas<sup>3-</sup> solution is 333.2 times faster than a 0.267 mM solution of oxas at a pH of 7.0, while manganese and magnesium are 48.2 and 13.6 times faster respectively. As can be readily seen, the experimental data supports this researcher's hypothesis that the mathematical description of the reaction scheme applicable to  $\beta$ -keto acids as proposed in the previous chapter is also valid for this system.

## VII. ENZYME ASSISTED DECARBOXYLATION OF OXALOSUCCINATE

The previous chapters in this research work were concerned with the non-enzymatic decarboxylation of oxalosuccinate. Reaction schemes for the spontaneous and metal-catalyzed reactions were proposed and verified by experimental rate data. This chapter will focus on the effect of the enzyme isocitrate dehydrogenase (ICDH) on the spontaneous and metal-catalyzed reaction rates. It will be divided into two sections: one for the kinetics of the oxas and ICDH alone, while the other will discuss the kinetics of the ternary oxas-metal ion-ICDH system. In the second section, the investigation and comparison of the two metals, zinc and magnesium, will be discussed. This section will then be followed by a summary.

The enzyme, ICDH, was purchased from the Sigma Chemical Company. This particular enzyme, which was extracted from pig hearts, is  $\text{NADP}^+$  specific. It was obtained in a 50% glycerol solution and was used without further purification. The concentration of the enzyme, as stated by Sigma, was 10 mg/ml. The actual concentration, determined in our lab, was 10.8 mg/ml. This measurement was taken on the Gilford 250 Spectrophotometer in the following way. A 2.0 ml blank solution of 50% glycerol/water was placed in a 1.0 cm cell. The absorbance at 280 nm was recorded. Next, 50  $\mu\text{l}$  of the stock enzyme was syringed

into the same cell, and another absorbance reading at 280 nm was recorded. The difference between the two measurements is the absorbance due to the enzyme. The blank solution was not corrected for dilution, since it was identical in composition to the semi-aqueous solvent of the enzyme. The absorbance difference can be converted into the concentration of ICDH (in mg/ml) in the cell by dividing this difference by 0.91 absorbance units/(mg/ml) (36).

A critical property of the enzyme is its activity. The activity of enzymes is dependent upon several parameters, such as pH, substrate concentration, cofactor concentrations, impurities, and temperature. In order to insure continuity throughout this investigation, the enzyme was assayed weekly using the procedure discussed in Chapter II. This weekly check also provided data concerning the stability of the enzyme over an extended period of time. From these weekly assays, the ICDH used had an activity of  $1.37 \pm 0.04$  units. For this research, one unit of activity converts one  $\mu$ mole of isocitrate to  $\alpha$ -KG per minute at 25°C at a pH of 7.8. It was therefore concluded that the enzyme was stable for the entire period of the investigation, and the kinetic results reported in this chapter are valid.

It was mentioned that the enzyme used was  $\text{NADP}^+$  specific. This coenzyme is needed in the dehydrogenase step of the overall isocitrate reaction as the proton acceptor during the oxidation of isocitrate.

It is not a requirement, however, for the decarboxylation step. Consequently, NADPH, which is the reduced form of the coenzyme and is present as oxas decarboxylates enzymatically, was not used in this study. This was done in order to simplify the system being analyzed. It is important to realize that formation constants, rate constants, and  $pK_a$  values determined in this reasearch would have been different if NADPH was used, since NADPH probably causes a conformational change in the enzyme (38,39,40). Therefore, the values presented are only valid for the coenzyme free system.

#### A. ICDH Assisted Decarboxylation of Oxalosuccinate

In order to analyze the kinetic data, some equilibrium data is needed. This data is in the form of appropriate  $pK_a$  values and formation constants for all complexes. In order to simplify the kinetic analysis, it would be helpful to determine these constants independently of the kinetic results. It was therefore decided to perform spectrophotometric titrations as a means of obtaining the desired values.

One titration, to determine the  $pK_a$  value for ICDH, is shown in Figure 37. The titration was done at 280 nm, which coincides with the only peak in the UV/vis spectrum of the enzyme. The titration was accomplished at 25°C in the Cary 14 as follows. 100  $\mu$ l of the stock enzyme solution (at a concentration of 0.186 mM) was syringed into

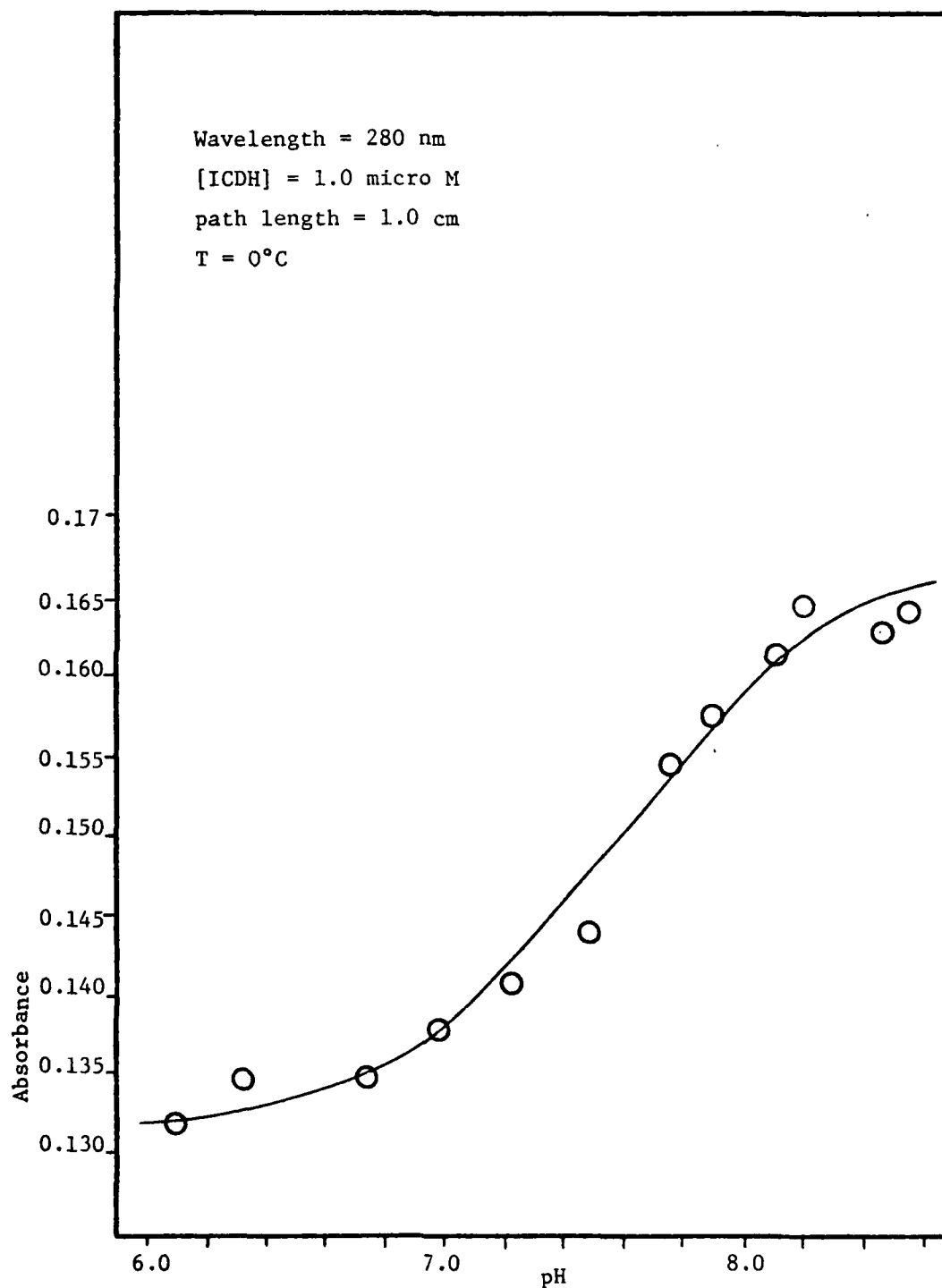


Figure 37. Spectrophotometric titration of isocitrate dehydrogenase.

49.5 ml of doubly distilled dimineralized water at 25°C. The pH was adjusted to approximately 6.0, then this solution was diluted to 50.0 ml. After recording the pH, the absorbance at 280 nm was determined. Next, 12.5  $\mu$ l of 1.00 N NaOH was added. The absorbance reading at this new pH was recorded. This was repeated using varying amounts of NaOH until a pH of 8.5 was attained. This data, shown in Figure 37 and tabulated in Appendix A, was analyzed by the program CORNEK. From this analysis, the  $pK_a$  of the enzyme is  $7.67 \pm 0.14$ . The calculated values are represented as the solid line in the figure.

It is very difficult to interpret this result based on the one experiment because of the complexity of the enzyme. Colman (38) studied the dependence of the Michaelis constant for the manganese<sup>2+</sup> - isocitrate substrate on the observed rates and the pH. From her analysis, the  $pK_a$  of the free enzyme, 6.01, is considerably lower than the value determined above. She also reported (38) a value of 5.71 for the  $pK_a$  of the enzyme-substrate complex and 6.55 for the enzyme-manganese<sup>2+</sup> complex. In another paper, Ehrlich and Colman (30) studied the loss of activity after treatment of ICDH with ethoxyformic anhydride. They reported that the observed loss of dehydrogenase activity depended upon the basic form of an ionizable group with a  $pK_a$  of 5.67, while the loss in decarboxylation activity was dependent upon an ionizable group with a  $pK_a = 7.05$ . It is apparent that the proton titrated



spectrophotometrically cannot be directly related to other published  $pK_a$  values. Therefore, the result of this titration will be a simple statement of fact: a proton, with a  $pK_a$  value of 7.67, was titrated from the enzyme. Further discussion will be deferred until the discussion of the kinetic data, which is included in the second section of this chapter.

The next step, then, was to observe the kinetics of the reaction under a wide range of conditions. The enzyme concentration was fixed at  $1.06 \times 10^{-6}$  M for all experiments. The concentration of oxas ranged from 0.151 mM to 2.72 mM in the pH range of 6.5 to 8.0. If the concentration of oxas was lower than 0.15 mM, it became extremely difficult to analyze the very small absorbance change of the reaction ( $\Delta$  absorbance = 0.005 absorbance units). That established 0.15 mM as the lowest concentration of oxas that could be used for the spectrophotometric analysis.

For the experiments at a pH of 6.5, MES was used as the buffer. HEPES was used for the pH range of 6.8 - 8.1. In either case, the final concentration of the buffer was fixed at 0.020 M. HEPES was selected because it does not bind with the metals used in this investigation. Although metals can bind to MES, they do not form very stable complexes. Consequently, their contribution to the overall system can be ignored.

The experiments were performed in the following way. A solution of oxas at the desired concentration was prepared at 0°C as described in the Experimental section of Chapter II, then neutralized with NaOH, which was also at 0°C. Then, 1.0 ml of this solution was syringed into a 1.0 cm quartz cell. This was followed by 12.5  $\mu$ l of the enzyme solution. Lastly, 1.0 ml of the buffer solution, heated to 55°C, was added. The reaction mixture, now at 25°C, was placed in the thermostatted cell compartment of the Gilford 250 Spectrophotometer to monitor the reaction. The ionic strength was maintained at 0.1 M by the addition of NaCl to the oxas solution.

Since the solution of oxas and ICDH will be essentially composed of oxas<sup>3-</sup>, it was decided to monitor the reaction at 255 nm and 240 nm, which were the same wavelengths used in the investigation of the non-enzymatic decarboxylation reaction. A typical trace of this reaction was similar to other traces; that is, a rapid absorbance increase followed by a slower absorbance decrease. The increase was attributed to the tautomerization of the non-enzyme bound oxas, while the decrease was due to the decarboxylation of the free and complexed acid. As before, tautomerization will be considered as a pre-equilibrium step and therefore ignored during the analysis of the kinetic data. The data was analyzed by the program RLXFT in a manner identical to the analysis of the spontaneous decarboxylation spectral changes.

Each data point reported in this portion of the investigation is the result of at least two separate experiments, one at 240 nm and another at 255 nm. Any discrepancies in these experiments were resolved by repeating the experiment a third time. This generally resulted in a confirmation of one of the previous values. This replication insured accurate data acquisition for this complex system.

Some of the observed rate constants as a function of pH are shown in Figure 38, while the rate data versus the concentration of oxas is shown in Figure 39. A complete table of the data can be found in Appendix C. Note that the range of observed rate constants is from  $2.5 \times 10^{-4}$  seconds<sup>-1</sup> to  $1.21 \times 10^{-3}$  seconds<sup>-1</sup>. Since the observed rate constants for the spontaneous decarboxylation of oxas were  $2.2 - 2.5 \times 10^{-4}$  seconds<sup>-1</sup> in this pH range, it is apparent that the enzyme is able to catalyze the reaction without the aid of any metal ion cofactors. This is in contrast to the oxidation of isocitrate, which has an absolute requirement for a metal ion (in addition to NADP<sup>+</sup>) in the enzymatic reaction. Also note that the observed rate constant decreases as the concentration of oxas increases. This is opposite of what would be anticipated in an enzyme system; that is, the rate increases as the level of substrate increases. This observation must be considered when proposing and verifying a model for this system.

It is also readily apparent that, at constant oxas concentration, as the pH increases, the observed rate decreases. This can be

Figure 38

Observed rate constant for the ICDH-oxalosuccinate system as a function of pH.

[buffer] = 0.020 M

T = 25°C

I = 0.1 M

(ICDH) =  $1.06 \times 10^{-6}$  M

○ [oxas] =  $1.51 \times 10^{-4}$  M

△ [oxas] =  $2.77 \times 10^{-4}$  M

◊ [oxas] =  $7.69 \times 10^{-4}$  M

□ [oxas] =  $2.72 \times 10^{-3}$  M

pH Range

6.4 - 6.8

6.8 - 8.1

Buffer Used

MES

HEPES

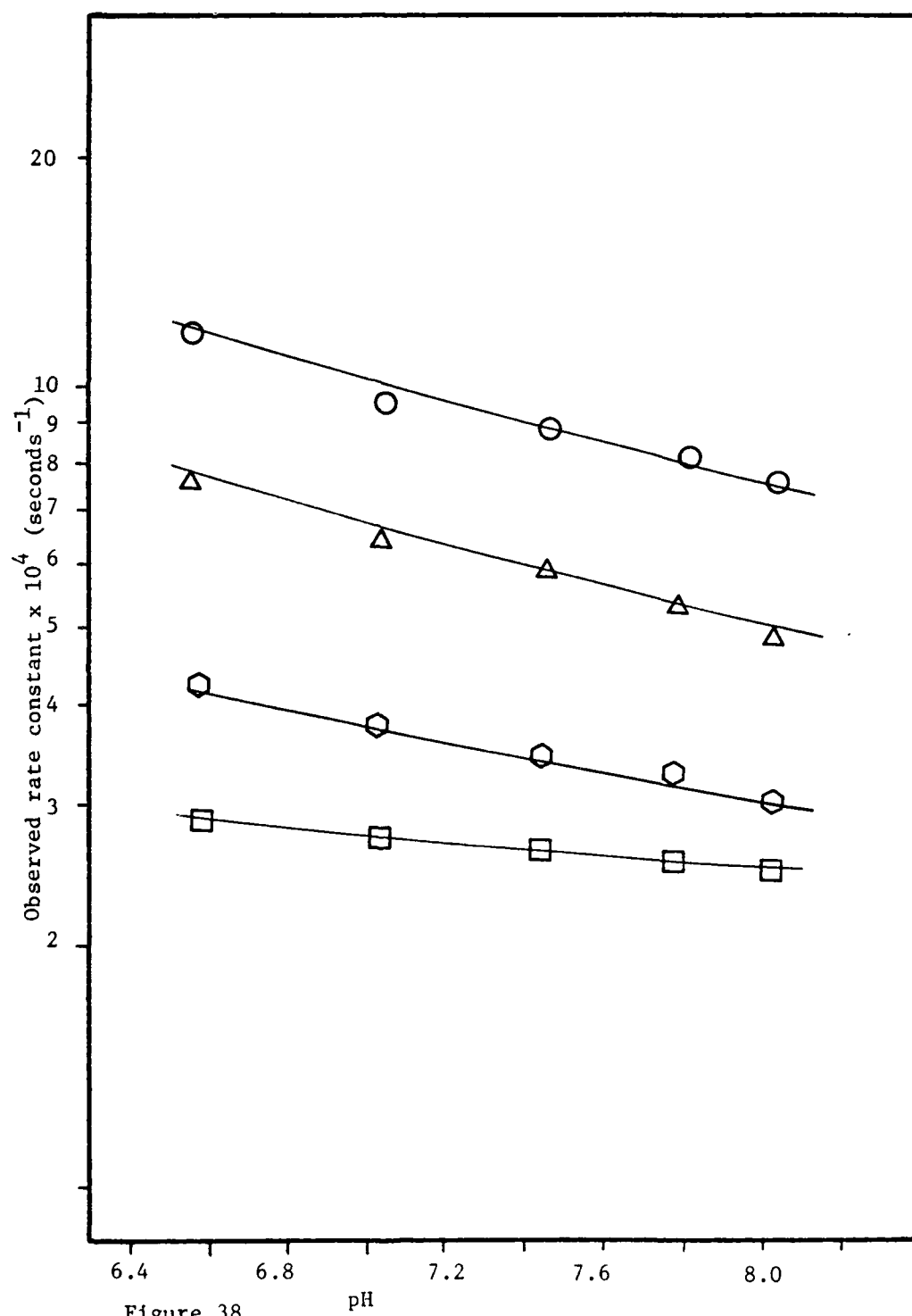


Figure 38.

Figure 39

Observed rate constant for the ICDH-oxalosuccinate system as a function of the concentration of oxalosuccinate.

[buffer] = 0.020 M

T = 25°C

I = 0.1 M

[ICDH] =  $1.06 \times 10^{-6}$  M

○ pH = 6.6

△ pH = 7.0

○ pH = 7.4

□ pH = 8.0

Buffers used are shown on Figure 38.

AD-A092 546

AIR FORCE INST OF TECH WRIGHT-PATTERSON AFB OH  
SPONTANEOUS, METAL-CATALYZED, AND ENZYME-CATALYZED DECARBOXYLAT--ETC(U)  
1980 S L SINCOFF  
AFIT-CI-80-270

F/G 7/3

UNCLASSIFIED

NL

3 of 4  
AD-A  
1782416



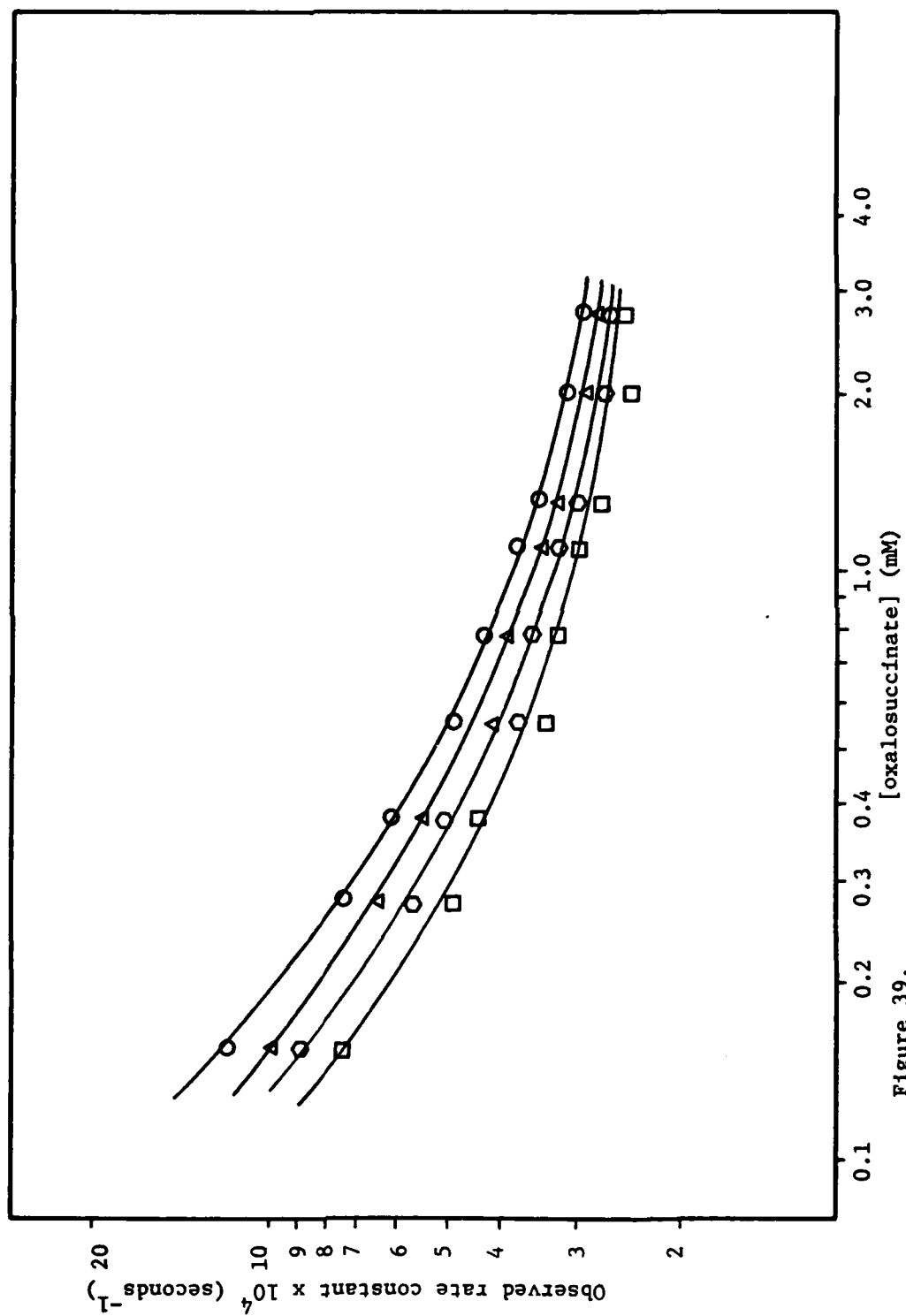
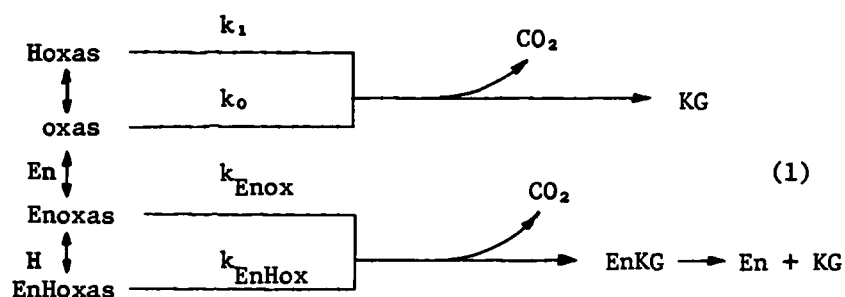


Figure 39.



accounted for by assuming that the ICDH-oxas complex deprotonates, forming either a non-decarboxylating complex or a less reactive, ionized complex. If the latter is assumed, then the reaction sequence, ignoring enol formation, is:



The charges on the complexes were omitted for simplicity. The other protonated forms of oxas were also omitted since they will be present in negligible quantities in the pH range of these experiments.

The rate law for this scheme is:

$$\begin{aligned}
 - \frac{d(\text{oxas})_{\text{total}}}{dt} &= k_{\text{obs}} [\text{oxas}]_{\text{total}} = k_1 [\text{Hoxas}] + k_o [\text{oxas}] \\
 &\quad + k_{\text{Enoxas}} [\text{Enoxas}] + k_{\text{EnHoxas}} [\text{EnHoxas}] \quad (2)
 \end{aligned}$$

By dividing Equation (2) by the total concentration of oxas, we obtain the mathematical expression for the reaction scheme (1), which is:

$$k_{\text{obs}} = k_1 \text{Fr}_{\text{Hoxas}} + k_0 \text{Fr}_{\text{oxas}} + k_{\text{Enoxas}} \text{Fr}_{\text{Enoxas}} + k_{\text{EnHoxas}} \text{Fr}_{\text{EnHoxas}} \quad (3)$$

where  $\text{Fr}_i$  is the fraction of oxas that is in the form of "i".

The experimental data tabulated in Appendix C was tested in the program CORNEK using this model. From the best fit of the data, the formation constant for the ICDH - oxas complex was  $10^{5.67 \pm 0.14}$  while the  $\text{pK}_a$  of the complex was  $7.22 \pm 0.10$ . The rate constant for the protonated ICDH-oxas complex was  $0.159 \pm 0.004 \text{ seconds}^{-1}$ , which is nearly two orders of magnitude faster than the free monoprotonated oxas complex. The rate constant for the deprotonated enzyme-oxas complex was  $0.0704 \pm 0.003 \text{ seconds}^{-1}$ . These rates are comparable to the zinc-oxas keto complex, which is  $0.136 \text{ seconds}^{-1}$ . For this analysis, the formation constant of the ICDH- $\alpha$ -KG complex was fixed at  $10^{4.987}$  (35).

Based on these values, it is necessary to determine if the model predicts the observations included in Figure 39. Recall that this figure shows that at constant pH, the observed and calculated rates decrease as the concentration of oxas increases. This statement contradicts the expectations of an enzyme system; that is, the rate should increase as the amount of substrate increases. The answer to this paradox lies in the mathematics of this system. Since the concentration of the enzyme is approximately 100 to 1000 times lower than the concentration of oxas, and since the formation constant for the

complex is so large, then the actual concentration of the ICDH-oxas complex is nearly unchanged while the concentration of the substrate changes by a factor of 18. According to the model, the observed rate is a function of the fractional distribution of oxas. Although the concentration of the complex is essentially unchanged, the fraction of oxas that is complexed to the enzyme will be much greater at the lower concentration of substrate, an observation reflected in Figure 39.

The solid lines in Figures 38 and 39 represent the theoretical values calculated from Equation (3). These plots indicate that the model proposed accurately describes the observed kinetics of this system.

Although the formation constant for the enzyme- $\alpha$ -KG complex has been published, it is necessary to optimize it for the conditions of this investigation. Therefore, the following experiments were performed. A 0.10 M solution of  $\alpha$ -KG was prepared. The ICDH, buffer, and oxas solutions were prepared as described previously in this chapter. After the oxas was syringed into the cell, 5  $\mu$ l of the  $\alpha$ -KG solution was added. This was followed by the enzyme and buffer as before, and analyzed in the Gilford 250 Spectrophotometer. The result of injecting a very small volume of concentrated  $\alpha$ -KG solution was to increase its concentration in the reaction cell without a drastic change in volume. The concentration of  $\alpha$ -KG can be varied by varying the volume added. The results of these experiments are shown in Table 19.

TABLE 19  
 $\alpha$ -KETOGLUTARATE INHIBITION ON THE  
 ICDH-OXALOSUCCINATE SYSTEM

$\alpha$ -Ketoglutarate Inhibition:  
 [oxas] = 0.252 mM; pH = 7.44

[KG] mM	k(obs)	k(calc)	% Dev	% ICDH Bound to:		
				KG	oxas	Hoxas
0.110	5.83E-4	5.78E-4	0.87	5.3	58.7	35.4
0.235	5.39E-4	5.56E-4	-3.06	10.7	55.4	33.4
0.607	5.11E-4	5.09E-4	0.39	23.4	46.7	29.5

Note: The rate constants are in units of seconds<sup>-1</sup>.

The observed rate constants for these experiments were analyzed with the other data points for this system in the program CORNEK to optimize the ICDH -  $\alpha$ -KG formation constant. The value resulting from this fit was  $10^{4.99}$ , the same value stated in the literature. The calculated values in the table were evaluated from Equation (3).

The next portion of this investigation was to study the effect of EDTA on the reaction rates. These experiments were conducted in the following way. Buffer, ICDH, and oxas solutions were prepared as previously described. The cold oxas solution, 1.0 ml, was syringed into a 1.0 cm quartz cell. Next, a  $\mu$ l volume of 0.100 M EDTA was added. This was followed by 12.5  $\mu$ l ICDH and 1.0 ml of buffer at 55°C. The cell was then placed in the Gilford 250 and monitored at 255 nm. Different concentrations of EDTA were obtained by varying the volume of EDTA added. The largest volume increment was 10.0  $\mu$ l, giving a concentration of 0.494 mM. Using this technique, the amount of EDTA in the reaction cell can be changed without a significant change in the total volume.

The results of this experiment are summarized in Table 20. The observed rate constant is plotted as a function of EDTA concentration in Figure 40 for an oxas concentration of 0.252 mM and a pH of 7.44. The effect of a 40  $\mu$ M concentration of EDTA on the pH profile is shown in Figure 41 for two different oxas concentrations. It is evident

TABLE 20

## EDTA INHIBITION ON THE METAL-FREE SYSTEM

<u>Reaction</u>	<u>Rate Constant</u>
E-oxas $\rightarrow$ CO <sub>2</sub>	7.04E-02
H-E-oxas $\rightarrow$ CO <sub>2</sub>	1.59E-01
H- oxas $\rightarrow$ CO <sub>2</sub>	1.69E-03
oxas $\rightarrow$ CO <sub>2</sub>	2.22E-04
<u>Complex</u>	<u>Log <math>\beta</math></u>
Enoxas	5.670
EnHoxas	12.890 (En + H <sup>+</sup> + oxas = EnHoxas)
Hoxas	4.467
En $\alpha$ -KG	4.987
H $\alpha$ KG	4.640
HEDTA	10.950
H <sub>2</sub> EDTA	17.220 (2H <sup>+</sup> + EDTA <sup>4-</sup> = H <sub>2</sub> EDTA <sup>2-</sup> )
EnHEDTA	17.960 (En + H <sup>+</sup> + EDTA <sup>4-</sup> = EnHEDTA)

Enzyme concentration = 1.06E-06 M for all experiments.

Data Set #1: [oxas] = 0.252 mM [ $\alpha$ KG] = 0.110 mM

Exp	[EDTA]	pH	k(obs)	k(calc)	% Dev
1	5.15E-05	7.44	3.75E-04	3.44E-04	8.36
2	2.13E-04	7.44	2.57E-04	2.61E-04	-1.39
3	5.15E-04	7.44	2.44E-04	2.40E-04	1.77

Data Set #2: [oxas] = 0.151 mM [ $\alpha$ KG] = 0.066 mM

4	4.00E-05	6.57	7.49E-04	8.14E-04	-8.65
5	4.00E-05	7.01	5.31E-04	5.31E-04	-0.01
6	4.00E-05	7.47	3.70E-04	3.84E-04	-3.71
7	4.00E-05	7.77	3.56E-04	3.40E-04	4.37
8	4.00E-05	8.01	3.20E-04	3.22E-04	-0.45

Table 20 (continued)

Exp	[EDTA]	pH	k(obs)	k(calc)	% Dev
Data set #3: [oxas] = 0.693 mM			[αKG] = 0.303 mM		
9	4.00E-05	6.57	4.13E-04	4.20E-04	-1.60
10	4.00E-05	7.01	3.45E-04	3.59E-04	-4.06
11	4.00E-05	7.47	3.23E-04	3.10E-04	4.09
12	4.00E-05	7.77	3.09E-04	2.91E-04	5.84
13	4.00E-05	8.01	2.99E-04	2.82E-04	5.76

Note: the rate constants have units of 1/seconds.

Figure 40

EDTA inhibition on the ICDH - oxalosuccinate system: rate constant versus [EDTA].

$T = 25^{\circ}\text{C}$

$I = 0.1 \text{ M}$

$\text{pH} = 7.44$

$[\text{HEPES}] = 0.020 \text{ M}$

$[\text{oxas}] = 0.252 \text{ mM}$

$[\alpha\text{KG}] = 0.110 \text{ mM}$

$[\text{ICDH}] = 1.06 \mu\text{M}$

The dotted line indicates the observed rate in the absence of EDTA.



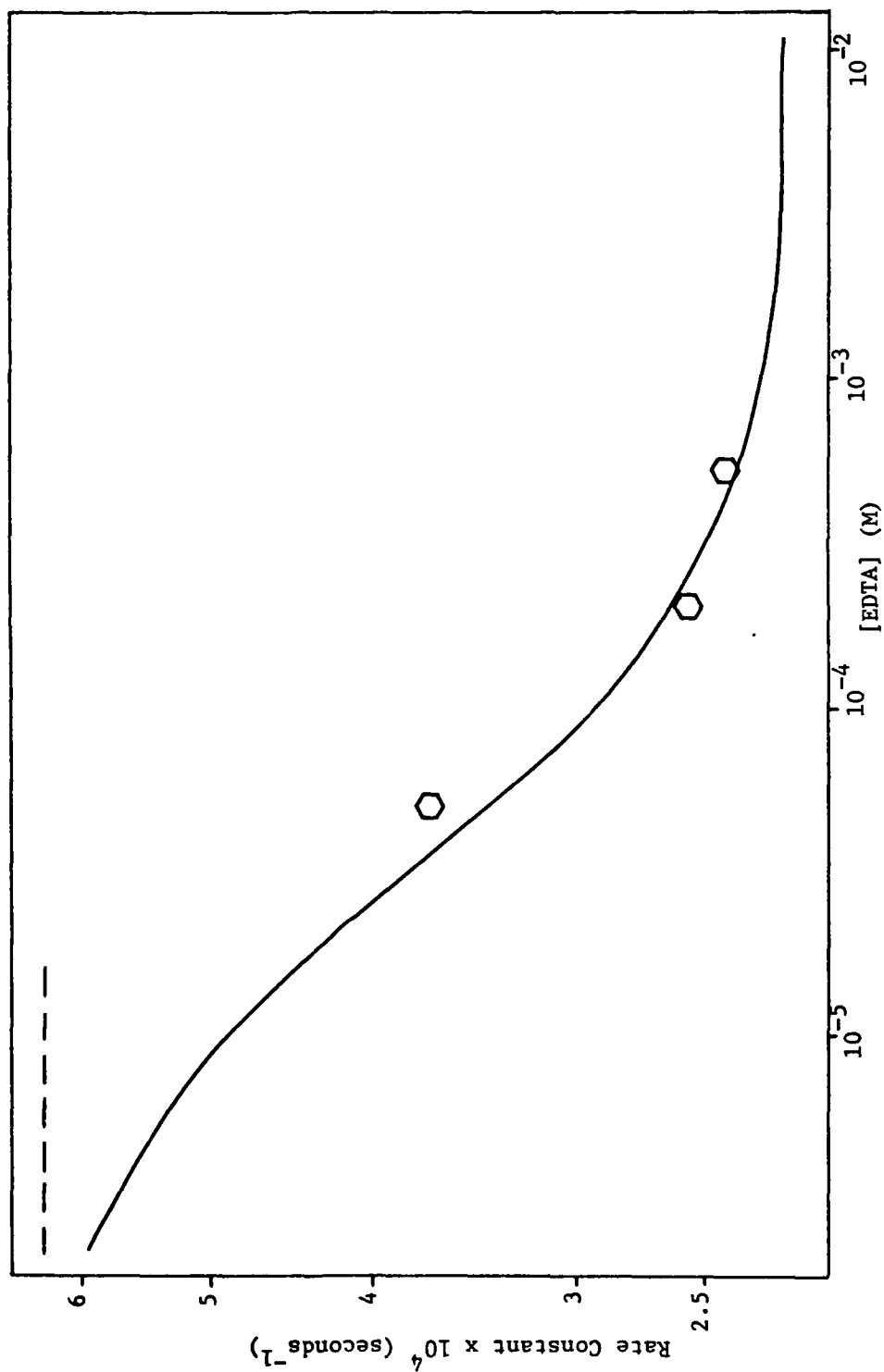


Figure 40.

Figure 41

EDTA inhibition on the ICDH - oxalosuccinate system: rate constant versus pH

$T = 25^{\circ}\text{C}$

$I = 0.1 \text{ M}$

$[\text{ICDH}] = 1.06 \mu\text{M}$

- $[\text{oxas}] = 0.151 \text{ mM}$ ; no EDTA
- $[\text{oxas}] = 0.151 \text{ mM}$ ;  $[\text{EDTA}] = 0.040 \text{ mM}$
- $[\text{oxas}] = 0.693 \text{ mM}$ ; no EDTA
- $[\text{oxas}] = 0.693 \text{ mM}$ ;  $[\text{EDTA}] = 0.040 \text{ mM}$

Buffer conditions are shown in Figure 38.

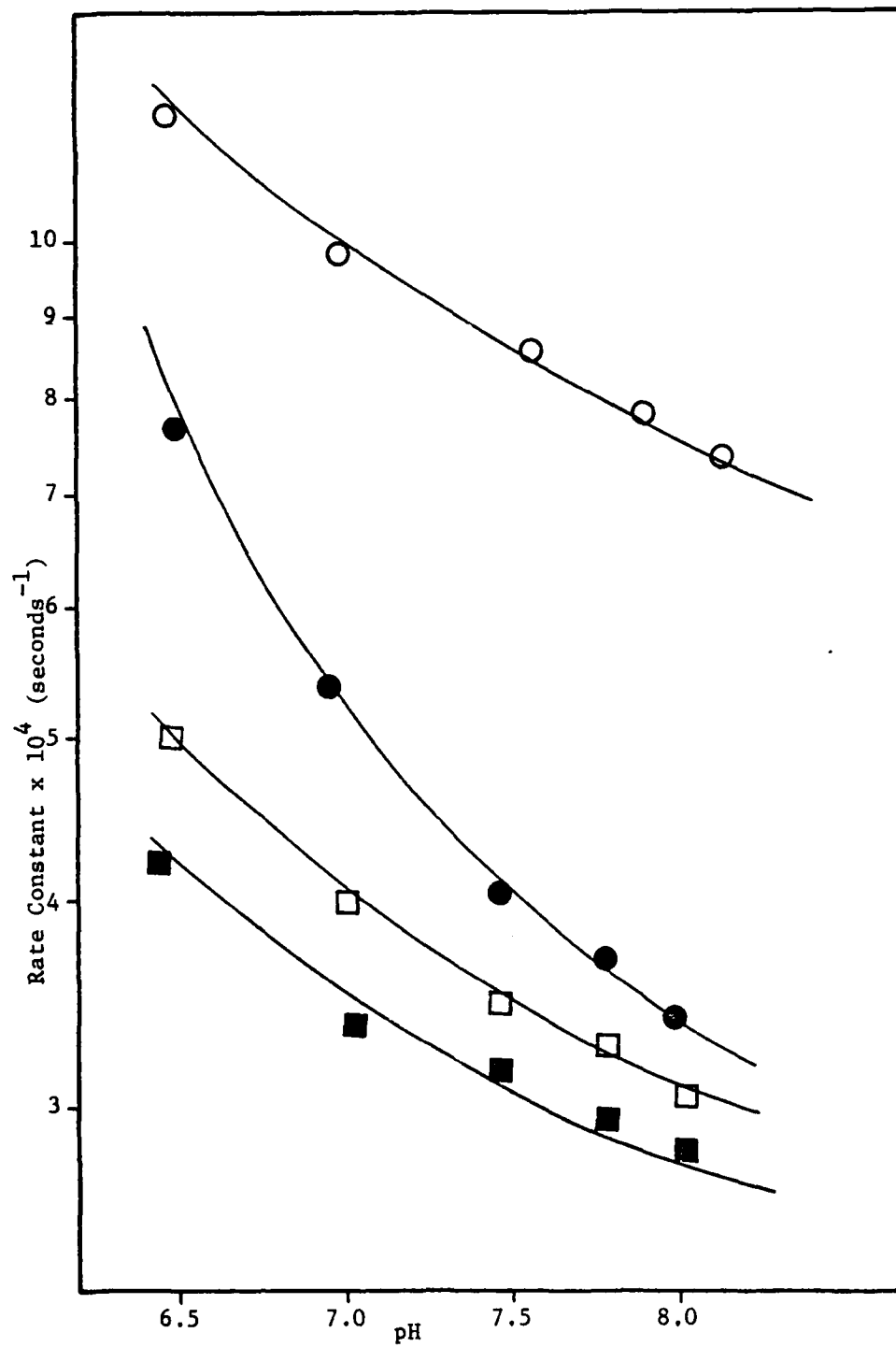


Figure 41.

that EDTA inhibits the reaction, but the question is: how does it inhibit? To begin answering this question, an attempt was made to fit the data to a model. It was first assumed that  $\text{EDTA}^{4-}$  binds to the enzyme with a particular formation constant. Thus,  $\text{EDTA}^{4-}$  competes with  $\text{oxas}^{3-}$  at the active site of the enzyme. Unfortunately, this model, tested via CORNEK, did not adequately describe the data due to relatively large deviations between observed and calculated rate constants.

The next model was to assume that EDTA was monoprotonated. This was a reasonable assumption since free EDTA is 63%  $\text{HEDTA}^{3-}$ /37%  $\text{H}_2\text{EDTA}^{2-}$  at pH = 6.5 and 98%  $\text{HEDTA}^{3-}$ /2%  $\text{H}_2\text{EDTA}^{2-}$  at pH = 8.0. When this model was tried in CORNEK, a good fit, based on the differences between the observed and calculated values, was obtained. This fit is represented as the solid lines in Figures 40 and 41, and is also shown in Table 20 as  $k(\text{calc})$ . The formation constant for the  $\text{ICDH-HEDTA}^{3-}$  complex is  $10^{17.96 \pm 0.02}$ . After accounting for the  $\text{pK}_a$  of EDTA (10.95), the effective formation constant of the  $\text{ICDH-EDTA}$  complex is  $10^{7.01}$ . This value is approximately 20 times higher than the  $\text{ICDH-oxas}$  complex.

This model states that  $\text{HEDTA}^{3-}$  binds to the enzyme, but does not rule out binding via trace metals in solution or enzyme-bound metal. To rule out the latter, consider the data in Table 21, which summarizes published data on the metal content of the apoenzyme. These data show that there is less than 1.5 mol %  $\text{Mn}^{2+}$  and less than 1.6 mol %  $\text{Zn}^{2+}$

TABLE 21  
METAL CONTENT OF ICDH

[ICDH]	M <sup>2+</sup>	[M <sup>2+</sup> ]	mol % M	Method	Reference
0.940 mM	Mn	0	0	epr	36
6.48 M	Mn	0.10 M	<1.5	AA	37
6.14 M	Zn	0.10 M	<1.6	AA	37
0.186 mM	Mg	0.014 mM	<7	AA	This work

bound to the enzyme. This researcher determined the  $\text{Mg}^{2+}$  content via atomic absorption. The investigation was done on a Perkin-Elmer 303 Spectrophotometer, using an air/acetylene flame with a 10.0 cm path length. The source was a magnesium hollow cathode lamp. The absorption line studied was 285.2 nm. The air flow rate was 9 ml/min., while the acetylene flow rate was 3 ml/min. The  $\text{Mg}^{2+}$  standard solutions were first prepared as an aqueous solution, then diluted by a factor of two with glycerol to match the enzyme solution. Using this method, the flame temperature was the same for the standard as well as the sample.

Using this method, it was found that the apoenzyme contained less than 7 mol %  $\text{Mg}^{2+}$ . Therefore, from this table, it is concluded that no more than 10 mol % of ICDH had bound metal. This value is an upper limit value and is set only by the detection limit of the analytical method.

The next step is to calculate the fractional distribution of ICDH in the ICDH-oxas- $\alpha$ -KG-HEDTA system based on a  $\log \beta_{\text{EnHEDTA}} = 17.96$ . This was done with the program GENDIS. It was found, based on  $[\text{oxas}] = 0.252 \text{ mM}$ ,  $[\alpha\text{-KG}] = 0.110 \text{ mM}$ ,  $[\text{ICDH}] = 1.06 \text{ }\mu\text{M}$ , and the pH of 7.44, that 31.6 mol % of the enzyme contained bound HEDTA when  $[\text{EDTA}^{4-}] = 1.0 \times 10^{-5} \text{ M}$ . At an  $\text{EDTA}^{4-}$  concentration of  $1.0 \times 10^{-4} \text{ M}$ , 82.6 mol % of ICDH contained bound HEDTA. Even at an  $\text{EDTA}^{4-}$  concentration of  $3.2 \times 10^{-6} \text{ M}$ , 12.7 mol % of ICDH contained bound HEDTA. Since ICDH is

no more than 10 mol % metallated, it is concluded that the binding of HEDTA does not result from any metal on the enzyme.

However, this does not rule out the possibility that EDTA is tying up trace metal contaminants in the solution. To eliminate this possibility, it is necessary to examine the experiments of Kratochvil and coworkers (41), who studied the effect of  $\text{Mg}^{2+}$ ,  $\text{Mn}^{2+}$ ,  $\text{Zn}^{2+}$ , and  $\text{Co}^{2+}$  on the overall ICDH reaction. They found that a small but measurable reaction is observed at 340 nm in the absence of metal ions. These experiments were repeated by this researcher with similar results. This effect was attributed to metal ion impurities in the reagents, since the activity was reduced to zero by the addition of EDTA. Their calculations, based on the level of residual activity, the amount of EDTA required to eliminate the residual activity, and the conditional formation constants, indicated that the trace metal causing the activity was  $10^{-7} \text{ M Mn}^{2+}$ .

To examine the hypothesis that EDTA is merely binding the trace metals in solution, consider a solution composed of 0.20 mM oxas, 1.06  $\mu\text{M}$  ICDH, and  $10^{-7} \text{ M Mn}^{2+}$ . If we now assume that this solution also contains  $10^{-7} \text{ M EDTA}^{4-}$ , then, from the program GENDIS, 29% of the  $\text{Mn}^{2+}$  is bound to  $\text{EDTA}^{4-}$ , while 0.02% of the  $\text{Mn}^{2+}$  is bound to ICDH. If the  $\text{EDTA}^{4-}$  concentration increases to  $10^{-5} \text{ M}$ , then 98.3% of  $\text{Mn}^{2+}$  is bound to  $\text{EDTA}^{4-}$ , whereas 99.8% of the  $\text{Mn}^{2+}$  is complexed to  $\text{EDTA}^{4-}$  in a solution composed of  $10^{-4} \text{ M EDTA}^{4-}$ . This means that essentially all of the manganese is bound to  $\text{EDTA}^{4-}$  at  $[\text{EDTA}^{4-}] = 10^{-5} \text{ M}$  or

greater. However, it is evident from Figure 40 that the observed rate constant dropped 40% as the level of  $\text{EDTA}^{4-}$  decreased from  $5 \times 10^{-5} \text{ M}$  to  $5 \times 10^{-4} \text{ M}$ . From the above discussion, this rate decrease cannot result solely from the binding of EDTA to trace metals in the solution.

It is concluded, then, that EDTA actively competes with oxas at the active site of the enzyme. The data presented on the inhibition of the reaction follows the binding of a monoprotinated EDTA complex to ICDH, with a  $\log \beta$  of 17.06. The data does not indicate that the role of EDTA is to remove trace metals from solution.

Now that the role of EDTA in this system has been discussed, let us look at the problem encountered by this researcher in attempting to determine the  $\text{pK}_a$  values of the apoenzyme from the kinetic data. This investigator found that this was impractical for the following reason. Due to the large complex formation constants, very little enzyme was unbound. Because of this, varying the  $\text{pK}_a$  from 6.0 to 7.7 did not change the computer fit of the data very much.

Consider, for example, a reaction mixture composed of  $1.06 \times 10^{-6} \text{ M}$  ICDH,  $2.52 \times 10^{-4} \text{ M}$  oxas, and  $1.10 \times 10^{-4} \text{ M}$  KG at a pH of 7.44. The observed rate constant was  $5.83 \times 10^{-4} \text{ seconds}^{-1}$ . If we assume a  $\text{pK}_a$  of 6.40 for the enzyme, then the calculated rate, using the model shown in reaction scheme (1), would be  $5.78 \times 10^{-4} \text{ seconds}^{-1}$ . If we now assume a  $\text{pK}_a$  of 7.67, which was the value found spectrophotometrically, the calculated rate becomes  $5.75 \times 10^{-4} \text{ seconds}^{-1}$ . This means



that changing the enzyme pK value by nearly 1.4 units resulted in a 0.52% decrease in the calculated rate!

It is unclear from the kinetic analysis how oxas is bound to the enzyme or why decarboxylation is accelerated. One explanation is that the substrate sits in a hydrophobic pocket. It has been shown (20) that oxaloacetate decarboxylates faster in a medium of lower dielectric constant. Birus and Leussing (44) provided good evidence for a hydrophobic pocket surrounding oxaloacetate in the enzyme pyruvate kinase. This may also be the case in this enzyme system. However, many more experiments are needed in order to resolve this question.

In summary, the model proposed and verified is as follows. Oxas binds to the enzyme and this complex decarboxylates without the aid of a metal ion. The formation constant of this complex is  $10^{5.67}$ . The decarboxylation rate was  $0.0704 \text{ seconds}^{-1}$ , which is faster than the non-enzymatic reaction. This complex can also protonate, with a  $pK_a$  of 7.22, to yield a more reactive complex. The rate constant for this complex is  $0.159 \text{ seconds}^{-1}$ . The enzyme can also form a competitive complex with  $\alpha$ -KG, with a formation constant of  $10^{4.987}$ . The important point here is that the enzyme can catalyze the reaction without the aid of a metal ion. This means that, in the overall ICDH reaction, the metal is only needed for the oxidation of isocitrate and not for the decarboxylation of oxas. This observation has not been

reported in the literature. The reaction is also inhibited by EDTA, which was attributed to the formation of a competitive ICDH-HEDTA<sup>3-</sup> complex ( $\log \beta = 17.96$ ) and not by the removal of trace metals by binding to EDTA.

B. Zinc (II) and Magnesium (II) Assisted Decarboxylation of the ICDH Oxalosuccinate System

The model presented in the first portion of this chapter on the nonmetal catalyzed enzymatic decarboxylation of oxas will now be extended to include the effects of two metal dications, zinc and magnesium. The zinc data was somewhat limited to the lower pH values due to the formation of the insoluble hydroxide, but this did not greatly affect the results. As will be seen, enough data was obtained to propose and verify a model for this system. The magnesium data was not affected by hydroxide formation, and is therefore more complete. The zinc system will be discussed first since it is less complicated. Note that only part of the data will be presented in this chapter and in the accompanying figures. These figures will provide a more than adequate representation of the data. All of the data is tabulated in Appendix C.

An important consideration for the investigation is to obtain the data over a wide range of conditions. This will insure that a proposed reaction scheme can be tested against all the system variables.

Therefore, the approach to data collection for this portion of the investigation is as follows. At an oxas concentration of 0.33 mM and a metal concentration of 3.28 mM, the pH was varied from 6.5 to 8.0. The metal concentration was increased to 6.28 mM, and the pH profile was repeated. This was repeated with metal ion increments of 3.28 mM until the metal ion concentration reached 19.8 mM. This entire procedure was repeated at an oxas concentration of 0.65 mM and 1.77 mM. The result is a data array that varies over a seven-fold change of metal concentration, five-fold change of oxas concentration, and a 1.5 pH unit range.

This approach worked well for magnesium, but was modified for zinc due to the hydroxide formation. The highest pH was 7.47, while the peak zinc level was 13.1 mM. The minimum zinc concentration was lowered to 1.97 mM. With this scheme, a sufficiently wide range of variables was still possible.

These experiments were performed in the following manner. The oxas solution was prepared as described previously; that is, the solution was neutralized and maintained at 0°C. The buffer was heated to 55°C, while the metal solutions were kept at room temperature. An important point in the experimental procedure is to determine the order in which the solutions will be added. To resolve this, the following two assumptions were made. First, it is not known if this reaction occurs via a random mechanism (61) or an ordered mechanism

(39). There is data to support both mechanisms. Thus, it was assumed that the actual order of the chemicals into the reaction cell was unimportant. This assumption will be justified later by experimentation. Second, it was assumed that protonation, deprotonation, and complexation are very rapid compared to decarboxylation.

From these assumptions, it was concluded that the order of transferring the reagents into the cell is not critical, but the last reagent transferred should be the key compound to initiate the reaction. Of all possible combinations, it was decided to add the metal last. Although the cell contained oxas, ICDH, and buffer, at 25°C prior to the addition of the metal, the observed half-life of that solution (> 12 minutes) is sufficiently long enough that only a small part of the reaction will be lost in the 30 seconds required to add the metal.

Therefore, the solutions were syringed into the 1.0 cm quartz cell in the following order: 1) 0.50 ml neutralized oxas at 0°C; 2) 25.0  $\mu$ l ICDH; 3) 0.50 ml of the appropriate buffer at 55°C; 4) 0.50 ml of the metal solution at room temperature. The cell was then placed in the thermostatted compartment of the Gilford 250 Spectrophotometer and monitored at 260 nm ( $\text{Mg}^{2+}$  system) or 284 nm ( $\text{Zn}^{2+}$  system). The ionic strength was maintained at 0.1 M by adding the calculated amount of NaCl to the metal solution. For the pH = 6.55 experiment, MES was used as the buffer, whereas HEPES was the buffer for the pH range of 6.9 to 8.1. In either case, the final buffer concentration was 0.020 M.

The UV trace representing the reaction showed the biphasic change as described previously in this research. The initial absorbance increase was tautomerization, and, as assumed throughout the experimental procedure, treated as a pre-equilibrium state. The slower absorbance decrease was decarboxylation. The spectrophotometric data was analyzed by the program RLXFT via the equation

$$A_{\text{obs}} = A_{\infty} + A_1 \exp(-k_1 t) + A_2 \exp(-k_2 t)$$

Various experiments were run to determine the effect of the order used in transferring the solutions into the reaction cell. A set of experiments were done by changing the order of reagents for the magnesium system. In one case, magnesium was added last; in another, ICDH was added last. In a third case, the buffer was added last. In the last check, oxas was added last. The observed decarboxylation rate constants determined by RLXFT for each of the four experiments were within experimental accuracy of each other. Therefore, the order is unimportant and the data obtained using the experimental procedure stated above (metal solution last) is reliable.

The zinc data is plotted in Figures 42 and 43. In Figure 42, the observed rate constant is plotted as a function of pH, whereas Figure 43 shows the same data set as a function of the zinc<sup>2+</sup> concentration. From these figures, some trends can be noted. First, from Figure 42,

Figure 42

Observed rate constant for the ICDH-zinc-oxalosuccinate system  
as a function of pH.

T = 25°C

I = 0.1 M

[buffer] = 0.020 M

○ [oxas] =  $6.68 \times 10^{-4}$  M; [Zn] =  $3.28 \times 10^{-3}$  M

▽ [oxas] =  $6.68 \times 10^{-4}$  M; [Zn] =  $1.97 \times 10^{-3}$  M

○ [oxas] =  $1.67 \times 10^{-3}$  M; [Zn] =  $3.28 \times 10^{-3}$  M

Buffers used are as shown in Figure 38.

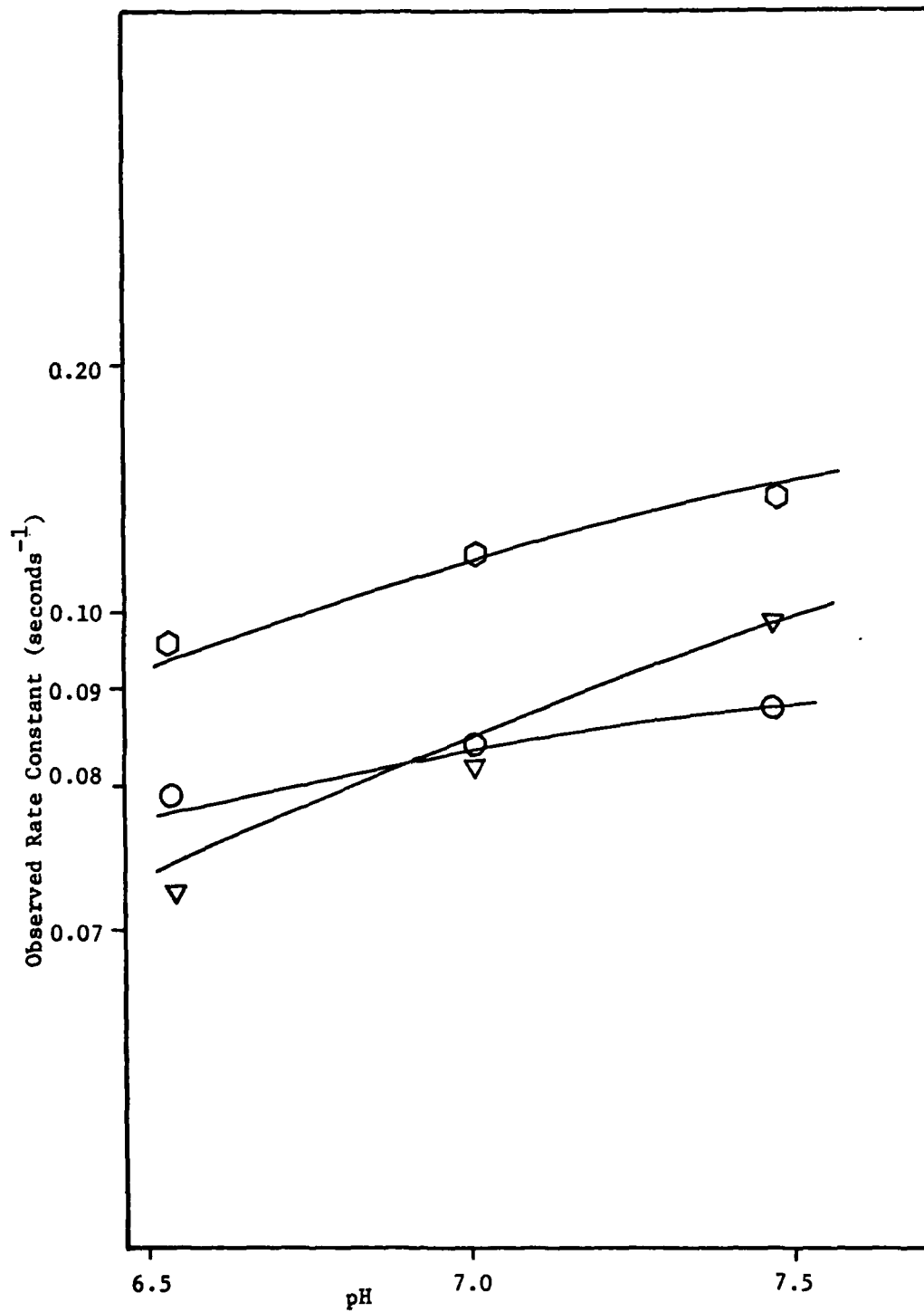


Figure 42.

Figure 43

Observed rate constant for the ICDH-zinc-oxalosuccinate system  
as a function of the zinc concentration.

$T = 25^{\circ}\text{C}$

$I = 0.1 \text{ M}$

$[\text{buffer}] = 0.020 \text{ M}$

○  $[\text{oxas}] = 0.349 \text{ mM}; \text{ pH} = 7.01$

⬡  $[\text{oxas}] = 0.349 \text{ mM}; \text{ pH} = 6.55$

□  $[\text{oxas}] = 0.668 \text{ mM}; \text{ pH} = 6.55$

Buffers used are as shown in Figure 38.



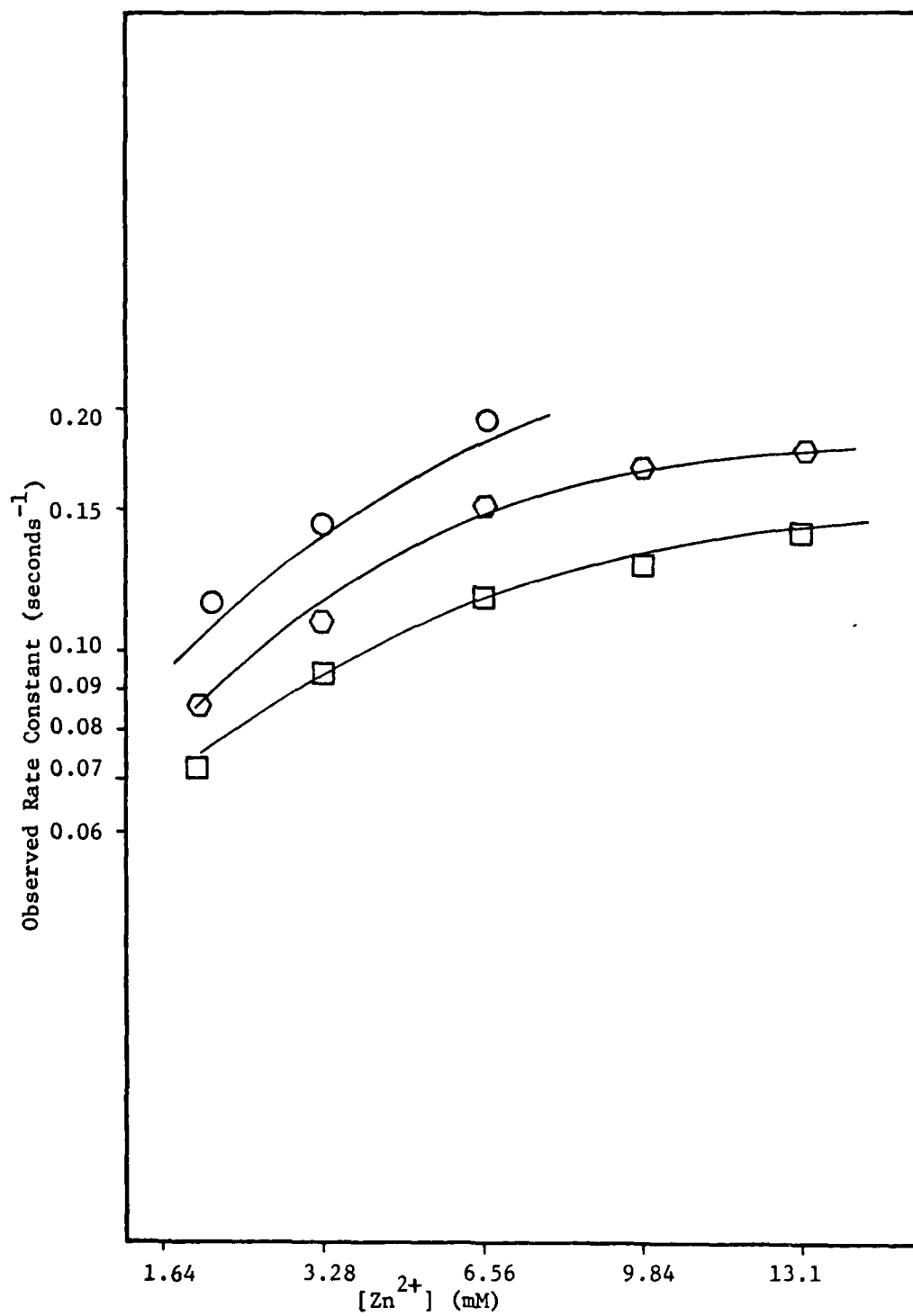
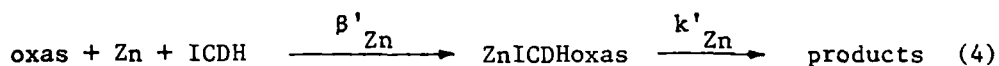


Figure 43.

as the pH increases, the observed rate increases. Since the amount of the binary zinc-oxas complex in solution will not change very much at this pH region for constant zinc and oxas concentration, the rate increase must be due to the increasing amount of the ICDH-zinc-oxas complex being formed. Since the figure does not show a maximum, then it is unlikely that an inhibition complex was formed.

Secondly, from the other plot, the observed rate increases as the metal ion increases, but appears to level off. This leveling could be due to an inhibition complex, but it could also be due to a saturation effect. A third observation, also from the second plot, is that the rate decreases as the concentration of oxas increases. This was the same trend observed in the ICDH-oxas binary system, and therefore comes as no surprise.

From these observations, the data can be qualitatively rationalized by adding reaction (4) to reaction scheme (1) shown earlier



in the chapter. In reaction (4), the primes on the constants indicate the ternary complex while the subscripts describe the metal ion in the complex. The rate law for this scheme now becomes:

$$k_{\text{obs}} = k_1 \text{Fr}_{\text{Hoxas}} + k_o \text{Fr}_{\text{oxas}} + k_{\text{Enoxas}} \text{Fr}_{\text{Enoxas}} + k_{\text{HENoxas}} \text{Fr}_{\text{HENoxas}} + k'_{\text{Zn}} \text{Fr}_{\text{ZnEnoxas}} \quad (5)$$

In addition to the above reaction, the model will also take into account the formation of two other complexes,  $\text{ICDH} - \text{Zn}^{2+}$ , and  $\text{ICDH} - \text{Zn}^{2+} - \alpha\text{KG}$ .

In order to characterize the system, we need to determine three complex formation constants,  $\text{ICDH} - \text{Zn}^{2+} - \text{oxas}$ ,  $\text{ICDH} - \text{Zn}^{2+} - \alpha\text{KG}$ , and  $\text{ICDH} - \text{Zn}^{2+}$ , and one rate constant. However, for the experiments described above, the relative amounts of oxas and  $\alpha\text{KG}$  in the cell were constant. It may be difficult, then, to resolve the absolute values for  $\beta_{\text{ICDH-Zn}^{2+}\text{-oxas}}$  and  $\beta_{\text{ICDH-Zn}^{2+}\text{-}\alpha\text{KG}}$ . In other words, since the ratio of [oxas] to [ $\alpha\text{KG}$ ] is constant, the respective enzyme ternary formation constants may be relative. In order to resolve this possibility, it was necessary to perform a series of experiments at constant oxas, ICDH, and  $\text{Zn}^{2+}$  concentrations and constant pH, but variable  $\alpha\text{KG}$  concentrations. This was done by adding  $\mu\text{l}$  volumes of 0.1 M  $\alpha\text{KG}$  solution to the reaction cell analogous to the EDTA investigation reported above.

All of the data was analyzed by the program CORNEK using this model. The results of the best fit are shown as the solid lines in Figures 42 and 43. Since the theoretical curves provide an excellent trace of the data, it must be concluded that the model proposed for the system is valid. The numerical values for the constants are:

$$\begin{aligned}
 k'_{\text{Zn}} &= 43.7 \pm 1.1 \text{ seconds}^{-1} \text{ (ICDHZnoxas} \rightarrow \text{CO}_2 + \text{products)} \\
 \text{Log } \beta'_{\text{Zn}} &= 7.96 + 0.01 \text{ (ICDH} + \text{Zn}^{2+} + \text{oxas}^{3-} = \text{ICDHZnoxas)} \\
 \text{Log } \beta_{\text{ICDH-Zn}} &= 2.74 \pm 0.15 \\
 \text{Log } \beta_{\text{ICDH-Zn-}\alpha\text{KG}} &= 7.32 \pm 0.08 \text{ (ICDH} + \text{Zn}^{2+} + \alpha\text{KG}^{2-} = \text{ICDHZn}\alpha\text{-KG)}
 \end{aligned}$$

The rate constant for the ICDH-Zn-oxas complex is 300 times faster than the comparable value for the Zn-oxas or the ICDH-oxas complexes. The half life of that reaction is approximately 16 mseconds. It is readily apparent that the  $\text{Zn}^{2+}$  ion has a powerful effect on the reactivity of enzyme-bound oxas. An expanded discussion of the rate constant as well as the significance of the magnitude of the formation constants will be deferred until after the magnesium data is presented.

The observed rate data for the  $\text{ICDH} - \text{Mg}^{2+} - \text{oxas}$  system is presented in Figures 44, 45, and 46. The data collection was accomplished in a manner identical to the  $\text{ICDH-Zn}^{2+}$ -oxas system. In Figure 44, the data is plotted as a function of pH for the case of  $[\text{oxas}]_{\text{total}} = 0.349 \text{ mM}$ . The rate profiles for oxas concentrations of 0.649 mM and 1.77 mM are very similar; the main difference is that for a given pH and magnesium concentration, the reaction rates decrease as the concentration of oxas increases. This observation, typical of these systems in the region of this investigation, is visualized in Figure 46. Figure 45 shows the same data as a function of the magnesium concentration. In the pH profiles shown in Figure 44, the observed rates

Figure 44

Observed rate constants for the ICDH-magnesium-oxalosuccinate system as a function of pH.

$T = 25^{\circ}\text{C}$

$I = 0.1 \text{ M}$

$[\text{buffer}] = 0.020 \text{ M}$

$[\text{oxas}] = 0.349 \text{ mM}$

◇  $[\text{Mg}] = 3.28 \text{ mM}$

▽  $[\text{Mg}] = 6.56 \text{ mM}$

□  $[\text{Mg}] = 9.84 \text{ mM}$

△  $[\text{Mg}] = 13.1 \text{ mM}$

⬡  $[\text{Mg}] = 16.4 \text{ mM}$

○  $[\text{Mg}] = 19.8 \text{ mM}$

Buffers used are as shown in Figure 38.

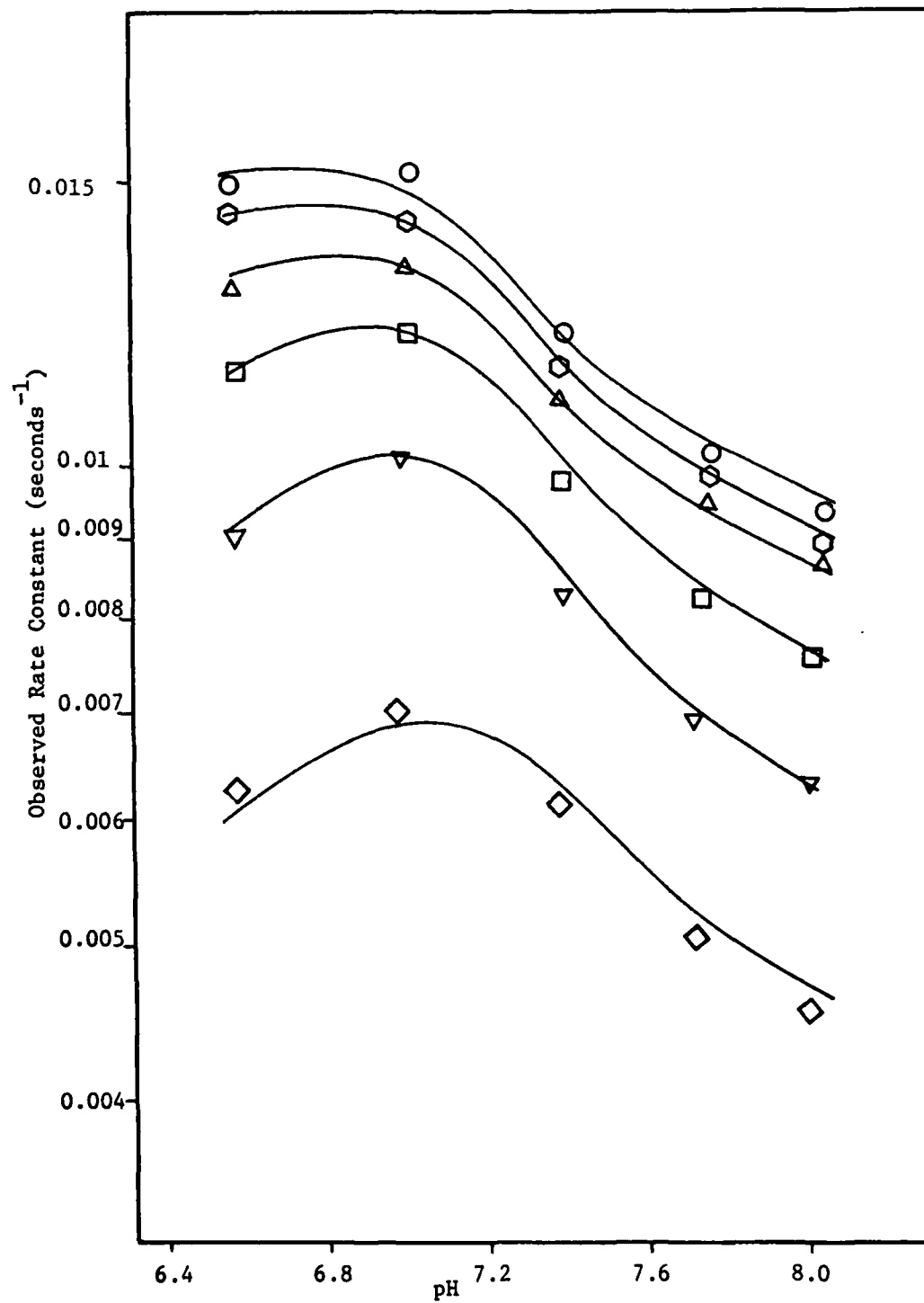


Figure 44.

Figure 45

Observed rate constant for the ICDH-magnesium-oxalosuccinate system  
as a function of the Magnesium concentration.

[oxas] = 0.349 mM

○ pH = 6.57

◊ pH = 7.01

△ pH = 7.47

□ pH = 7.77

▽ pH = 8.01

Other experimental conditions are stated in Figure 44.

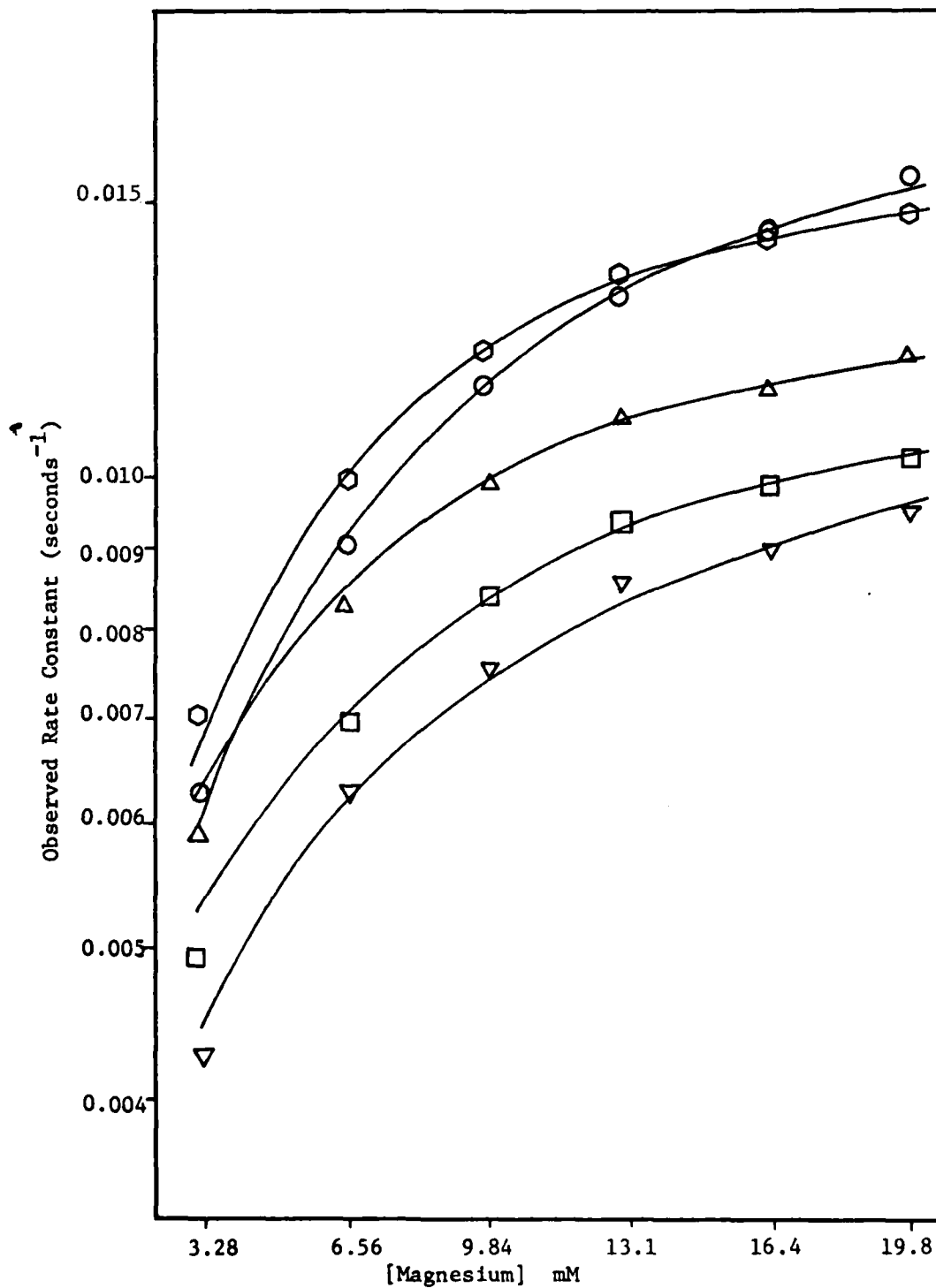


Figure 45.



Figure 46

Observed rate constant for the ICDH-magnesium-oxalosuccinate system as a function of the oxalosuccinate concentration.

- [Mg] = 16.4 mM; pH = 8.01
- ◊ [Mg] = 9.84 mM; pH = 7.77
- △ [Mg] = 6.56 mM; pH = 8.01
- [Mg] = 3.28 mM; pH = 6.57

Other experimental conditions are stated in Figure 44.

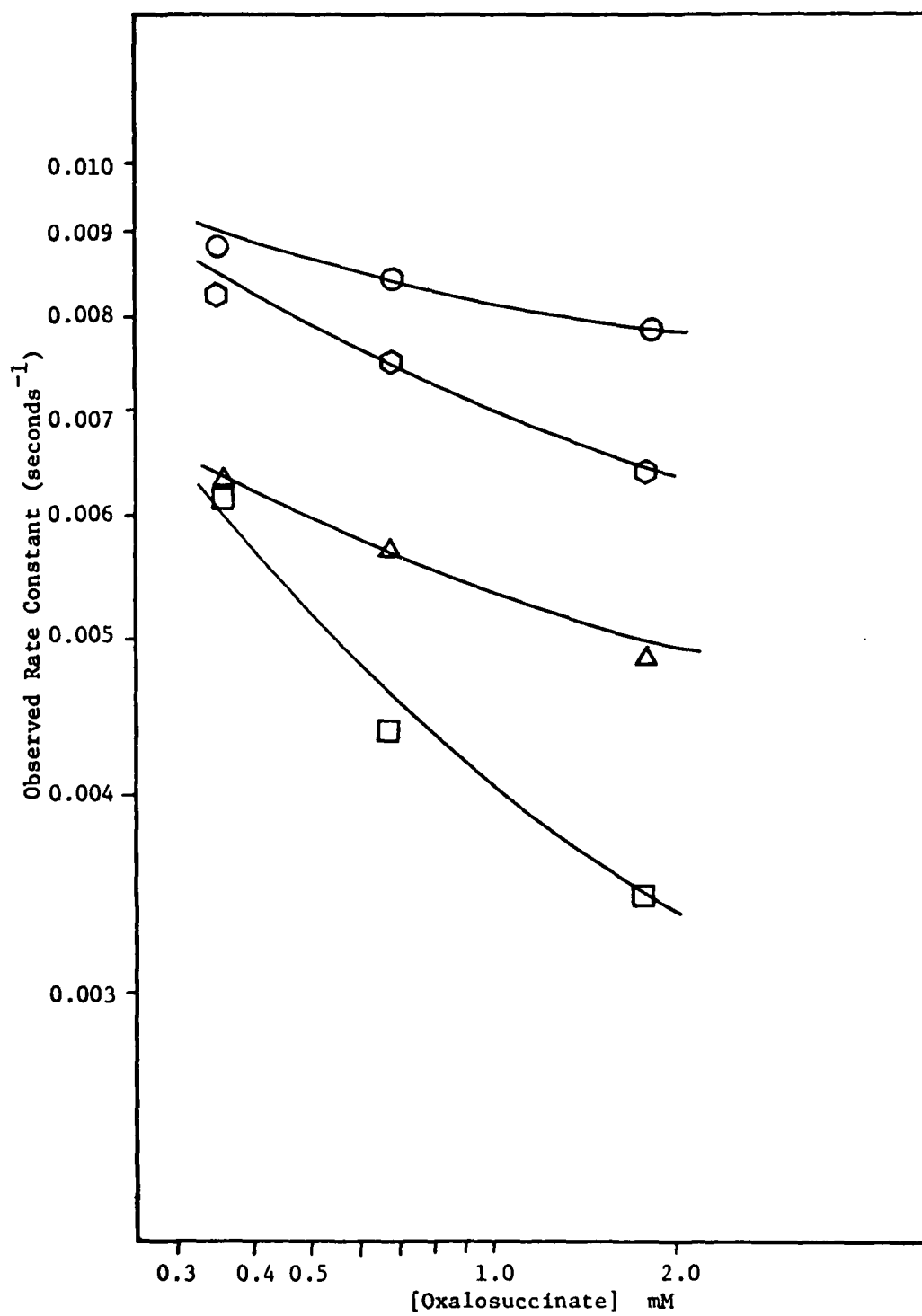
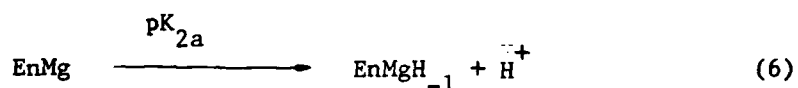


Figure 46.

reach a maximum at pH 7.0 - 7.2. This differs from the zinc system, which had no peaks in the profile. In the magnesium profile in Figure 45, various sets of iso-pH data cross. The zinc model predicts that the pH profile will approach a maximum value asymptotically. It cannot account for a maximum rate as shown in Figure 44. Therefore, the model for the magnesium system must include an inhibition complex.

In order to analyze the data using the following models, some of the data for the rate versus pH was replotted in Figure 47, while some data for the rate versus the magnesium concentration was replotted in Figure 48. Using the pyruvate kinase - oxaloacetate system as a base, we will first consider the formation of a deprotonated ICDH-Mg complex as shown in (6). Inclusion of this



complex to the model does not alter the form of the rate law, equation (5), since it only serves to tie up the enzyme and decrease the amount of oxas-bound complexes.

The results of the best fit from the program CORNEK using this model are shown as the dashed lines in Figures 47 and 48. Although the use of this model results in a graphic similarity with the experimental data, it still does not provide an adequate representation of the data. Therefore, in order to improve the model, it was

Figure 47

Comparison of enzyme models for the ICDH-magnesium-oxalosuccinate system versus pH.

[oxas] = 0.349 mM

○ [Mg] = 19.8 mM

△ [Mg] = 9.84 mM

--- ICDH-Mg-H<sub>-1</sub> only

— ICDH-Mg-H<sub>-1</sub> and ICDH-Mg-oxas-H<sub>-1</sub>

Other experimental conditions are stated in Figure 44.

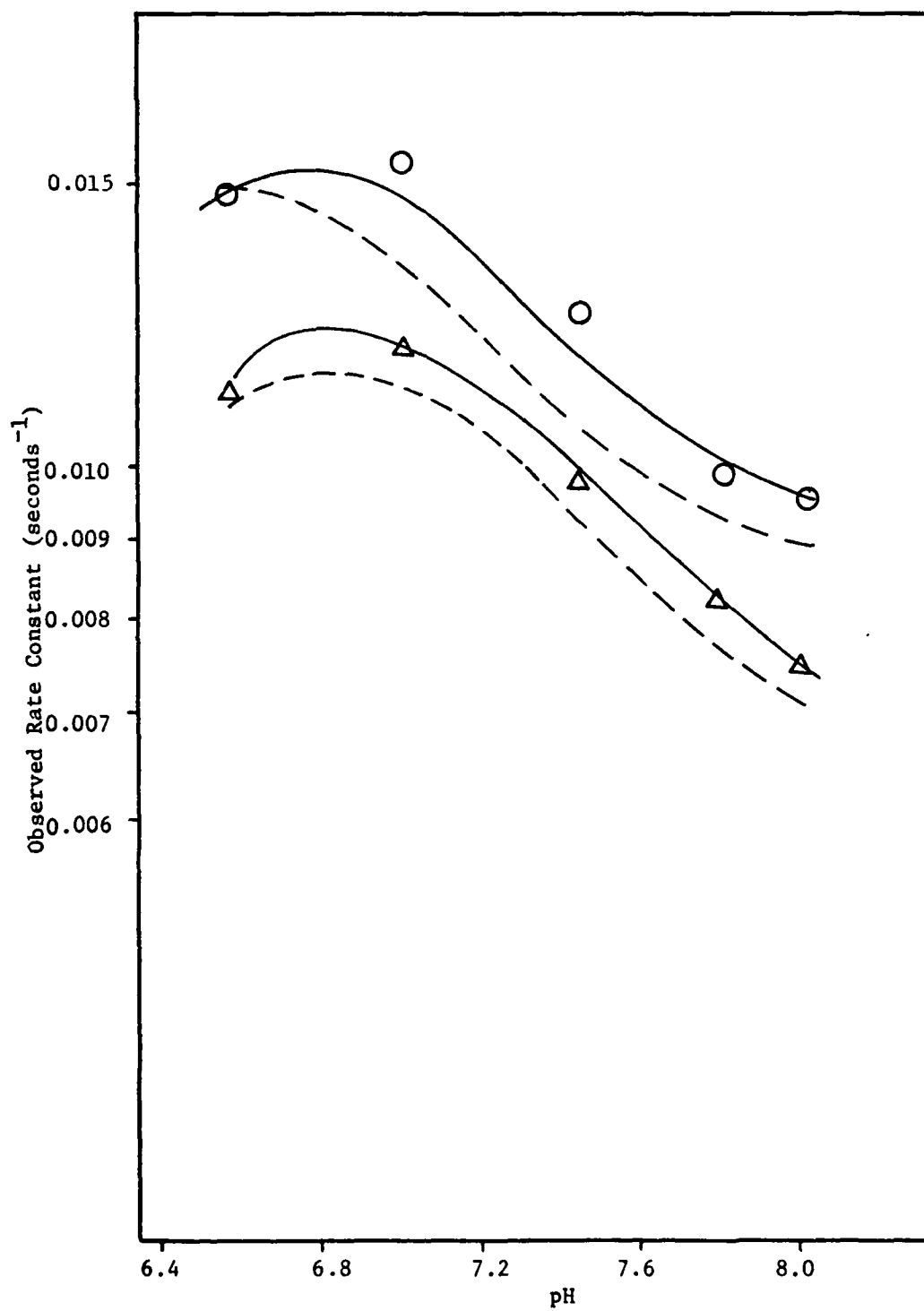


Figure 47.

Figure 48

Comparison of enzyme models for the ICDH-magnesium-oxalosuccinate system versus the magnesium concentration.

[oxas] = 0.349 mM

○ pH = 7.01

◇ pH = 8.01

--- ICDH-Mg-H<sub>-1</sub> only

— ICDH-Mg-H<sub>-1</sub> and ICDH-Mg-oxas-H<sub>-1</sub>

Other experimental conditions are stated in Figure 44.

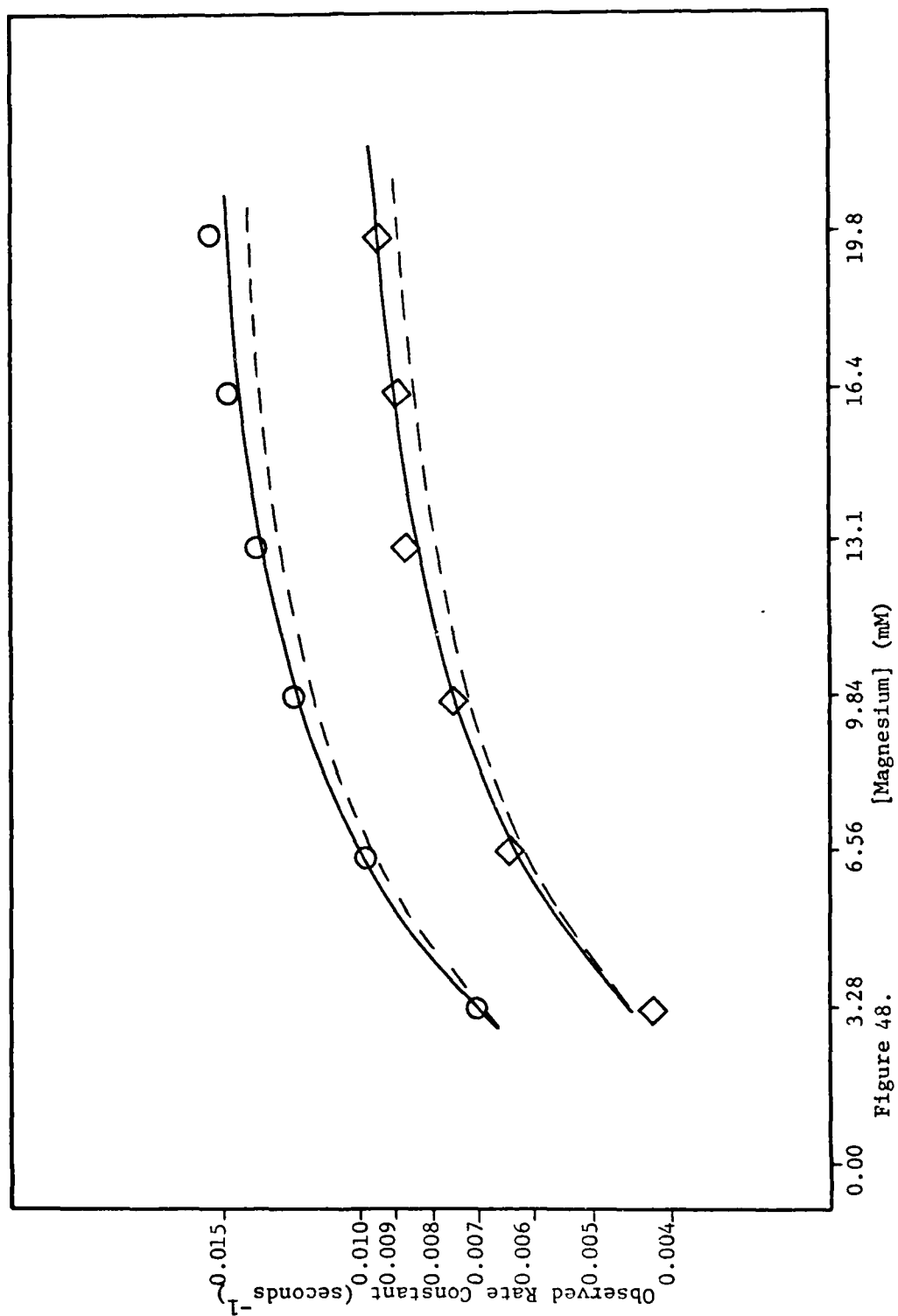
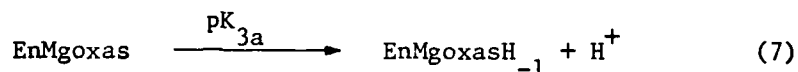


Figure 48.

necessary to add one more reaction. This reaction, shown below, is the deprotonation of the ternary ICDH-Mg-oxas complex to yield a second non-reactive, inhibition complex.



When this complex is added to the model, the result is the solid lines in Figures 47 and 48. This gives the best fit of the several models attempted. The solid lines in Figures 44 and 45, which represent all the data at an oxas concentration of 0.349 mM, as well as those in Figure 46 were calculated based on the formation of both inhibition complexes. This model not only provides an excellent mathematical expression of the data, but also accurately predicts the pH value corresponding to the peak rate in Figure 44.

The numerical values of the appropriate constants are as follows:

$$k'_{\text{Mg}} = 41.3 \pm 0.8 \text{ seconds}^{-1} \quad (\text{EnMgoxas} \rightarrow \text{CO}_2 + \text{products})$$

$$\log \beta'_{\text{Mg}} = 6.67 \pm 0.01 \quad (\text{En} + \text{Mg}^{2+} + \text{oxas}^{3-} = \text{EnMgoxas})$$

$$\log \beta_{\text{En-Mg}} = 3.94 \pm 0.08$$

$$\log \beta_{\text{En-Mg-}\alpha\text{KG}} = 6.16 \pm 0.15 \quad (\text{En} + \text{Mg}^{2+} + \alpha\text{KG} = \text{EnMg}\alpha\text{KG})$$

$$\text{pK}_{2a} = 7.64 \pm 0.09 \quad (\text{EnMg} = \text{EnMgH}_{-1} + \text{H}^+)$$

$$\text{pK}_{3a} = 5.72 \pm 0.01 \quad (\text{EnMgoxas} = \text{EnMgoxasH}_{-1} + \text{H}^+)$$

In comparing the numbers obtained in the two metal systems, the first observation is that the rate constant for the ICDH-Mg-oxas



complex is essentially equal to the rate constant for the ICDH-Zn-oxas complex. This was also observed in the pyruvate kinase-oxaloacetate system between manganese and magnesium. The significance of this will be discussed in more detail later in the chapter.

The two inhibition complexes,  $\text{EnMgH}_{-1}$  and  $\text{EnMgoxasH}_{-1}$ , result from the deprotonation of an amino acid residue on the enzyme. These ionized complexes are unreactive towards decarboxylation. The  $\text{pK}_a$  value for the metallated enzyme,  $\text{EnMg}$ , is 7.64. This is remarkably close to the  $\text{pK}_a$  of 7.67 determined by the spectrophotometric titration of the apoenzyme. The only amino acids with a comparable  $\text{pK}_a$  value are cystine, which has a  $\text{pK}_a$  of 7.85, or cysteine, with a  $\text{pK}_a$  of 8.3. Ehrlich and Colman (39) reported that N-ethylmaleimide inactivates ICDH by altering an average of two cysteinyl residues. They also report in the same paper that treatment of the enzyme with 5,5'-dithiobis(2-nitrobenzoic acid) and cyanide modified an average of four cysteinyl residues. This latter thiocyno enzyme shows a loss of the ability to bind NADPH and the manganese-isocitrate substrate, but the binding of manganese or isocitrate alone is unaltered. It was concluded that the critical cysteinyl residues participate in the tight binding of manganese isocitrate.

Colman and Chu (64) found 13 mols of cysteic acid per mol of ICDH after the oxidation of ICDH with performic acid. This was the same number of free -SH groups observed by the reaction with 5,5'-dithiobis(2-nitrobenzoic acid) after denaturation. Performic acid

will oxidize all cysteinyl and cystinyl residues to yield cysteic acid, whereas 5,5'-dithiobis(2-nitrobenzoic acid) only reacts with the sulfhydryl group. It was therefore concluded that ICDH contains no disulfide bonds. This means that the proton titrated via the spectrophotometric titration, as described in the beginning of the chapter, as well as the residue undergoing ionization to form the  $\text{EnMgH}_{-1}$  complex may, in fact, be the sulfhydryl proton of a cysteine residue.

The other ionized complex,  $\text{EnMgoxash}_{-1}$ , has a  $\text{pK}_a$  of 5.72. This number has been referenced several times in other investigations of the ICDH reactions. Ehrlich and Colman (30) studied the loss of ICDH activity after treating the enzyme with ethoxyformic anhydride, a reagent which preferentially carbethoxylates histidyl residues. These workers used 0.05 M MES ( $\text{pH} = 5.0 - 7.0$ ) and 0.05 M HEPES ( $\text{pH} = 7.0$  and above) buffers in their work. They found that the loss of dehydrogenase activity, which is the oxidation of isocitrate to yield oxas, is dependent upon the basic form of an ionizable group with a  $\text{pK}_a$  of 5.67. In this work, manganese was the metal ion cofactor.

In another paper by Ehrlich and Colman (38), it was reported that the pH dependence of the maximum velocity of ICDH activity was dependent upon the form of a single ionizable group in the ICDH - manganese-isocitrate complex with a  $\text{pK}_a$  of 5.71. These results along with other data (30) indicate that histidine ( $\text{pK}_a = 6.04$ ) may be

involved at the active site. The results presented in this research indicate that the ICDH-Mg-oxas complex ionizes the same critical histidine residue as ICDH-Mn-isocitrate, since nearly identical  $pK_a$  values were found.

It is assumed that the actual substrate for this reaction is the metal-oxas complex, since that is true for the isocitrate reaction. It is possible to calculate the formation constant of the ternary complex by assuming it forms from the enzyme and the metal-oxas binary complex. Consider equations (8) and (9).

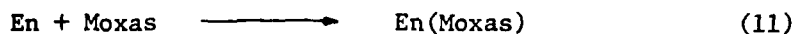
$$\beta_{\text{EnMoxas}} = \frac{[\text{EnMoxas}]}{[\text{En}][\text{M}][\text{oxas}]} \quad (8)$$

$$\beta_{\text{Moxas}} = \frac{[\text{Moxas}]}{[\text{M}][\text{oxas}]} \quad (9)$$

By dividing Equation (8) by Equation (9), one obtains:

$$\frac{\beta_{\text{EnMoxas}}}{\beta_{\text{Moxas}}} = \frac{[\text{EnMoxas}]}{[\text{En}][\text{Moxas}]} \quad (10)$$

The right side of Equation (10) describes the equilibrium constant for the reaction



Equation (10) reduces to

$$\log \beta_{\text{En(Moxas)}} = \log \beta_{\text{EnMoxas}} - \log \beta_{\text{Moxas}} \quad (12)$$

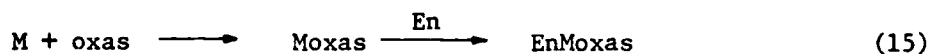
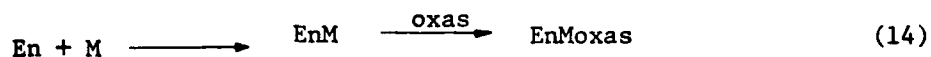
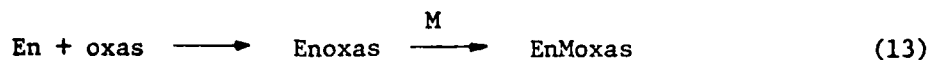
From Equation (12), we can compare the formation constants of the various metal-oxas complexes for the different metals as shown by reaction (11). The calculated values are:

$$\log \beta_{\text{En(Mgoxas)}} = 6.67 - 1.99 = 4.68$$

$$\log \beta_{\text{En(Znoxas)}} = 7.96 - 3.02 = 4.94$$

The stability constants show that the enzyme binds the Mg-oxas complex and the Zn-oxas complex with comparable stability. They further show that the larger formation constant of the zinc ternary complex is primarily due to the larger formation constant for the Zn-oxas binary complex. Unfortunately, these values cannot be used to confirm nor deny the true nature of the substrate.

From the data presented thus far, it is unclear as to which of the reactions below is the actual path in the formation of the ternary complex. From the stability constants of the intermediate



binary complexes, the En-oxas complex is the most stable, whereas M-oxas is the least stable. If one examines the equilibrium concentrations of all the enzyme species, the dominant form of the enzyme is the binary enzyme-oxas complex. Thus, based on the stability constants, the formation of the ternary complex via path (13) would be favored thermodynamically. However, in order to resolve this question properly, it would be necessary to obtain kinetic data on the time scale of the complexation reaction. This could also resolve the ambiguity as to whether or not the reaction mechanism is random or ordered.

The data show that the ICDH-Mg complex ( $\log \beta_{\text{EnMg}} = 3.94$ ) is considerably more stable than the ICDH-Zn complex ( $\log \beta_{\text{EnZn}} = 2.74$ ). Published literature values for ICDH - metal complexes are lacking. Villafranca and Colman (35) reported a formation constant of  $10^{4.35}$  for the ICDH-Mn complex. One would therefore predict that the stability constant for ICDH-Mg should be somewhat smaller than  $10^{4.35}$ , which was predicted and observed, while the same constant for zinc should be somewhat larger, which was predicted but not observed.

The greater stability for the magnesium complex cannot be due to the size of the ions. The ionic radius of  $\text{Mg}^{2+}$  is  $0.66 \text{ \AA}$ , compared to  $0.73 \text{ \AA}$  for  $\text{Zn}^{2+}$ . However, the manganous ion, which is considered to be the best activator, has an ionic radius of  $0.79 \text{ \AA}$ , while  $\text{Cd}^{2+}$ , another activator, has an ionic radius of  $0.96 \text{ \AA}$ . Since the zinc ion

is intermediate in size to the magnesium and manganese ions, the difference in stabilities is not due to ionic size.

This effect cannot be due to a greater affinity for the metal to the particular ligands on the enzyme, since zinc binds better to amino acids than magnesium. It is possible, however, that the metals differ in their coordination number in the metal-enzyme complex. It is also possible that a change in conformation of the enzyme results from a change in the metal ion.

Another possibility is that the different metals do not bind in precisely the same spot on the enzyme, although they still catalyze the reaction. This type of behavior has been observed in the binding of copper<sup>2+</sup> and zinc<sup>2+</sup> by myoglobin (63). These ions compete for binding to the enzyme, but x-ray diffraction studies show the existence of two separate sites. The Zn<sup>2+</sup> binding groups are asparagine (GH4), lysine(A14), and a histidine (GH1). On the other hand, the Cu<sup>2+</sup> binding groups include asparagine (CH4) and lysine (A14), but it involves a different histidine (A10). The Zn<sup>2+</sup> site and the Cu<sup>2+</sup> site are 7 Å apart.

In the case of ICDH, strong evidence has been provided by Colman (37) to indicate that the five activating dications -- manganese, magnesium, zinc, cadmium, and cobalt -- have different binding sites. Since the discussion of the kinetic data provided in this chapter is highly dependent on the above premise, this researcher will devote the

next few paragraphs summarizing the work of Colman (37). The experimental details can be found in the published paper.

The Michaelis constants for the five metals were determined for the overall oxidative decarboxylation of isocitrate (4.0 mM) with 0.1 mM  $\text{NADP}^+$  and 0.20 M acetate buffer at a pH of 5.5. The respective constants are:

<u>Metal Ion</u>	<u>Michaelis Constant (<math>\mu\text{M}</math>)</u>
$\text{Mn}^{2+}$	11.1
$\text{Cd}^{2+}$	16.6
$\text{Zn}^{2+}$	13.9
$\text{Co}^{2+}$	19.1
$\text{Mg}^{2+}$	126.0

The maximum observed rates for the reaction in order of decreasing effectiveness are  $\text{Mn}^{2+} > \text{Cd}^{2+} > \text{Zn}^{2+} > \text{Co}^{2+} > \text{Mg}^{2+}$ . Note that this data was obtained spectrophotometrically at 340 nm.

The relative effectiveness of the metals on oxas decarboxylation was then examined. This data was obtained by a pH stat experiment, which measures the rate of proton uptake. The metal concentrations were set approximately twenty times greater than their Michaelis constants, while the concentration of oxas was 2.3 mM. The pH was 5.5 and the solutions were unbuffered. In this case, the relative rate of oxas decarboxylation was  $0.22 \text{ mM } \text{Mn}^{2+} > 0.35 \text{ mM } \text{Cd}^{2+} > 3.00 \text{ mM } \text{Mg}^{2+} > 0.4 \text{ mM } \text{Co}^{2+} = 0.3 \text{ mM } \text{Zn}^{2+} = 0$ . The observed decarboxylation produced by  $\text{Zn}^{2+}$  and  $\text{Co}^{2+}$  were attributed to the high rate of the non-enzymatic decarboxylation catalyzed by these metals.

The relative rates for the metal assisted reverse reactions were monitored spectrophotometrically at 340 nm. The relative rates for the reductive carboxylation ( $\alpha$ KG + CO<sub>2</sub> + NADPH  $\rightarrow$  isocitrate + NADP<sup>+</sup>) were 0.22 mM Mn<sup>2+</sup> > 0.30 mM Zn<sup>2+</sup> > 0.40 mM Co<sup>2+</sup> > 0.40 mM Cd<sup>2+</sup> > 3.00 mM Mg<sup>2+</sup>. The relative rates for the oxalosuccinate reductase reaction (oxas + NADPH  $\rightarrow$  isocitrate + NADP<sup>+</sup>) were 0.22 mM Mn<sup>2+</sup> > 0.40 mM Cd<sup>2+</sup> > 0.30 mM Zn<sup>2+</sup> > 0.40 mM Co<sup>2+</sup> > 3.00 mM Mg<sup>2+</sup>. Both experiments were done at a pH of 5.5.

If one examines the relative effectiveness of the metals at concentrations that are approximately twenty times their Michaelis constants, it is apparent that the partial reactions are affected differently by each metal. Colman reasoned that this could result if the metals did not bind precisely at the same spot on the protein. A consequence of this might be a distinction between the metals in their influence on the reactivity of a particular amino acid residue modified by the appropriate chemical reagent. This hypothesis was tested by inactivating the enzyme with diazo-lH-tetrazole.

Although the diazo-lH-tetrazole reagent modified histidyl, tyrosyl, and lysyl residues, it was shown by Colman that only the lysyl residues are affected if the enzyme is treated with dilute (0.20 mM) reagent in 0.065 M triethanolamine buffer at a pH of 7.7 in the presence of 0.20 M sodium sulfate and 6.5% glycerol at 0°C. The enzyme treated in this



way had 16% residual activity compared to the native enzyme. However, the amount of residual activity could be varied by careful control of the experimental conditions. This resulted in a series of modified enzymes whose activity varied from 8% to 82% when compared to the untreated enzyme.

The next step was to correlate the residual activity with the lysine content of ICDH. The lysine content was measured by the quantitative ninhydrin reaction using leucine as a standard. Each analysis reported was an average of at least five determinations. A total of 25 lysine residues were detected on the unmodified enzyme which represents 100% residual activity. A total of 22 lysyl groups were detected in the modified enzyme that had 58% residual activity. Under different experimental conditions, one modified enzyme had 20% residual activity. From the analysis of this enzyme, 20 lysyl groups were detected.

Thus, there was a good correlation between residual activity and the measurable lysine content. If the number of measurable lysyl groups is plotted as a function of the corresponding residual activity, a fairly smooth curve results. This curve is in fact linear in the range of 10% to 80% residual activity.

This correspondence was tested for the metals. In this set of experiments, the metal ions were added to the enzyme just prior to the

addition of diazo-1H-tetrazole. The metal ion concentration used gave the maximum effect on inactivation by the reagent. This modified enzyme was tested as before for the residual activity and lysine content. It was found that the 1.0 mM  $\text{Mn}^{2+}$  and 1.0 mM  $\text{Co}^{2+}$  data points for residual activity versus measurable lysine residues lie fairly close to the line. Under these experimental conditions, the residual activity (63%) and number of lysine residues (22) determined for the cobalt treated enzyme were nearly the same values as those determined for the enzyme treated with the reagent in the absence of any metal ion. It was concluded that cobalt does not affect the reaction between ICDH and diazo-1H-tetrazole. This was the same result seen in the presence of 5.0 mM  $\text{Mg}^{2+}$ . Although manganese was also close to the line, it enhanced the extent of inactivation (10% residual activity) as well as the number of lysyl groups modified (20) compared to the nonmetal treated enzyme. It was reasoned that manganese increases the reactivity or availability of the amino acid groups that react with the reagent in the absence of the metal ions.

For the case of the enzyme treated with 0.5 mM  $\text{Zn}^{2+}$ , the number of lysine residues detected, 24, correspond to an enzyme with 70% activity, yet this enzyme was only 4% as active. In the presence of 1.0 mM  $\text{Cd}^{2+}$ , the enzyme was 7% as active as the untreated enzyme. However, the number of lysines detected, 22, corresponds to an enzyme

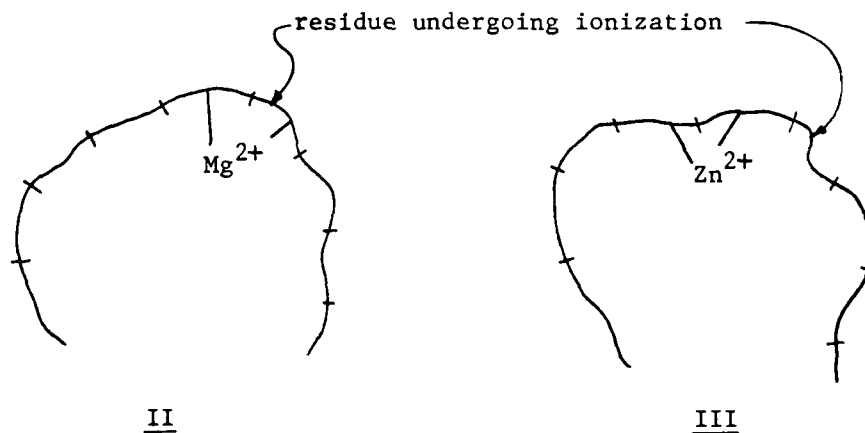
with about 60% residual activity. Therefore, the modification of other amino acid residues in addition to lysine must be responsible for the greater inactivation observed in the presence of zinc and cadmium ions.

The different effect of the metals on the inactivation of ICDH, as well as the differing abilities to enhance the partial reactions in this system, can best be explained if it is assumed that the binding sites for each metal are different. Since manganese, zinc, and cadmium enhance the inactivation by diazo-1H-tetrazole, then these metals must be located at sites not sensitive to the reagent. Magnesium and cobalt must be present at sites that protect the residues which undergo a modification from the reagent.

The existence of separate binding sites could also explain why the two inhibition complexes were required to fit the kinetic data for the magnesium system, but were not needed to fit the zinc data. It is possible that the residue undergoing ionization in the metallated enzyme is involved in the binding of  $Mg^{2+}$  but not in the binding of  $Zn^{2+}$ . This same statement holds true for the ionization of the ternary complex which yields  $EnMgOxasH_{-1}$ . If the zinc ion was found in a conformation and setting identical to the magnesium ion, one would expect to see the  $EnZnH_{-1}$  and the  $EnZnOxasH_{-1}$  complexes form since  $Zn^{2+}$  is a stronger Lewis acid than  $Mg^{2+}$ . But no evidence was seen in this investigation indicating the presence of these complexes.

Thus, published results as well as the data in this research work support the fact that the binding of different metals to ICDH is different for each metal, which in turn could induce a conformational change in the enzyme.

It is possible that the binding is as shown in I and II, which represent the  $Mg^{2+}$  and  $Zn^{2+}$  binding respectively. The curved line



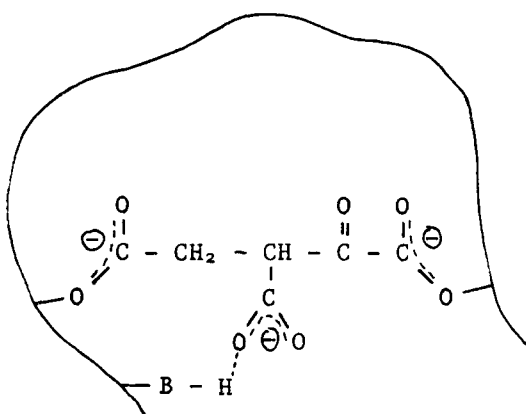
represents the enzyme, while the segments in the line represent the various amino acid residues. It can be seen that the two binding sites for the metals are different, yet they are located in the same general area. Note that the  $Mg^{2+}$  ion is bound to the residue that

undergoes ionization, forming the  $\text{EnMgH}_{-1}$  and  $\text{EnMgoxasH}_{-1}$  complexes, whereas  $\text{Zn}^{2+}$  is not bound to that residue. This explains the observed relative stabilities of the ICDH - M complexes as well as the observation that only  $\text{Mg}^{2+}$  forms non-reactive, ionized complexes.

Although the evidence presented strongly suggests a different mode of binding for the two metals to the enzyme, one point should still remain clear: the ternary ICDH-metal-oxas complex decarboxylates at the same rate for both metals investigated. Considering the fact that oxas binds very tightly to the enzyme without the aid of a metal ion ( $\log \beta = 5.67$ ) and this complex decarboxylates at an accelerated rate, it is concluded that the role of the metal ion is to aid in the binding of oxas to the enzyme, but other functional groups on the enzyme promote decarboxylation.

Recall that ICDH forms a very stable complex with oxas without the help of a metal ion. This complex decarboxylates at a rate two orders of magnitude faster than the non-ICDH bound molecule. Therefore, there are functional groups inherent to the enzyme that promote decarboxylation. One possible explanation for this is the straining of the bond between the 3-carbon and the 3-carboxylate, the leaving group. This could result from a hydrogen bond between the 3-carboxylate group and the enzyme. The effect is to strain the bond, thereby forcing it to break easier and faster. Once the bond is broken, the

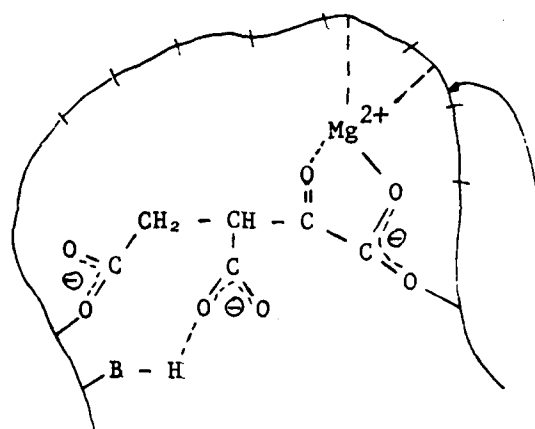
CO<sub>2</sub> gas is initially hydrogen bonded to the enzyme. Since this bond is not very strong, the CO<sub>2</sub> is eventually released, but this release does not immediately follow decarboxylation. This postulate is shown in III. This is consistent with the work of O'Leary and Limburg (43),



III

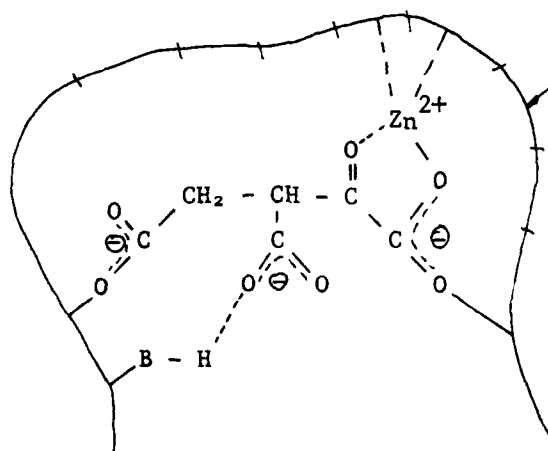
who claimed that the rate of product release was two or more orders of magnitude slower than the decarboxylation step.

When the metal is added to the system, the following occurs. Binding of the metal to the enzyme pulls the oxas molecule towards the metal binding site. This is shown in IV for  $\text{Mg}^{2+}$  as the binding metal and in V as  $\text{Zn}^{2+}$  as the binding metal. This strains the carbon-carbon bond even more than the case shown in III. This results in a still faster reaction due to the added strain. This explains why the ICDH-M-oxas decarboxylation rate is independent of the metal ion.



IV

residue under-  
going ionization



V

### C. Summary

This chapter discussed the catalysis of the enzyme isocitrate dehydrogenase on the decarboxylation of oxalosuccinate, as well as the influence of two divalent metal ions, zinc and magnesium, on the reaction. It was observed that oxas binds very tightly to the enzyme

in the absence of metal ions ( $\log \beta = 5.67$ ), and this complex decarboxylates approximately 320 times faster than free oxas<sup>3-</sup>. Furthermore, at lower pH values, this binary complex can protonate ( $pK_{1a} = 7.22$ ), and decarboxylate twice as fast as the unprotonated form. No pH maxima were observed in the range of 6.5 - 8.0, although the rate increased as the pH decreased. It was observed that EDTA inhibited the reaction. This inhibition was due to the binding of the monoprotonated molecule, HEDTA<sup>3-</sup>, with ICDH. The log of the formation constant was 17.96. The inhibition was not due to EDTA binding with trace metals in solution or bound to the enzyme.

Next, the effects of the two metals were investigated. The following was observed. First, the binary ICDH-Mg complex was more stable than the ICDH-Zn complex. This is the reverse order that is expected when comparing the binding of these two metals on a particular ligand. Second, the zinc rate data increased as pH increased, indicating the formation of a simple, ternary ICDH-Zn-oxas complex. However, the magnesium data showed a maximum rate at pH = 7.0 - 7.2 (the actual peak was a function of the metal concentration), indicating the formation of various inhibition complexes. The magnesium data was resolved by including the formation of two ionized, non-reactive complexes,  $EnMgH_{-1}$  and  $EnMgOxasH_{-1}$ , whereas these complexes were not needed to resolve the zinc data.



Another observation was that the actual decarboxylation rate constant for the EnMoxas complex was very rapid ( $t_{1/2} = 16$  mseconds) and independent of the metal. Since it was shown that the enzyme accelerates the decarboxylation rate of oxas in the absence of metals, it is concluded that the function of the metal ion is to aid in the binding of oxas to the enzyme but other functional groups on the enzyme promote decarboxylation. Thus, it is only important for the metal to place oxas in a more favorable geometry relative to the enzyme, and this is independent of the nature of the ICDH-metal bond. From the data collected in this study, it is concluded that: (1) the actual binding site for the metals on the enzyme are different for the two metals; and (2) the role of the metal ion is to create a more favorable geometry of oxas at the active site of the enzyme. This new geometry, then, establishes a structure within the enzyme for the other functional groups at the active site to better promote decarboxylation.

#### REFERENCES

1. Ochoa, S., Journal of Biological Chemistry, 159, 243 (1945).
2. Ochoa, S., Journal of Biological Chemistry, 174, 123 (1948).
3. Moyle, J., and Dixon, M., Biochimie Biophysica Acta, 252, 2455 (1955).
4. Moyle, J., and Dixon, M., Biochemical Journal, 63, 548 (1956).
5. Moyle, J., and Dixon, M., Biochemical Journal, 63, 552 (1956).
6. Siebert, G., et al, Journal of Biological Chemistry, 226, 965 (1957).
7. Siebert, G., et al, Journal of Biological Chemistry, 226, 977 (1957).
8. Brummond, D.O., and Burris, R.H., Proceeds of the National Academy of Sciences, 39, 754 (1953).
9. Ochoa, S., Journal of Biological Chemistry, 174, 115 (1948).
10. Lynen, F., and Scherer, H., Liebigs Ann., 560, 163 (1948).
11. Ochoa, S., Kornberg, A., and Mehler, A.H., Journal of Biological Chemistry, 174, 159 (1948).
12. Chen, R.F., and Plaut, G.W.E., Biochemistry, 2, 752 (1963).
13. Pederson, K.J., Journal of the American Chemical Society, 51, 2098 (1929).
14. Steinberger, R., and Westheimer, F.H., Journal of the American Chemical Society, 73, 429 (1951).
15. Lienhard, G.E., and Rose, I.A., Biochemistry, 3, 185 (1964).
16. Danziel, K., and Londesborough, J.C., Biochemical Journal, 110, 223 (1968).

17. Steinberger, R., and Westheimer, F.H., Journal of the American Chemical Society, 71, 4158 (1949).
18. Pederson, K.J., Journal of the American Chemical Society, 58, 240 (1936).
19. Raghaven, N.V. and Leussing, D.L., Journal of the American Chemical Society, 98, 723 (1976).
20. Gelles, E., Journal of the Chemical Society, 4736 (1956).
21. Gelles, E. and Salama, A., Journal of the Chemical Society, 3689 and 3864 (1958).
22. Reyes-Zamora, C. and Tsai, C.S., Chemical Communications, 1047 (1971).
23. Gelles, E. and Hay, R.W., Journal of the Chemical Society, 3683 (1958).
24. Kosicki, G.W. and Lipovac, S.N., Canadian Journal of Chemistry, 42, 403 (1964).
25. Larson, D.W. and Lister, M.W., Canadian Journal of Chemistry, 46, 823 (1968).
26. Covey, W.D. and Leussing, D.L., Journal of the American Chemical Society, 96, 3860 (1974).
27. Gelles, E. and Hay, R.W., Journal of the Chemical Society, 3673 (1958).
28. Wolff, L., Ann. Chem. 305, 154 (1899).
29. Ochao, S. and Weisz-Tabori, E., Journal of Biological Chemistry, 159, 245 (1945).
30. Colman, R.F. and Ehrlich, R.S., European Journal of Biochemistry, 89, 575 (1978).
31. Atkinson, D.E., Hathaway, J.A., and Smith, E.C., Journal of Biological Chemistry, 240, 2682 (1965).
32. Suittie, J.W., Introduction to Biochemistry, Holt, Rinehart, and Winston, New York, p. 306, 1977.

33. Londesborough, J.C. and Dalziel, K., *Biochemical Journal*, 110, 217 (1968).
34. Colman, R.F., *Journal of Biological Chemistry*, 243, 2454 (1968).
35. Colman, R.F. and Villafranca, J.J., *Journal of Biological Chem.*, 247, 209 (1972).
36. Levy, R.S. and Villafranca, J.J., *Biochemistry*, 16, 3293 (1977).
37. Colman, R.F., *Journal of Biological Chemistry*, 247, 215 (1972).
38. Colman, R.F. and Ehrlich, R.S., *Biochemistry*, 15, 4034 (1976).
39. Ehrlich, R.S. and Colman, R.F., *Biochemistry*, 14, 5008 (1975).
40. Rose, Z.B., *Journal of Biological Chemistry* 235, 938 (1960).
41. Kratochvil, B., Boyer, S.L., and Hicks, G.P., *Analytical Chem.*, 39, 45 (1967).
42. Ingebretsen, O.C. and Sanner, T., *Arch. Biochem. Biophys.* 176, 442 (1976).
43. O'Leary, M.H. and Limburg, J.A., *Biochemistry*, 16, 1129 (1977).
44. Birus, M. and Leussing, D.L., unpublished results.
45. Schwarzenbach, G. and Flaschka, H., *Complexometric Titrations*, 2nd English Edition, Methuen, London, 1966.
46. Albery, W.J., Bell, R.P., and Powell, A.J., *Trans. Farad Soc.*, 61, 1194 (1965).
47. P.L. Biochemicals, Inc., Circular OR-10.
48. Sigma Chemical Company, Technical Bulletin No. 153-UV, "The Ultraviolet Determination of Isocitrate Dehydrogenase."
49. Dubois, J.E. and Toullec, J., *Tetrahedron Letters*, 37, 3373 (1971).
50. Bell, R.P. and Smith, P.W., *Journal of the Chemical Society (B)*, 241 (1966).

51. Langes' Handbook of Chemistry, John A. Dean, Ed., McGraw-Hill Book Co., New York, 11th Edition, 1973.
52. Sharma, V.S. and Leussing, D.L., Talanta, 18, 1137 (1971).
53. Sadtler Infrared Reference Spectrum No. 21260K.
54. Cooper, A.J.L. and Redfield, A.G., Journal of Biological Chemistry, 250, 527 (1975).
55. Emly, M., Ph.D. Dissertation, The Ohio State University (1978).
56. Methods in Enzymology, Volume 13, 455 (1969).
57. Katsuki, H., Yoshida, T., Tanegashima, C., and Tanaka, S., Analytical Biochemistry, 43, 349 (1971).
58. Kalnitsky, G., Journal of Biological Chemistry, 201, 817 (1953).
59. Kalnitsky, G., and Rachis, J.J., Journal of Biological Chemistry, 225, 751 (1957).
60. Anshütz, W., and Datta, S.N., Liebigs Ann. Chem., 1971 (1975).
61. Tallman, D.E. and Leussing, D.L., Journal of the American Chemical Society, 91, 6256 (1969).
62. Northrop, D.B., and Cleland, W.W., Journal of Biological Chemistry, 249, 2928 (1974).
63. Banaszak, L.J., Watson, H.C., and Kendrew, J.C., Journal of Molecular Biology, 12, 130 (1965).
64. Colman, R.F. and Chu, R., Journal of Biological Chemistry, 245, 608 (1970).

APPENDIX A

Absorbance Data for the Various  
Oxalosuccinate-Metal-Alpha-Ketoglutarate Systems

-----

ALPHA-KETOGLUTARATE ABSORBANCE DATA  
AT 255 NM

-----

SPECIES/COMPLEX			EXT COEF	STD DEV	
H2KG			34.1	2.78	
H KG			143.6	2.43	
KG			195.4	3.29	
-----					
COMPLEX			LOG BETA		
H2KG			6.780		
H KG			4.861		
-----					
EXP	(KG)	PH	A(OBS)	A(CALC)	% DEV
1	7.26E-4	1.44	0.046	0.045	3.16
2	7.11E-4	1.75	0.053	0.056	-5.08
3	7.05E-4	2.06	0.068	0.069	-1.31
4	6.99E-4	2.46	0.087	0.083	4.12
5	6.97E-4	2.78	0.091	0.091	-0.17
6	6.96E-4	3.03	0.098	0.095	3.06
7	6.95E-4	3.92	0.104	0.103	1.18
8	6.94E-4	4.01	0.105	0.104	1.42
9	6.92E-4	4.46	0.108	0.109	-1.27
10	6.92E-4	4.65	0.110	0.113	-2.65
11	6.90E-4	4.98	0.115	0.119	-3.78
12	6.88E-4	5.14	0.118	0.122	-3.50
13	6.84E-4	5.26	0.120	0.124	-2.95
14	6.80E-4	5.38	0.121	0.125	-3.05
15	6.78E-4	5.54	0.130	0.126	2.78
16	6.73E-4	5.72	0.133	0.127	4.30
17	6.72E-4	9.71	0.139	0.131	5.52

## NOTES:

1. THE DATA WAS OBTAINED AT 0 C.
2. A 1.0 CM QUARTZ CELL WAS USED.

OXALOSUCCINATE ABSORBANCE DATA  
AT 255 NM

SPECIES/COMPLEX			EXT COEF	STD DEV
H3OX			353.4	17.02
H2OX			466.6	18.16
H OX			446.6	13.30
OX			277.2	6.19
COMPLEX			LOG BETA	
H3OX			9.277	
H2OX			7.402	
H OX			4.631	

EXP	(OX)	(KG)	PH	A(OBS)	A(CALC)	% DEV
1	1.25E-3	9.05E-4	6.42	0.511	0.525	-2.77
2	1.23E-3	9.11E-4	6.17	0.513	0.522	-1.81
3	1.21E-3	9.17E-4	6.01	0.531	0.519	2.20
4	1.21E-3	9.19E-4	5.69	0.537	0.525	2.24
5	1.18E-3	9.25E-4	5.22	0.572	0.534	6.66
6	1.16E-3	9.33E-4	4.76	0.591	0.561	5.13
7	1.15E-3	9.41E-4	4.17	0.612	0.608	6.61
8	1.14E-3	9.51E-4	3.68	0.622	0.631	-1.46
9	1.12E-3	9.61E-4	3.31	0.623	0.632	-1.48
10	1.11E-3	9.70E-4	3.03	0.617	0.630	-2.08
11	1.10E-3	9.80E-4	2.88	0.611	0.625	-2.23
12	1.08E-3	9.91E-4	2.66	0.605	0.610	-0.77
13	1.07E-3	1.00E-3	2.54	0.596	0.600	-0.59
14	1.05E-3	1.01E-3	2.40	0.582	0.581	0.13
15	1.04E-3	1.02E-3	2.26	0.567	0.564	0.46
16	1.03E-3	1.03E-3	2.14	0.558	0.548	1.89
17	1.01E-3	1.04E-3	2.04	0.537	0.527	1.79
18	9.99E-4	1.05E-3	1.87	0.498	0.501	-0.65
19	9.87E-4	1.07E-3	1.57	0.483	0.460	4.87
20	9.73E-4	1.08E-3	1.29	0.409	0.426	-4.23

## NOTES:

1. A 1.0 CM QUARTZ CELL WAS USED.
2. THE EXPERIMENTS WERE CARRIED OUT AT 0 C.
3. THE DATA FOR ALPHA-KETOGLUTARATE USED FOR THE CALCULATED ABSORBANCE VALUES WERE OBTAINED FROM THE PREVIOUS TABLE.



ALPHA-KETOGLUTARATE ABSORBANCE DATA  
AT 260 NM

SPECIES/COMPLEX			EXT COEF	STD DEV	
H2KG			24.8	2.75	
H KG			123.9	2.50	
KG			172.5	3.44	
COMPLEX			LOG BETA		
H2KG			6.780		
H KG			4.861		
EXP	(KG)	PH	A(OBS)	A(CALC)	% DEV
1	7.26E-4	1.44	0.038	0.036	5.41
2	7.11E-4	1.75	0.043	0.046	-7.25
3	7.05E-4	2.06	0.056	0.058	-3.74
4	6.99E-4	2.46	0.075	0.071	4.96
5	6.97E-4	2.78	0.080	0.078	2.12
6	6.96E-4	3.03	0.083	0.082	1.45
7	6.95E-4	3.92	0.089	0.089	0.52
8	6.94E-4	4.01	0.093	0.090	3.62
9	6.92E-4	4.46	0.094	0.095	-1.21
10	6.92E-4	4.65	0.097	0.098	-1.50
11	6.90E-4	4.98	0.098	0.105	-6.64
12	6.88E-4	5.14	0.105	0.107	-2.03
13	6.84E-4	5.26	0.106	0.109	-2.35
14	6.80E-4	5.38	0.107	0.110	-2.44
15	6.78E-4	5.54	0.114	0.111	2.42
16	6.73E-4	5.72	0.117	0.112	4.30
17	6.72E-4	9.71	0.122	0.116	4.99

## NOTES:

1. THE DATA WAS OBTAINED AT 0 C.
2. A 1.0 CM QUARTZ CELL WAS USED.

OXALOSUCCINATE ABSORBANCE DATA  
AT 260 NM

SPECIES/COMPLEX			EXT COEF	STD DEV		
H3OX			236. 4	7. 86		
H2OX			337. 0	9. 01		
H OX			407. 6	7. 25		
OX			224. 7	3. 30		
-----						
COMPLEX			LOG BETA			
H3OX			9. 277			
H2OX			7. 402			
H OX			4. 631			
-----						
EXP	(OX)	(KG)	PH	A(OBS)	A(CALC)	% DEV
1	1. 25E-3	9. 05E-4	6. 42	0. 430	0. 440	-2. 31
2	1. 23E-3	9. 11E-4	6. 17	0. 433	0. 438	-1. 22
3	1. 21E-3	9. 17E-4	6. 01	0. 440	0. 437	0. 80
4	1. 21E-3	9. 19E-4	5. 69	0. 448	0. 443	1. 14
5	1. 18E-3	9. 25E-4	5. 22	0. 473	0. 456	3. 66
6	1. 16E-3	9. 33E-4	4. 76	0. 504	0. 487	3. 35
7	1. 15E-3	9. 41E-4	4. 17	0. 543	0. 538	0. 94
8	1. 14E-3	9. 51E-4	3. 68	0. 552	0. 557	-0. 86
9	1. 12E-3	9. 61E-4	3. 31	0. 549	0. 548	0. 26
10	1. 11E-3	9. 70E-4	3. 03	0. 521	0. 532	-2. 13
11	1. 10E-3	9. 80E-4	2. 88	0. 504	0. 519	-2. 96
12	1. 08E-3	9. 91E-4	2. 66	0. 490	0. 493	-0. 56
13	1. 07E-3	1. 00E-3	2. 54	0. 472	0. 477	-1. 07
14	1. 05E-3	1. 01E-3	2. 40	0. 457	0. 454	0. 60
15	1. 04E-3	1. 02E-3	2. 26	0. 436	0. 433	0. 59
16	1. 03E-3	1. 03E-3	2. 14	0. 422	0. 414	1. 79
17	1. 01E-3	1. 04E-3	2. 04	0. 408	0. 395	3. 22
18	9. 99E-4	1. 05E-3	1. 87	0. 362	0. 369	-1. 79
19	9. 87E-4	1. 07E-3	1. 57	0. 332	0. 328	1. 09
20	9. 73E-4	1. 08E-3	1. 29	0. 294	0. 298	-1. 49

## NOTES:

1. A 1.0 CM QUARTZ CELL WAS USED.
2. THE EXPERIMENTS WERE CARRIED OUT AT 0 C.
3. THE DATA FOR ALPHA-KETOGLUTARATE USED FOR THE CALCULATED ABSORBANCE VALUES WERE OBTAINED FROM THE PREVIOUS TABLE.

-----

ALPHA-KETOGLUTARATE ABSORBANCE DATA  
AT 272 NM

-----

SPECIES/COMPLEX			EXT COEF	STD DEV	
H2KG			17. 6	2. 18	
H KG			107. 0	2. 04	
KG			146. 8	2. 80	
-----					
COMPLEX			LOG BETA		
H2KG			6. 780		
H KG			4. 861		
-----					
EXP	(KG)	PH	A(OBS)	A(CALC)	% DEV
1	7. 26E-4	1. 44	0. 031	0. 029	6. 66
2	7. 11E-4	1. 75	0. 035	0. 038	-9. 10
3	7. 05E-4	2. 06	0. 047	0. 049	-4. 30
4	6. 99E-4	2. 46	0. 065	0. 061	6. 25
5	6. 97E-4	2. 78	0. 070	0. 067	3. 90
6	6. 96E-4	3. 03	0. 071	0. 070	0. 83
7	6. 95E-4	3. 92	0. 074	0. 077	-2. 97
8	6. 94E-4	4. 01	0. 079	0. 077	2. 29
9	6. 92E-4	4. 46	0. 082	0. 082	0. 11
10	6. 92E-4	4. 65	0. 084	0. 084	-0. 51
11	6. 90E-4	4. 98	0. 087	0. 089	-3. 33
12	6. 88E-4	5. 14	0. 091	0. 092	-0. 79
13	6. 84E-4	5. 26	0. 092	0. 093	-0. 67
14	6. 80E-4	5. 38	0. 094	0. 094	0. 53
15	6. 78E-4	5. 54	0. 096	0. 095	1. 22
16	6. 73E-4	5. 72	0. 097	0. 096	1. 83
17	6. 72E-4	9. 71	0. 099	0. 099	0. 38

## NOTES:

1. THE DATA WAS OBTAINED AT 0 C.
2. A 1.0 CM QUARTZ CELL WAS USED.

OXALOSUCCINATE ABSORBANCE DATA  
AT 272 NM

SPECIES/COMPLEX			EXT COEF	STD DEV		
H3OX			125.1	6.54		
H2OX			149.6	7.92		
H OX			266.7	7.01		
OX			102.1	3.30		
COMPLEX			LOG BETA			
H3OX			9.277			
H2OX			7.402			
H OX			4.631			
EXP	(OX)	(KG)	PH	A(OBS)	A(CALC)	% DEV
1	1.25E-3	9.05E-4	6.42	0.251	0.263	-4.77
2	1.23E-3	9.11E-4	6.17	0.253	0.264	-4.14
3	1.21E-3	9.17E-4	6.01	0.267	0.264	1.16
4	1.21E-3	9.19E-4	5.69	0.201	0.270	3.96
5	1.18E-3	9.25E-4	5.22	0.301	0.285	5.32
6	1.16E-3	9.33E-4	4.76	0.323	0.316	2.18
7	1.15E-3	9.41E-4	4.17	0.371	0.362	2.37
8	1.14E-3	9.51E-4	3.68	0.370	0.376	-1.68
9	1.12E-3	9.61E-4	3.31	0.364	0.363	0.17
10	1.11E-3	9.70E-4	3.03	0.337	0.343	-1.86
11	1.10E-3	9.80E-4	2.88	0.317	0.328	-3.60
12	1.08E-3	9.91E-4	2.66	0.302	0.302	-0.04
13	1.07E-3	1.00E-3	2.54	0.283	0.287	-1.57
14	1.05E-3	1.01E-3	2.40	0.268	0.269	-0.24
15	1.04E-3	1.02E-3	2.26	0.252	0.252	0.03
16	1.03E-3	1.03E-3	2.14	0.243	0.238	2.09
17	1.01E-3	1.04E-3	2.04	0.238	0.225	5.44
18	9.99E-4	1.05E-3	1.87	0.204	0.208	-1.72
19	9.87E-4	1.07E-3	1.57	0.181	0.183	-0.87
20	9.73E-4	1.08E-3	1.29	0.164	0.165	-0.54

## NOTES:

1. A 1.0 CM QUARTZ CELL WAS USED.
2. THE EXPERIMENTS WERE CARRIED OUT AT 0 C.
3. THE DATA FOR ALPHA-KETOGLUTARATE USED FOR THE CALCULATED ABSORBANCE VALUES WERE OBTAINED FROM THE PREVIOUS TABLE.

-----

ALPHA-KETOGLUTARATE ABSORBANCE DATA  
AT 284 NM

-----

SPECIES/COMPLEX			EXT COEF	STD DEV	
H2KG			30.5	3.21	
H KG			86.8	2.56	
KG			121.8	3.50	
COMPLEX			LOG BETA		
H2KG			6.780		
H KG			4.861		
EXP	(KG)	PH	A(OBS)	A(CALC)	% DEV
1	7.26E-4	1.44	0.032	0.032	-1.02
2	7.11E-4	1.75	0.038	0.038	0.36
3	7.05E-4	2.06	0.043	0.045	-3.66
4	6.99E-4	2.46	0.058	0.052	10.39
5	6.97E-4	2.78	0.059	0.056	5.17
6	6.96E-4	3.03	0.058	0.058	0.09
7	6.95E-4	3.92	0.061	0.062	-2.38
8	6.94E-4	4.01	0.064	0.063	1.67
9	6.92E-4	4.46	0.065	0.067	-2.84
10	6.92E-4	4.65	0.066	0.069	-4.89
11	6.90E-4	4.98	0.068	0.074	-8.21
12	6.88E-4	5.14	0.074	0.075	-3.39
13	6.84E-4	5.26	0.074	0.076	-3.33
14	6.80E-4	5.38	0.075	0.077	-3.04
15	6.78E-4	5.54	0.084	0.078	6.60
16	6.73E-4	5.72	0.086	0.079	8.03
17	6.72E-4	5.71	0.087	0.082	5.93

## NOTES:

1. THE DATA WAS OBTAINED AT 0 C.
2. A 1.0 CM QUARTZ CELL WAS USED.

OXALOSUCCINATE ABSORBANCE DATA  
AT 284 NM

SPECIES/COMPLEX				EXT COEF	STD DEV
H3OX				73.6	2.36
H2OX				56.5	2.58
H OX				126.3	2.18
OX				41.4	1.11

COMPLEX				LOG BETA
H3OX				9.277
H2OX				7.402
H OX				4.631

EXP	(OX)	(KG)	PH	A(OBS)	A(CALC)	% DEV
1	1.25E-3	9.05E-4	6.42	0.159	0.163	-2.52
2	1.23E-3	9.11E-4	6.17	0.161	0.164	-1.56
3	1.21E-3	9.17E-4	6.01	0.164	0.164	0.02
4	1.21E-3	9.19E-4	5.69	0.169	0.166	1.60
5	1.18E-3	9.25E-4	5.22	0.177	0.172	2.65
6	1.16E-3	9.33E-4	4.76	0.190	0.185	2.44
7	1.15E-3	9.41E-4	4.17	0.202	0.206	-1.77
8	2.65E-3	9.51E-4	3.68	0.214	0.211	1.44
9	1.12E-3	9.61E-4	3.31	0.201	0.203	-1.04
10	1.11E-3	9.70E-4	3.03	0.189	0.192	-1.41
11	1.10E-3	9.80E-4	2.88	0.180	0.184	-2.08
12	1.08E-3	9.91E-4	2.66	0.172	0.170	1.07
13	1.07E-3	1.00E-3	2.54	0.164	0.163	0.64
14	1.05E-3	1.01E-3	2.40	0.157	0.154	1.83
15	1.04E-3	1.02E-3	2.26	0.148	0.147	0.92
16	1.03E-3	1.03E-3	2.14	0.141	0.141	0.20
17	1.01E-3	1.04E-3	2.04	0.134	0.136	-1.10
18	9.99E-4	1.05E-3	1.87	0.127	0.129	-1.24
19	9.87E-4	1.07E-3	1.57	0.119	0.120	-0.43
20	9.73E-4	1.08E-3	1.29	0.114	0.113	0.81

## NOTES:

1. A 1.0 CM QUARTZ CELL WAS USED.
2. THE EXPERIMENTS WERE CARRIED OUT AT 0 C.
3. THE DATA FOR ALPHA-KETOGLUTARATE USED FOR THE CALCULATED ABSORBANCE VALUES WERE OBTAINED FROM THE PREVIOUS TABLE.

MAGNESIUM-OXALOSUCCINATE ABSORBANCE DATA  
AT 260 NM

SPECIES/COMPLEX		EXT. COEF.	STD DEV
MGOXAS		329.2	9.61
MG AKG		200.0	
OXAS		225.0	
H OXAS		408.0	
H2OXAS		337.0	
H3OXAS		236.0	
AKG		173.0	
H AKG		124.0	
H2 AKG		24.8	

COMPLEX		LOG BETA
MGOXAS		1.918
MG AKG		0.353
H OXAS		4.631
H2OXAS		7.402
H3OXAS		9.277

EXP	(MG)	(OXAS)	(AKG)	PH	ABSORBANCE	
					OBS	CALC
1	5.00E-3	7.71E-4	3.37E-4	4.88	0.283	0.281
2	4.99E-3	7.58E-4	3.42E-4	5.32	0.273	0.263
3	4.98E-3	7.32E-4	3.51E-4	5.50	0.257	0.254
4	4.97E-3	7.21E-4	3.56E-4	5.83	0.251	0.248
5	4.96E-3	7.08E-4	3.62E-4	6.63	0.253	0.243
6	1.20E-2	6.92E-4	3.65E-4	6.57	0.261	0.255
7	1.20E-2	6.79E-4	3.71E-4	6.22	0.248	0.252
8	1.19E-2	6.65E-4	3.76E-4	5.44	0.245	0.251
9	1.19E-2	6.52E-4	3.81E-4	4.84	0.262	0.257
10	1.18E-2	6.36E-4	3.85E-4	4.78	0.243	0.257

## NOTES:

1. CONCENTRATION UNITS ARE MOLAR.
2. A 1 CM QUARTZ CELL WAS USED.
3. THE EXPERIMENT WAS CARRIED OUT AT 0 DEGREES CELCIUS.

ZINC-OXALOSUCCINATE ABSORBANCE DATA  
AT 255 NM

SPECIES/COMPLEX			EXT. COEF.	STD DEV
ZNOXAS			2205.0	68.49
ZN AKG			956.0	
OXAS			277.0	
H OXAS			447.0	
H2OXAS			467.0	
H3OXAS			353.0	
AKG			195.0	
H AKG			143.0	
H2 AKG			34.1	

COMPLEX		LOG BETA
ZNOXAS		3.017
ZN AKG		1.630
H OXAS		4.631
H2OXAS		7.402
H3OXAS		9.277

EXP	(ZN)	(OXAS)	(AKG)	PH	ABSORBANCE	
					OBS	CALC
1	4.96E-4	7.35E-4	3.49E-4	5.89	1.200	1.457
2	4.96E-3	7.19E-4	3.55E-4	6.35	1.360	1.439
3	1.21E-2	6.83E-4	3.69E-4	5.83	1.480	1.554
4	1.20E-2	6.65E-4	3.76E-4	5.16	1.480	1.480
5	1.20E-2	6.48E-4	3.83E-4	4.86	1.410	1.410
6	1.19E-2	6.29E-4	3.90E-4	4.09	1.240	1.149
7	1.19E-2	6.12E-4	3.98E-4	3.63	1.020	0.865
8	1.89E-2	5.93E-4	4.05E-4	3.46	0.946	0.857
9	1.88E-2	5.74E-4	4.13E-4	4.29	1.280	1.224
10	1.87E-2	5.58E-4	4.22E-4	4.64	1.330	1.276
11	1.87E-2	5.41E-4	4.32E-4	5.15	1.360	1.317
12	1.86E-2	5.24E-4	4.42E-4	5.88	1.350	1.325

## NOTES:

1. CONCENTRATION UNITS ARE MOLAR.
2. A 1 CM QUARTZ CELL WAS USED.
3. THE EXPERIMENT WAS CARRIED OUT AT 0 DEGREES CELCIUS.



ZINC-OXALOSUCCINATE ABSORBANCE DATA  
AT 284 NM

SPECIES/COMPLEX		EXT. COEF.	STD DEV
ZNOXAS		209.7	14.00
ZN AKG		256.0	
OXAS		41.4	
H OXAS		126.0	
H2OXAS		56.5	
H3OXAS		73.6	
AKG		122.0	
H AKG		86.8	
H2 AKG		30.5	

COMPLEX		LOG BETA
ZNOXAS		3.017
ZN AKG		1.630
H OXAS		4.631
H2OXAS		7.402
H3OXAS		9.277

EXP	(ZN)	(OXAS)	(AKG)	PH	ABSORBANCE	
					OBS	CALC
1	5.00E-3	7.71E-4	3.37E-4	4.92	0.151	0.175
2	4.98E-3	7.53E-4	3.43E-4	5.21	0.177	0.177
3	4.96E-4	7.35E-4	3.49E-4	5.89	0.232	0.180
4	4.96E-3	7.19E-4	3.55E-4	6.35	0.255	0.179
5	1.21E-2	6.83E-4	3.69E-4	5.83	0.257	0.193
6	1.20E-2	6.65E-4	3.76E-4	5.16	0.209	0.184
7	1.20E-2	6.48E-4	3.83E-4	4.86	0.189	0.177
8	1.19E-2	6.29E-4	3.90E-4	4.09	0.148	0.153
9	1.19E-2	6.12E-4	3.98E-4	3.63	0.117	0.134
10	1.89E-2	5.93E-4	4.05E-4	3.46	0.117	0.132
11	1.88E-2	5.74E-4	4.13E-4	4.29	0.152	0.159
12	1.87E-2	5.58E-4	4.22E-4	4.64	0.153	0.167
13	1.87E-2	5.41E-4	4.32E-4	5.15	0.158	0.177
14	1.86E-2	5.24E-4	4.42E-4	5.88	0.175	0.183

## NOTES:

1. CONCENTRATION UNITS ARE MOLAR.
2. A 1 CM QUARTZ CELL WAS USED.
3. THE EXPERIMENT WAS CARRIED OUT AT 0 DEGREES CELCIUS.

---

ISOCITRATE DEHYDROGENASE  
ABSORBANCE DATA AT 280 NM

---



---

SPECIES	EXT COEF	STD DEV
ICDH	1.701E+5	2.60E+3
H-ICDH	1.309E+5	1.49E+3

---

PK = 7.667

---



---

EXP	(ICDH)	PH	A(OBS)	A(CALC)	% DEV
1	3.72E-7	6.10	4.90E-2	4.91E-2	-0.14
2	3.72E-7	6.31	5.00E-2	4.93E-2	1.41
3	3.71E-7	6.77	5.00E-2	5.02E-2	-0.38
4	3.71E-7	6.98	5.10E-2	5.10E-2	-0.06
5	3.70E-7	7.29	5.20E-2	5.27E-2	-1.37
6	3.69E-7	7.52	5.30E-2	5.43E-2	-2.47
7	3.68E-7	7.74	5.70E-2	5.60E-2	1.79
8	3.68E-7	7.87	5.80E-2	5.70E-2	1.68
9	3.66E-7	8.11	5.90E-2	5.84E-2	0.94
10	3.65E-7	8.26	6.00E-2	5.92E-2	1.39
11	3.63E-7	8.48	5.90E-2	5.98E-2	-1.42
12	3.61E-7	8.53	5.90E-2	5.97E-2	-1.17

---

NOTES:

1. A 1.0 CM QUARTZ CELL WAS USED.
2. THE DATA WAS OBTAINED AT 25 C.

APPENDIX B

pH Titration Data

ALPHA-KETOGLUTARATE TITRATION  
AT 25.0 DEGREES C

CHISQ = 1.9340 -3

CONST.	VARIED	FORM.	CONST	STAND. DEVS.
1		4.4644D	4	4.7244D 2
2		4.5906D	6	9.8743D 4

LOG BETA		MATRIX	
		KG	H
1	4.64976	1	1
2	6.66187	1	2

TITRATION 1

INITIAL CONCENTRATIONS OF INDEPENDENT SPECIES:

	KG	H
1	59000 -2	
3	18000 -2	

INITIAL VOLUME:  
20.0000

TITRANT CONCENTRATION:  
-0.1000

ACTIVITY COEFF:  
0.8250

VOLUME ADDED	PH OBS.	PH CALC	% DEV. IN H	FRAC TITR
0.100	2.160	2.173	2.941	0.016
0.150	2.170	2.182	2.871	0.024
0.200	2.179	2.192	3.066	0.031
0.250	2.189	2.202	3.054	0.039
0.300	2.198	2.212	3.310	0.047
0.350	2.203	2.222	3.359	0.055
0.400	2.215	2.233	4.159	0.062
0.450	2.229	2.243	3.319	0.070
0.500	2.240	2.254	3.232	0.078
0.550	2.252	2.265	2.943	0.086
0.600	2.268	2.276	1.750	0.094
0.650	2.272	2.287	3.428	0.102
0.700	2.291	2.298	1.603	0.110
0.750	2.301	2.309	1.941	0.118
0.800	2.311	2.321	2.323	0.126
0.850	2.326	2.333	1.575	0.134
0.900	2.338	2.345	1.577	0.142
0.950	2.351	2.357	1.393	0.149
1.000	2.360	2.369	2.195	0.157

## INITIAL CONCENTRATIONS OF INDEPENDENT SPECIES:

KG 1.59000 -2  
H 3.18000 -2

INITIAL VOLUME:  
20.0000

TITRANT CONCENTRATION:  
-0.1000

ACTIVITY COEFF:  
0.8250

VOLUME ADDED	PH OBS.	PH CALC	% DEV. IN H	FRAC TITR
1.100	2.396	2.395	-0.242	0.173
1.200	2.412	2.421	2.196	0.189
1.300	2.448	2.449	0.225	0.204
1.400	2.475	2.478	0.619	0.220
1.500	2.508	2.508	-0.076	0.236
1.600	2.542	2.539	-0.668	0.252
1.700	2.582	2.572	-2.253	0.267
1.800	2.625	2.607	-4.079	0.283
1.900	2.651	2.644	-1.654	0.299
2.000	2.691	2.683	-1.844	0.314
2.100	2.742	2.725	-3.896	0.330
2.200	2.800	2.770	-6.748	0.346
2.300	2.847	2.818	-6.419	0.362
2.400	2.899	2.871	-6.248	0.377
3.700	4.119	4.078	-8.978	0.582
3.800	4.192	4.157	-7.765	0.597
3.900	4.259	4.230	-6.526	0.613
4.000	4.329	4.298	-6.963	0.629
4.100	4.389	4.362	-6.085	0.645
4.200	4.439	4.423	-3.679	0.660
4.300	4.495	4.481	-3.109	0.676
4.400	4.542	4.538	-0.920	0.692
4.500	4.598	4.593	-1.072	0.708
4.600	4.648	4.648	-0.062	0.723
4.700	4.692	4.702	2.240	0.739
4.800	4.741	4.755	3.370	0.755
4.900	4.792	4.809	4.098	0.770
5.000	4.840	4.864	5.726	0.786
5.100	4.889	4.920	7.411	0.802
5.200	4.940	4.978	9.033	0.818
5.300	5.010	5.037	6.488	0.833
5.400	5.068	5.100	7.649	0.849
5.500	5.129	5.167	9.048	0.865

## MAGNESIUM/ALPHA-KETOGLUTARATE TITRATION

CHISQ = 3.981D -4

CONST. VARIED	FORM. CONST	STAND. DEVS.
1	2.2563D 0	1.6693D -1

LOG BETA		MATRIX		
		MG	KG	H
1	0.35339	1	1	0
2	4.64976	0	1	1
3	6.66187	0	1	2

## TITRATION 1

INITIAL CONCENTRATIONS OF INDEPENDENT SPECIES:

MG	2.9530D -2
KG	1.0000D -2
H	2.0000D -2

INITIAL VOLUME:	TITRANT CONCENTRATION:	ACTIVITY COEFF:
10.0000	-0.1000	0.8250

VOLUME ADDED	PH OBS.	PH CALC	% DEV. IN H	FRAC TITR
1.250	4.289	4.264	-5.685	0.625
1.300	4.379	4.364	-3.461	0.650
1.350	4.461	4.457	-0.879	0.675
1.375	4.502	4.502	0.024	0.688
1.400	4.544	4.546	0.500	0.700
1.425	4.586	4.589	0.586	0.713
1.450	4.628	4.631	0.805	0.725
1.475	4.668	4.674	1.429	0.738
1.500	4.709	4.717	1.807	0.750
1.525	4.752	4.760	1.745	0.763
1.550	4.798	4.803	1.057	0.775
1.561	4.816	4.822	1.313	0.781
1.571	4.831	4.839	1.891	0.786
1.580	4.849	4.855	1.380	0.790
1.590	4.868	4.873	1.077	0.795
1.600	4.885	4.890	1.273	0.800
1.610	4.902	4.908	1.507	0.805
1.620	4.921	4.927	1.316	0.810
1.631	4.942	4.947	1.136	0.816
1.640	4.961	4.964	0.611	0.820
1.650	4.980	4.982	0.487	0.825
1.660	5.002	5.001	-0.184	0.830
1.673	5.030	5.026	-0.816	0.837
1.680	5.044	5.040	-0.859	0.840
1.690	5.068	5.060	-1.765	0.845
1.700	5.101	5.081	-4.577	0.850

## MANGANESE/ALPHA-KETOGLUTARATE TITRATION

CHISQ = 6.213D -4

CONST. VARIED	FORM. CONST	STAND. DEVS.
1	4.9244D 0	2.5541D -1

## LOG BETA      MATRIX

		MN	KG	H
1	0.69235	1	1	0
2	4.64976	0	1	1
3	6.66187	0	1	2

## TITRATION      1

INITIAL CONCENTRATIONS OF INDEPENDENT SPECIES:

MN	3.0000D -2
KG	1.0000D -2
H	2.0040D -2

INITIAL VOLUME:	TITRANT CONCENTRATION:	ACTIVITY COEFF:
10.0000	-0.1000	0.8250

VOLUME ADDED	PH OBS.	PH CALC	% DEV. IN H	FRAC TITR
1.325	4.401	4.377	-5.402	0.661
1.350	4.441	4.423	-4.047	0.674
1.375	4.481	4.468	-2.924	0.686
1.400	4.522	4.512	-2.215	0.699
1.425	4.564	4.556	-1.880	0.711
1.450	4.604	4.598	-1.416	0.724
1.475	4.644	4.641	-0.795	0.736
1.500	4.686	4.683	-0.648	0.749
1.526	4.728	4.728	-0.085	0.761
1.550	4.768	4.769	0.218	0.773
1.575	4.810	4.812	0.572	0.786
1.600	4.851	4.857	1.328	0.798
1.625	4.893	4.902	2.083	0.811
1.650	4.939	4.948	2.192	0.823
1.677	4.989	5.000	2.654	0.837
1.700	5.033	5.046	3.143	0.848
1.725	5.083	5.099	3.717	0.861
1.750	5.146	5.154	1.923	0.873
1.775	5.206	5.213	1.732	0.886
1.800	5.266	5.277	2.664	0.898

## ZINC/ALPHA-KETOGLUTARATE TITRATION

CHISQ = 1.227D -4

CONST. VARIED	FORM. CONST	STAND. DEVS.
1	4.3320D 1	2.9559D -1

LOG BETA		MATRIX		
		ZN	KG	H
1	1.63669	1	1	0
2	4.64976	0	1	1
3	6.66187	0	1	2

## TITRATION 1

INITIAL CONCENTRATIONS OF INDEPENDENT SPECIES:

ZN	3.0000D -2
KG	1.0000D -2
H	2.0000D -2

INITIAL VOLUME:	TITRANT CONCENTRATION:	ACTIVITY COEFF:
10.0000	-0.1000	0.8250

VOLUME ADDED	PH OBS.	PH CALC	% DEV. IN H	FRAC TITR
1.150	3.770	3.781	2.552	0.575
1.200	3.882	3.889	1.717	0.600
1.225	3.932	3.941	2.088	0.613
1.250	3.982	3.991	2.088	0.625
1.275	4.032	4.039	1.554	0.638
1.300	4.080	4.086	1.384	0.650
1.325	4.139	4.132	-1.567	0.663
1.350	4.181	4.178	-0.577	0.675
1.375	4.228	4.223	-1.150	0.688
1.401	4.271	4.269	-0.548	0.701
1.425	4.315	4.310	-1.228	0.713
1.450	4.358	4.353	-1.185	0.725
1.475	4.400	4.396	-0.938	0.738
1.500	4.440	4.439	-0.220	0.750
1.525	4.484	4.482	-0.367	0.763
1.550	4.528	4.526	-0.420	0.775
1.576	4.571	4.572	0.308	0.788
1.600	4.616	4.616	0.095	0.800
1.625	4.661	4.663	0.381	0.813
1.651	4.711	4.712	0.267	0.826
1.675	4.759	4.759	0.104	0.838
1.700	4.810	4.811	0.168	0.850
1.725	4.862	4.865	0.586	0.863
1.751	4.922	4.924	0.423	0.876
1.776	4.982	4.985	0.666	0.888
1.801	5.049	5.051	0.452	0.901



APPENDIX C

Decarboxylation Rate Data for the Various  
Enzyme/Oxalosuccinate/Metal Systems

SPONTANEOUS DECARBOXYLATION OF  
OXALOSUCCINIC ACID

REACTION	RATE CONSTANT	STD DEV
H3OXAS $\rightarrow$ CO <sub>2</sub> + A-KG	3.704E-04	2.655E-05
H2OXAS $\rightarrow$ CO <sub>2</sub> + A-KG	1.036E-03	9.085E-05
H OXAS $\rightarrow$ CO <sub>2</sub> + A-KG	1.697E-03	4.535E-05
OXAS $\rightarrow$ CO <sub>2</sub> + A-KG	2.222E-04	5.709E-06
COMPLEX	LOG BETA	
H3OXAS	4.467	
H2OXAS	7.127	
H OXAS	8.991	

EXP	(OXAS)	PH	K(OBS)	K(CALC)	% DEV
1	4.00E-04	0.04	3.90E-04	3.91E-04	-0.27
2	4.00E-04	2.36	1.18E-03	1.10E-03	6.84
3	4.00E-04	2.51	1.22E-03	1.20E-03	1.95
4	4.00E-04	2.56	1.22E-03	1.23E-03	-0.57
5	4.00E-04	2.84	1.30E-03	1.38E-03	-5.80
6	4.00E-04	2.89	1.25E-03	1.40E-03	-11.73
7	4.00E-04	3.17	1.47E-03	1.48E-03	-0.65
8	4.00E-04	3.46	1.50E-03	1.50E-03	0.35
9	4.00E-04	3.50	1.61E-03	1.49E-03	7.41
10	4.00E-04	3.58	1.74E-03	1.48E-03	15.04
11	4.00E-04	3.64	1.43E-03	1.47E-03	-2.45
12	4.00E-04	4.06	1.36E-03	1.20E-03	6.26
13	4.00E-04	4.49	9.06E-04	9.41E-04	-3.84
14	4.00E-04	4.78	7.19E-04	7.06E-04	1.86
15	4.00E-04	5.05	5.49E-04	5.29E-04	3.81
16	4.00E-04	5.15	4.49E-04	4.76E-04	-6.00
17	4.00E-04	5.44	3.54E-04	3.64E-04	-2.87
18	4.00E-04	5.45	3.27E-04	3.61E-04	-10.47
19	4.00E-04	5.91	2.55E-04	2.74E-04	-7.28
20	4.00E-04	6.04	2.70E-04	2.61E-04	3.48
21	4.00E-04	6.41	2.61E-04	2.39E-04	8.49
22	4.00E-04	7.06	2.30E-04	2.26E-04	1.75
23	4.00E-04	7.44	2.27E-04	2.24E-04	1.42
24	4.00E-04	7.48	2.31E-04	2.24E-04	3.19
25	4.00E-04	9.14	2.20E-04	2.22E-04	-1.02

## NOTES:

- 1) MOLAR CONCENTRATIONS ARE USED.
- 2) UNITS ON THE RATE CONSTANTS ARE 1/SEC.

MAGNESIUM CATALYZED DECARBOXYLATION  
OF OXALOSUCCINIC ACID

REACTION	RATE CONSTANT	STD DEV
MGOXAS $\rightarrow$ CO <sub>2</sub> + A-KG	1. 254E-02	3. 641E-04
H3OXAS $\rightarrow$ CO <sub>2</sub> + A-KG	3. 704E-04	
H2OXAS $\rightarrow$ CO <sub>2</sub> + A-KG	1. 036E-03	
H OXAS $\rightarrow$ CO <sub>2</sub> + A-KG	1. 697E-03	
OXAS $\rightarrow$ CO <sub>2</sub> + A-KG	2. 222E-04	

COMPLEX	LOG BETA
MGOXAS	1. 993
H3OXAS	4. 467
H2OXAS	7. 127
H OXAS	8. 991

OXALOSUCCINATE CONCENTRATION = 2. 67E-04 M  
FOR ALL EXPERIMENTS

EXP	(MG)	PH	K(OBS)	K(CALC)	% DEV
1	3. 33E-03	2. 84	1. 50E-03	1. 52E-03	-1. 63
2	6. 67E-03	2. 84	1. 59E-03	1. 57E-03	1. 16
3	1. 00E-02	2. 84	1. 61E-03	1. 62E-03	-0. 51
4	1. 33E-02	2. 84	1. 64E-03	1. 66E-03	-1. 46
5	1. 67E-02	2. 84	1. 65E-03	1. 71E-03	-3. 68
6	2. 00E-02	2. 84	1. 64E-03	1. 76E-03	-7. 06
7	3. 33E-03	3. 30	1. 75E-03	1. 72E-03	1. 66
8	6. 67E-03	3. 30	1. 91E-03	1. 89E-03	0. 84
9	1. 00E-02	3. 30	2. 11E-03	2. 06E-03	2. 32
10	1. 33E-02	3. 30	2. 27E-03	2. 22E-03	2. 13
11	1. 67E-02	3. 30	2. 41E-03	2. 38E-03	1. 16
12	2. 00E-02	3. 30	2. 62E-03	2. 53E-03	3. 32

EXP	(MG)	PH	K(OBS)	K(CALC)	% DEV
13	3.33E-03	3.54	1.84E-03	1.84E-03	-0.14
14	6.67E-03	3.54	2.18E-03	2.15E-03	1.22
15	1.00E-02	3.54	2.47E-03	2.45E-03	0.98
16	1.33E-02	3.54	2.88E-03	2.72E-03	5.56
17	1.67E-02	3.54	3.11E-03	2.99E-03	3.95
18	2.00E-02	3.54	3.38E-03	3.23E-03	4.35
19	3.33E-03	3.61	1.94E-03	1.87E-03	3.75
20	6.67E-03	3.61	2.11E-03	2.22E-03	-5.00
21	1.00E-02	3.61	2.54E-03	2.54E-03	-0.03
22	1.33E-02	3.61	2.90E-03	2.84E-03	1.93
23	1.67E-02	3.61	3.09E-03	3.14E-03	-1.55
24	2.00E-02	3.61	3.27E-03	3.41E-03	-4.18
25	3.33E-03	4.03	2.09E-03	2.17E-03	-3.81
26	6.67E-03	4.03	2.77E-03	2.92E-03	-5.25
27	1.00E-02	4.03	3.74E-03	3.56E-03	4.82
28	1.33E-02	4.03	4.43E-03	4.12E-03	7.02
29	1.67E-02	4.03	4.75E-03	4.63E-03	2.52
30	2.00E-02	4.03	5.11E-03	5.07E-03	0.89
31	3.33E-03	4.59	2.55E-03	2.63E-03	-3.19
32	6.67E-03	4.59	3.92E-03	3.94E-03	-0.62
33	1.00E-02	4.59	4.56E-03	4.95E-03	-8.55
34	1.33E-02	4.59	5.21E-03	5.74E-03	-10.16
35	1.67E-02	4.59	5.95E-03	6.40E-03	-7.53
36	2.00E-02	4.59	6.46E-03	6.93E-03	-7.23
37	3.33E-03	4.96	2.99E-03	2.85E-03	4.57
38	6.67E-03	4.96	4.53E-03	4.41E-03	2.63
39	1.00E-02	4.96	5.19E-03	5.54E-03	-6.69
40	1.33E-02	4.96	5.90E-03	6.38E-03	-8.21
41	1.67E-02	4.96	6.86E-03	7.07E-03	-3.03
42	2.00E-02	4.96	7.20E-03	7.60E-03	-5.56
43	3.33E-03	5.32	3.07E-03	2.97E-03	3.12
44	6.67E-03	5.32	4.67E-03	4.66E-03	0.22
45	1.00E-02	5.32	5.68E-03	5.84E-03	-2.84
46	1.33E-02	5.32	6.56E-03	6.71E-03	-2.29
47	1.67E-02	5.32	7.16E-03	7.40E-03	-3.33
48	2.00E-02	5.32	7.59E-03	7.93E-03	-4.45

EXP	(MG)	PH	K(OBS)	K(CALC)	% DEV
49	3.33E-03	6.91	3.17E-03	3.08E-03	2.95
50	6.67E-03	6.91	4.73E-03	4.87E-03	-2.99
51	1.00E-02	6.91	6.06E-03	6.10E-03	-0.59
52	1.33E-02	6.91	7.13E-03	6.98E-03	2.12
53	1.67E-02	6.91	7.93E-03	7.67E-03	3.30
54	2.00E-02	6.91	8.76E-03	8.19E-03	6.48
55	3.33E-03	7.38	3.14E-03	3.08E-03	1.96
56	6.67E-03	7.38	4.74E-03	4.87E-03	-2.85
57	1.00E-02	7.38	6.39E-03	6.10E-03	4.53
58	1.33E-02	7.38	7.65E-03	6.98E-03	8.71
59	1.67E-02	7.38	8.11E-03	7.67E-03	5.39
60	2.00E-02	7.38	8.78E-03	8.20E-03	6.64
61	3.33E-03	7.71	3.22E-03	3.08E-03	4.38
62	6.67E-03	7.71	4.81E-03	4.88E-03	-1.38
63	1.00E-02	7.71	6.06E-03	6.10E-03	-0.69
64	1.33E-02	7.71	7.68E-03	6.99E-03	9.05
65	1.67E-02	7.71	8.02E-03	7.67E-03	4.31
66	2.00E-02	7.71	8.86E-03	8.20E-03	6.41

## NOTES:

1. UNITS OF CONCENTRATION ARE MOLAR.
2. UNITS OF RATE CONSTANTS ARE 1/SECONDS.

MANGANESE CATALYZED DECARBOXYLATION  
OF OXALOSUCCINIC ACID

REACTION	RATE CONSTANT	STD DEV
MNOXAS $\rightarrow$ CO <sub>2</sub> + A-KG	2.003E-02	4.830E-04
H3OXAS $\rightarrow$ CO <sub>2</sub> + A-KG	3.704E-04	
H2OXAS $\rightarrow$ CO <sub>2</sub> + A-KG	1.036E-03	
H OXAS $\rightarrow$ CO <sub>2</sub> + A-KG	1.697E-03	
OXAS $\rightarrow$ CO <sub>2</sub> + A-KG	2.222E-04	

COMPLEX	LOG BETA
MNOXAS	2.565
H3OXAS	4.467
H2OXAS	7.127
H OXAS	8.991

OXALOSUCCINATE CONCENTRATION = 2.67E-04 M  
FOR ALL EXPERIMENTS

EXP	(MN)	PH	K(OBS)	K(CALC)	% DEV
1	3.33E-03	3.57	3.57E-03	3.42E-03	4.12
2	6.67E-03	3.57	5.27E-03	4.99E-03	5.35
3	1.00E-02	3.57	6.63E-03	6.28E-03	5.24
4	1.33E-02	3.57	7.51E-03	7.37E-03	1.94
5	1.33E-02	3.57	7.99E-03	7.37E-03	7.83
6	1.67E-02	3.57	8.45E-03	8.32E-03	1.58
7	2.00E-02	3.57	8.81E-03	9.11E-03	-3.45
8	3.33E-03	3.87	4.75E-03	4.86E-03	-2.33
9	6.67E-03	3.87	7.18E-03	7.26E-03	-1.05
10	1.00E-02	3.87	9.19E-03	9.00E-03	2.11
11	1.33E-02	3.87	1.08E-02	1.03E-02	4.52
12	1.67E-02	3.87	1.15E-02	1.14E-02	1.08
13	2.00E-02	3.87	1.21E-02	1.22E-02	-0.89

EXP	(MN)	PH	K(OBS)	K(CALC)	% DEV
14	3.33E-03	3.95	5.02E-03	5.11E-03	-1.82
15	6.67E-03	3.95	7.61E-03	7.63E-03	-0.28
16	1.00E-02	3.95	9.60E-03	9.43E-03	1.82
17	1.33E-03	3.95	1.18E-02	1.08E-02	8.82
18	1.67E-02	3.95	1.22E-02	1.18E-02	3.08
19	2.00E-02	3.95	1.29E-02	1.27E-02	1.94
20	1.00E-02	5.24	1.35E-02	1.52E-02	-12.72
21	3.33E-03	5.53	9.61E-03	1.01E-02	-5.20
22	6.67E-03	5.53	1.28E-02	1.35E-02	-5.47
23	1.00E-02	5.53	1.45E-02	1.51E-02	-4.41
24	1.33E-02	5.53	1.57E-02	1.61E-02	-2.72
25	1.67E-02	5.53	1.69E-02	1.68E-02	0.59
26	2.00E-02	5.53	1.82E-02	1.73E-02	5.14
27	3.33E-03	7.15	1.12E-02	1.09E-02	2.82
28	6.67E-03	7.15	1.39E-02	1.42E-02	-1.83
29	1.00E-02	7.15	1.53E-02	1.57E-02	-2.65
30	1.33E-02	7.15	1.69E-02	1.66E-02	1.75
31	1.67E-02	7.15	1.87E-02	1.72E-02	7.98
32	2.00E-02	7.15	1.90E-02	1.76E-02	7.26
33	3.33E-03	7.62	1.07E-02	1.09E-02	-1.77
34	6.67E-03	7.62	1.29E-02	1.42E-02	-9.76
35	1.00E-02	7.62	1.49E-02	1.57E-02	-5.34
36	1.33E-02	7.62	1.71E-02	1.66E-02	2.88
37	1.67E-02	7.62	1.90E-02	1.72E-02	9.41
38	2.00E-02	7.62	1.99E-02	1.76E-02	11.44

-----

NOTES:

1. UNITS OF CONCENTRATION ARE MOLAR.
2. UNITS OF THE RATE CONSTANTS ARE 1/SECONDS.

ZINC CATALYZED DECARBOXYLATION  
OF OXALOSUCCINIC ACID

REACTION	RATE CONSTANT	STD DEV
ZNOXAS $\rightarrow$ CO <sub>2</sub> + A-KG	1. 360E-01	2. 130E-03
H3OXAS $\rightarrow$ CO <sub>2</sub> + A-KG	3. 704E-04	
H2OXAS $\rightarrow$ CO <sub>2</sub> + A-KG	1. 036E-03	
H OXAS $\rightarrow$ CO <sub>2</sub> + A-KG	1. 697E-03	
OXAS $\rightarrow$ CO <sub>2</sub> + A-KG	2. 222E-04	

COMPLEX	LOG BETA
ZNOXAS	3. 016
H3OXAS	4. 467
H2OXAS	7. 127
H OXAS	8. 991

OXALOSUCCINATE CONCENTRATION = 2. 67E-04 M  
FOR ALL EXPERIMENTS

EXP	(ZN)	PH	K(OBS)	K(CALC)	% DEV
1	3. 33E-3	3. 17	1. 23E-2	1. 25E-2	-1. 21
2	6. 67E-3	3. 17	2. 37E-2	2. 14E-2	9. 90
3	1. 00E-2	3. 17	2. 88E-2	2. 87E-2	0. 29
4	1. 33E-2	3. 17	3. 53E-2	3. 49E-2	1. 22
5	1. 67E-2	3. 17	4. 29E-2	4. 03E-2	6. 11
6	2. 00E-2	3. 17	4. 62E-2	4. 48E-2	3. 01
7	3. 33E-3	3. 41	1. 93E-2	2. 01E-2	-3. 87
8	6. 67E-3	3. 41	3. 63E-2	3. 31E-2	8. 79
9	1. 00E-2	3. 41	4. 66E-2	4. 28E-2	8. 25
10	1. 33E-2	3. 41	5. 20E-2	5. 01E-2	3. 61
11	1. 67E-2	3. 41	5. 76E-2	5. 61E-2	2. 54
12	2. 00E-2	3. 41	6. 48E-2	6. 09E-2	6. 05
13	3. 33E-3	3. 61	3. 01E-2	2. 96E-2	1. 58
14	6. 67E-3	3. 61	4. 57E-2	4. 60E-2	-0. 69
15	1. 00E-2	3. 61	6. 05E-2	5. 67E-2	6. 36
16	1. 33E-2	3. 61	6. 71E-2	6. 41E-2	4. 53
17	1. 67E-2	3. 61	7. 17E-2	6. 97E-2	2. 79
18	2. 00E-2	3. 61	7. 72E-2	7. 39E-2	4. 27



EXP	(ZN)	PH	K(OBS)	K(CALC)	% DEV	269
19	3.33E-3	3.96	4.64E-2	4.56E-2	1.77	
20	6.67E-3	3.96	5.85E-2	6.39E-2	-9.23	
21	1.00E-2	3.96	7.09E-2	7.38E-2	-4.05	
22	1.33E-2	3.96	8.33E-2	7.99E-2	4.10	
23	1.67E-2	3.96	9.00E-2	8.42E-2	6.46	
24	2.00E-2	3.96	9.41E-2	8.72E-2	7.32	
25	3.33E-3	4.54	5.51E-2	6.52E-2	-18.35	
26	6.67E-3	4.54	7.25E-2	8.12E-2	-12.06	
27	1.00E-2	4.54	8.64E-2	8.83E-2	-2.23	
28	1.33E-2	4.54	9.78E-2	9.23E-2	5.64	
29	1.67E-2	4.54	9.91E-2	9.49E-2	4.24	
30	2.00E-2	4.54	1.07E-1	9.67E-2	9.63	
31	3.33E-3	4.92	5.85E-2	7.11E-2	-21.56	
32	6.67E-3	4.92	8.06E-2	8.57E-2	-6.32	
33	1.00E-2	4.92	9.21E-2	9.18E-2	0.33	
34	1.33E-2	4.92	9.82E-2	9.51E-2	3.13	
35	1.67E-2	4.92	1.03E-1	9.73E-2	5.56	
36	2.00E-2	4.92	1.07E-1	9.87E-2	7.74	
37	3.33E-3	5.57	6.27E-2	7.44E-2	-18.76	
38	6.67E-3	5.57	8.95E-2	8.81E-2	1.55	
39	1.00E-2	5.57	9.52E-2	9.37E-2	1.62	
40	1.33E-2	5.57	9.77E-2	9.66E-2	1.09	
41	1.67E-2	5.57	1.05E-1	9.86E-2	6.41	
42	2.00E-2	5.57	1.08E-1	9.98E-2	7.58	
43	3.33E-3	7.18	6.35E-2	7.53E-2	-18.62	
44	6.67E-3	7.18	8.35E-2	8.87E-2	-6.27	
45	1.00E-2	7.18	9.58E-2	9.41E-2	1.75	
46	1.33E-2	7.18	9.72E-2	9.70E-2	0.17	
47	1.67E-2	7.18	1.01E-1	9.89E-2	2.09	
48	2.00E-2	7.18	1.05E-1	1.00E-1	4.66	
49	3.00E-2	3.91	9.16E-2	8.75E-2	4.49	
50	4.00E-2	3.88	8.97E-2	8.98E-2	-0.10	
51	3.00E-2	4.44	9.19E-2	9.37E-2	-1.97	
52	3.00E-2	6.32	8.65E-2	9.63E-2	-11.33	
53	4.00E-2	6.35	8.83E-2	9.72E-2	-10.08	
54	9.09E-2	3.76	8.86E-2	9.35E-2	-5.48	

NOTES:

1. UNITS OF CONCENTRATION ARE MOLAR.
2. UNITS OF RATE CONSTANTS ARE 1/SECONDS.

---

 ICDH/OXAS DECARBOXYLATION DATA
 

---

REACTION	RATE CONSTANT	STD DEV
H-E-OX $\rightarrow$ CO <sub>2</sub>	1.591E-1	4.32E-3
E-OX $\rightarrow$ CO <sub>2</sub>	7.040E-2	2.86E-3
H- OX $\rightarrow$ CO <sub>2</sub>	1.690E-3	
OX $\rightarrow$ CO <sub>2</sub>	2.222E-4	

---

COMPLEX	LOG BETA
E-OXAS	5.670
H-E-OXAS	12.890
E- KG	4.987
H-OXAS	4.467
H- EN	6.67

---

THE CONCENTRATION OF ENZYME FOR ALL  
EXPERIMENTS WAS 1.06E-6 M

---

EXP	PH	K(OBS)	K(CALC)	% DEV
DATA SET 1: [OXAS] = 2.72E-3 M [KG] = 1.17E-3 M				
1	6.60	2.910E-4	2.870E-4	1.38
2	7.03	2.770E-4	2.727E-4	1.55
3	7.46	2.610E-4	2.613E-4	-0.11
4	7.74	2.520E-4	2.557E-4	-1.47
5	8.02	2.500E-4	2.522E-4	-0.87
DATA SET 2: [OXAS] = 1.99E-3 M [KG] = 8.69E-4 M				
6	6.55	3.140E-4	3.091E-4	1.56
7	7.03	2.810E-4	2.898E-4	-3.12
8	7.46	2.730E-4	2.751E-4	-0.77
9	7.75	2.620E-4	2.677E-4	-2.18
10	8.02	2.430E-4	2.630E-4	-8.22
DATA SET 3: [OXAS] = 1.29E-3 M [KG] = 5.63E-4 M				
11	6.60	3.590E-4	3.471E-4	3.32
12	7.04	3.410E-4	3.238E-4	5.03
13	7.54	3.240E-4	2.997E-4	7.50
14	7.78	3.010E-4	2.912E-4	3.27
15	8.03	2.780E-4	2.848E-4	-2.46

EXP	PH	K(OBS)	K(CALC)	% DEV
DATA SET 4: [OXAS] = 1.09E-3 M [KG] = 4.76E-4 M				
16	6.56	3.890E-4	3.704E-4	4.78
17	6.97	3.610E-4	3.460E-4	4.15
18	7.44	3.400E-4	3.187E-4	6.26
19	7.73	3.170E-4	3.055E-4	3.62
20	7.97	3.140E-4	2.978E-4	5.16
DATA SET 5: [OXAS] = 7.69E-4 M [KG] = 3.36E-4 M				
21	6.56	4.430E-4	4.274E-4	3.52
22	7.03	4.030E-4	3.909E-4	3.01
23	7.47	3.650E-4	3.562E-4	2.41
24	7.47	3.510E-4	3.379E-4	3.73
25	8.02	3.370E-4	3.274E-4	2.86
DATA SET 6: [OXAS] = 5.44E-4 M [KG] = 2.37E-4 M				
26	6.61	4.920E-4	5.027E-4	-2.17
27	7.02	4.120E-4	4.601E-4	-11.67
28	7.49	3.830E-4	4.090E-4	-6.79
29	7.76	3.540E-4	3.861E-4	-9.08
30	8.03	3.420E-4	3.702E-4	-8.24
DATA SET 7: [OXAS] = 3.75E-4 M [KG] = 1.64E-4 M				
31	6.55	6.380E-4	6.316E-4	1.01
32	7.01	5.730E-4	5.667E-4	1.10
33	7.46	5.330E-4	4.965E-4	6.85
34	7.73	4.770E-4	4.625E-4	3.03
35	8.02	4.550E-4	4.371E-4	3.93
DATA SET 8: [OXAS] = 2.77E-4 M [KG] = 1.21E-4 M				
36	6.54	7.600E-4	7.733E-4	-1.76
37	7.03	6.660E-4	6.825E-4	-2.47
38	7.51	5.820E-4	5.832E-4	-0.21
39	7.75	5.390E-4	5.440E-4	-0.91
40	8.02	4.910E-4	5.126E-4	-4.39
DATA SET 9: [OXAS] = 1.51E-4 M [KG] = 6.59E-5 M				
41	6.57	1.210E-3	1.213E-3	-0.21
42	7.04	1.010E-3	1.057E-3	-4.61
43	7.49	9.110E-4	8.871E-4	2.64
44	7.80	8.340E-4	7.966E-4	4.48
45	8.04	7.560E-4	7.485E-4	1.00

## NOTE:

THE RATE CONSTANTS HAS UNITS OF 1/SECONDS.

---

MAGNESIUM/ICDH/OXAS DECARBOXYLATION DATA

---

REACTION	RATE CONSTANT	STD DEV
MG-E-OX → CO <sub>2</sub>	4.128E+1	7.82E-1
H-E-OX → CO <sub>2</sub>	1.591E-1	
E-OX → CO <sub>2</sub>	7.040E-2	
H- OX → CO <sub>2</sub>	1.690E-3	
OX → CO <sub>2</sub>	2.222E-4	

---

COMPLEX	LOG BETA
MG-E	3.944
MG-E-OXAS	6.662
MG- OXAS	1.993
MG- KG	0.353
MG-E- KG	6.157
-1H-MG-E	-3.684
-1H-MG-E-OXAS	0.980
E-OXAS	5.670
H-E-OXAS	12.890
E- KG	4.987
H-OXAS	4.467
H- EN	6.67

---

THE CONCENTRATION OF ENZYME FOR ALL  
EXPERIMENTS WAS 2.97E-6 M

---

EXP	[MG]	PH	K(OBS)	K(CALC)	% DEV
DATA SET 1: [OXAS] = 3.49E-4 M [KG] = 1.52E-4 M					
1	3.28E-3	6.57	6.31E-3	6.01E-3	4.75
2	3.28E-3	7.01	7.06E-3	6.86E-3	2.80
3	3.28E-3	7.47	5.88E-3	6.28E-3	-6.85
4	3.28E-3	7.77	4.89E-3	5.27E-3	-7.86
5	3.28E-3	8.01	4.20E-3	4.54E-3	-8.22
6	6.56E-3	6.57	8.99E-3	9.16E-3	-1.88
7	6.56E-3	7.01	9.92E-3	1.01E-2	-1.81
8	6.56E-3	7.47	8.13E-3	8.61E-3	-5.93
9	6.56E-3	7.77	6.91E-3	7.22E-3	-4.50
10	6.56E-3	8.01	6.40E-3	6.38E-3	0.34

EXP	[NG]	PH	K(OBS)	K(CALC)	% DEV
11	9.84E-3	6.57	1.12E-2	1.14E-2	-1.81
12	9.84E-3	7.01	1.22E-2	1.21E-2	0.98
13	9.84E-3	7.47	9.77E-3	9.99E-3	-2.21
14	9.84E-3	7.77	8.27E-3	8.46E-3	-2.27
15	9.84E-3	8.01	7.50E-3	7.59E-3	-1.18
16	1.31E-2	6.57	1.24E-2	1.30E-2	-5.03
17	1.31E-2	7.01	1.36E-2	1.33E-2	1.95
18	1.31E-2	7.47	1.11E-2	1.09E-2	1.95
19	1.31E-2	7.77	9.49E-3	9.31E-3	1.88
20	1.31E-2	8.01	8.82E-3	8.44E-3	4.27
21	1.64E-2	6.57	1.43E-2	1.42E-2	0.61
22	1.64E-2	7.01	1.47E-2	1.42E-2	3.64
23	1.64E-2	7.47	1.12E-2	1.15E-2	-2.84
24	1.64E-2	7.77	9.84E-3	9.94E-3	-1.06
25	1.64E-2	8.01	8.84E-3	9.06E-3	-2.49
26	1.98E-2	6.57	1.48E-2	1.51E-2	-1.99
27	1.98E-2	7.01	1.58E-2	1.47E-2	6.79
28	1.98E-2	7.47	1.26E-2	1.20E-2	4.84
29	1.98E-2	7.77	9.96E-3	1.04E-2	-4.78
30	1.98E-2	8.01	9.41E-3	9.60E-3	-1.97
DATA SET 2: [OXAS] = 6.50E-4 M [KG] = 2.84E-4 M					
31	3.28E-3	6.57	4.27E-3	4.65E-3	-8.93
32	3.28E-3	7.01	4.93E-3	5.15E-3	-4.43
33	3.28E-3	7.47	4.98E-3	4.85E-3	2.47
34	3.29E-3	7.77	4.33E-3	4.28E-3	0.83
35	3.28E-3	8.01	4.02E-3	3.89E-3	3.36
36	6.56E-3	6.57	7.43E-3	7.24E-3	2.53
37	6.56E-3	7.01	8.22E-3	7.85E-3	4.48
38	6.56E-3	7.47	7.13E-3	7.01E-3	1.62
39	6.56E-3	7.77	6.30E-3	6.21E-3	1.50
40	6.56E-3	8.01	5.95E-3	5.72E-3	3.87
41	9.84E-3	6.57	8.82E-3	9.13E-3	-3.50
42	9.84E-3	7.01	9.59E-3	9.63E-3	-0.45
43	9.84E-3	7.47	8.51E-3	8.38E-3	1.52
47	9.84E-3	7.77	7.50E-3	7.44E-3	0.60
45	9.84E-3	8.01	6.86E-3	6.95E-3	-1.38
46	1.31E-2	6.57	1.07E-2	1.05E-2	1.46
47	1.31E-2	7.01	1.10E-2	1.09E-2	1.32
48	1.31E-2	7.47	9.83E-3	9.32E-3	5.19
49	1.31E-2	7.77	8.87E-3	8.36E-3	5.80
50	1.31E-2	8.01	7.98E-3	7.84E-3	1.80

EXP	[MG]	PH	K(OBS)	K(CALC)	% DEV
51	1.64E-2	6.57	1.14E-2	1.16E-2	-2.16
52	1.64E-2	7.01	1.20E-2	1.17E-2	2.20
53	1.64E-2	7.47	1.07E-2	1.00E-2	6.41
54	1.64E-2	7.77	9.39E-3	9.03E-3	3.87
55	1.64E-2	8.01	8.54E-3	8.51E-3	0.39
56	1.98E-2	6.57	1.22E-2	1.25E-2	-2.67
57	1.98E-2	7.01	1.25E-2	1.24E-2	0.83
58	1.98E-2	7.47	1.09E-2	1.06E-2	3.19
59	1.98E-2	7.77	9.32E-3	9.56E-3	-2.56
60	1.98E-2	8.01	9.07E-3	9.04E-3	0.32

DATA SET 3: [OXAS] = 1.77E-3 M [KG] = 7.73E-4 M

61	3.28E-3	6.57	3.43E-3	3.48E-3	-1.56
62	3.28E-3	7.01	3.65E-3	3.67E-3	-0.55
63	3.28E-3	7.47	3.55E-3	3.58E-3	-0.90
64	3.28E-3	7.77	3.43E-3	3.38E-3	1.49
65	3.28E-3	8.01	3.31E-3	3.23E-3	2.50
66	6.56E-3	6.57	5.43E-3	5.57E-3	-2.53
67	6.56E-3	7.01	5.79E-3	5.83E-3	-0.67
68	6.56E-3	7.47	5.32E-3	5.53E-3	-3.95
69	6.56E-3	7.77	4.99E-3	5.22E-3	-4.65
70	6.56E-3	8.01	4.85E-3	5.04E-3	-3.83
71	9.84E-3	6.57	7.32E-3	7.09E-3	3.18
72	9.84E-3	7.01	7.46E-3	7.33E-3	1.72
73	9.84E-3	7.47	7.24E-3	6.85E-3	5.33
74	9.84E-3	7.77	6.39E-3	6.49E-3	-1.61
75	9.84E-3	8.01	6.09E-3	6.29E-3	-3.33
76	1.31E-2	6.57	8.92E-3	8.24E-3	7.66
77	1.31E-2	7.01	9.05E-3	8.42E-3	6.94
78	1.31E-2	7.47	8.12E-3	7.80E-3	3.90
79	1.31E-2	7.77	7.59E-3	7.41E-3	2.34
80	1.31E-2	8.01	7.18E-3	7.21E-3	-0.37
81	1.64E-2	6.57	9.95E-3	9.15E-3	8.05
82	1.64E-2	7.01	1.01E-2	9.25E-3	8.39
83	1.64E-2	7.47	8.94E-3	8.53E-3	4.63
84	1.64E-2	7.77	8.28E-3	8.12E-3	1.96
85	1.64E-2	8.01	7.94E-3	7.91E-3	0.41
86	1.98E-2	6.57	1.09E-2	9.90E-3	9.16
87	1.98E-2	7.01	1.06E-2	9.91E-3	6.49
88	1.98E-2	7.47	9.75E-3	9.10E-3	6.65
89	1.98E-2	7.77	9.59E-3	8.67E-3	9.47
90	1.98E-2	8.01	9.07E-3	8.47E-3	6.61

DATA SET 4: [OXAS] = 3.30E-4 M

EXP	[MG]	[KG]	PH	K(OBS)	K(CALC)	% DEV
91	3.28E-3	4.18E-4	7.01	6.82E-3	6.83E-3	-0.11
92	3.28E-3	9.27E-4	7.01	6.36E-3	6.46E-3	-1.52
93	3.28E-3	1.22E-3	7.01	6.16E-3	6.27E-3	-1.87
94	9.84E-3	4.18E-4	7.01	1.28E-2	1.20E-2	6.31
95	9.84E-3	9.27E-4	7.01	1.11E-2	1.14E-2	-2.97
96	9.81E-3	1.22E-3	7.01	1.05E-2	1.11E-2	-6.21
97	1.98E-2	4.18E-4	7.01	1.47E-2	1.46E-2	0.64
98	1.98E-2	9.27E-4	7.01	1.42E-2	1.40E-2	1.15
99	1.98E-2	1.22E-3	7.01	1.39E-2	1.38E-2	1.06
100	9.84E-3	1.22E-3	6.57	1.09E-2	1.08E-2	1.19
101	9.84E-3	1.22E-3	7.47	9.22E-3	9.61E-3	-4.18
102	9.84E-3	1.22E-3	7.77	8.22E-3	8.35E-3	-1.58
103	9.84E-3	1.22E-3	8.01	7.86E-3	7.57E-3	0.94

NOTE:

THE RATE CONSTANTS HAVE UNITS OF 1/SECONDS.

AD-A092 546

AIR FORCE INST OF TECH WRIGHT-PATTERSON AFB OH  
SPONTANEOUS, METAL-CATALYZED, AND ENZYME-CATALYZED DECARBOXYLAT--ETC(U)  
1980 S L SINCOFF

F/G 7/3

UNCLASSIFIED

AFIT-CI-80-270

NL

4 of 4  
AD-A  
PAGE



END  
DATE  
FILMED  
-81  
DTIC



---

 ZINC/ICDH/OXAS DECARBOXYLATION DATA
 

---

REACTION	RATE CONSTANT	STD DEV
ZN-E-OX → CO <sub>2</sub>	4.370E+1	1.08E-0
H-E-OX → CO <sub>2</sub>	1.591E-1	
E-OX → CO <sub>2</sub>	7.040E-2	
H- OX → CO <sub>2</sub>	1.690E-3	
OX → CO <sub>2</sub>	2.222E-4	

---

COMPLEX	LOG BETA
ZN-E	2.740
ZN-E-OXAS	7.960
ZN- OXAS	3.016
ZN- KG	1.630
ZN-E KG	7.324
E-OXAS	5.670
H-E-OXAS	12.890
E- KG	4.987
H-OXAS	4.467
H- EN	6.67

---

THE CONCENTRATION OF ENZYME FOR ALL  
EXPERIMENTS WAS 2.97E-6 M

---

EXP	[ZN]	PH	K(OBS)	K(CALC)	% DEV
DATA SET 1: [OXAS] = 3.33E-4 M [KG] = 1.45E-4 M					
1	1.97E-3	6.55	8.55E-2	8.96E-2	-4.78
2	3.28E-3	6.55	1.07E-1	1.14E-1	-6.51
3	6.56E-3	6.55	1.53E-1	1.50E-1	1.90
4	9.84E-3	6.55	1.71E-1	1.71E-1	0.15
5	1.31E-2	6.55	1.77E-1	1.83E-1	-3.43
6	1.97E-3	7.01	1.18E-1	1.09E-1	7.90
7	3.28E-3	7.01	1.45E-1	1.41E-1	2.52
8	6.56E-3	7.01	1.98E-1	1.86E-1	6.14

EXP	[ZN]	PH	K(OBS)	K(CALC)	% DEV	
DATA SET 2: [OXAS] = 6.68E-4 M [KG] = 2.92E-4 M						
9	1.97E-3	6.55	7.15E-2	7.47E-2	-4.49	
10	3.28E-3	6.55	9.57E-2	9.43E-2	1.49	
11	6.56E-3	6.55	1.18E-1	1.20E-1	-1.95	
12	9.84E-3	6.55	1.29E-1	1.35E-1	-4.66	
13	1.31E-2	6.55	1.43E-1	1.45E-1	-1.16	
14	1.97E-3	7.01	7.95E-2	8.36E-2	-5.20	
15	3.28E-3	7.01	1.09E-1	1.08E-1	1.16	
16	6.56E-3	7.01	1.38E-1	1.40E-1	-1.28	
17	1.97E-3	7.47	9.36E-2	9.27E-2	0.98	
18	3.28E-3	7.47	1.13E-1	1.20E-1	-6.28	
DATA SET 3: [OXAS] = 1.67E-3 M [KG] = 7.29E-4 M						
19	3.28E-3	6.55	7.94E-2	7.74E-2	2.66	
20	6.56E-3	6.55	1.07E-1	9.94E-2	7.09	
21	9.84E-3	6.55	1.14E-1	1.10E-1	3.62	
22	1.31E-2	6.55	1.19E-1	1.17E-1	2.14	
23	3.28E-3	7.01	8.34E-2	8.20E-2	1.74	
24	6.56E-3	7.01	1.10E-1	1.07E-1	2.58	
25	9.84E-3	7.01	1.18E-1	1.19E-1	-0.89	
26	1.31E-2	7.01	1.33E-1	1.26E-1	5.18	
27	3.28E-3	7.47	8.68E-2	8.64E-2	0.48	
DATA SET 4: [OXAS] = 3.39E-4 M						
EXP	[ZN]	[KG]	PH	K(OBS)	K(CALC)	% DEV
28	3.28E-3	4.54E-4	6.55	1.04E-1	1.08E-1	-3.97
29	3.28E-3	9.97E-4	6.55	9.74E-2	1.02E-1	-4.65
30	3.28E-3	1.41E-3	6.55	9.58E-2	9.86E-2	-2.93
31	1.97E-3	4.54E-4	6.55	8.39E-2	8.67E-2	-3.30
32	1.97E-3	9.97E-4	6.55	8.00E-2	8.33E-2	-4.07
33	1.97E-3	1.41E-3	6.55	7.82E-2	8.12E-2	-3.84
34	6.56E-3	4.54E-4	6.55	1.32E-1	1.34E-1	-1.57
35	6.56E-3	9.97E-4	6.55	1.16E-1	1.21E-1	-4.55
36	6.56E-3	1.41E-3	6.55	1.09E-1	1.16E-1	-6.10
37	6.56E-3	4.54E-4	7.01	1.47E-1	1.51E-1	-2.36
38	6.56E-3	1.41E-3	7.01	1.23E-1	1.20E-1	2.11

## NOTE:

THE RATE CONSTANTS ARE IN UNITS OF 1/SECONDS.

APPENDIX D

Computer Listing of the Program CORNEK

```

C      MODE=1, CORNEX
C      MODE=2, ABSORBANCE FIT
C      MODE=3 P4-FIT
C      MODE=4, METAL-P4-FIT
      IMPLICIT REAL*8(A-H,C-Z)
      INTEGER BV,CV,DCN
      DIMENSION FRIC(30)
      DIMENSION VI(5),CHXI(5),TSPI(7,7),VQRS(7,25),PHQRS(7,25),FBETA(20)
1,A(20),B(20),DERIV(20),SIGA(20),BETA(20),RV(20),CV(20),DCN(20),
2 EQNMAT(15,10,15),TITLE(7,40),WEIGHT(125,8),FRAC(125,30)
      COMMON/A/TSP(125,7),SP(7),COMP(20),BETA(20),M(7,20),AR(6,7)
      COMMON/B/CGN(20,8),DCCN(125,8),P(2,2)
      COMMON/C/TLIM1,NIND,NASS,NKN,NUNK,NC,NENTL,MODE
      COMMON/D/ ALPH(20,20),ARRAY(20,20)
21 FORMAT(40A2)
22 FORMAT(16(I3,2X))
23 FORMAT(12(F10.3),12(I3,2X))
24 FORMAT(D10.3,20A2)
25 FORMAT (10(D8.3))
31 FORMAT('      CHISQ= ',1PD10.2)
32 FORMAT('1',40A2)
33 FORMAT(//,40A2,/)
34 FORMAT(5X,I3,I3,5X,10A2,2(3X,1PD10.3))
36 FORMAT(5X,I3,3X,3(1PD10.3),10(2X,I3))
37 FORMAT(5X,I3,3X,1PD10.3,10X,1PD10.3,10(2X,I3))
38 FORMAT(5X,I3,9(2X,1PD10.3))
41 FORMAT (5X,I3,15(2X,F5.2))
42 FORMAT (5X,I3,10(1PD10.3))
422 FORMAT ('      NUMBER OF CYCLES = ',I3)
      READ (5,22) NSET
      DO 1000 ISET=1,NSET
      DO 20 J=1,6
      READ (5,21) (TITLE(J,I), I=1,40)
20 CONTINUE
      READ(5,22) NRT
      WRITE(6,22) NRT
      READ(5,22) NIND,NASS,NKN,NENTL,NCNT,MODE
      WRITE(6,22) NIND,NASS,NKN,NENTL,NCNT,MODE
      NUNK=NIND-NKN
      DO 30 I=1,NASS
      READ(5,23) BETA(I),FBETA(I),(M(J,I),J=1,NIND)
      WRITE(6,23) BETA(I),FBETA(I),(M(J,I),J=1,NIND)
30 BETA(I)=10**BETA(I)
      READ(5,22) NDV

```

```

WRITE(6,22)NBV
IF(NBV.LE.0) GO TO 40
READ(5,22) (BV(I),I=1,NBV)
WRITE(6,22) (BV(I),I=1,NBV)
40 IF (MODE.GE.3) GO TO 90
READ(5,22) NCON,NDCN
WRITE(6,22)NCON,NDCN
DO 50 K=1,NDCN
DO 50 I=1,NCON
READ(5,24) CON(I,K),(EQNMAT(I,J,K),J=1,10)
50 WRITE(6,24) CON(I,K),(EQNMAT(I,J,K),J=1,10)
READ(5,22) NCV
WRITE(6,22)NCV
IF(NCV.LE.0) GO TO 70
READ(5,22) (CV(I),DCN(I),I=1,NCV)
WRITE(6,22) (CV(I),DCN(I),I=1,NCV)
70 READ(5,22) NEX
WRITE(6,22) NEX
AMIN=1000
DO 80 I=1,NEX
READ(5,25) (TSP(I,J),J=1,NIND),(DCON(I,K),K=1,NDCN)
IF(AMIN.GT.DCON(I,K)) AMIN=DCON(I,K)
80 CONTINUE
DO 85 I=1,NEX
WEIGHT(I,K)=AMIN/DCON(I,K)
85 WRITE(6,25) (TSP(I,J),J=1,NIND),(DCON(I,K),WEIGHT(I,K),K=1,NDCN)
GO TO 111
90 NCV=0
NCON=0
NCCT=0
NEX=0
NDCN=1
READ(5,22) NTR
WRITE(6,22)NTR
DO 110 I=1,NTR
READ(5,22) NPTS
WRITE(6,22)NPTS
NEX=NEX + NPTS
READ(5,25) VI(I),CHXI(I),(TSP(I,J),J=1,NIND)
WRITE(6,25) VI(I),CHXI(I),(TSP(I,J),J=1,NIND)
DO 110 K=1,NPTS
NCCT=NCCT+1
READ(5,25) VOBS(I,K),PHOBS(I,K)
WRITE(6,25) VOBS(I,K),PHOBS(I,K)

```

```

V=VI(I)+VOBS(I,K)
N=NCCT
DO 100 L=1,NIND
100 TSP(N,L)=TSP(I,L)+VI(I)/V
IF (MODE.EQ.4) GO TO 101
TSP(N,NIND)=TSP(N,NIND)+CHXI(I)+VOBS(I,K)/V
GO TO 102
101 TSP(N,L)=TSP(N,L)+CHXI(I)+VOBS(I,K)/V
102 CCON(N,1)=PHOBS(I,K)
110 WEIGHT(N,1)=1.0
111 NTERM=NCV+N2V
NFREE=NEX-NTERM
NC=NUNK+1
TLIM1=1.0D-6
NCC=0
CHISV=1.0E-27
FLANC=0.001
120 CH2X=0.0
IF (NTERM.EQ.0) GO TO 231
DO 130 I=1,NTERM
BETA(I)=0.0
DO 130 J=1,NTERM
130 ALPHA(I,J)=0.0
DO 190 I=1,NEX
IF (NBV.LE.0) GO TO 161
DO 160 K=1,NBV
J=BV(K)
A(K)=BETA(J)
AJ=A(K)
DELTA=FBETA(J)+AJ
BETA(J)=AJ+DELTA
YFIT=0.0
CALL GENDIS(I)
DO 140 L=1,NCCN
CALL FITFC(YFIT1,I,L)
140 YFIT=YFIT+YFIT1*WEIGHT(I,L)
YFIT1=YFIT
YFIT=0.0
BETA(J)=AJ-DELTA
CALL GENDIS(I)
DO 150 L=1,NCCN
CALL FITFC(YFIT2,I,L)
150 YFIT=YFIT+YFIT2*WEIGHT(I,L)
YFIT2=YFIT

```

```

      DERIV(K)=(YFIT1-YFIT2)/(2.0*DELTA)
160 BETA(J)=A(K)
161 CALL GENDIS(I)
      IF(NCV.LE.0) GO TO 171
      DO 170 K=1,NCV
        J=CV(K)
        N=DCN(K)
        A(NBV+K)=CON(J,N)
        AJ=A(NBV+K)
        DELTA=0.11*AJ
        CON(J,N)=AJ*DELTA
        CALL FITFC(YFIT1,I,N)
        YFIT1=WEIGHT(I,N)*YFIT1
        CON(J,N)=AJ*DELTA
        CALL FITFC(YFIT2,I,N)
        YFIT2=WEIGHT(I,N)*YFIT2
        DERIV(NBV+K)=(YFIT1-YFIT2)/(2.0*DELTA)
170 CON(J,N)=A(NBV+K)
171 N=0
      CHIX=0.0
      DO 180 J=1,NDCN
        CALL FITFC(YF,I,J)
        IF(WEIGHT(I,J).NE.0.0) N=N+1
        YF=YF+WEIGHT(I,J)
180 CHIX=CHIX+YF**2
      CHIX=CHIX/N
      CHIX2=CHIX2+CHIX
      DO 190 J=1,NTERM
        BEDA(J)=BEDA(J)-YF*DERIV(J)
      DO 190 K=1,J
190 ALPH(J,K)=ALPH(J,K)+DERIV(J)*DERIV(K)
191 DO 200 J=1,NTERM
      DO 199 K=1,J
      ARRAY(J,K)=ALPH(J,K)/(DSQRT(ALPH(J,J))*DSQRT(ALPH(K,K)))
199 ARRAY(K,J)=ARRAY(J,K)
200 ARRAY(J,J)=1.0+FLAND
      CALL MATINV(NTERM)
      DO 210 J=1,NTERM
        B(J)=A(J)
      DO 210 K=1,NTERM
        B(J)=B(J)+BEDA(K)*ARRAY(J,K)/(DSQRT(ALPH(J,J))*DSQRT(ALPH(K,K)))
      IF(A(J).GE.0.0) GO TO 209
      IF(B(J).GT.0.1*A(J)) B(J)=0.1*A(J)
      IF(B(J).LT.10.0*A(J)) B(J)=10.0*A(J)

```

```

      GO TO 210
209 IF(B(J).LT.0.1*A(J)) B(J)=0.1*A(J)
   IF(B(J).GT.10.0*A(J)) B(J)=10.0*A(J)
210 CONTINUE
   IF(NBV.LE.0) GO TO 221
   DO 220 J=1,NBV
   K=BV(J)
220 BETA(K)=B(J)
221 IF(NCV.LE.0) GO TO 231
   DO 230 J=1,NCV
   K=CV(J)
   N=DCN(J)
230 CON(K,N)=B(NBV+J)
231 CH12R=0.0
   DO 250 I=1,NEX
   N=0
   CHIX=0.0
   CALL GENDIS(I)
   DO 240 J=1,NDCN
   CALL FITFC(YF,I,J)
   IF(WEIGHT(I,J).NE.0.0) N=N+1
   YF=YF*WEIGHT(I,J)
240 CHIX=CHIX+YF**2
   CHIX=CHIX/N
250 CH12R=CH12R+CHIX
   IF (INTERM.EQ.0) GO TO 291
   IF(CH12R.LE.CH12X) GO TO 260
   FLAMD=10.0*FLAMD
   GO TO 191
260 CONTINUE
   WRITE(6,31) CH12R
   WRITE(6,25) (CON(I,1),I=1,NDCN)
   WRITE(6,25) (BETA(I),I=1,NASS)
   CHISQ=CH12R
   IF(DABS(CHISQ-CHISV)/CHISV.LE.0.0001) GO TO 270
   FLAMD=0.1*FLAMD
   CHISV=CHISQ
   NCC=NCC+1
   IF(NCC.LE.NCNT) GO TO 120
270 DO 280 J=1,INTERM
   DO 280 K=1,J
   ARRAY(J,K)=ALPH(J,K)/(DSQRT(ALPH(J,J))*DSQRT(ALPH(K,K)))
280 ARRAY(K,J)=ARRAY(J,K)
   CALL MATINV(INTERM)

```



```

      DO 290 I=1,NTERM
290  SIGA(I)=DSQRT(ARRAY(I,I)*CHI2R/(ALPH(I,I)*NFREE))
291  CHISQ=CHI2R/NFREE
      WRITE(6,32) (TITLE(1,I),I=1,40)
      WRITE (6,31) CHISQ
      WRITE(6,422) NCC
      IF(NCON.LE.0) GO TO 301
      WRITE(6,33) (TITLE(2,I),I=1,40)
      N=1
      DO 300 K=1,NCON
      DO 300 I=1,NCON
      IF((NCV.EQ.0).OR.(CV(N).NE.I)) GO TO 299
      IF(DCN(N).NE.K) GO TO 299
      WRITE(6,34) K,I,(EQNMAT(I,J,K),J=1,10),CON(I,K),SIGA(NBV+N)
      IF(N.LT.NCV) N=N+1
      GO TO 300
299  WRITE(6,34) K,I,(EQNMAT(I,J,K),J=1,10),CON(I,K)
300  CONTINUE
301  WRITE(6,33) (TITLE(3,I),I=1,40)
      N=1
      DO 310 I=1,NASS
      TD=DLOG10(BETA(I))
      IF((NBV.EQ.0).OR.(BV(N).NE.I)) GO TO 309
      WRITE(6,36) I,BETA(I),SIGA(N),TD,(M(J,I),J=1,NIND)
      IF(N.LT.NBV) N=N+1
      GO TO 310
309  WRITE(6,37) I,BETA(I),TD,(M(J,I),J=1,NIND)
310  CONTINUE
      WRITE(6,33) (TITLE(4,I),I=1,40)
      DO 320 I=1,NEX
      CALL GENDIS(I)
      N=1
      IF(WEIGHT(I,N).EQ.0.0) GO TO 320
      CALL FITFC(FIT,I,N)
      DCAL=DCON(I,N)-FIT
      IF(MODE.NE.3) FIT=FIT*100.0/DCCN(I,N)
      WRITE(6,38) I,(TSP(I,J),J=1,NIND),DCON(I,N),DCAL,FIT
320  CONTINUE
      WRITE (6,33) (TITLE(5,I),I=1,40)
      NASS1=NASS+1
      DO 326 I=1,NEX
      CALL GENDIS(I)
      FRIC(I)=SP(2)*100.0/TSP(I,2)
      DO 325 ISP=1,NASS

```

```

      FRIC(ISP+1)=COMP(ISP)*100.0/TSP(I,2)
      IF (M(2,ISP).EQ.0) FRIC(ISP+1)=0.0
325  CONTINUE
326  WRITE (6,41) I,(FRIC(IJ),IJ=1,NASS1)
      WRITE (6,33) (TITLE(6,I),I=1,40)
      DO 329 I=1,NEX
      CALL GENDIS(I)
      FRIC(I)=SP(I)*100.0/TSP(I,1)
      DO 327 ISP=1,NASS
      FRIC(ISP+1)=COMP(ISP)*100.0/TSP(I,1)
      IF (M(1,ISP).EQ.0) FRIC(ISP+1)=0.0
327  CONTINUE
328  WRITE (6,41) I,(FRIC(IJ),IJ=1,NASS1)
1000 CONTINUE
      STOP
      END
      SUBROUTINE MATINV(INTERM)
      IMPLICIT REAL*8(A-H,O-Z)
      COMMON/D/ ALPH(20,20),ARRAY(20,20)
      DIMENSION IK(20), JK(20)
      DET=1.0
      DO 100 K=1,INTERM
      AMAX=1.0D-10
      DO 30 I=K,INTERM
      DO 30 J=K,INTERM
      IF(DABS(ARRAY(I,J)/AMAX).LE.1.0) GO TO 30
      AMAX=ARRAY(I,J)
      IK(K)=I
      JK(K)=J
30  CONTINUE
      I=IK(K)
      IF(I.EQ.K) GO TO 51
      DO 50 J=1,INTERM
      SAVE=ARRAY(K,J)
      ARRAY(K,J)=ARRAY(I,J)
50  ARRAY(I,J)=-SAVE
51  J=JK(K)
      IF(J.EQ.K) GO TO 61
      DO 60 I=1,INTERM
      SAVE= ARRAY(I,K)
      ARRAY(I,K)=ARRAY(I,J)
60  ARRAY(I,J)=-SAVE
61  DO 70 I=1,INTERM
70  IF(I.NE.K) ARRAY(I,K)=-ARRAY(I,K)/AMAX

```

```

      DO 90 I=1, NTERM
      IF(I.EQ.K) GO TO 90
      DO 80 J=1, NTERM
80    IF(J.NE.K) ARRAY(I,J)=ARRAY(I,J)+ARRAY(I,K)*ARRAY(K,J)
90    ARRAY(K,I)=ARRAY(K,I)/AMAX
      ARRAY(K,K)=1.0/AMAX
100   DET=DET*AMAX
      DO 130 L=1, NTERM
      K=NTERM-L+1
      J=IK(K)
      IF(J.LE.K) GO TO 111
      DO 110 I=1, NTERM
      SAVE=ARRAY(I,K)
      ARRAY(I,K)=-ARRAY(I,J)
110   ARRAY(I,J)=SAVE
111   I=JK(K)
      IF(I.LE.K) GO TO 130
      DO 120 J=1, NTERM
      SAVE=ARRAY(K,J)
      ARRAY(K,J)=-ARRAY(I,J)
120   ARRAY(I,J)=SAVE
130   CONTINUE
      RETURN
      END
      SUBROUTINE GENDIS(I)
      IMPLICIT REAL*8(A-H,C-Z)
C
C      DIMENSION AR(NUNK,NC)
C
      COMMON/A/TSP(125,7), SP(7), COMP(20), BETAI(20), M(7,20), AR(6,7)
      COMMON/C/TLIM1, NIND, NASS, NKN, NUNK, NC, NCNTL, MODE
110   DO 10 J=1, NIND
10    SP(J)=TSP(I,J)
      IF(NUNK.NE.NIND) SP(NC)=10**(-TSP(I,NC))
      TLIM=TLIM1*SP(1)
      NCNT=0
      UL=9.0
      PL=0.9
20    DO 30 J=1, NUNK
      AR(J,NC)=TSP(I,J)-SP(J)
      DO 30 K=1, NASS
      COMP(K)=BETAI(K)
      DO 29 L=1, NIND
29    IF(M(L,K).NE.0) COMP(K)=COMP(K)*(SP(L))**M(L,K)

```

```

30 AR(J,NC)=AR(J,NC)-M(J,K)*COP(K)
   DO 40 J=1,NUNK
   IF(DABS(AR(J,NC)).GT.TL1*) GO TO 42
40 CONTINUE
   RETURN
42 DO 50 J=1,NUNK
   DO 49 K=1,NUNK
   AR(J,K)=0.0
   DO 48 L=1,NASS
48 IF((P(K,L).NE.0).AND.(M(J,L).NE.0)) AR(J,K)=AR(J,K)+P(J,L)*M(K,L)*
   ICOMP(L)
49 AR(J,K)=AR(J,K)/SP(K)
50 AR(J,J)=AR(J,J)+1.0000
   K1=NUNK-1
   DO 70 J=1,K1
   K2=J+1
   DO 70 K=K2,NUNK
   IF(AR(K,J).EQ.0.0) GO TO 70
   R=AR(K,J)/AR(J,J)
   IF(DABS(R).LE.1.0) GO TO 61
   DO 60 N=J,NC
   T=AR(K,N)
   AR(K,N)=AR(J,N)
60 AR(J,N)=T
   R=AR(K,J)/AR(J,J)
61 DO 69 L=J,NC
69 AR(K,L)=AR(K,L)-R*AR(J,L)
70 CONTINUE
   DO 80 J=1,NUNK
   NU=NC-J
   L=J-1
   IF(L.LE.0) GO TO 80
   DO 79 K=1,L
   N=NC-L
79 AR(NU,NC)=AR(NU,NC)-AR(NU,N)*AR(N,NC)
80 AR(NU,NC)=AR(NU,NC)/AR(NU,NU)
   DO 90 J=1,NUNK
   IF(AR(J,NC).GT.UL*SP(J)) AR(J,NC)=UL*SP(J)
   IF(-AR(J,NC).GT.PL*SP(J)) AR(J,NC)=-PL*SP(J)
90 SP(J)=SP(J)+AR(J,NC)
   NCNT=NCNT+1
   IF(NCNT.GT.NCNTL) GO TO 100
   IF(NCNT.NE.NCNTL/2) GO TO 20
   UL=1.0

```

```
PL=0.5
GO TO 20
100 WRITE(6,101) I
101 FORMAT(5X,'NONCONVERGENCE FOR EXP. #',I5)
I=I+1
GO TO 110
END
SUBROUTINE FITEC(DET,I,N)
IMPLICIT REAL*8(A-H,C-Z)
COMMON/A/TSP(125,7),SP(7),COMP(20),BETA(20),M(7,20),AR(6,7)
COMMON/B/CON(20,8),DCON(125,8),P(2,2)
COMMON/C/TLIM1,NIND,NASS,NKN,NUNK,NC,NCNTL,MODE
DET=DCON(I,N)-DCALC
RETURN
END
```

APPENDIX E

Computer Listings of the Various FITFC Subroutines Used  
for the Program CORNEK

C THIS SUBROUTINE IS FOR METAL/ENZYME/CXAS DECARBOXYLATION  
C NOTE : TSP(1,2) = TOTAL CXAS CONCENTRATION

CXTOT=TSP(1,2)  
FOX=SP(2)/CXTOT  
FENOX=COMP(1)/CXTOT  
FMOX=COMP(3)/CXTOT  
FHOX=COMP(4)/CXTOT  
FMOX=COMP(5)/CXTOT  
FEHGX=COMP(9)/CXTOT  
DCALC=CON(1,1)\*FENOX+CON(2,1)\*FENOX+  
1CON(3,1)\*FEHGX+CON(4,1)\*FHOX+CON(5,1)\*FOX+CON(6,1)\*FMOX

C THIS SUBROUTINE IS FOR FREE CXAS DECARBOXYLATION ONLY  
C NOTE : TSP(1,2) = TOTAL CXAS CONCENTRATION

CXTOT=TSP(1,1)  
FOX=SP(1)/CXTOT  
FHOX=COMP(1)/CXTOT  
FH2OX=COMP(2)/CXTOT  
FH3OX=COMP(3)/CXTOT  
DCALC=CON(2,1)\*FH2OX+CON(1,1)\*FH3OX+CON(3,1)\*FHOX+CON(4,1)\*FOX

C THIS SUBROUTINE IS FOR METAL/CXAS DECARBOXYLATION ONLY  
C NOTE : TSP(1,2) = TOTAL CXAS CONCENTRATION

ENCL=0.22  
CXTOT=TSP(1,2)  
FMOX=COMP(1)\*(1.0-ENCL)/CXTOT  
FOX=SP(2)/CXTOT  
FHOX=COMP(2)/CXTOT  
FH2OX=COMP(3)/CXTOT  
FH3OX=COMP(4)/CXTOT  
TERM1=CON(1,1)\*FMOX  
TERM2=0.00  
DCALC=TERM1+CON(2,1)\*FH3OX+CON(3,1)\*FH2OX+CON(4,1)\*FHOX  
1+CON(5,1)\*FOX+TERM2

- C     THIS SUBROUTINE IS FOR OXAS TAUTOMERIZATION RATIOS  
 $OXTOT = TSP(1,1)$   
 $FOX = SP(1)/OXTOT$   
 $FH0X = COMP(1)/OXTOT$   
 $FH20X = COMP(2)/OXTOT$   
 $FH30X = COMP(3)/OXTOT$   
 $DCALC = FOX * CON(4,1) + FH0X * CON(3,1) + FH20X * CON(2,1) + FH30X * CON(1,1)$
- C     THIS SUBROUTINE IS FOR OXAS ENOLATE SPECTROPHOT. DATA  
 $DCALC = SP(1) * CON(1,1) + SP(2) * CON(3,1) + COMP(1) * CON(2,1)$
- C     THIS SUBROUTINE IS FOR ABSORBANCE DATA (KG)  
 $DCALC = SP(1) * CON(1,1) + COMP(1) * CON(2,1) + COMP(2) * CON(3,1)$
- C     THIS SUBROUTINE IS FOR METAL-KG ABSORBANCE DATA  
 $DCALC = SP(2) * CON(2,1) + COMP(1) * CON(1,1) + COMP(2) * CON(3,1) + COMP(3) * CON(4,1)$
- C     THIS SUBROUTINE IS FOR ABSORBANCE DATA (OXAS)  
 $DCALC = SP(1) * CON(1,1) + COMP(1) * CON(2,1) + COMP(2) * CON(3,1) + COMP(3) * CON(4,1) + SP(2) * CON(5,1) + COMP(4) * CON(6,1) + COMP(5) * CON(7,1)$
- C     THIS SUBROUTINE IS FOR METAL-OXAS ABSORBANCE DATA  
 $DCALC = SP(2) * CON(3,1) + SP(3) * CON(7,1) + COMP(1) * CON(1,1) + COMP(2) * CON(2,1) + COMP(3) * CON(4,1) + COMP(4) * CON(5,1) + COMP(5) * CON(6,1) + COMP(6) * CON(8,1) + COMP(7) * CON(9,1)$
- C     THIS ROUTINE IS FOR ENZYME ABSORBANCE DATA  
 $DCALC = SP(1) * CON(1,1) + COMP(1) * CON(2,1)$

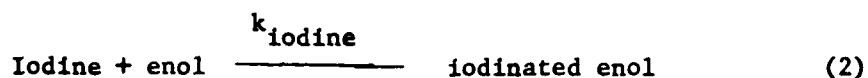


C        THIS ROUTINE IS FOR ENZYME/OXAS/KG ABSORBANCE DATA .  
         DCALC=SP(1)\*CON(1,1)+COMP(1)\*CON(2,1)+COMP(3)\*CON(3,1)+  
         1SP(2)\*CON(5,1)+COMP(4)\*CON(6,1)+SP(3)\*CON(7,1)+COMP(5)\*CON(8,1)  
         2+COMP(2)\*CON(4,1)  
         3+COMP(6)\*CON(9,1)

APPENDIX F

Investigation of the Spontaneous Tautomerization of  
Oxalosuccinate via the Method of Iodination

It was shown in Chapter IV that the rapid initial absorbance increase seen during the decarboxylation of oxas was due to tautomerization. It would seem that an alternate method to study that reaction is through iodination of the enol. The reactions involved are shown below. It was also shown in Chapter IV that iodination of the enol



was very rapid compared to tautomerization. Thus, the rate of disappearance of iodine should be comparable to the rate of enolization,  $k_b$ .

However, a plot of the rate of iodination, measured at 352 nm to monitor the species  $\text{I}_3^-$ , does not bear out this point. This can be seen in Figure 49. This figure shows the data for the rate of iodine uptake as a function of pH. Also shown on this figure is the tautomerization relaxation rate determined spectrophotometrically at 255 nm as reported in Chapter IV. Recall that this relaxation rate is actually  $k_f + k_b$ . Since  $K_T$ , the equilibrium constant for reaction (1), is  $k_f/k_b$ , then

$$k_{\text{obs}} (255 \text{ nm}) = k_b (1 + K_T) \quad (3)$$

Figure 49

Tautomerization rate and iodination rate versus pH.

$T = 25^{\circ}\text{C}$

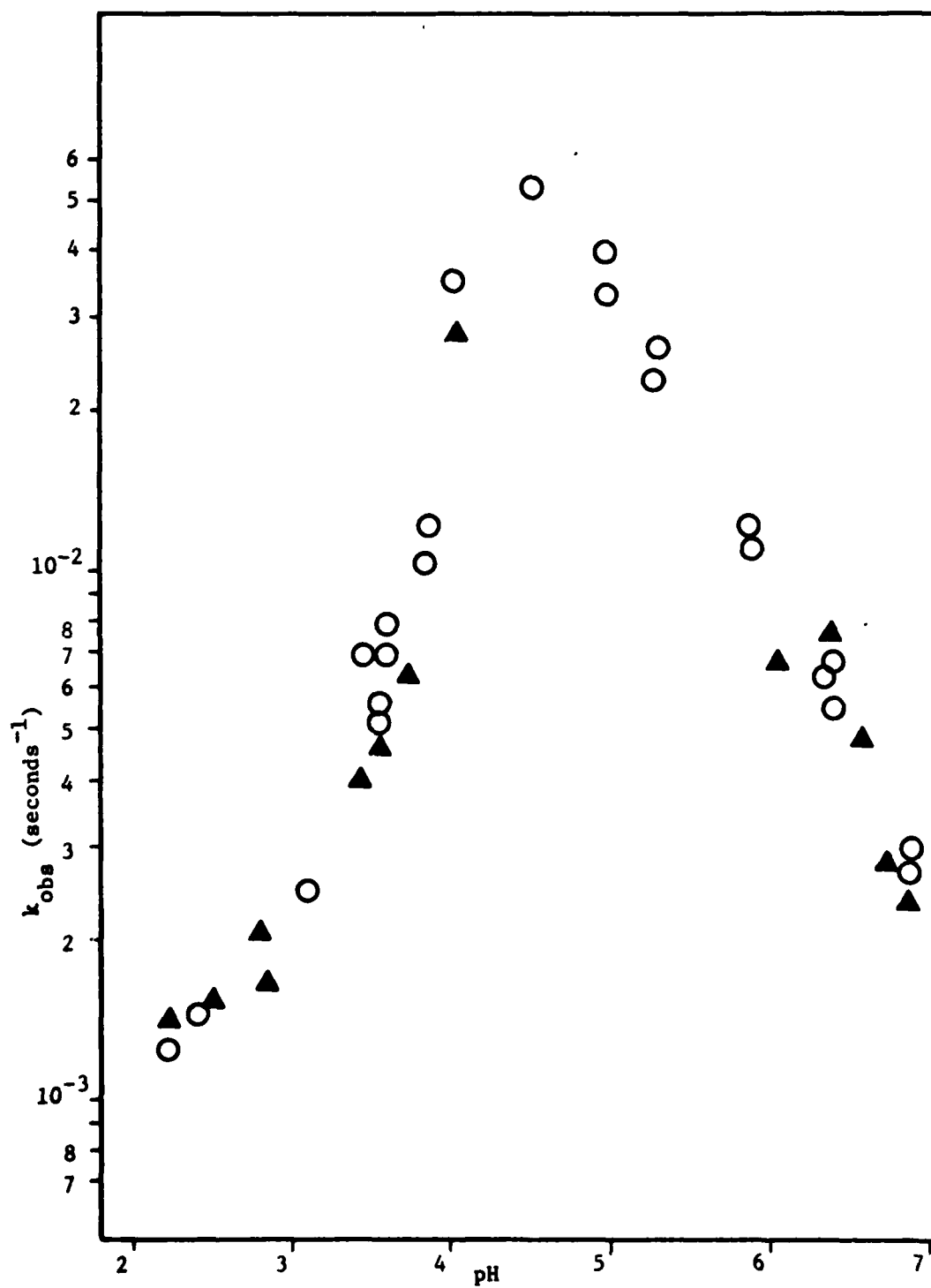
▲ Tautomerization rate at 255 nm.

○ Iodination rate at 352 nm

$[\text{I}^{-}] = 0.090 \text{ mM}$

$[\text{oxas}] = 0.336 \text{ mM}$

Other experimental conditions are as stated in Figure 21.



or

$$k_b = k_{obs} / (1 + K_T) \quad (4)$$

From the data in Chapter IV, the lowest value of  $K_T$  is 289. Thus,  $k_b$ , or the enolization rate, is at least two orders of magnitude smaller than the observed relaxation rate.

However, the rate of iodine uptake is not equal to the rate of enolization. It is instead comparable to the relaxation rate, or  $k_f + k_b$ . Due to the large equilibrium constant, the relaxation rate is essentially equal to the rate of ketonization. This means that the rate of iodine consumed, measured at 352 nm, is the same as the rate of ketonization, not enolization.

From the data presented, no conclusions can be made as to why the rate of iodine reacted did not equal the enolization rate. Therefore, further investigations will be required to deduce the iodination mechanism that is consistent with the data.